Johan Mendoza Chacón
Mestre em Ciência e Tecnologia Alimentar

Exploring and improving the color stability of natural anthocyanins and synthetic derivatives and their application as pH/light-sensitive systems.

Dissertação para obtenção do Grau de Doutor em Química Sustentável

Orientador: Doutor Fernando Jorge da Silva Pina, Professor Catedrático Jubilado da Faculdade de Ciências e Tecnologia da Universidade NOVA de Lisboa.
Co-orientador: Doutor Nuno Miguel Jesuíno Basílio, Investigador Auxiliar da Faculdade de Ciências e Tecnologia da Universidade NOVA de Lisboa.

Júri:

Presidente:	Doutora Susana Filipe Barreiros, Professora Catedrática da Faculdade de Ciências e Tecnologia da Universidade NOVA de Lisboa.
Arguente(s):	Doutor António Luís Vieira de Andrade Maçanita, Professor Catedrático Jubilado do Instituto Superior Técnico da Universidade de Lisboa.
	Doutora Erika Salas Muñoz, Full Professor da Facultad de Ciencias Químicas da Universidad Autónoma de Chihuahua.
Vogal(ais):	Doutor João Carlos dos Santos Silva e Pereira de Lima, Professor Associado, com agregação da Faculdade de Ciências e Tecnologia da Universidade NOVA de Lisboa.
	Doutor Luis Miguel Neves Ferreira Serra Cruz, Investigador da Faculdade de Ciências da Universidade do Porto.
	Doutor Nuno Miguel Jesuíno Basílio, Investigador Auxiliar da Faculdade de Ciências e Tecnologia da Universidade NOVA de Lisboa.

FACULDADE DE CIÊNCIAS E TECNOLOGIA
UNIVERSIDADE NOVA DE LISBOA

Novembro, 2020

Exploring and improving the color stability of natural anthocyanins and synthetic derivatives and their application as pH/light-sensitive systems.

To my parents, to whom I owe everything.
A mis padres, a quienes les debo todo.

Acknowledgements

First, and most of all, I would like to express my gratitude to God, who always lit my path since the beginning of my existence, and has put all the wonderful people and blessings around me. My enormous gratitude also for my dear mentor Professor Fernando Pina, who accepted me as an apprentice in the last years before his jubilee. Professor Pina has always been incredibly supportive and helpful, always ready to share his vast knowledge with that strong passion and unrelenting commitment characteristic in him. Professor's Pina child-like curiosity is inspiring; anyone who knows him knows about this attribute that only he can convey. His guidance, without doubts, has positively impacted my professional growth, teaching me how to drive forward the generation of results. Professor, I sincerely appreciate your time and advice during these four years; thank you for your trust and the opportunity to learn from one of the most prominent researchers in photochemistry and the field of flavylium derivatives. I consider myself extremely lucky to have the opportunity to work with you and the CHARM group.

Particular thanks must be expressed to my co-supervisor, Doctor Nuno Basílio, who I consider my friend. Like any good friend in our lives, you came to my professional life unexpectedly. I did not choose you, and probably neither did you, but without doubts, you have been one of the greatest blessings. Thank you, Nuno, for your constant and tireless support, for your availability and dedication, but above all, thank you for your enormous PATIENCE. You know I have great admiration for your time management, the way you think, and your conviction; these and other attributes make you a great friend, researcher and advisor. I hope to have learned something about this under your tutelage. As your fist Ph.D. pupil, I hope I was the worst in your fruitful starting career as advisor; even if you consider me good enough, I'm pretty sure you deserve the best students, rest assured now I am a different person and a better researcher after all your guidance and advises, and I will be pleased to be part of future collaborations wherever fate leads us.

I would like also to thank Professor João Carlos Lima (a.k.a. WikiLima, who was introduced to me like that at the very beginning) and Professor Jorge Parola for their support, anytime I needed some advice you were there, thank you so much. Thanks also to the other experienced members of the photo group; Artur Moro, Andreia Forte, João Avô, Tiago Moreira, Noemi Jordão, Hugo Cruz, Claudia Pereira, Sandra Gago, and believe or not my good friend

André Seco, who always were there to help me out with my experiments. Special thanks to my friend and colleague Miguel Santos who was also my personal Portuguese teacher during the first year (and beyond). I have to thank the other group members for their company and emotional support, thank you Rita João, Marisa Noijens, my friend Ana Lúcia Pinto, and the members of the foreign legion: Ambrósio Camuenho, Mani Otis (now Portuguese), Jack Fletcher, Massimo Tosolini, Karolina Zalewska, Zeljko Petrovsky (also Portuguese now), María Cámara, Alfonso Alejo, and my good friends Miguel (Migue) Romero, Eva Mariasole Angelin and Javier (Xavi) Díaz.

Here, I would like to thank Professor Victor de Freitas and his group at the University of Porto, thank you for your trust and support. I hope we can contribute to the future with new collaborations. Special thanks to Luis Cruz, Joana Oliveira, and my friend Paula (Paulinha) Araújo.

This thesis would not be possible without the financial support of the National Council on Science and Technology (CONACyT, Ref. 288188) from the Mexican government and the economic support from the CHARM group, thanks for the money.

Cambiando a mi lengua madre, tengo que agradecer también el infinito apoyo de mis amigos principalmente el de mi mejor amigo Diego Carballo, gracias carnal por estar siempre cuando mas lo necesitaba. A mis otros amigos que estuvieron brindando apoyo desde lejos; Dk, Ily, Brenda, Dr. Cacho, Mayte, Dany, Denisa (y el bebé que viene en camino), Dra. Lula, Dra. Layla, Dr. Victor, Rulo, Cynthia, Ever, Perla, Mariana y Maveth. En mi paso por Portugal también encontré buenos amigos que han ayudado mucho a mantenerme constante en este viaje, muchas gracias a mi mejor amiga Gaby (bebeshita), Gonzálo, Isela, Alina, Rafa, Alheli, Lupita, Luis, Liz, Sofia, Mani (obrigado meu), Mario (grazie mille), Erick, Ricardo, Andrea, Anabel, Bernie, Chris y Estrella. Gracias también a los del nuevo club Andrés, Vetho y Ariel.

Por último pero no menos importante, he de agradecer a mi familia, a mis padres Héctor y María Elena, por haberme dado todo lo que tengo y que gracias a ellos soy todo lo que soy. Gracias a mis hermanos y mis sobrinos por todo el apoyo recibido desde lejos antes y después de llegar hasta aquí. He de agradecer también a mi familia Luso-mexicana, quienes me han tratado como parte de su familia, gracias Sandra, Miguel, Gabo y Dário por siempre recibirme en su casa y ser tan buenos conmigo.

"I think Nature's imagination is so much greater than man's,
she's never gonna let us relax!"-Richard Phillip Feynman

Abstract

The color expression in Nature deserves the attention of scientists searching eco-friendly solutions to substitute pollutant synthetic dyes used in industrial processes. Being natural pigments, anthocyanins represent an affordable alternative; unfortunately, the colored structures in anthocyanins are only stable in very acidic conditions, forming colorless products as the pH increases, precluding a more widespread utilization of these compounds as dyes. This has motivated significant research efforts focusing on the development of new strategies toward color stabilization in anthocyanins and their application in formulations with different pHs in the coloring industry. On the other hand, the colorless structures are light-sensitive being responsible for the photochromic properties in some anthocyanins and synthetic derivatives. The study of photochromic transformations between uncolored and colored forms is important in the development of photochromic devices in the materials industry. In this thesis, a deep physical-chemical analysis of some natural mechanisms for color stabilization such as self-association, aggregation, and co-pigmentation was performed in anthocyanins and synthetic derivatives, in order to understand how Nature rules the expression of color. Some other methods based on supramolecular assemblies as host-guest interactions and micelle inclusions were also studied for the stabilization of both, colored and uncolored species, searching for the stabilization of color and improvement and application of the photochromic properties. Some results in natural anthocyanins indicate that the inter and intramolecular interactions during their self-association and aggregation processes, as well as the number of acylated units, result crucial in the stabilization of color and their water solubility. The co-pigmentation effect of the caffeine over the color stabilization was evaluated in a systematic way, employing a developed new method to explain the higher affinity of the co-pigment for the chromophores. The inclusion of anthocyanins and their synthetic derivatives into host receptors as molecular clips, calix[n]arenes, and micellar environments proved a high stabilization of the color along the pH scale. On the other hand, the photochromic properties of some synthetic flavylium systems were explored; the quantum yield of photoisomerization between uncolored and colored species was increased by the complexation with cyclodextrin as a host. The pH and light-sensitive properties of anthocyanins derivatives were exploited in the construction of a molecular timer controlled by changes in the pH and a system able to control the dissociation of boronate esters by photoisomerization.

Keywords: Anthocyanins, Host-guest, Self-association, Copigmentation, Photochromism.

Resumo

A expressão da cor na Natureza merece a atenção dos cientistas em busca de soluções verdes para a substituição de corantes sintéticos poluentes usados em processos industriais. Por serem pigmentos naturais, as antocianinas representam uma alternativa acessível; infelizmente, as estruturas coloridas nas antocianinas são estáveis apenas em condições muito ácidas, formando produtos incolores com o aumento do pH, impossibilitando uma utilização mais ampla desses compostos como corantes. Isso tem motivado esforços de pesquisa significativos com foco no desenvolvimento de novas estratégias para a estabilização da cor em antocianinas e sua aplicação em formulações com diferentes pHs na indústria de corantes. Por outro lado, as estruturas incolores são sensíveis à luz, sendo responsáveis pelas propriedades fotocrómicas de algumas antocianinas e derivados sintéticos. O estudo das transformações entre formas incolores e coloridas é importante no desenvolvimento de dispositivos fotocrómicos na indústria dos materiais. Nesta tese, foi realizada uma análise físico-química profunda de alguns mecanismos naturais de estabilização de cor tais como a autoassociação, agregação e co-pigmentação em antocianinas e derivados sintéticos, a fim de compreender como a Natureza rege a expressão da cor. Alguns outraos métodos baseados em montagens supramoleculares como interações hospedeiro-hóspede e inclusões micelares também foram estudadas para a estabilização de espécies coradas e incolores, procurando a estabilização da cor e o aperfeiçoamento e aplicação das propriedades fotocrómicas. Alguns resultados em antocianinas naturais indicam que as interações inter e intramoleculares durante seus processos de autoassociação e agregação, bem como o número de unidades aciladas, são cruciais na estabilização da cor e sua solubilidade em água. O efeito da co-pigmentação da cafeína sobre a estabilização da cor foi avaliado de forma sistemática, empregando-se um novo método desenvolvido para explicar a maior afinidade do co-pigmento pelos cromóforos. A inclusão de antocianinas e seus derivados sintéticos em receptores supramoleculares como clipes moleculares, calix[n]arenos e ambientes micelares provou uma alta estabilização da cor ao longo da escala de pH. Por outro lado, as propriedades fotocrómicas de alguns sistemas baseados en flavílios sintéticos foram exploradas; o rendimento quântico da fotoisomerização entre espécies não coloridas e coloridas foi aumentado pela complexação com ciclodextrina como hospedeiro. As propriedades de sistemas de derivados de antocianinas sensíveis ao pH e à luz foram exploradas na construção de um cronômetro molecular controlado por mudanças no pH e de um sistema capaz de controlar a disociação de ésteres de boronato por fotoisomerização.

Palavras-chave: Antocianinas, Hospedeiro-hóspede, Auto-associação, Copigmentação, Fotocromismo.

Contents

List of Figures

List of Tables

Glossary

Actinometry	Technique used to measure the intensity of a lamp using an actinometer; a chemical system or a physical device by which the number of photons in a beam absorbed into the defined space of a chemical reactor can be determined integrally or per time.
Biomimmicry	A practice that learns from and mimics the strategies found in nature to solve human design challenges.
Chromophore	Part of a molecule or molecules that absorb particular wavelengths of visible light, and are responsible for its color.
Co-pigmentation	Phenomenon in which the pigments and other colorless organic compounds, or metallic ions, form molecular or complex associations, generating a change or an increment in the color intensity.
Cotton effect	Characteristic change circular dichroism experiments. In a wavelength region where the light is absorbed, the absolute magnitude of the optical rotation at first varies rapidly with wavelength, crosses zero at maximum absorption and then again varies rapidly with wavelength but in the opposite direction.
Direct pH jump	A fast solution pH change to less acidic conditions commonly achieved after addition of an strong base.
Equilibrium	State in which the rate of the forward reaction equals the rate of the backward reaction. In other words, there is no net change in concentrations of reactants and products.
Flavylium	Member of the class of chromenyliums that is chromenylium with a phenyl substituent at position 2.
Flavylium multi-state	Different species obtained along the pH scale in aqueous solutions containing flavylium-based compounds.

Functional food product	Foods that have a potentially positive effect on health beyond basic nutrition. Proponents of functional foods say they promote optimal health and help reduce the risk of disease.
Molecular timer	A set of molecules that are interconnected that responds to external stimuli followed by a kinetic process that controls an specific event.
Molecular switch	Molecule that can be reversibly shifted between two or more stable states. The molecules may be shifted between the states in response to environmental stimuli, such as changes in pH, light, temperature, an electric current, microenvironment, or in the presence of ions and other ligands.
Photo-stationary state	Steady state reached by a photochemical reaction in which the rates of formation and disappearance of transient species are equal.
Photochromism	Reversible transformation of a chemical species between two forms by the absorption of electromagnetic radiation (photoisomerization).
Pseudo-equilibrium	Transition state obtained in a consecutive set of reactions, where one of the last reaction rates is sufficiently slow, and the concentrations of the reactants and products keep relatively constant for a considerable period of time.
Reverse pH jump	A fast solution pH change to more acidic conditions commonly achieved after addition of an strong acid.
Self-association	Intra-molecular interaction or also defined as intermolecular interactions between molecules of the same type.
Sustainable	Scientific concept that seeks to improve the efficiency with which natural resources are used to meet human needs for chemical products and services.

Acronyms

βCD	β-Cyclodextrin
μM	Micromolar
μl	Microliters
ΔG^0	Gibbs Free Energy
^{1}H NMR	Proton Nuclear Magnetic Resonance
^{13}C NMR	Carbon-13 Nuclear Magnetic Resonance
2′OH-5′Me	2′-Hydroxy-5′-methylflavylium
3-DAs	3-Deoxyanthocyanins
4′OH	4′-Hydroxyflavylium
7OH4'TEG	7-Hydroxy-4'-triethylenglycol flavylium
8,4′OH	8,4′-Dihydroxyflavylium
8OH4′TMA	8-hydroxy,4′-(3-trimethylammonio) propoxyflavylium
A	Quinoidal Base
Abs	Absorbance
AH^+	Flavylium Cation
B	Carbinol pseudo-base/Hemiketal
Cn	Calix[n]arenes
CBn	Curcubit[n]urils
CB^	Conjugated base species of AH^+ at the pseudo-equilibrium
CB′	Conjugated base species of AH^+ at the equilibrium
Cc	*cis*-Chalcone
CCC	Countercurrent Chromatography
CD	Circular Dichroism
CDs	Cyclodextrins
cm	Centimeters

CMC	Critical Micelle Concentration
Ct	*trans*-Chalcone
DFT	Density Functional Theory
DNA	Deoxyribonucleic Acid
DSSC	Dye Sensitized Solar Cells
EPS	Electronic Potential Surface
FDA	Food Drug and Administration
Fla	Flavanone
Fle	Flavanone phenoxide ion
Fle^-	Flavanone phenoxide dianion
GHF	7-β-D-glucopyranosyloxy-4′-hydroxyflavylium
HBA1	Heavenly Blue Anthocyanin
HBA2	Bisdeacyl HBA
HBA3	Trisdeacyl HBA
HPLC	High-Performance Liquid Chromatography
ITC	Isothermal Titration Calorimetry
M	Molar
MHz	Megahertz
min	Minutes
ml	Milliliters
mM	Milimolar
MPLC	Medium-Pressure Liquid Chromatography
ms	Miliseconds
MS	Mass Spectrometry
Mv3Coum	Malvidin 3-O-(6-O-*p*-coumaroyl) glucoside
nm	nanometers
NMR	Nuclear Magnetic Resonance
NOE	Nuclear Overhauser Effect

PBA	Phenylboronic acid
ROS	Reactive Oxygen Species
s	Seconds
SBE-βCD	Sulfobutylether-β-Cyclodextrin
SC*4*	*p*-sulfonated calix[*4*]arene
SC*6*	*p*-sulfonated calix[*6*]arene
SC*8*	*p*-sulfonated calix[*8*]arene
SC*n*	Sulfonated Calix[*n*]arenes
SDS	Sodium Dodecyl Sulfate
TFA	TriFluoroacetic Acid
UV	Ultraviolet
UV-B	Ultraviolet-B
UV-vis	Ultraviolet-visible

CHAPTER 1

Introduction

The practice of a specific technique makes humans became masters; consequently, masters contribute to making perfection. To reach perfection is necessary to use time, the most valuable thing that someone can spend. With billions of years of evolution that support it, *Mother Nature* is the clearest example of perfection. It is not strange that Nature's genius serves for inspiration in science and technology, and the practice of copying mechanisms to produce functional materials and make synthetic chemical compounds based on them is one of the most followed protocols to research in different areas. Nature-inspired design served for these proposes is known as *biomimicry*.

1.1 Biomimicry and its relationship with sustainability

The term biomimicry, derived from the Greek *"bio"* which means life and *"mimesis"* that means simulation or imitation.[1, 2] The term appeared for the first time published in 1982,[3] a work that describes organometallic complexes which mimic the active site function of two enzymes. Biomimicry is a branch of science that aims to identify and study the basics of the mechanisms, materials, and structures found in nature and then convert them in the knowledge that can be applied in problem-solving.[2] Janine Benyus popularized the term of biomimicry in her book published in 1997 [1], later she founded *The Biomimicry Institute* that promotes the transfer of ideas, designs, and strategies from biology to sustainable human systems design.

On the other hand, the *Oxford English Dictionary* defines *sustainability* as "capable of being upheld; maintainable"the term derives from the French verb *"soutenir"*, which means "to hold up"or "support". The concept of sustainability had been modified and adapted by different societies, including aspects related to sustainable energy, society, economy, agriculture, and biological resource use.[4, 5, 6] In general, sustainability is based on the fact that resources are finite, and it is essential to maximize their use during the production

processes. Here, the application of biological systems that serve as models plays an essential role in proposing various strategies to increase the benefits of the resources and reduce production costs.[2]

1.2 Copying Nature as an opportunity in the science of color

Colorants extracted from plants, animals, and minerals were used since prehistoric times. The animal instinct of humans to mark our territory comes from more than 30,000 years ago. Later, the Egyptians and Chinese dominated some dyeing techniques using dyes principally extracted from plants and insects and some mineral pigments; other cultures in America and other continents also developed different techniques with other kinds of colorants.[7] The Greeks and Romans used different colorants obtained from natural sources. Later, they were spread, modified, and diversified in Europe during medieval times and worldwide with the industrial revolution and modern age.[8] In 1856 the first synthetic organic dye was incidentally discovered; the mauveine or Perkin's mauve has pioneered the development of other synthetic dyes as azo and di-azo compounds. During the chemical industry expansion in the 19th century, the natural pigments chemical structure also served as inspiration for the synthesis of useful substances in terms of product quality and cost-effectiveness.[9] Many natural pigments, obtained typically by extraction and purification, were replaced by their synthetic versions through the history.[8, 10]

During ancient times, the cost of colored articles, in therm of chemistry and applications, was high, and only the wealthiest people could afford them, now they are accessible by almost all. In early times, the effects of colorant extraction, production, and waste generation over the environment, health, and toxicity were unknown.[7, 11] Nowadays, color occupies an essential role in our lives, from the clothes we wear, the documents we read, food we eat and in general, everything we see. Hence, the rapid industrialization and the high demand for colorants for different proposes is affecting the dyeing industry.

Among the dying industries, textile is one of the most polluting activities. Synthetic dyestuffs used to dye fabrics give color to the water. Some of them are toxic; this reduces the water permeability to light and oxygen that may cause the extinction of living beings and restrict the reuse of the water.[7] Today, natural colorants are hardly used in the textile sector.[12] Furthermore, the food industry uses synthetic and natural colorants to influence the food appearance to attract consumers. Synthetic compounds are widely used due to their effectiveness, but they can cause toxic or carcinogenic effects in humans. On the other hand, natural colorants are usually non-toxic and posses some beneficial health effects as anti-carcinogenic, antioxidant, bactericidal, anti-viral, and anti-mutagenic activities. Cosmetic products also have many colorants on their formulations, they have rarely been associated with health hazards, but long-term effects have not been evaluated. However, some

of them cause allergic reactions and exhibit possible carcinogenic or mutagenic effects.[7, 11]

Consequently and given the above findings, environmental and health legislation have a stricter control, but necessary, over the colorant usage. In 1881, the United States Department of Agriculture began research on the colorants used in food. Later, the Federal Drug and Administration (FDA) was founded and is now responsible for protecting public health in the US. In Europe, the European Parliament appointed the European Commission, and now every country around the world has its own institution to regulate these affairs. These institutions regularly publish a series of specifications and recommendations in the use of natural and synthetic colorants and their prohibitions in different industries.[11, 13]

Natural dyes are not entirely safe, but they are less toxic than their synthetic counterparts. Many of them are biodegradable and cost-effective, have pharmacological effects and possible health benefits, and come from renewable sources.[14] Unfortunately, there is a series of disadvantages to the use of natural pigments in the coloring industry. Some examples include their extraction, which is time-consuming, they tend to fade faster than synthetic dyes (lower stability) and are not entirely compatible with synthetic fibers for their use in the textile industry.[5]

Whatever view is taken on this, the interest of using dyes and pigments derived from natural sources is increasing during the last years. The study of the natural compounds applying biomimetic techniques led to obtaining discoveries about the science of color, this, in turn, contributes to obtain industrial innovations.[7] An example of Nature's inspiration is, in fact, the synthesis of dyes and pigments previously mentioned, as well as the study of natural photosynthetic mechanisms to obtain energy from the sun. All the photosynthetic organisms, the best solar cells on earth, are considered sustainable because there is no waste in these natural systems. The environment is not affected when the organism born or dies. Investing in the study and partial or total application of their mechanism features to obtain renewable energy technologies leads to achieving a truly sustainable energy source.[15]

1.3 Anthocyanins as natural dyes

Anthocyanins are the most important pigments of the vascular plants; they are produced as secondary metabolites to attract animals to promote pollination and seed dispersal. They also play an important role in plant protection against ultraviolet (UV) light damage and photo-oxidative stress.[16] Natural anthocyanins have served as bio-inspiration for the design of synthetic flavylium-based compounds. In turn, the study of the thermodynamic and kinetic behaviors of the pH-dependent network of chemical reactions in such compounds has substantially contributed to a better understating of the complicated system behavior as the anthocyanins one.[17] Understanding the anthocyanins behavior is essential to evaluate the role of these natural compounds in health-related benefits, their use as colorants, and

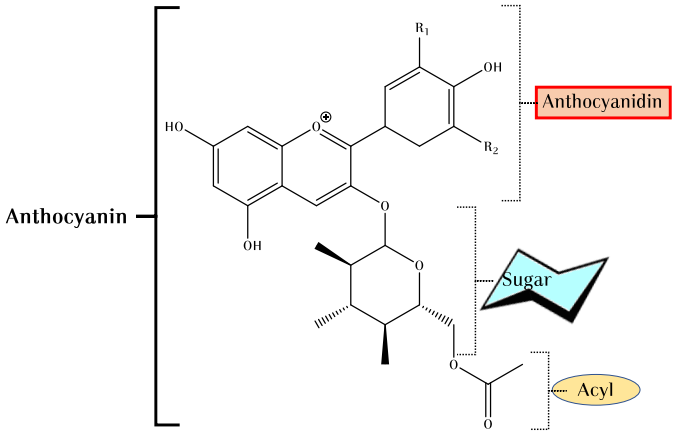

Scheme 1.1: Typical representation of an anthocyanin and its fragments.

their applications in different areas that will go deeply forward in this chapter.

Anthocyanins belong to the family of flavonoids, the largest group of pigments in the Plant Kingdom. These phenolic compounds are responsible for blue, orange, violet, purple, pink, and red colors in many flowers, leaves, roots, seeds, stems, and fruits. They are heterosides, composed of an anthocyanidin (aglycone), derived from the 2-phenylbenzopyrylium (flavylium), and one or various sugar moieties that confers water solubility and can be or not acylated with aromatic or aliphatic organic acids (Scheme 1.1).[18] Most anthocyanins are glycosylated at position C3 (see Figure 1.1), but they can be found bearing sugars in positions C5,C7,C3',C5' or C4'.[18] Meanwhile, the acylation is one of the most common modifications in plant secondary metabolites as the anthocyanins. The hydroxycinnamoyl groups are commonly the main aromatic substituents, and the aliphatic acyl substituents, including malonyl, acetyl, succinyl, and malyl, among others, can be generally linked to the glucosyl moieties. The acylated compounds are more stable than their non-acylated parent compounds.[19] By this time, the structure of more than 700 anthocyanins have been identified in extracts obtained from Nature, and around 65% of them are acylated.[20]

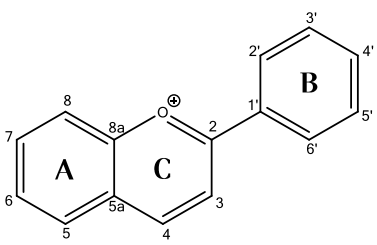

Anthocyanidin	3,5,7	3'	4'	5'
Pelargonidin (Pg)	OH	H	OH	H
Cyanidin (Cy)	OH	OH	OH	H
Delphinidin (Dp)	OH	OH	OH	OH
Peonidin (Pn)	OH	OCH_3	OH	H
Petunidin (Pt)	OH	OH	OCH_3	OH
Malvidin (Mv)	OH	OCH_3	OH	OCH_3

Figure 1.1: The 2-phenylbenzopyrylium structure and the most common anthocyanidins found in Nature.

Chemically, the flavylium backbone or 2-phenylbenzopyrylium is composed by an aromatic ring (A) bonded to an oxygen heterocycle (C), which is also bonded to a third aromatic ring (B), some H are commonly substituted by methoxy or hydroxyl functional groups (Figure 1.1) to form the anthocyanidins, that acts as the chromophore.[21] In Figure 1.1, the substitution pattern of the most important anthocyanidins is presented.

The flavylium cation usually represents anthocyanins and related compounds because they are generally isolated as flavylium chloride salts,[22] which is the dominant form in acidic aqueous solutions. However, this structure is only one of the species involved in the pH-dependent flavylium multi-state (see Section 1.4). A positive charge is always represented over the oxygen in the heterocycle, but it is delocalized through all the pyrylium structure, being C2 and C4 the most electron-deficient atoms.[23]

1.3.1 Stability of anthocyanins

Anthocyanins are the flavonoids with high sensibility to thermal and pH degradation, their aglycones are only stable under highly acidic conditions and are degraded in less than an hour at physiological conditions (37°C and pH=7.4).[24] The increasing $^{-}$OH concentration may boost the degradation reactions in anthocyanins, while the hydroxyl group in position C3 in anthocyanidins makes them unstable. Both anthocyanidins and anthocyanins are not stable above neutral pH and the pathways for their degradation include hydrolytic and autoxidative processes with cleavage of the C2-C1', C2-C3 and C3-C4 bonds (Figure 1.2).[24, 25] These reactions are irreversible and represent a drain from the flavylium multi-state system detailed below in Section 1.4.

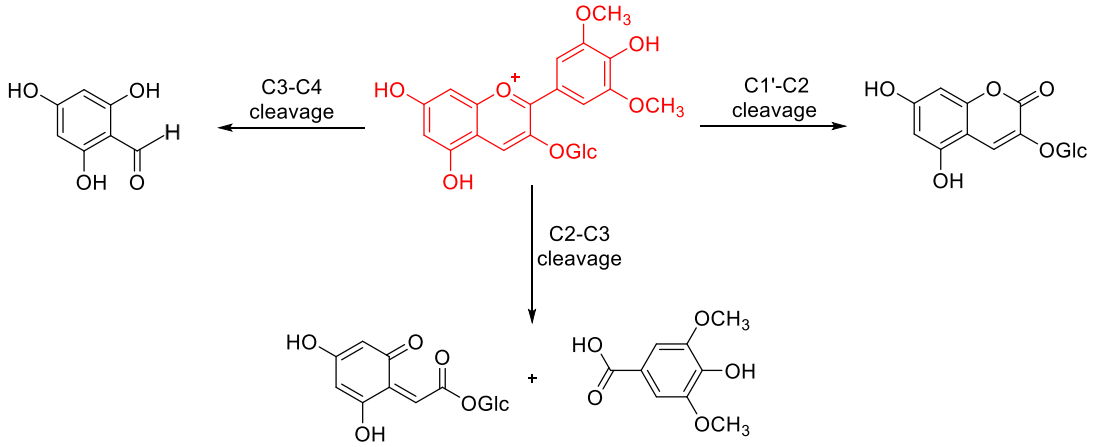

Figure 1.2: Pathways of the anthocyanins degradation by cleavage of the C2-C1', C2-C3 and C3-C4 bonds.

On the other hand, the polyphenolic structure of anthocyanidins adds a hydrophobic characteristic on them, and makes them soluble in organic solvents, such as ethanol and

methanol. The sugar moiety provides higher solubility to the anthocyanins when they are dissolved in aqueous media; thus, the aglycones are found in fresh plant tissues in a lower proportion. The level of glycosylation is also important in terms of stability; an extra sugar in position 5 improves the stabilization of 3-O-glycosides.[26] Sugars can be substituted or acylated by aliphatic, hydroxybenzoic, or hydroxycinnamic acids. Polyacylated anthocyanins that contain more than one glycosyl and/or acyl groups have been identified in different plant tissues.[27]. The acylated derivatives are typically more stable than non-acylated because they offered resistance to the hydration reaction[18] (see Section 1.4) and higher resistance to light and heat. The substituents in the B ring also influence the stability of anthocyanins, the more hydroxyl groups, the more unstable. Otherwise, the methoxyl groups can bring certain stability. Accordingly, Pelargonidin would be the most stable anthocyanidin (Figure 1.1). Other compounds as pyranoanthocyanins and 3-deoxyanthocyanins are more stable than the anthocyanins; because the former have a substitution in position 4 and are less susceptible to hydration[28], while the absence of substituent in position 3 in deoxyanthocyanins not only make them resistant to hydration at high pH, making their quinoidal bases more stable than the hemiketal form, but also they are stable to temperature degradation.[29, 30, 31] The isolated anthocyanins stability can be also affected negatively by the presence of enzymes, heat-humidity, oxygen, and light exposure leading to their degradation.[32, 33]

1.3.2 Color expression

The π-conjugated structures in flavylium-based compounds are responsible for the absorption of green and yellow wavelengths (expressing red to blue colors), while the chalcones can sometimes absorb blue wavelengths providing yellow colors.[34] The UV/Vis absorption spectra are commonly attributed to electronic transition between the π-type molecular orbitals and have been defined by different quantum chemical methods.[35] Almost all the anthocyanins present an absorption band in the visible region of the electromagnetic spectrum, around 500-535nm, and a second band in the UV region around 265-275nm. When an aromatic organic acid acylates an anthocyanin, the absorption in the UV-B range is increased.[36] After a proton lost in the flavylium cation, the anthocyanins' conjugate base maximizes its electron delocalization over the three rings, and typically, a red-shift is observed in the wavelength absorption, and the color turns from red to purple-blue. The number and type of substituent in the flavylium backbone, as well as the site of substitution, are responsible for the variation in color in this family.[9, 34] The color of these compounds can also be modulated by controlling the pH of the solution, metal complexation, and intermolecular interactions, which may induce co-pigmentation detailed below in sections 1.5 and 1.6.

1.3.3 Anthocyanins sources

During the last decades, an increasing number of reports in the literature regarding the sources and the development of novel techniques to separate and purify anthocyanins, their application, color tracking and pigment changes, quantitative analysis, and the effect of the plant stress over the anthocyanin production have been published. The source and applications of some natural anthocyanins and their synthetic parent compounds will be summarized in this and the next subsection.

As previously pointed out, anthocyanins are spread in the Plantae Kingdom. The most common sources in human feeding are fruits and vegetables. Principally from fruits of the family *Rosaceae* (Blueberries, blackberries, strawberries, cherries, etc.), but they are also abundant in some cereals, leafy vegetables, and roots such in purple potatoes, eggplant, red onion and cabbage, beans, purple corn, among others.[37] Processed foods have been much less studied for their anthocyanin content because usually, the extraction of these compounds leads to their degradation after their storage. Wine is maybe the processed product with more research about anthocyanin content; during the aging, the anthocyanin levels decrease, but other derivatives as stable pyranoanthocyanins use to appear.[28]

Anthocyanins are polar molecules, and typically they are obtained by solvent extraction using acidified aqueous mixtures of methanol, ethanol, or acetone. This method can not separate other polar molecules like sugars or organic acids; then, a separation technique must be applied to purify the pigments. The most used techniques to separate them are the solid phase extraction, countercurrent, medium pressure, and high-performance liquid chromatography (CCC, MPLC, and HPLC, respectively). After isolation, the mass spectrometry (MS) and nuclear magnetic resonance (NMR) of ^{1}H and ^{13}C are the most used techniques for the identification of anthocyanins.[21]

1.3.4 Applications of anthocyanins and related compounds

Besides their use as natural colorants, many other uses and applications of anthocyanins and their flavylium derivatives have been discovered, mostly in food processing, pharmaceutical industry, cosmetic manufacturing, solar cell development, biosensors, molecular switches, and drug delivery assemblies.

The European Union and the United States approve the use of anthocyanins as natural food additives to impart color. Usually, they are used as raw extracts or concentrated juices obtained from different edible sources.[18] Their use is limited to foodstuffs with sufficiently acidic pH, not extremely heated or without sulfites (except for the wine, commonly used as food preservatives); in those conditions, they are unstable. Because of this, they are used in dairy products, jams, candies, soft drinks, etc. Due to their health promotion properties, anthocyanins have been included in many foods products not only because of their colors

but also for the formulation of functional food products.[38, 39] The previous statement is attributed because anthocyanins have been identified to exhibit a strong antioxidant activity. They can transfer electrons to reactive oxygen species (ROS), protecting those biomolecules able to oxidize as DNA, proteins, and polyunsaturated fatty acids.[24] This property is related to the prevention of neuronal and cardiovascular illnesses, cancer, inflammation, and diabetes, among other diseases.[40, 41] As an active pharmaceutical additive, some anthocyanins have been associated with antimicrobial effects and good visual health goodnesses.[42, 43] These are some of the reasons why natural anthocyanins are considered important in the pharmaceutical sector.

Some cosmetic topical formulations rich in anthocyanins have shown reliable protection in human skin against the aging damage produced by UV light, such as oxidative damage in the epidermis, dermis and, adnexal organs of the skin.[44, 45, 46] This photo-protective effect is related to the anthocyanins UV light absorption, mainly in acylated and polyacylated ones. Conversely, another effect observed in cosmetics with anthocyanins is the inhibition of hyperpigmentation by inhibition of the tyrosinase activity in melanocytes.[47] The tyrosinase inhibitors are commonly used for whitening skin in cosmetic formulations; unfortunately, the common inhibitors are related to cancer and neurodegenerative diseases as Parkinson's[48], then the use of natural inhibitors as anthocyanins can be suitable for their substitution.

Natural anthocyanins with a catechol group in the B ring can be used as light harvesters in dye-sensitized solar cells (DSSC), based on the principle that they can link to the titanium dioxide in their quinoidal base form, then light excitation of the chromophore lads to the electron injection to the TiO_2 conduction band producing electric current.[49, 50] Anthocyanins nano-encapsulation has demonstrated enhanced optical properties as chromophores or fluorescent active biomolecules used as green constituents for electro-chromic applications and photonic devices.[51, 52, 53] Anthocyanins have served as bioinspiration for the application of synthetic flavylium compounds, and in counterpart, the study of some synthetic flavylium model compounds have contributed to a better understanding of the anthocyanins properties. Since natural anthocyanins tend to degrade and/or hydrate to form other species along the time (see sections 1.3.1 and 1.4), some bioinspired stable synthetic flavylium compounds have been tested in DSSC with high performances.[54] The synthetic flavylium-based compounds have served as light, and pH-dependent molecular switches, chemosensors for water/humidity, and photo triggered drug delivery assemblies, among other applications.[22, 55, 56, 57]

Research on anthocyanins and in general flavylium-based compounds has evolved during the last two decades. New natural compounds have been discovered and characterized, their mechanism of color has been clarified, the interaction with other molecules been studied, and new applications been discovered.[22] All this has only been possible because of a better

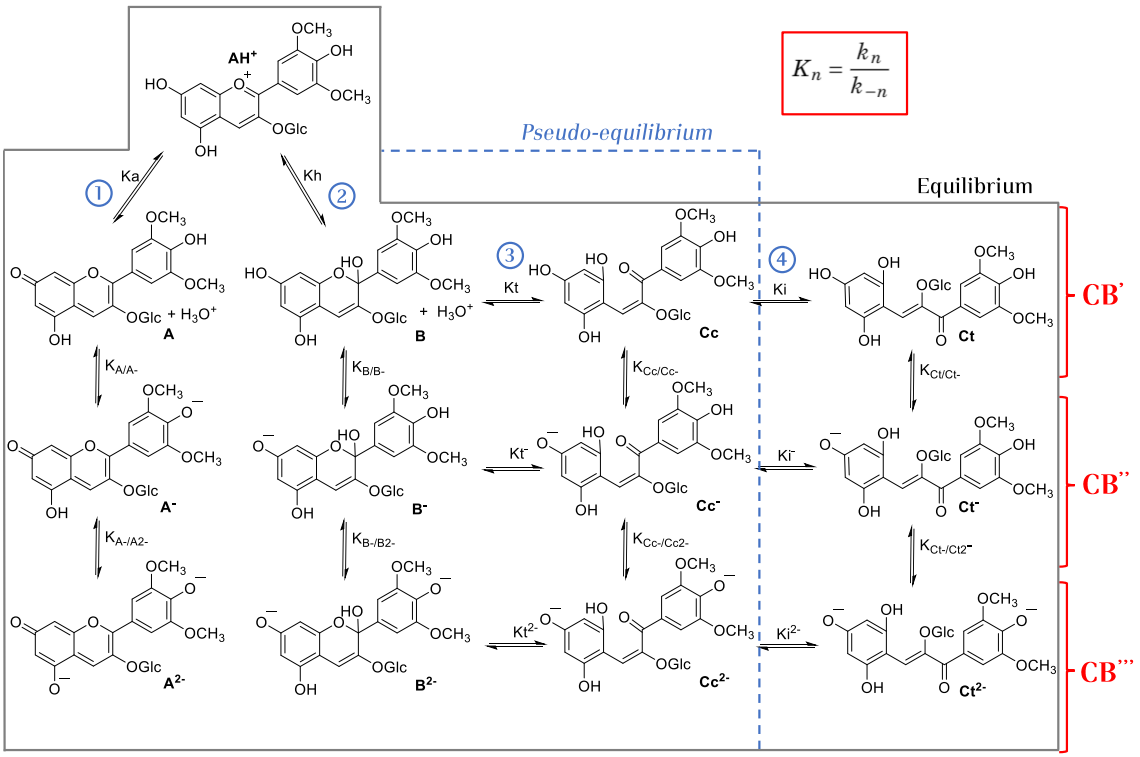

Scheme 1.2: The Oenin flavylium multi-state by means of pH changes. The deprotonated species are highly unstable for this anthocyanin.

understanding of the behavior of complex flavylium multi-state in different situations.

1.4 The flavylium multi-state

Flavylium derivatives have the peculiarity of change their color when they are dissolved in water at different pH values. They are involved in a reversibly interconnected series of chemical reactions producing five different species and their deprotonated forms, described in detail below. Scheme 1.2 shows the possible species formed in the anthocyanin Oenin through pH changes and serves as an example for the other flavylium-based systems. Five different species and their deprotonated forms interconnected by four chemical reactions can be observed defining the *flavylium multi-state*.[58] It is important to note that the commonly colored species are the flavylium cation **AH⁺**, the quinoidal base **A** and their deprotonated forms, the last ones red-shifted compared with the former.[22] The **AH⁺** is the only stable species at very acidic solutions (generally pH<1), but when the pH is higher than 1, the production of the other species in the multi-state is triggered.

1.4.1 A brief history of flavylium-based compounds research

To understand the peculiar behavior of the flavylium multi-state was necessary the investment of decades of work and research by many scientists, including the Nobel Prize winners

Richard Willstätter (1915) and Robert Robinson (1947).[58]

It was Büllow[59] who, in 1901, published the first synthetic flavylium compound settling the basis of the study of this family. However, the interest in the change of color in these compounds was early expressed; in 1664, Robert Boyle placed his curiosity on the color changes in flower extracts treated with acids or alkalis.[60, 61]

Ludwing Clamor Marquart coined the term *Anthocyanin* in 1835, coming from the Greek *Anthos* that means flower and *kyanos*, meaning blue.[22] In 1913, Willstätter started the journey studying natural anthocyanins, with initial studies focused on understanding their role in flower coloration.[62] Later he studied these compounds in water solutions at different pH values, clarifying the color change.[63] Willstätter introduced the therm *anthocyanidin* to describe those anthocyanins without a sugar attached.[22] In 1924 Willstätter and his students published the first synthesized anthocyanidins, the pelargonidin, and the cyanidin.[64] Willstätter studied the variation of the anthocyanin colors at different pH values and their conformational arrangement and interaction with other plant constituents (other phenolic compounds, metal ions, hydrocolloids, etc.) forming supramolecular complexes.[65]

In 1925, Robinson[66] synthesized the anthocyanidins by condensing an aromatic O-hydroxyaldehyde and an acetophenone, including a final demethylation step, this mechanism is still used for the synthesis of flavylium salts with a series of modifications. The product demonstrated the same properties as the compound obtained from natural sources.[9] Later in 1927, the inclusion of an attached sugar residue leads Robinson to synthesize the firsts anthocyanin-like compounds. Robinson also made contributions to the understanding of the co-pigmentation process.[67]

In the 60's decade, when the works published by Sondheimer[68] opened the doors for a more systematic study for the anthocyanins, Sondheimer calculated the pelargonidin 3-monoglucoside acidity constant. Timberlake and Bridle firstly observed the effect of the light on the flavylium system an noticed that the true equilibrium is only achieved in total darkness, because light affects isomerization of chalcones, [69] however, they worked with natural anthocyanins where the *trans*-chalcone (**Ct**) molar fraction is low. Later this effect was clarified with synthetic flavylium compounds (7,4'-dihydroxyflavylium and 5,7,4'-trimethoxyflavylium) by Jurd, who explained the photoisomerization of **Ct** to the *cis*-chalcone (**Cc**) followed by the formation of $\mathbf{AH^+}$ through the hemiketal (**B**).[70] In the 80's, McClelland and his colleagues clarify the behavior of the flavylium-based compounds in aqueous solutions at different pH values.[71, 72] Brouillard, Dubois, and Delaporte elucidated the equilibria among the anthocyanin structures (explained below in detail) in 1977. An important discovering was the fact that the quinoidal base does not hydrate in moderately acidic medium.[73, 74] Later, Brouillard and co-workers studied the isomerization

process in anthocyanins chalcones.[75] The complete flavylium multi-state system elucidation was carried out by Santos and co-workers using one- and two-dimensional NMR spectroscopy.[76]

1.4.2 The flavylium multi-state chemical reactions

Any alteration to higher pH values in a solution sufficiently acid to ensure the presence of the **AH$^+$** as the single species makes that two different reactions take place (Scheme 1.2). (1) deprotonation of the most acidic H^+ in the hydroxyl groups to produce the colored quinoidal base **A** and (2) water attack on the C2 or C4 to give the colorless hemiketal **B** (carbinol pseudo-base) through a hydration reaction, the 4-hydroxy adduct is thermodynamically less favored, so C2 hydration mainly takes place. Kinetically, the proton transfer that converts **AH$^+$** into **A** is the fastest reaction, occurring on the sub-microseconds timescale,[77] while the water attack over the **AH$^+$** is a slower process, within times between minutes and seconds. The hydration rate is a strictly pH-dependent reaction, increasing at higher H^+ concentrations. Only the flavylium cation is hydrated by the water in moderately acidic pH values and not the quinoidal base.[74] Consequently, the higher the pH, the fewer **AH$^+$** available to hydrate and the slower the hydration rate, however at high $^-$OH concentrations, the **A** can react with the hydroxyl and hydrate and then the hydration rate can be proportional to the hydroxide concentration.

The **B** form can eventually suffer a ring-opening leading to the *cis*-chalcone **Cc** formation mean a tautomerization process, step (3) in Scheme 1.2. This process is commonly faster than hydration (except at very acidic conditions) and occurs in the sub-seconds scale. Finally, in the last step (4), an isomerization reaction conducts to the *trans*-chalcone **Ct** formation form **Cc**, a process that can take a few seconds, minutes, hours, or even days.[22, 23]

The set of reactions reported in Scheme 1.2 can be written as:

Proton transfer

$$AH^+ + H_2O \overset{K_a}{\rightleftharpoons} A + H_3O^+ \tag{1.1}$$

Hydration

$$AH^+ + 2H_2O \overset{K_h}{\rightleftharpoons} B + H_3O^+ \tag{1.2}$$

Tautomerization

$$B \overset{K_t}{\rightleftharpoons} Cc \tag{1.3}$$

Isomerization

$$Cc \overset{K_i}{\rightleftharpoons} Ct \tag{1.4}$$

The flavylium multi-state can be simplified if it is considered as a single *acid-base* reaction,

involving just the **AH⁺** and its conjugate base **CB**, which is the sum of the other species[74, 75], thus:

$$AH^+ + 2H_2O \rightleftharpoons CB + H_3O^+ \tag{1.5}$$

with [**CB**] = [**A**] + [**B**] + [**Cc**] + [**Ct**]
The equilibrium constant K'_a for Eq.1.5 is defined then as:

$$K'_a = K_a + K_h + K_h K_t + K_h K_t K_i \tag{1.6}$$

For flavylium-based compounds in which isomerization is the slowest process, a *pseudo-equilibrium* can be set, this equilibrium is between the **AH⁺**, **B** and **Cc**. With a small modification of equations 1.5 and 1.6 can be represented as:

$$AH^+ + 2H_2O \rightleftharpoons \tilde{CB} + H_3O^+ \tag{1.7}$$

with [$\tilde{\textbf{CB}}$] = [**A**] + [**B**] + [**Cc**]
And the equilibrium constant $\tilde{K_a}$ for Eq.1.7 is defined then as:

$$\tilde{K_a} = K_a + K_h + K_h K_t \tag{1.8}$$

As all the reactions exposed in Scheme 1.2 are reversible, acidification of the media reverts the equilibria to the **AH⁺** form or the most stable species at the final pH value. At higher pH values, all the species suffer a second or even a third deprotonation (see eq.1.9 and 1.10), leading to the formation of other species with different colors, generally absorbing at higher wavelengths than their protonated forms.

$$CB + H_2O \rightleftharpoons CB^- + H_3O^+ \tag{1.9}$$

$$CB^- + H_2O \rightleftharpoons CB^{-2} + H_3O^+ \tag{1.10}$$

with [$\textbf{CB}^{\textbf{-}}$] = [$\textbf{A}^{\textbf{-}}$] + [$\textbf{B}^{\textbf{-}}$] + [$\textbf{Cc}^{\textbf{-}}$] + [$\textbf{Ct}^{\textbf{-}}$] and [$\textbf{CB}^{\textbf{-2}}$] = [$\textbf{A}^{\textbf{-2}}$] + [$\textbf{B}^{\textbf{-2}}$] + [$\textbf{Cc}^{\textbf{-2}}$] + [$\textbf{Ct}^{\textbf{-2}}$]
And the equilibrium constant K''_a for Eq.1.9 and K'''_a for Eq.1.10 defined then as:

$$K''_a = \frac{K_{A/A^-}K_a + K_{B/B^-}K_h + K_{Cc/Cc^-}K_h K_t + K_{Ct/Ct^-}K_h K_t K_i}{K'_a} \tag{1.11}$$

$$K'''_a = \frac{K_{A^-/A^{-2}}K_{A/A^-}K_a + K_{B^-/B^{-2}}K_{B/B^-}K_h + K_{Cc^-/Cc^{-2}}K_{Cc/Cc^-}K_h K_t + K_{Ct^-/Ct^{-2}}K_{Ct/Ct^-}K_h K_t K_i}{K'_a K''_a} \tag{1.12}$$

with K_{X/X^-} and $K_{X^-/X^{-2}}$ representing the first and second deprotonation reactions for each species, see more details about the mathematical deduction of these expressions in Appendix A.

The *equilibrium* (K) and *kinetic* (k) constants control the amount of the flavylium multi-state species at the equilibrium and pseudo-equilibrium and their rate of formation respectively. Both constants depend on the flavylium chemical nature, intermolecular and intramolecular interactions, solvent mixtures, environment conditions, etc. Typically, in anthocyanins, the species **B**, **Cc**, and **Ct** are more stable than **A**, and once it is formed as a kinetic product is totally or partially converted into the other species after the equilibrium.[22]

1.4.3 Photochemistry in the flavylium multi-state system

Some flavylium multi-state species are sensitive to photochemical transformations when exposed to a continuous or pulsed light stimulus. In general, anthocyanins are poorly fluorescent compounds, with typical fluorescent quantum yields lower than 4×10^{-3}.[78] The interesting effect is that the flavylium cation is a strong acid when it is in the excited state, even at very acidic pH values, this transfer the proton to the solvent in a picoseconds scale, later its quinoidal base in the excited state is deactivated thermically (non-radiative processes) and by fluorescence (radiative process), being **A** responsible for the emission spectra[79].

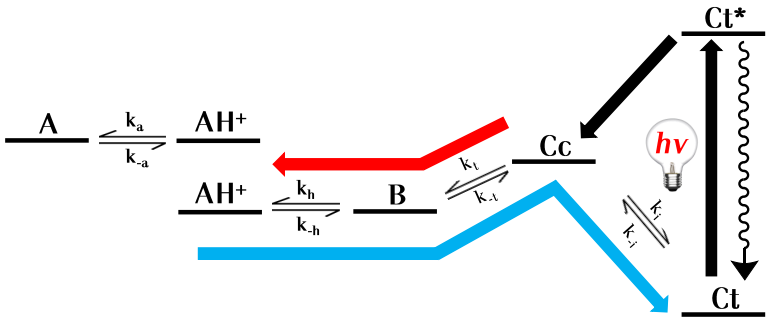

Figure 1.3: General representation for the photochemical process in flavylium-based compounds. Photochromism is only observable if the *cis-trans* isomerization barrier is high.

Furthermore, the *photochromism* phenomenon occurs in many flavylium derivative multi-states, including some deoxyanthocyanins. The *cis* and *trans* chalcones in the flavylium multi-state system have a particular feature; they can be photo-isomerized in mildly acidic media exhibiting photochromism. The general *cis-trans* photochromism is presented in Figure 1.3, once the *cis*-chalcone has been formed through the photoisomerization process (black arrows), as it is not thermodynamically stable, it can take two different routes: a) going thermally backwards to the recovery of **Ct** (perceptible only in compounds with low *cis-trans* isomerization barrier) and/or b) forward to the formation of the other species in the pseudo-equilibrium (red arrow); **B**, and **A** or $\mathbf{AH^+}$ depending of the pH of the solution and the K_a. Eventually, the solution will achieve the equilibrium thermically to the most stable species (blue arrow). As will be discussed in section 1.4.4, the rate constants are dependent

on the pH; thus, the photochromism in flavylium-based compounds can be controlled by the H^+ concentrations in the solution.

1.4.4 Study of the flavylium multi-state system

To understand the behavior of a specific flavylium-based compound, when it is dissolved in water, there is a convenient way to study the kinetic and thermodynamic constants, controlling the flavylium multi-state species, this method is the performance of pH jumps. A *direct pH jump* is defined as the addition of base to an equilibrated aqueous solution increasing its pH value. Generally, in the flavylium multi-state, it starts at pH=1 or any pH where the **AH$^+$** be the only species. In the same way, a *reverse pH jump* can be performed; this is the addition of acid to equilibrated solutions decreasing their pH value. Usually the final pH is 1 or any pH where the **AH$^+$** be the most stable species.[32] After the pH jump, the system starts to evolve toward the formation of other species, following Le Chatelier's principle, where the kinetics can be tracked by common UV-Vis and stopped-flow spectrophotometry and/or by NMR spectroscopy depending on the kinetics lifetime.

As seen previously, the kinetics after a direct pH jump, follow a reversible first-order set of reactions, and is possible to deduce their complete mathematical resolution.[80, 81] The first step is the proton transfer, and due to the fast conversion between **AH$^+$** and **A**, they are commonly considered as a single species **AH$^+$/A** when the kinetics are followed, the same thing when any other anionic species and its protonated form are involved. For this reason, all the proton transfer reactions can not be followed during a pH jump not even by stopped-flow spectrophotometry, to follow this kind of fast reactions is necessary to use special techniques, such as temperature jumps or nanosecond flash photolysis.[74, 77] The first kinetic step is expressed as shown in Eq.1.13.

$$k_1 = k_a + k_{-a}[H^+] \tag{1.13}$$

In compounds with high *cis-trans* isomerization barrier as the anthocyanins (Figure 1.4), the UV-vis spectra can be recorded immediately after a direct pH jump as shown in Figure 1.5a. The kinetics, commonly represented at a wavelength with higher variation in the spectra along the time until the equilibrium, can be adjusted by a bi-exponential curve, see insets in Figure 1.5a.

The first exponential represents the hydration followed immediately by the tautomerization which is faster, so the rate-determining step is the hydration (at very acidic pH values the hydration becomes faster than the tautomerization, *change of regime*).[58] At the end of this step, the species **AH$^+$**, **A**, **B**, and **Cc** can be present, and the pseudo-equilibrium can be defined since the isomerization is the slowest process in the anthocyanins. The hydration

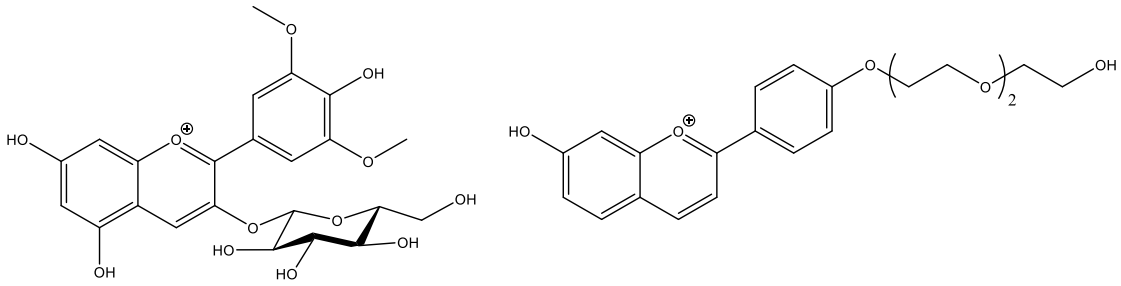

Figure 1.4: Structure of **a)** Oenin and **b)** 7-hydroxy-4'triethylenglycol flavylium (7OH4'TEG) as examples of flavylium-based compounds with and without high *cis-trans* isomerization barrier.

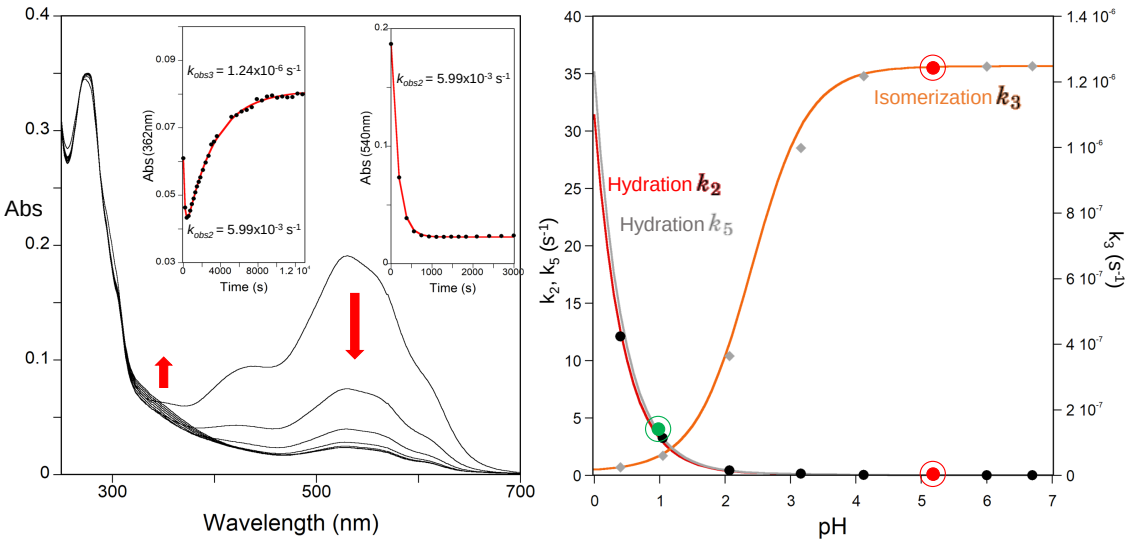

Figure 1.5: Representation of a typical direct pH jump, data obtained for Oenin. **a)** Kinetics followed after a pH jump from pH 1 to 5.2 by common spectrophotometry adjusted by a bi-exponential curve (insets), **b)** pH dependence of k_2 Eq.1.14, k_3 Eq.1.15 and k_5 Eq.1.17 using $K_a = 1.58 \times 10^{-4}$, $k_h = 0.12 s^{-1}$, $K_t = 3.4 \times 10^{-3}$, $k_{-h} = 35 M^{-1} s^{-1}$, $k_i = 1.2 \times 10^{-5} s^{-1}$ and $k_{-i} = 1.3 \times 10^{-8} s^{-1}$. [82]

can be represented by Eq.1.14.

$$k_2 = \chi_{AH^+} k_h + \chi_B k_{-h}[H^+] = \frac{[H^+]}{[H^+]+K_a} k_h + \frac{1}{1+K_t} k_{-h}[H^+] \tag{1.14}$$

Where the molar fraction of **AH$^+$**, χ_{AH^+} (obtained from the equilibrium with **A**), is multiplied by the direct hydration constant, k_h, and the molar fraction of **B**, χ_B (obtained from the equilibrium of **B** with **Cc**), by the reverse rate constant k_{-h}.

The isomerization is represented by a second exponential in Eq.1.15, where the mole fraction of **Cc**, X_{Cc} is multiplied by the direct rate constant k_i, the reverse constant k_{-i} is just added.

$$k_3 = \chi_{Cc} k_i + k_{-i} = \frac{K_h K_t}{[H^+]+K_a+(1+K_t)K_h} k_i + k_{-i} \tag{1.15}$$

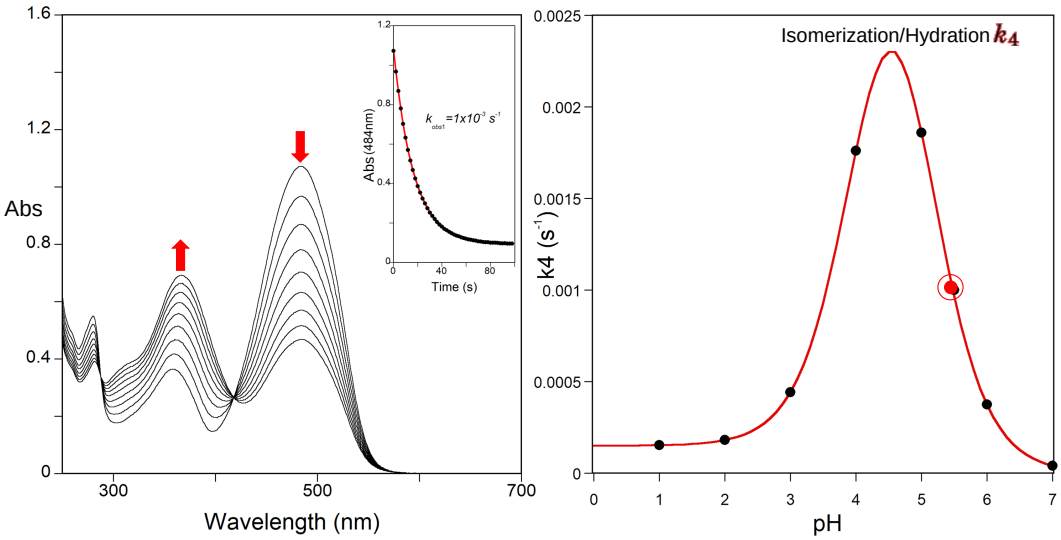

Figure 1.6: Representation of a typical direct pH jump, data obtained for 7OH4'TEG. **a)** Kinetics followed after a pH jump from pH 1 to 5.5 by common spectrophotometry adjusted by a mono-exponential curve, **b)** pH dependence of k_4 Eq.1.16, using $K_a = 6.3 \times 10^{-5}$, $K_h K_t k_i = 3.6 \times 10^{-7} M s^{-1}$, $K_t k_i / k_{-h} = 2 \times 10^{-5} M$ and $k_{-i} = 2.7 \times 10^{-4} s^{-1}$. Reproduced from the work of Basílio et. al.[58]

Other flavylium-based compounds without a high *cis-trans* isomerization barrier (Figure 1.4) can be also followed by UV-Vis spectroscopy after the pH jumps (Figure 1.6a), but in this case, the kinetics are described by a unique exponential curve. Thus, the hydration is slower than the tautomerization, but also than the isomerization, being the rate-determining step. This unique observed step, after the proton transfer reaction, leads to the equilibrium and

the pseudo-equilibrium is not observed, the Eq.1.16 is representative of this event.

$$k_4 = \frac{\frac{[H^+]}{[H^+]+K_a} K_h K_t k_i + k_{-i}[H^+]}{[H^+] + \frac{K_t k_i}{k_{-h}}} \tag{1.16}$$

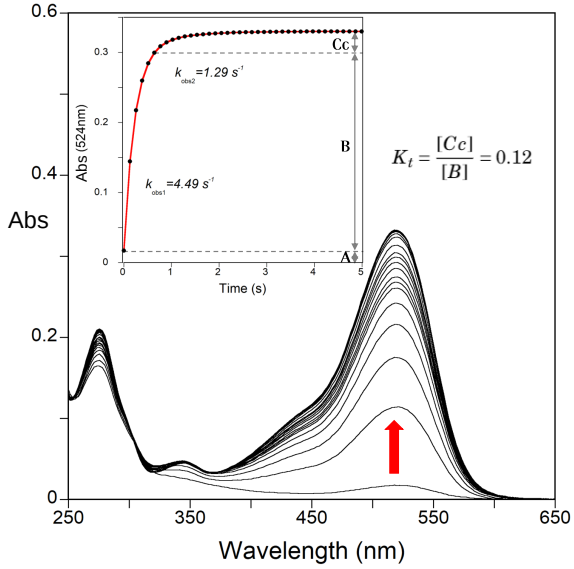

Figure 1.7: A typical reverse pH jump kinetics (from pH 5.2 to 0.93) of a equilibrated Oenin solution followed by stopped flow spectrophotometry. The molar fraction of **A**, **B** and **Cc** have been calculated from the pre-exponential factors in the fitted curve.

Sometimes, the reverse pH jumps can help to calculate the thermodynamic and kinetics constants in compounds with high *cis-trans* isomerization barrier.[82] When an equilibrated solution goes back to a pH where the **AH$^+$** is thermodynamically stable, the kinetics can be followed by stopped flow spectrophotometry (Figure 1.7). The curve followed in the flavylium maximum wavelength absorption can be adjusted by a mono, bi or tri-exponential curve, depending of the species present in the equilibrium/pseudo-equilibrium. The first absorption registered is due the **A** that is transformed into **AH$^+$** during the mixing time of the stopped flow. The fist exponential in the curve (hydration rate) corresponds to the conversion of **B** into **AH$^+$** (k_5 in Eq.1.17), the next step is controlled by the tautomerization rate (k_6 in Eq.1.18) by conversion of **Cc** into more flavylium through **B**, and finally, the last step typically observed by normal spectrophotometry is the conversion of **Ct** into **AH$^+$** through **B** and **Cc** (not shown in Figure 1.7 because anthocyanins have a small amount of **Ct** in the equilibrium).This is possible due the change of regime. The equilibrium constant K_t can be also calculated indirectly from the ratio of the pre-exponential factors $K_t = [Cc]/[B]$.

$$k_5 = \frac{[H^+]}{[H^+]+K_a} k_h + k_{-h}[H^+] \tag{1.17}$$

$$k_6 = k_{-t} + k_{-t}^{H}[H^+] + k_{-t}^{OH}[OH^-] \tag{1.18}$$

For illustrative purposes, an example of the kinetic process after a direct pH jump of the anthocyanin Oenin and the synthetic 7-hydroxy-4'-triethylenglycol flavylium (7OH4'TEG in Figure 1.4) is represented in Figures 1.5 and 1.6 respectively. In Figure 1.5b the representation of the pH-dependent Eqs. 1.14, 1.15 and 1.17 is observed. In contrast, in Figure 1.6b, only the representation of the Equation 1.16 for compounds without a *cis-trans* isomerization barrier is shown, the black points represent the experimentally observed constants result of the exponential fittings, the big colored points are the representation of the direct (red) and reverse (green) pH jumps in Figures 1.5a, 1.4a, and 1.7

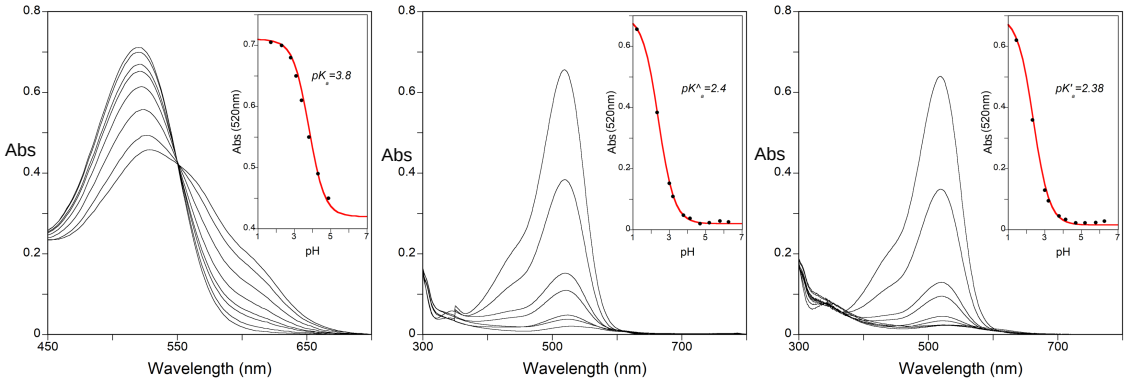

Figure 1.8: Absorption spectra of Oenin after a direct pH jump to different pH values: a) taken immediately after the jump, $pK_a = 3.8$, b) the same in the pseudo-equilibrium, $pK\hat{}_a = 2.4$ and c) in the equilibrium, $pK'_a = 2.38$.

The acid-base constant K_a can be calculated by collecting immediately the absorption spectra after a pH jump to different pH values, before $\mathbf{AH^+}$ or **A** hydrate. Furthermore, the $K\hat{}_a$ and K'_a are calculated, collecting the absorption spectra when the system has reached the pseudo-equilibrium, and the equilibrium, respectively, Figure 1.8 shows an example in the calculation of the three constants for the Oenin. Unlike other flavylium-based compounds, common anthocyanins have less than a 5% of **Ct** in the equilibrium, making it difficult to distinguish from the spectra in the pseudo-equilibrium.[32]

Once the flavylium multi-state thermodynamic constants had been calculated, the system can be represented employing the pH-dependent molar fraction of each species.[83] The set of equations compiled in Eq. 1.19 can be applied to calculate the molar fractions; after the proton transfer (the immediate spectra registered after the direct pH jump; EC=K_a), in the pseudo-equilibrium (for those compounds without high *cis-trans* isomerization barrier (EC=$K\hat{}_a$) and in the equilibrium (EC=K'_a). Figure 1.9 shows the molar fraction distribution in a pH range between and 7 for the Oenin.

$$\chi_{AH^+} = \frac{[H^+]}{[H^+]+EC}; \chi_A = \frac{K_a}{[H^+]+EC}; \chi_B = \frac{K_h}{[H^+]+EC}; \chi_{Cc} = \frac{K_h K_t}{[H^+]+EC}; \chi_{Ct} = \frac{K_h K_t K_i}{[H^+]+K_a'} \tag{1.19}$$

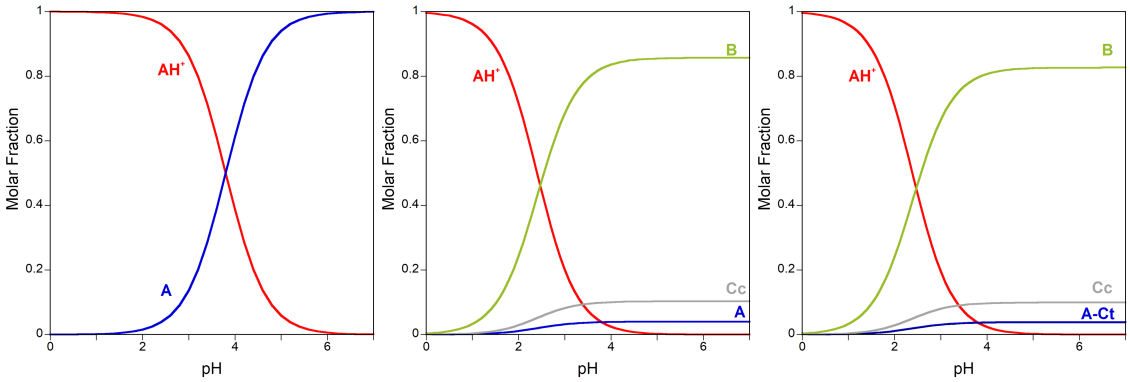

Figure 1.9: Molar fraction distribution of the five species in the flavylium multi-state for Oenin **a)** immediately after the pH jump **b)** at the pseudo-equilibrium and **c)** at the equilibrium.

The use of an energy level diagram as the one shown in Scheme 1.3 is also a valuable tool to study the flavylium multi-state. Here the relative free Gibbs energies of all the species are represented using the **AH⁺** as reference. The free Gibbs energy can be easily calculated from the expression $\Delta G^0 = -RT\ln K_{eq}$, where ΔG^0 is the Gibbs free energy, R is the ideal gas constant (8.314J mol^{-1}K^{-1}), T is the temperature expressed in Kelvin scale, and K_{eq} is the equilibrium constant.[58, 83, 84]. When the pH increase, the energy of **AH⁺** also increase, this means a destabilization and formation of other species in the equilibrium.

According to Scheme 1.3, the Oenin **AH⁺** is the most stable species at pHs lower than 2.47 (pK_h). After a direct pH jump to pH=pKa, half of **AH⁺** and **A** are formed, however **B** is more stable at this pH and the system goes forward to form **B** and **Cc**; **Ct** is only stable at pH above 3.8. In most common anthocyanins the most stable species at the equilibrium is the hemiketal, and the *cis* and *trans* chalcones are less stable, being the last almost imperceptible. In 3-substituted flavylium compounds **AH⁺** and **Ct** usually are in equilibrium as the unique species. On the other hand the equilibrium between the flavylium cation and **B** is common in C4 and C5-substituted compounds.[22]

The photochemistry of the flavylium-based compounds is interesting, as was pointed out in section 1.4.3. The quantum yields of the photoisomerization reaction (Φ) can be calculated registering an absorption spectra of solutions, after being irradiated with light along a certain time, Eq.1.20.

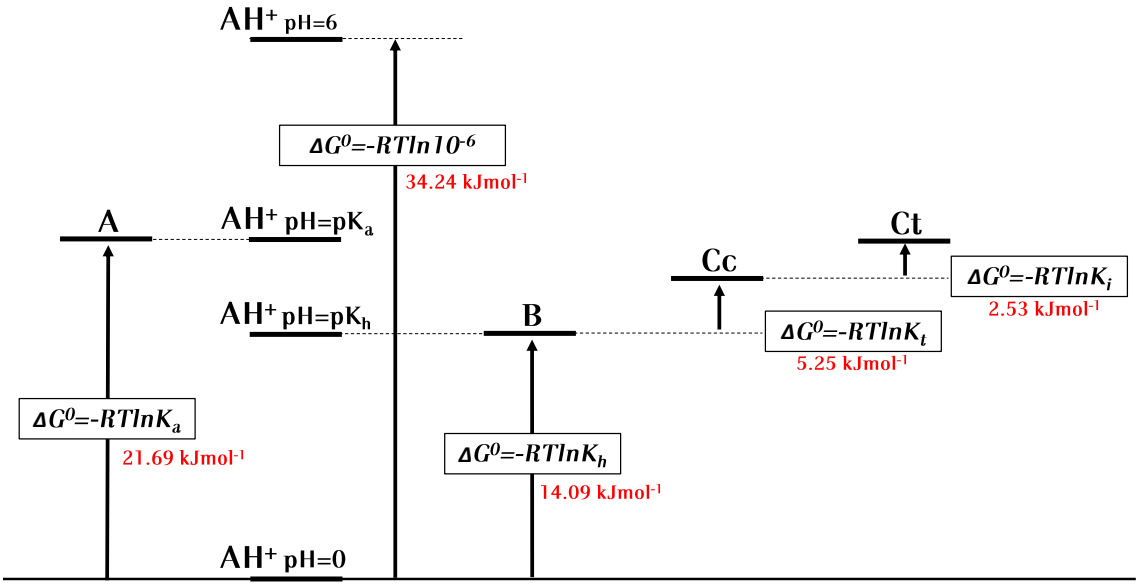

Scheme 1.3: Free Gibbs energy level diagram of the multi-state of Oenin.

$$\Phi = \frac{V_{sol}\frac{\Delta A_{\lambda obs}}{b\Delta\epsilon_{\lambda obs}}}{\Delta t I_0(1-10^{-A_{\lambda irr}})} \tag{1.20}$$

where V_{sol} is the volume of the solution expressed in L, b is the optical path, λ_{obs} and λ_{irr} are the observation and irradiation wavelengths respectively, Δt is the time and I_0 is the intensity of the incident light (measured by actinometry).[85] Note that this equation assumes that the photoproduct does not absorb light in the irradiation wavelength and the reactant does not absorb in the measured wavelength.

Figure 1.10 shows an example for the variation of the UV-Vis spectra of an equilibrated solution 1.5×10^{-5}M of the compound 7-hydroxy-4'triethylenglycol flavylium in water at pH=3.1 upon irradiation at 375 nm. As can be observed the representative absorption band of **Ct** at 370 nm disappears, while the **AH⁺** absorption band (453 nm) appears along the time of exposure to the light stimulus, the calculated quantum yield is $\Phi = 0.05$.

The quantum yield of formation of **AH⁺** is pH-dependent; in slightly acidic solutions, where the hydration is the rate-determining step, **B** and **Cc** can be considered as a unique species, **B:Cc** reacts to form **AH⁺** by one side (Eq.1.21) and back to **Ct** by the other (Eq.1.22), the contribution of k_{-i} is very small as well as $k_h[H^+]/([H^+]+K_a)$ due the fact that the hydration is the rate-determining step, therefore both can be neglected.[17] For those compounds with high *cis-trans* isomerization barrier the contribution of the backward process can be also neglected.

$$k_{fw} = \frac{k_{-h}[H^+]}{1+K_t} \tag{1.21}$$

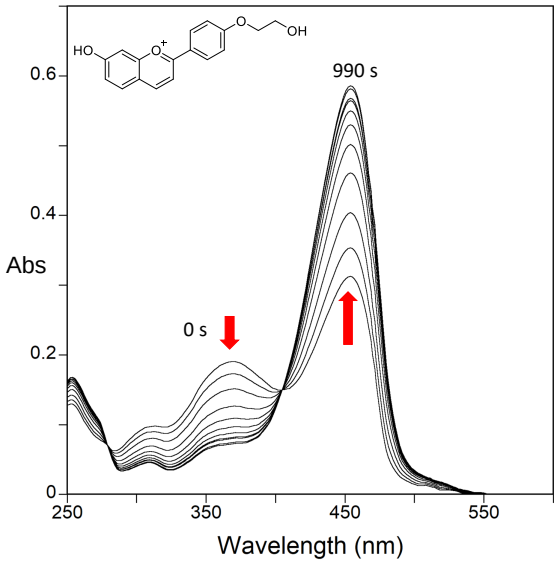

Figure 1.10: Spectral variations of the compound 7-hydroxy-4'triethylenglycol flavylium, 1.5×10^{-5} M in water at pH=3.1, irradiation at 375 nm, $\Phi = 0.05$. Reproduced from the work of Gago et.al.[86]

$$k_{bw} = \frac{K_t}{1+K_t} k_i \tag{1.22}$$

Then, the pH-dependent quantum yield of reaction can be expressed as:

$$\Phi = \Phi_0 \frac{k_{fw}}{k_{fw} + k_{bw}} = \Phi_0 \frac{[H^+]}{[H^+] + \frac{K_t k_i}{k_{-h}}} \tag{1.23}$$

where Φ_0 represents the quantum yield of photoisomerization of **Ct** to **Cc** and further conversion into $\mathbf{AH^+}$ at pH=1.

By the other hand, when the tautomerization is the rate-determining step in acid pH (change of regime), the quantum yield is represented by:

$$\Phi = \Phi_0 \frac{k_{-t} + k^H[H^+] + k^{OH}[OH^-]}{k_{-t} + k^H[H^+] + k^{OH}[OH^-] + k_i} \tag{1.24}$$

Pina and Maestri[87] introduced the flash photolysis as a powerful technique to obtain information about the photochemical process when a flashlight hits on an equilibrated solution with enough **Ct**. The maximum wavelength of the flavylium or the chalcones can be tracked by common spectroscopy, and the events shown in Figure 1.11 take place. For practical purposes only one wavelength is followed at the time, and its absorbance is set to zero before the flash. An immediate bleaching can be observed in the tracking of the chalcone wavelength after the light pulse, this because the **Ct** is photoisomerized into **Cc** which absorption coefficient is lower.[17, 88] An increasing mono-exponential process can also be observed immediately due to the formation of more **Cc** (in those compounds with

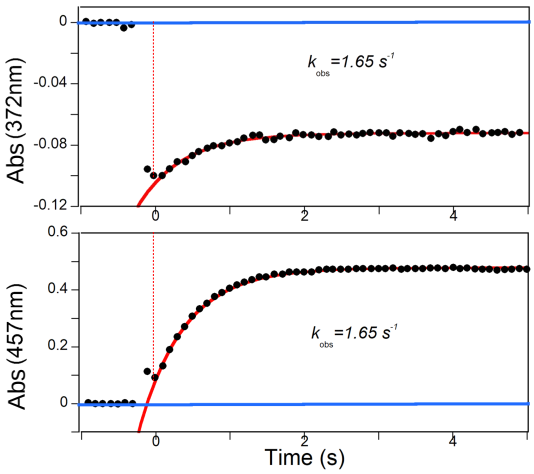

Figure 1.11: Typical representation of a flash photolysis traces after a light flash over an equilibrated solution with enough **Ct**. Kinetic followed in the maximum wavelength of the *trans*-chalcone (up) and the flavylium cation (down).

a low *cis-trans* isomerization barrier the thermal recovery of **Ct** can be observed). At the bottom of Figure 1.11 the wavelength of the formation of $\mathbf{AH^+}$ is shown, these processes are pH-dependent and follow first-order kinetics. The rate constants can be calculated by means of the exponential changes in both the chalcones and the flavylium maximum absorption wavelength. In the pH interval where the rate-determining step is the hydration, the Eq.1.14 can be applied to fit the rate constants obtained from the flash photolysis experiments. At lower pH, once we overpass the isomerization mean the use of light, the hydration is faster than the tautomerization (change of regime), being the last the rate-determining step and Eq.1.25 must be used to describe the phenomena.

$$k_7 = k_{-t} + k^H[H^+] + k^{OH}[OH^-] \tag{1.25}$$

In compounds without *cis-trans* isomerization barrier, the photochemical studies represent an indispensable tool to accurate calculation of all the equilibrium and rate constants.

1.5 Stabilization of the flavylium multi-state species by natural co-pigmentation effect

As mentioned before, it is well-known that the stability of **A** in simple anthocyanins is low, and its formation is transient in many cases, leading to the formation of the uncolored species of the multi-state. However, the presence of the colored forms is commonly extended to higher pH values in plant tissues; this is an indication of a series of protection mechanisms employed by Nature over **A** and $\mathbf{AH^+}$ species. Being the former responsible for many

blue shades and the flavylium cation of red hues in plants.

The stability and diversity of the colors that we see in Nature, such as in flowers or fruits, depends on several factors when to anthocyanins concern. In addition to the number, type, and position of the substituents in the flavylium backbone and other intramolecular interactions, the anthocyanins colored forms are stabilized through complex mechanisms in biological systems related to intermolecular interactions. By this way Nature couple the chromophores in anthocyanins with other molecules stabilizing them. In this manner, the control of their transformation in other species is mediated by the intermolecular interactions in the vacuolar environment inside plant cells. Since the concept of supramolecular chemistry was introduced by Lenh in 1995[89] these complex natural mechanisms have been studied in a systematic way.

The interaction of anthocyanins with colorless molecules to produce a color intensification and different shades of color is known as *co-pigmentation*. The interaction molecule known as *co-pigment* can be a metal, ion or another organic compound, such flavonoids, polysaccharides, amino acids, organic acids or another anthocyanin.[90] In general, an organic molecule shall comply with the following characteristics to be considered a co-pigment; must be a π-conjugated system able to favor the π-π stacking interactions (see below), or be a hydrogen bond developer. For this reason, some investigations have centered their focus on the study and stabilization of the anthocyanins' colored species by this method.[27, 91, 92, 93, 94, 95]

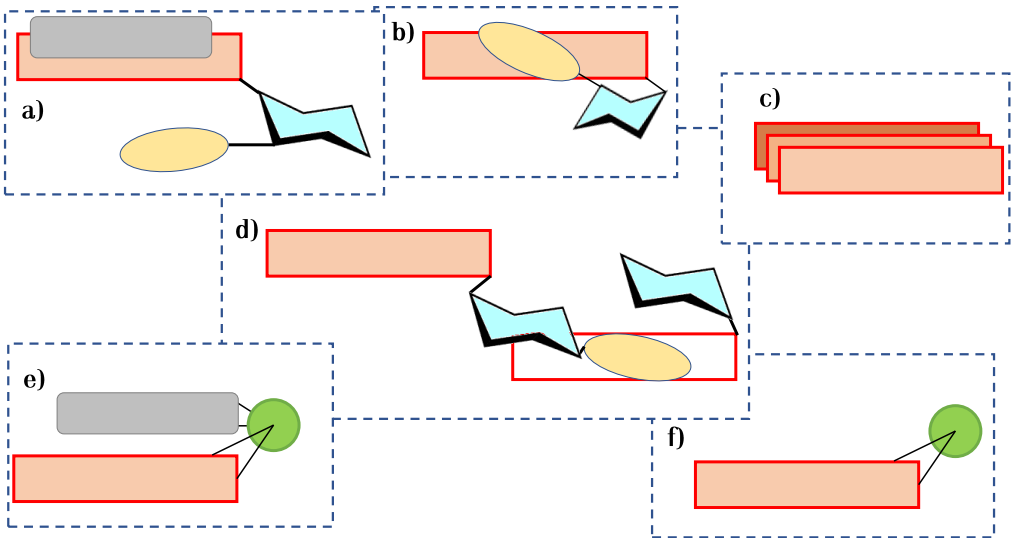

Figure 1.12: Co-pigmentation effect by interactions between an anthocyanin and **a)** a colorless organic pigment, **b)** its acylated moiety (intramolecular interaction), **c)** another anthocyanin (self-association), **d)** the acyl moiety of another molecule, **e)** a colorless organic pigment and a metal and **f)** a metal.

Co-pigmentation can be classified according to the kind of co-pigment with which the chromophore interacts (Figure 1.12); if there is another molecule forming a π-π stacking with the anthocyanin, an intermolecular co-pigmentation takes place (Figure 1.12a and d), if the co-pigment is part of the structure or another anthocyanin, an intramolecular co-pigmentation or self-association is formed (Figure 1.12b and c), the co-pigment can also be a metal, forming a simple metal-anthocyanin interaction or a triad with the anthocyanin and another organic molecule (Figure 1.12f and e).

The intermolecular interactions between the flavylium multi-state species with other organic co-pigments, of the same or other species, have been attributed to hydrophobic effect, mostly driven by dispersion interactions that lead to the displacement of water out of the solvation shells.[24, 96, 97] Typically, the co-pigmentation involves charge-transfer complex formation and/or π-stacking interactions between the planar polarizable nuclei of the colored forms of the flavylium multi-state and the co-pigment, this is because the co-pigments regularly are rich in π-electrons and associate with the poor deficient $\mathbf{AH^+}$.[21, 24] The π-stacking interactions can be exemplified by the binding of the anthocyanins with other phenol (Figure 1.12b) and the self-association (Figure 1.12c). This arrangement protects the chromophore from nucleophilic attacks, inhibiting the formation of the uncolored species or degradation products.[18]

Regularly, the co-pigments are uncolored compounds. Once they form the association with the flavylium-based pigments, a bathochromic shift is observed in the absorption spectra. Therefore changes in color intensity are just a reflection of differences in molar absorption coefficients in free and paired molecules.[24] The stabilization of the flavylium cation is also observed in the equilibrium; and then, the red color remains at pH values when the molar fractions of the complex are compared with the pigment by itself, this is traduced to a hyperchromic effect. The combination of both, hyperchromic and bathochromic effects makes co-pigmentation one of the most important natural mechanisms used by Nature to vary and stabilize colors.[21] The affinity of the co-pigment is measured by its thermodynamic binding constant, being higher for planar flavonoids and lower for hydroxybenzoic acids in anthocyanins.[24]

A different process of co-pigmentation occurs at intra-molecular level, in acylated anthocyanins; for example, the acyl units can serve as a co-pigment, while sugars act as bridges, allowing the molecule to fold. This co-pigmentation effect is produced when the π-orbitals of the aromatic acyl group interact with the flavylium backbone.[18, 93, 98] The possibility to form π-stacking interactions with other molecules is also increased with acylation.[24] The gentiodelphin (*Gentiana makinoi*), heavenly blue anthocyanin (HBA in *Iponema tricolor* cv. heavenly blue) and ternatin (*Cliteria ternatea*) for example, bear polyacylated branched chains, which adopt conformations where the acyl groups stack on both sides of the chromophore, protecting it from water attack.[35] These kinds of structures will be studied

deeply in Chapter 2.

1.5.1 Self-association

Self-association is common in anthocyanins because flavylium compounds tend to aggregate, hence the concentration of the flavylium-based compounds is an important feature to take into account when the equilibrium of the multi-state is studied. The self-association was first proposed by Asen[90] describing the stabilization of the colored species and was adopted as another way used by Nature to stabilize the colored species of the flavylium multi-state in slightly acidic to neutral media in flowers, for example, this is because self-association decreases the efficiency in hydration reaction, this means that the pK_h and pK'_a increase with the concentration.[82, 99]

Solutions with concentrations up to 1mM of some common anthocyanins have shown stabilization of $\mathbf{AH^+}$, but the effect over the UV-Vis absorption spectra causes a band broadening and a decrease on the maximum molar absorptivity. Besides this, the aggregates can stack in a left-handed or right-handed screw axis; as demonstrated for 3,5-diglucosides and 3-monoglucosides.[100] Solutions with anthocyanins aggregates exhibit negative Cotton effect signals in circular dichroism, and increasing concentrations leads to chemical shifts in ^{1}H NMR spectra.[100, 101] These methods represent a feasible way to identify the self-association effect. The association constants in self-association processes are higher in the interaction between neutral quinoidal bases because of the lack of the electrostatic repulsion between molecules, something that occurs in the flavylium cation and quinoidal base deprotonated forms.[24]

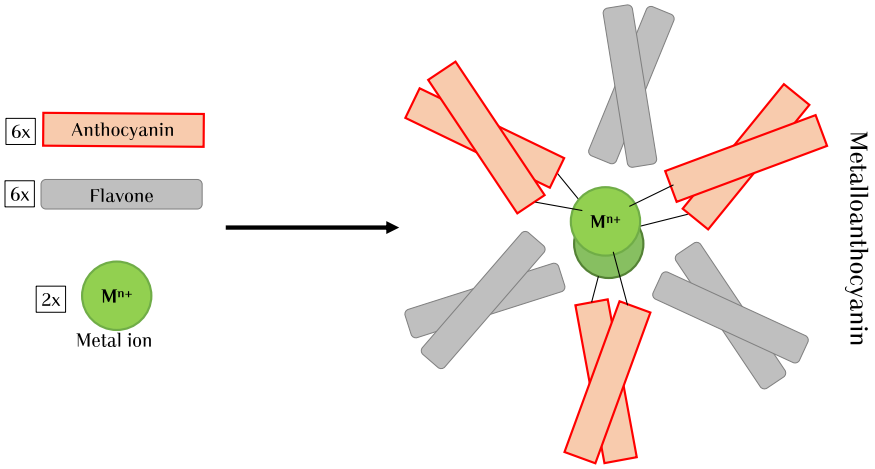

Figure 1.13: Representation of the three element (triad) interaction in the metalloanthocyanin found in *Commelina communis*. Adaptation of the structure obtained by Yoshida et. al.[91]

1.5.2 Metal complexation.

Another mechanism that influences the color of the anthocyanins is their complexation with metals. Metal chelation occurs mainly with flavylium-based compounds with a *ortho*-dihydroxy system (catechol or pyrogallol groups) as cyanidin, delphinidin and petunidin, which can form complexes with di or tri-valent metals M^{n+} (Cu^{+2}, Mg^{+2}, Fe^{+3}, Al^{+3}, Cr^{+3}, Ga^{+3}).[102] Flavylium with a single OH substituent or with one or two methoxyl groups, as malvidin, peonidin, and petunidin, can also form chelation but is less favorable.[103] This mechanism involves the complexation of the metal with the anionic quinoidal base form, this happens because the metal chelation is a competitive process for the hydration reaction, consequently, the **A** and its deprotonated forms are stabilized. Likewise other co-pigmentation effects, this complex causes a bathochromic shift, due to the additional proton loss of C3'-OH, turning absorption bands of some anthocyanins closer to the infrared zone.[19]

A high-level complex can also be formed between an anthocyanin, a co-pigment, and a metal. These triads enhance the co-pigmentation effect as demonstrated in some reported works about blue flowers color expression.[27, 94] In the beginning, the participation of metal ions in co-pigmentation was ignored, because of the founding of stable nonmetallic pigment-copigment assemblies in Nature, that express the blue hues as the polyacylated anthocyanins aforementioned, despite of this, Shibata and co-workers reported the metal complex theory for the blue color in 1919.[104] In 1992, the structure of commelinin was identified by X-ray crystallography, as responsible for the intense blue colors in *Commelina communis*.[93] The existence of a helical aggregate with malonylawobanin (the acylated pigment) and flavocommelin (the flavone glycosylated co-pigment) are stacked in a chiral left-handed arrangement as shown in Figure 1.13; this anthocyanin represents only an example of the supramolecular structures found in Nature where the color is stabilized. The use of anthocyanins-metal complexes in the food industry takes more participation during the last years, this interaction can serve as an alternative to stabilize blue colors using metals included in the essential minerals in the diet. Conversely, the works on natural supramolecular assembling have served as inspiration for anthocyanins-metal complexations in naturally dye-sensitized TiO_2-based solar cells or their use in textile industry.[103]

1.5.3 Ion-pair co-pigmentation

The stabilization of color by ions is one of the strategies used by Nature, high concentrations of salts have been tested to stabilize the flavylium cation along the pH scale in some experiments trying to mimic the environment in plant tissues. Co-pigmentation with anions as Cl^-, Br^- and ClO_4^- have been tested to stabilize the flavylium cation of Malvidin and the synthetic 4',7-dihydroxyflavylium, increasing considerably the pK'_a in more than 0.5 units in the scale of pH. [105]

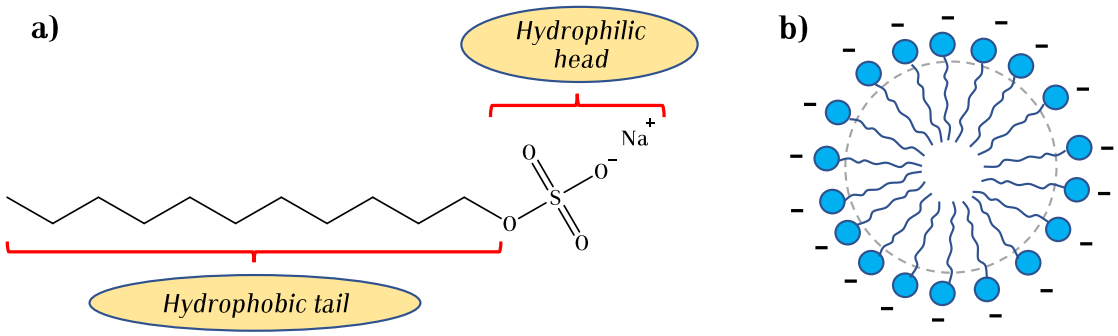

Figure 1.14: **a)** Sodium Dodecyl Sulfate (SDS) molecular structure and **b)** its association to form external anionic micelles.

1.6 Stabilization of the flavylium multi-state species by non-natural mechanisms

Other mechanisms for the stabilization of the flavylium multi-state species have been proposed and are mainly based on supramolecular interactions with compounds not found in the Nature, or at least not complexed with the anthocyanins, especially with the host-guest complexation with macrocycles as calix[*n*]arnes, cyclodextrins, crown ethers, molecular clips and curcubit[*n*]urils. These compounds can shield the chromophore from the contact with water and, therefore, protect it from its attack (hydration reactions).

1.6.1 Micelles

Some micellar solutions have been used as a host system for natural and synthetic organic compounds. Four different micelles can be produced depending on the surfactant nature; they can produce anionic, cationic, uncharged and zwitterionic micelles. The external charge in micelles plays an essential role in the interaction of them with the organic molecules, as well as their size and the presence of co-surfactants or salts in the solution.[106] The anionic micelles are used to stabilize the colored species in the flavylium multi-state system selectively. In the other hand, the cationic and neutral surfactant micelles are known to stabilize the uncolored species.[107, 108]

The SDS (Sodium Dodecyl Sulfate in Figure 1.14) negatively charged micelles provide chemical stability in anthocyanins and other flavylium based compounds, where the hydration and deprotonation of the $\mathbf{AH^+}$ is slightly slowed [106, 109], the isomerization constant was not affected by the presence of the micelles in the aqueous media. This behavior can explain the localization of the the positive charge of the flavylium cation on the negative charged micelle surface.[110]

In the anthocyanins stabilized by SDS micelles a red-shift is observed in the absorbance spectra. The stability of the flavylium cation is increased along the pH scale, raising the K'_a. At higher pH values the total amount of **Ct** and **A** are increased at the equilibrium at expenses of **B**.[108]

1.6.2 Cyclodextrins.

Cyclodextrins, formed naturally by enzymatic modification of starch, are cyclic oligosaccharides composed by six (α-cyclodextrin), seven (β-cyclodextrin), eight (γ-cyclodextrin) or more glucopyranose units linked by α-(1,4) bonds (Figure 1.15). These macrocycles have been used as pharmaceutical excipients due their ability to complex with drugs by means of host-guest interactions. Once the complex has been formed, some chemical and physical properties of the drugs change, including the increase of solubility, stability and bioavailability, in addition to the improvement of some organoleptic properties.[111] Some synthetic modifications on the structure of cyclodextrins had changed their properties and their use in different research areas.

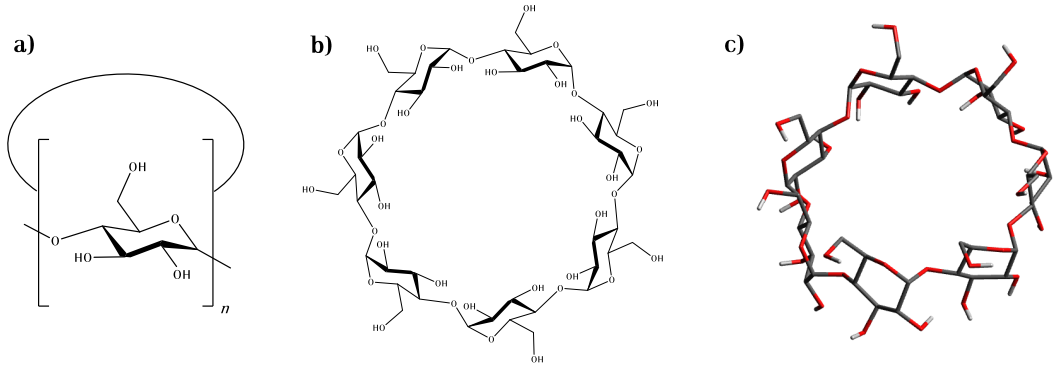

Figure 1.15: Representation of the a cyclodextrin in its **a)** simplified, **b)** seven units bi-dimensional and **c)** tri-dimensional form.

The modified β-cyclodextrin with seven sulfobutylether residues, also known as Captisol®, has an hydrophobic cavity which enables it to the complexation with compounds of the same nature. Conversely, the exterior is hydrophilic, thanks to the sulfonate groups, making it ideal for the use in aqueous media. The cavity size offers selectivity for specific guest molecules, always depending on their association constants.[112] This macrocycle is widely used in pharmaceutic formulations because it increases the solubility of many water insoluble drugs[111], it is also applied in the complexation with natural polyphenols[113, 114, 115, 116, 117, 118]. The complexation with some anthocyanidins has been explored, improving the storage stability of the pigments, which are sensitive to oxidation.[119] Some studies of the complexation of β-cyclodextrins with anthocyanins have been also performed. The protective effect of some natural anthocyanins against oxidation, thermal degradation and digestive damage was demonstrated.[120, 121]

β-Cyclodextrins have an anti co-pigmentation effect on anthocyanins, due they are have more affinity for uncolored forms[122]. In order to clarify the effect of this cyclodextrin on the multi-state species in flavylium-based compounds, the complexation with the synthetic compound 3',4',7-trihydroxyflavylium was investigated, the **Ct** form is favourable for complexation, while the $\mathbf{AH^+}$ interaction was negligible, a slight increment in the photoisomerization process was also observed. The **Ct** photoisomerization to **Cc**, and further transformation into $\mathbf{AH^+}$, also induce the guest exit from the host cavity, due the low association constant with the flavylium cation.[123].

1.6.3 Cucurbit[*n*]urils.

Other macrocyclic hosts that can be used to complex the falvylium multi-state species are the cucurbit[*n*]urils (CB*n*), these compounds represent a family of cyclic hosts composed by *n* glycoluril units (*n*=5-10), linked by methylene bridges, see Figure 1.16.[124, 125] This family has showed higher binding constants on their host-guest complexes than the ones obtained for cyclodextrins complexes.[125] The interactions between CB*n* molecules with their guests is in general driven by ion-dipole interactions or by hydrophobic effect. The two carbonyl-fringed portals have a negative charge density, which is suitable for metal ions and/or cationic organic compounds interaction. The cavity in the other hand, is hydrophobic and can host neutral molecules. The rigid structure in curcubit[*n*]urils make them attractive not only as synthetic receptor but also as a building blocks in supramolecular systems.[125, 126]

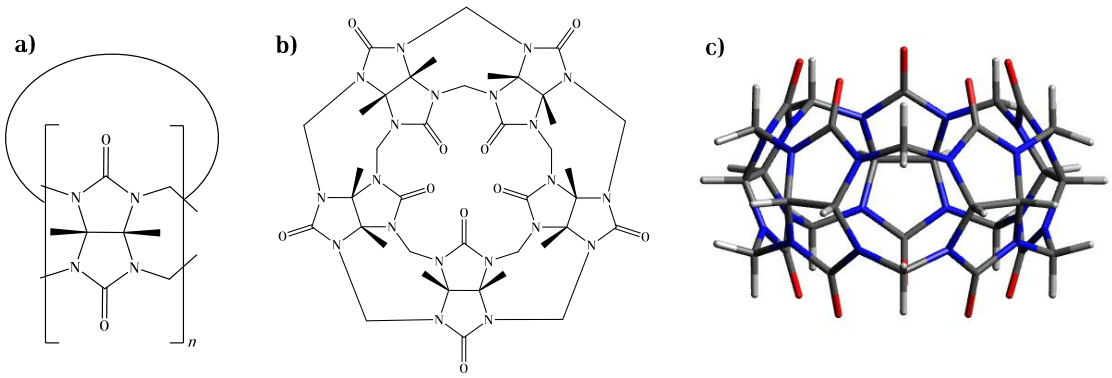

Figure 1.16: Representation of the **a)** glycoluril basic unit in Curcubitn]urils, **b)** bi-dimensional structure of CB5 and **c)** its tri-dimensional form.

The charge distribution in the flavylium multi-state species allows for the possibility to use them as guest molecules, especially for the flavylium cation form in anthocyanins derivatives.[127, 128, 129] CB7 is one of the most used compounds of this family, because its large enough cavity size of 279 Å and high water solubility, when it is compared with other members of the family. CB7 displays affinity for hydrophobic flavylium-based compounds, and it is higher for those bearing amino substituents.[128] This macrocycle is able to improve

the color in solutions stabilizing and extending the pH domain of the **AH**$^+$ form and also protecting it from hydration enhancing the stability of **A** in many flavylium derivatives, also the stability of the anthocyanidins is enhanced in presence of CB7, the protection against the hydration is the main reason, since there is evidence that their degradation take place via chalcone formation.[129]

1.6.4 Calix[*n*]arenes.

The Calix[*n*]arenes (C*n*) are oligomeric macrocycles linking a series of phenolic units through methylene bridges, they are obtained from the condensation reaction between *para*-*t*-butyl phenol and formaldehyde. They adopt the form of a vase, hence the name, having a wide and a narrow rim that can be chemically modified to functionalize them.[130] Figure 1.17 provides a generalized chemical structure of calix[*n*]arene, the size depend of the number of base units (n=4,5,6,7,8-20). Among their characteristics, they are resistant to high temperatures without degradation, but their water-solubility is limited being soluble in some organic solvents.[131]

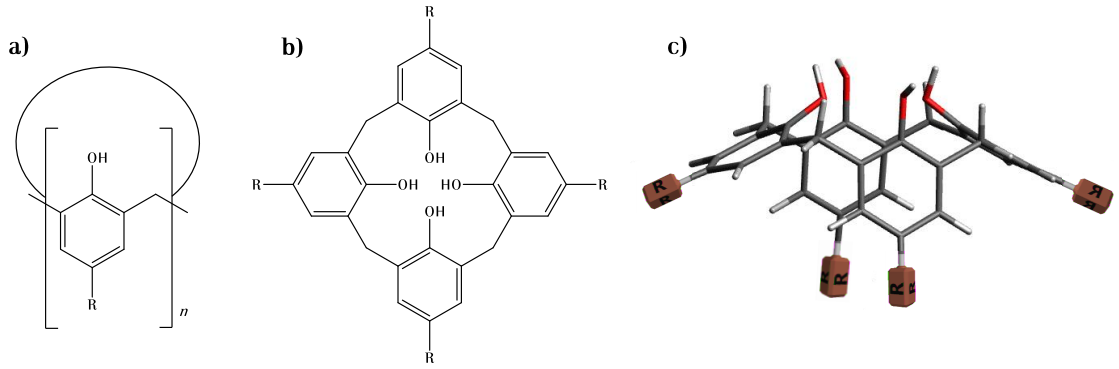

Figure 1.17: Representation of the **a)** basic unit in calix[*n*]arenes, **b)** bi-dimensional structure of the calix[4]arene and **c)** its tri-dimensional form.

The modified C*n* with sulfonated moieties have been used as hosts receptors in many biological applications to encapsulate compounds as toxins, biomolecules DNA, amino acids and some neurotrasnmiters as acetylcholine.[132, 133, 134, 135] These macrocycles have a π-electron rich aromatic cavity able to host ions and the sulfonate groups provides enough water solubility and the capacity for link selectively some cationic guests.[131]

The host-guest association constants of the sulfonated calix[*4*]arene (Figure 1.17b and c with R=SO_3) with various flavylium-based compounds are in the submillimolar range for the **AH**$^+$ form, while the **Ct** form is weakly binded. This discovering is important in the application in light triggered release of some biologically relevant guest as amino acids from inside the calix[*4*]arene cavity by means of photoisomerization of the **Ct** to **AH**$^+$, which occupies the cavity instead the amino acid.[136]

1.6.5 Molecular clips.

Taking advantage from the knowledge acquired trough the years about hydrophobic intermolecular π-π stacking interactions, the design and synthesis of tweezers and molecular clips for inclusion of electron-poor guest has increasingly attracted attention.[137, 138, 139] The structure of a typical molecular clip is presented in Figure 1.18a, where two electron-rich sidewalls are linked by a spacer.

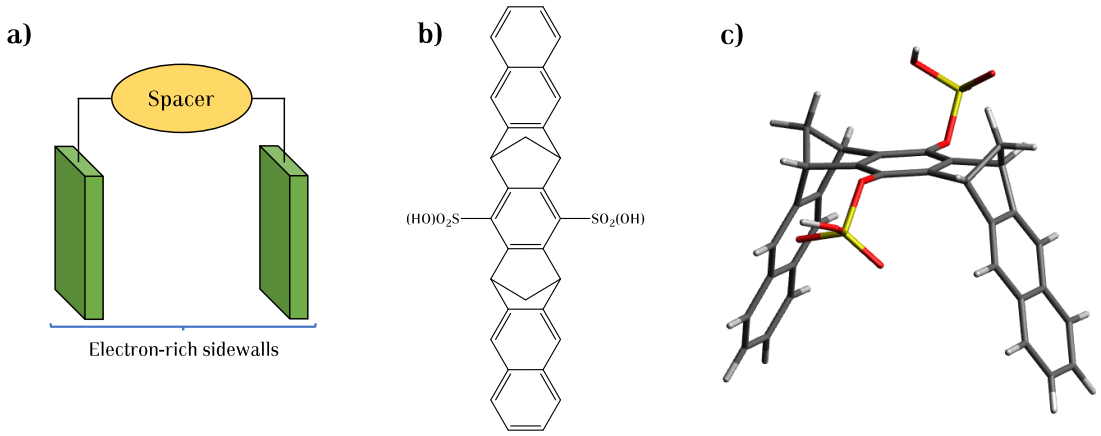

Figure 1.18: Representation of the **a)** a typical molecular clip, **b)** bi-dimensional structure of a sulfonated molecular clip and **c)** its tri-dimensional form.

Naphtalene sidewalls molecular clips with a central benzene spacer have been tested to capture electron-poor guests with high association constants, because they provide an extremely electron-rich cavity.[140, 141, 142] To increase the water solubility of these molecular clips, some esterifications with phosphonate or sulphonated groups had been made. [140] These guest molecules interact with the host by means of π-π, CH-π, and π-cation interactions inside the concave cavity, as well as by solvophobic effects.[138, 143]

The co-pigmentation of molecular clips with the flavylium multi-state species has been barely studied, some sulfonated and phosphonated naphtalen-based clips shows complexation with some flavylium derivatives in its $\mathbf{AH^+}$ and **A** forms in methanol and water (with poor solubility).[143] The complexation with **Ct** species was also measured for the sulfonated clips, which show a higher complex solubility. In general, the proton dissociation inside the cavity occurs at higher pH values and the pK_a is increased, also the flavylium domain along the pH scale is enhanced (higher pK_a') as indicative of the flavylium cation stabilization. Hydration and isomerization processes are also affected with the presence of the sulfonated clips, being both retarded. The use of these and other molecular clips in flavylium-based compounds is challenging, first because of their solubility not only of themselves but also of the complexes.

1.7 Objectives

The stabilization of the flavylium multi-state species and their distribution along the pH scale can be affected by inter and intramolecular interactions found in nature in compounds as anthocyanins and also in their derivative compounds. A deep study of the physical and chemical properties of these pigments were studied in this thesis following the next general objectives:

- Study of the stabilization of the colored species in natural Anthocyanins by self-association and intramolecular interactions.
- Color stabilization of the flavylium compounds by intermolecular interactions.
- Application of the flavylium multistate properties as pH and photoresponsive systems.

CHAPTER 2

Natural color stabilization in anthocyanins by self-association and intermolecular interactions

Anthocyanins are commonly found naturally in the vacuoles of many plant cells. As a secondary metabolite, they have been associated with different physiological roles in plant tissues. Their biosynthesis is greatly influenced by external stimuli that usually stress the plant. These include intense exposition to light, UV-B radiation, extreme temperatures, drought, ozone, nitrogen and phosphorus deficiencies, infections, wounding, herbivory, herbicides, and other pollutants.[144] Considering that the pH inside the plant cell vacuoles could be as low as 2.0 in citrus fruits,[145] and as high as 7.7 in some flowers,[92] the typical red color provided by the flavylium cation may be achieved at mildly acidic pH values by simple co-pigmentation or self-association. As reviewed in Chapter 1, these two effects can be attained by intra and intermolecular interactions.

On the other side, the expression of the stable pink, violet, and blue colors, characteristic of the quinoidal base species, is controlled in Nature, in addition to the co-pigmentation and self-association, by the development of more complex systems that have been widely described by some researchers.[91] Among the strategies used to stabilize the quinoidal base (**A**) species and their deprotonated forms, the metalloanthocyanins[91, 93] and intermolecular sandwich-type stacking of polyacylated anthocyanins are highlighted.[91] Regarding the last strategy, there is structural evidence accumulated over the last decades, indicating that the acylated sugars play an essential role in the anthocyanins stabilization.[146, 147, 148, 149] However, this stabilization is not possible if the acyl group is linked directly to the flavylium backbone; to this end, an acylated sugar that serves as a bridge is necessary.

The acylated and polyacylated anthocyanins with hydroxycinnamic acids have been identified as more stable than their nonacylated parent compounds. The folded conformations adopted by some acylated anthocyanins, where the acyl unit connects with the chromophore through van der Waals interactions (confirmed by long-range NMR NOE correlations), causes sandwich-type intramolecular associations.[150] It is also common to observe intermolecular self-association due to the aggregation of two or more molecules by chiral stacking of the chromophores,[151] see Figure 2.1.

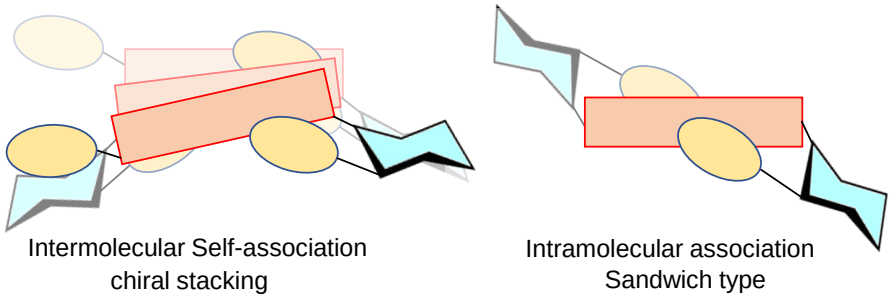

Figure 2.1: Representation of the inter and intramolecular interactions in polyacylated anthocyanins.

The anthocyanins are surrounded by different kind of molecules when they are in their natural environment. Once they are extracted and isolated is not unusual to observe different behaviors on their properties because the intermolecular interactions with other different type molecules affect them, these effects will be described in detail in Chapter 3. The study of their physical-chemical properties is difficult when they are interacting with other different molecules as in their natural environment; therefore, the isolation and study of these natural pigments is essential in understanding which factors related to their chemical structure affect their properties. The historical description of the self-association phenomenon, as well as its comparison with self-aggregation, was summarized by Yoshida[150, 152] as well as by Trouillas[35]. In general, the stability of colored species upon co-pigmentation has been associated with the protective effect for the water nucleophilic attack in position C2 of the flavylium ion.[153] Therefore, the intra and intermolecular interactions in anthocyanins with mono and polyacylated sugars are studied in this Chapter, evaluating their effectiveness in the stability of all the species in the flavylium multi-state at different pH values.

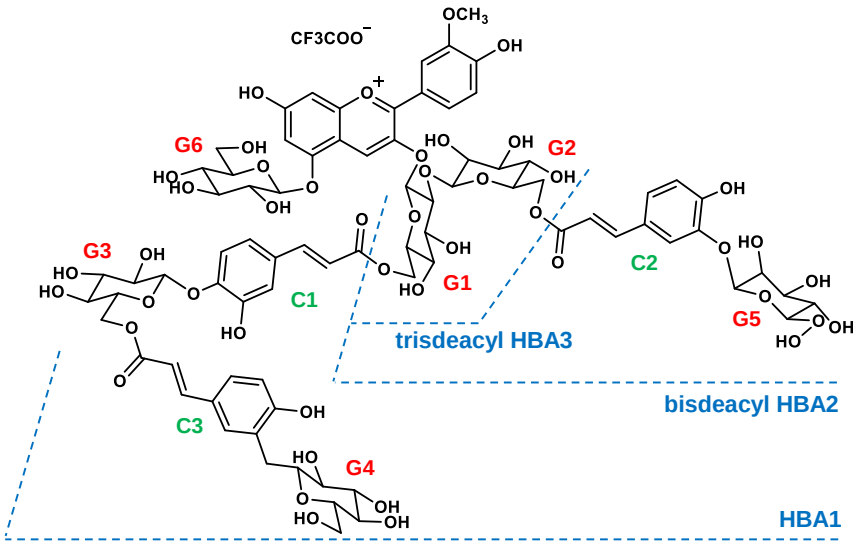

Scheme 2.1: Heavenly Blue Anthocyanin HBA1 and the respective deacylated derivatives, bisdeacyl HBA2 and trisdeacyl HBA3.

2.1 The natural color stabilization in polyacylated anthocyanins

.

Generally, poly-acylation makes anthocyanin coloration highly stable with blue-shifted hues at higher pH values[19], thus playing a key role in the stabilization of quinoidal base forms in many flowers such as gentian (*Gentiana triflora*), cineraria (*Senecio cruentus*), and butterfly pea (*Clitoria ternatea*).[98] Both the blue-shifting and the stabilization effect depends on the position and the number of acylated units. Aromatic acylated units in position C3' and C7 provide the most stable blue colors in anthocyanins.[98]

As other polyacylated anthocyanins the Heavenly Blue Anthocyanin (HBA1) extracted from the morning glory flower (*Ipomoea tricolor cv*), Scheme 2.1, has attracted the attention of the scientific community because their peculiar properties; particularly, the fact that this is the only anthocyanin found in buds and the petals of the open flowers, conferring both reddish and blue colors respectively.[92] This phenomenon is possible thanks to the control over the vacuolar pH, achieving an alkalinization from pH 6.6 to 7.7, allowing the change of color when the flower opens.[154] The HBA1 is a Peonidin derivative with a branched-chain containing three glucolylcaffeic acid moieties at C3; two of them with a glucose unit in the *m*-position of the caffeic acid and one on the *p*-position. The structure of HBA1 was previously reported[27] and is very consistent with the theory of intramolecular stacking, as shown in Figure 2.1. However, there is no kinetic and thermodynamic information regarding the pH-dependant multi-state of chemical species to describe this anthocyanin's behavior.

Before the publication of the work presented in this section, the scientific paper reported

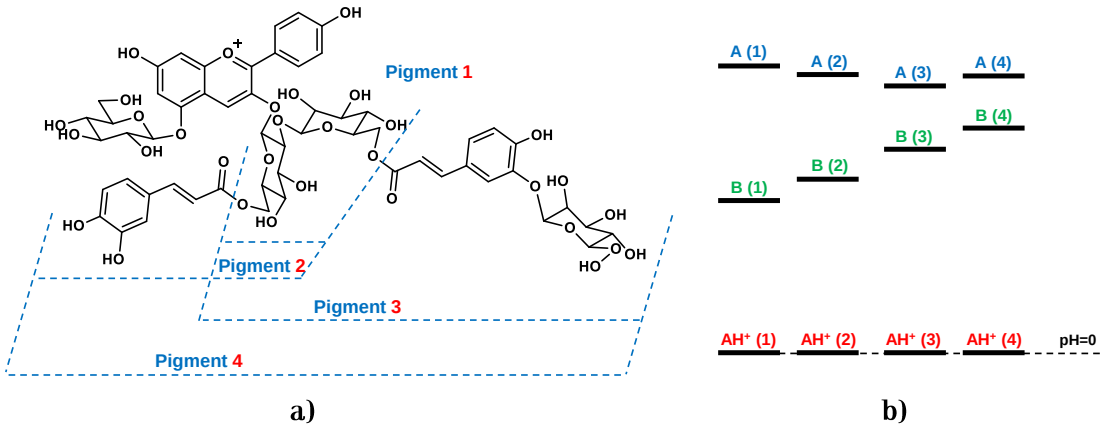

Scheme 2.2: a) Polyacylated anthocyanins reported by Dangles, and b) representation of an energy level diagram of the **AH⁺**, **A**, and **B** species calculated from the equilibrium constants reported by Dangles.[155]

in 1993 by Dangles and colleagues[155] was maybe the most complete study regarding kinetic and thermodynamic of poly-acylated anthocyanins. A Pelargonidin derivative extracted from the flower *Pharbitis Ipomoea nil* and three deacylated derivatives were investigated, see Scheme 2.2. When comparing the chemical structures of HBA1 and the polyacylated anthocyanin in Scheme 2.2, the most relevant difference is the presence of a larger three acylated moiety, which can form a more efficient stacking. This theory lies in the fact that as observed in Scheme 2.2b, the more acylated units, the more unstable the **B** species are, while the **A** species also result slightly stabilized. The protective effect of the acylated units against the flavylium cation's hydration has been attributed to the intermolecular stacking. In order to evaluate the impact of the HBA1 large acylated moiety on the stability of the colored species over the pH scale, the kinetic and thermodynamic properties not only of the HBA1 but also of two deacylated derivatives, HBA2 and HBA3 (Scheme 2.1), were calculated and presented.

2.1.1 The reaction network

Like many other flavylium-based compounds, when an aqueous solution of HBA1, HBA2, or HBA3 is prepared in HCl 0.1 M, the sole stable species is the flavylium cation (**AH⁺**). After rising the pH of the solution the set of reactions described previously in Chapter 1 takes place leading to the formation of the **A**, **B**, **Cc**, **Ct**, species as well as their deprotonated forms, similarly as previously described for the Oenin in Scheme 1.2. In this case, an increase in the colored species' stabilization, mainly the **A** and its ionized species, is expected as the number of acylated units increase in number.

2.1.2 Equilibrium and rate constants

The theory of the kinetic and thermodynamic of the anthocyanins and, in general, other flavylium-based compounds was addressed in Chapter 1. For the acylated anthocyanins and other synthetic flavylium-based compounds, which usually produce stable species at higher pH values, it is necessary to extend the mathematical treatment to the basic medium.[156] Before describing the kinetics of the HBA flavylium multi-state is important to emphasize that all the chemical reactions described henceforth are reversible pseudo-first-order reactions. These reactions follow the typical behavior of the anthocyanins with a high *cis-trans* isomerization barrier. The fastest reaction is the deprotonation to form the quinoidal base or any of the other deprotonated forms. Deprotonation reactions are not observable by conventional methods, but the formation of the subsequent species can be followed by stopped-flow and conventional UV-Vis spectroscopy after a pH jump (see 1.4.4).

As a polyacid, it is easy to predict the number of deprotonated species observable in an anthocyanin. After a pH jump to high pH values, the first deprotonation in HBA1 is expected in position C7,[22] leading to the formation of **A** and the subsequent formation of the other species in **CB**. The **A**, as well as the other three species in **CB** can deprotonate in position C4' to produce the first negatively charged species. There is one more possibility of deprotonation in any of the acyl residues. These hydroxyls have an identical environment in the sugar structure, and a stochastic behavior is expected, leading to a unique inflection point in the absorption spectra, mainly detected around 350-370nm. When the study of the flavylium multi-state is extended to the basic region is possible to observe all these transformations. The complete mathematical expression for thee acid-base equilibria is presented in Appendix A.

The pH dependant absorption spectra of HBA1, HBA2, and HBA3 obtained immediately after a pH jump (10 ms) to different pH values is shown in Figure 2.2. The spectra of HBA1 and HBA2 are compatible with a three acid-base equilibria involving flavylium cation, quinoidal base, deprotonated quinoidal base, and di-deprotonated quinoidal base, this last as a result of the deprotonation of the acyl residues. Inspection of the HBA1 and HBA2 spectra in Figure 2.2 indicate that the absorption spectra of $\mathbf{A^-}$ and $\mathbf{A^{2-}}$ are very similar in the visible region (purple and blue lines), but with an important variation in the UV region around 350 nm, demonstrating a deprotonation in the acyl residues (Figures 2.2a and b). The lack of acyl residues in HBA3 makes no possible a third deprotonation for the **A** species, and the $\mathbf{CB^{2-}}$ at this time scale does not exist, extending the domain of the $\mathbf{A^-}$ species (Figure 2.2c). With the pK_a values calculated, it is clear that the HB3 flavylium cation is the most stable when it is compared only with its quinoidal base immediately after the deprotonation, this because of the high pK_{a1} value (4.2), it is surprising to note that the fist deprotonation in HBA2 is lower than in HBA1 and HBA3. This means that the mono-acylated anthocyanin stabilizes more the quinoidal base over the flavylium cation.

Regarding the quinoidal bases blue-shift, the HBA1 has a higher shift, with up to 17 nm when compared with the $\mathbf{A^-}$ species in HBA3, this could indicate a higher interaction in the intermolecular stacking.

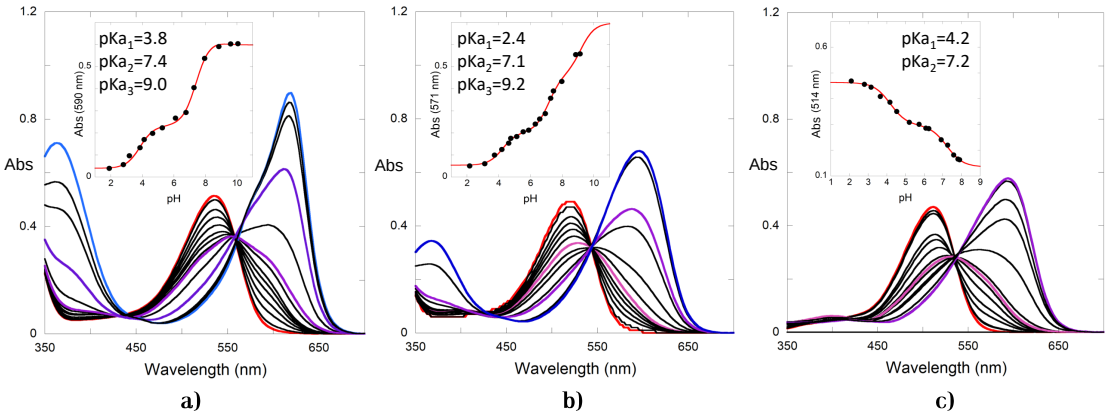

Figure 2.2: a) Absorption spectra of HBA1, 3.5×10^{-4}M taken 10 ms after a direct pH jump from pH=1 to higher pH values, followed by stopped flow, red line=$\mathbf{AH^+}$, pink line=$\mathbf{A}$, violet line=$\mathbf{A^-}$ and blue line=$\mathbf{A^{2-}}$, b) the same for HBA2, and c) the same for HBA3.

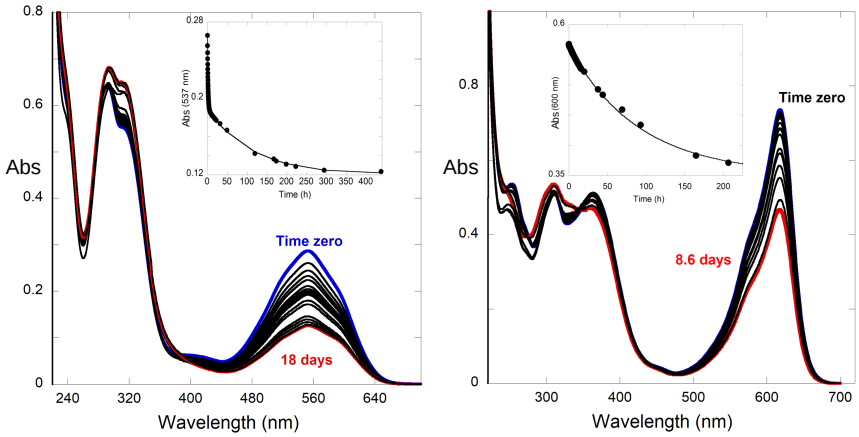

Figure 2.3: a) Spectral variations of a solution of HBA1, 3.5×10^{-4}M upon a direct pH jump from pH=1.0 to pH=6.4 kinetics fitted with a bi exponential, rate constants of $2.1 \times 10^{-4} s^{-1}$ and $2.4 \times 10^{-6} s^{-1}$. b) The same to pH=9.4, fitting achieved with a mono exponential, rate constant of $2.5 \times 10^{-4} s^{-6}$.

Once the quinoidal base species has been formed, the system evolves to produce the pseudo-equilibrium species during an exponential process that corresponds to the second and third steps of the kinetics. The variation on the spectra observed in HBA1 solutions and its derivatives after a direct pH jump indicates a behavior qualitatively similar to the one in common anthocyanins.[58] Two examples of this event are shown in Figure 2.3 with direct pH jumps from pH=1 to pH=6.4 and 9.4 in HBA1 solutions. The spectrum of the quinoidal

base in Figure 2.3a clearly disappears trough a bi-exponential kinetic process. The first exponential leads to the pseudo-equilibrium, a process composed of the hydration followed by the tautomerization and controlled by the former. The second exponential is a slower decay corresponding to the isomerization of **Cc** for the **Ct** formation. The kinetics in Figure 2.3b has a unique slow decay also controlled by the hydration but unusual in non-acylated anthocyanins; the second decay is not observed. In HBA2 and HBA3 solutions above pH=7, some degradation was observed before reaching the pseudo-equilibrium, also the case in HBA1 before reaching the equilibrium. The partial recovery of **AH$^+$** after a reverse pH jump to pH=1 confirmed the compound degradation.

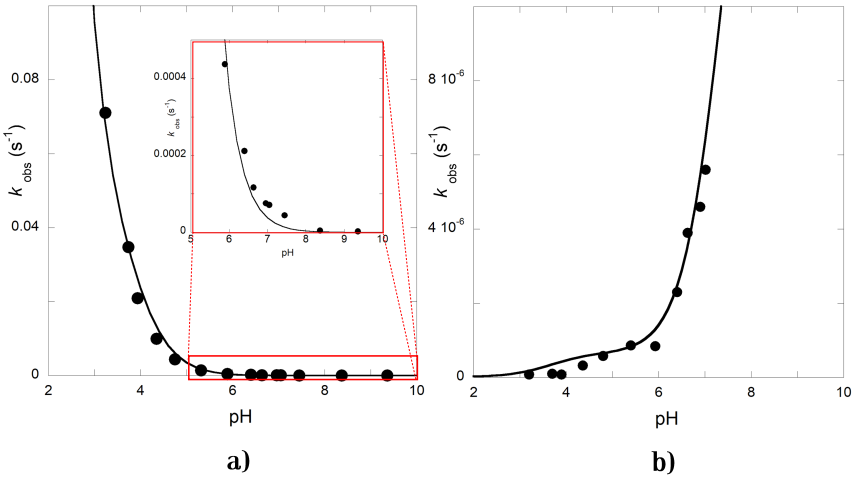

Figure 2.4: a) Representation of the second kinetic toward the equilibrium as a function of pH in HBA1 solutions; fitting was achieved with eq.1.15 for $pK_{a1} = 3.76$, $k_h = 0.01s^{-1}$, and $k_{-h}/(1+K_t) = 185M^{-1}s^{-1}$. b) Same for the third step; fitting achieved with eq1.16 for the mole fractions in the pseudo-equilibrium and $k_i = 2\times10^{-6}s^{-1}$ and $k_{-i} = 5\times10^{-7}s^{-1}$.

Representation of the rate of the second step of the pH-dependent kinetics is reported in Figure 2.4a. In HBA1, the flavylium cation hydration tends to zero; this seems to indicate that not only the **A** but also the **A$^-$** are difficult to hydrate. This is a feature not observed in other flavylium-based compounds, where the quinoidal base species suffer the attack of the $^-$OH in the basic medium, and the representation of the hydration rate constant at different pH values exhibits a U-shape.[157] The experimental data can be fitted exclusively with eq.1.15 for $pK_{a1} = 3.76$, $k_h = 0.01s^{-1}$, and $k_{-h}/(1+K_t) = 185M^{-1}s^{-1}$, because the [OH$^-$] has no effect on the hydration rate. The isomerization rate is represented in Figure 2.4b. At higher pH values, the system is not completely stable for the long time scale involved in this step, and only the isomerization of **Cc** and **Cc$^-$** was considered, the kinetic process is fitted by eq.2.1.

$$k_7 = \chi_{Cc}k_i + k_{-i} + \chi_{Cc-}k_{i-} + k_{-i-} \tag{2.1}$$

where χ_{Cc} and χ_{Cc-} are the mole fraction of **Cc** and **Cc$^-$** at the pseudo-equilibrium, k_i and

k_{-i} the direct isomerization rates constants from **Cc** and **Cc**$^{-}$ respectively, while k_{i-} and k_{-i-} are the equivalent for the reverse reaction. The accuracy to obtain the reverse isomerization rate constant of the mono deprotonated species (k_{-i-}) is low because of some decomposition at higher pH values and substantial time involved to reach the equilibrium.

Although HBA compounds are not entirely stable at moderately basic pH values compared with neutral and acidic medium, the blue color of the deprotonated quinoidal base remains during several days in the HBA1. Even though the behavior of HBA1 and its derivatives is very similar to non-acylated anthocyanins, it is worth to note the much higher mole fractions of colored species at the pseudo-equilibrium and the equilibrium. Not only the amount of quinoidal bases is different, but also the lifetime required to reach the equilibrated states, which is much higher for the HBA1, not the same for HBA2 and HBA3, which have a shorter lifetime.

The pH-dependent spectra of the three compounds at the pseudo-equilibrium are shown in Figure 2.5. The fitting of the experimental data obtained at a specific wavelength along the pH scale let to calculate the $pK_a^{\wedge}$ values for each compound, as observed in the inset of Figure 2.5. For HBA3, only the $pK_a^{\wedge}$, the fist deprotonation product, was calculated, and no significant amount of quinoidal bases was observed at the pseudo-equilibrium. In the case of HBA2, some **A** species remain at the pseudo-equilibrium, but with a high degradation degree at pH values up to pH 7, for this reason, the spectra of solutions in alkaline medium were not included.

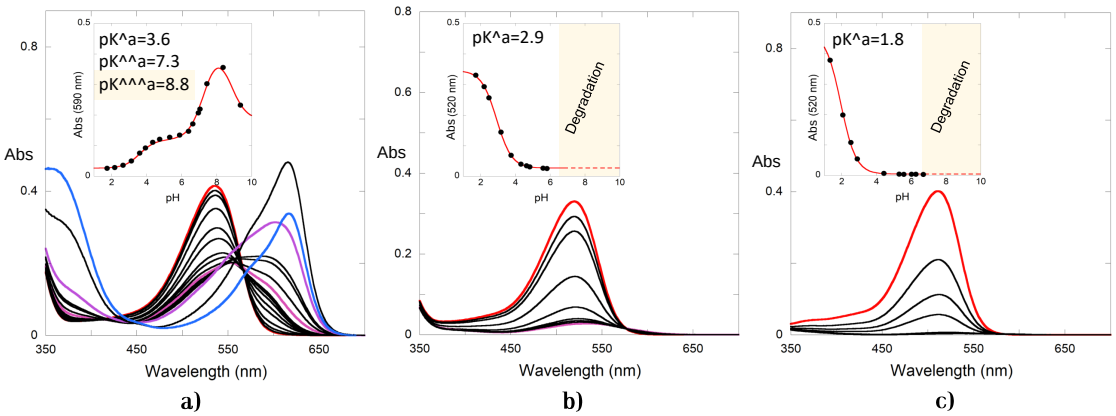

Figure 2.5: a) Absorption spectra of HBA1, 3.5×10^{-4}M at the pseudo-equilibrium upon a direct pH jump from pH=1.0 to higher pH values, red line=**AH**$^{+}$, pink line=**A**, violet line=**A**$^{-}$ and blue line=**A**$^{2-}$, b) the same for HBA2, and c) the same for HBA3.

On the other hand, for the HBA1, a considerable amount of the quinoidal bases are present at the pseudo-equilibrium. Therefore the kinetics of the HBA1 solutions were followed until the equilibrium. The HBA1 absorption spectra at the equilibrium is shown in

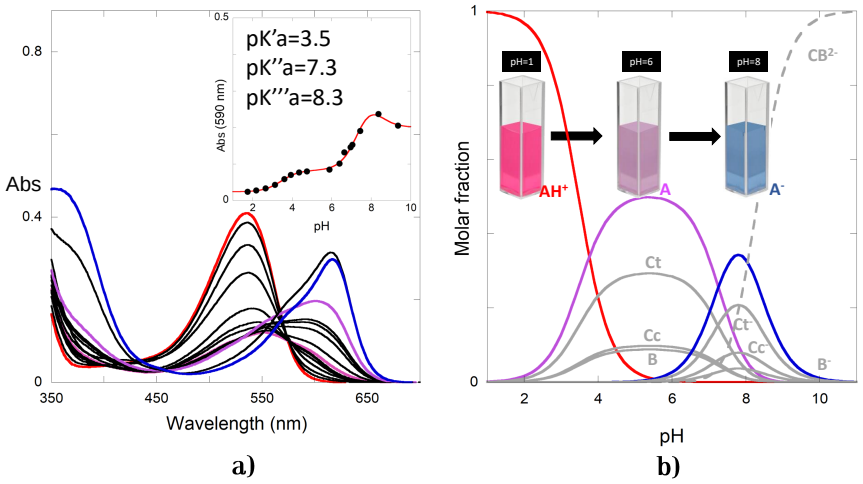

Figure 2.6: a) Absorption spectra of HBA1, 3.5×10^{-4}M at the equilibrium upon a direct pH jump from pH=1.0 to higher pH values, red line=**AH$^+$**, pink line=**A**, violet line=**A$^-$** and blue line=**A^{2-}**. b) Mole fraction distribution of HBA1 at the equilibrium of all the multi-state species including mono deprotonated species.

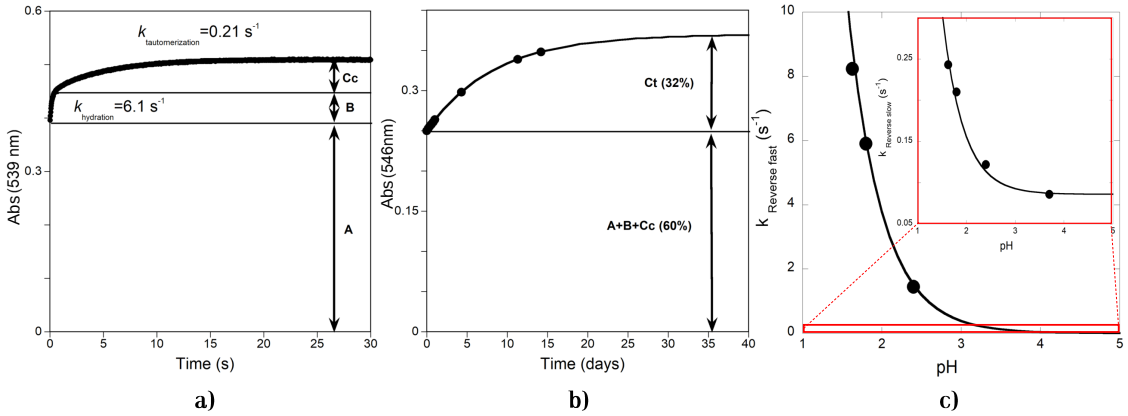

Figure 2.7: a) Reverse pH jump of a HBA1 solution 2.64×10^{-5}M at the pseudo-equilibrium from pH=6 to 1.9, followed by stopped-flow. b) Reverse pH jump of a HBA1 solution 1.76×10^{-5}M at the pseudo-equilibrium from pH=5.35 to 1. c) Representation of the rate constants for the reverse pH jumps carried out from the pseudo-equilibrium, followed by stopped-flow.

Figure 2.6a, and the molar fractions of all the species in the flavylium multi-state also in the equilibrium are shown in Figure 2.6b. The most notable difference, between the absorption spectra observed in Figure 2.6a and those obtained at the equilibrium in common anthocyanins, is the significant increase of the absorption bands relative to the purple quinoidal base (**A**) and the blue ionized quinoidal base (**A$^-$**). In common anthocyanins, the equilibrium takes a few hours or days to be achieved; in the case of the HBA1 is worth noting that the equilibrium takes several days, particularly at high pH values. However, for pH values higher than 8, the solutions are not completely stable, and some decomposition was observed after several days proved by the partial conversion into **AH$^+$** after a reverse pH jump to

pH=1. The equilibrium of HBA2 and HBA3 is not presented because of the decomposition make its calculation inaccurate.

The reverse pH jumps of solutions at the pseudo-equilibrium or equilibrium are usually employed to calculate the contributions of the **AH$^+$**, the neutral, mono, and di-deprotonated species in **CB**, **CB$^-$** and **CB^{2-}** respectively. Also these experiences contribute to calculate the thermodynamic and kinetic constants. Figure 2.7a shows a typical reverse pH jump of a HBA1 solution from the pseudo-equilibrium at pH=6 back to pH=1.9 followed by stopped-flow, the contributions of the **A**, **B**, and **Cc** species are ruled by the fast formation of **AH$^+$** in a three exponential pH-dependant kinetic process (the first exponential is to fast to be seen by stopped-flow). Figure 2.7b shows a reverse pH jump from the equilibrium at pH=5.35 back to pH=1, the formation of the flavylium cation through **A**, **B**, and **Cc** is achieved 25 seconds after the jump, while the **Ct** contribution takes more than 15 days to reach the equilibrium. It is interesting to note the high amount of **Ct** in the equilibrium, and the long time it takes to reach the full equilibrium, something unusual in common anthocyanins. The pH-dependant first and second steps observed after a reverse pH jump from the pseudo-equilibrium are presented in Figure 2.7c, the faster process represents the hydration and the second and slower is the tautomerization, the experimental data was fitted by eq.1.17 and eq.1.18 respectively for $k_h = 0.01 s^{-1}$ and $k_{-h} = 377 s^{-1}$; $k_{-t} = 0.086 s^{-1}$ and $k_{-t}^H = 7 M^{-1} s^{-1}$.

Table 2.1: Equilibrium and rate constants between **AH$^+$** and **CB** in the HBA series.

Compound	pK'_a	pK_a	pK_{a1}	K_h/M	K_t	K_i
HBA1	3.47	3.64	3.76	2.65×10^{-5}	1.05	3.98
HBA2[a]		2.92	4.23	8.3×10^{-4}	0.35	
HBA3[b]		1.92	4.19	8.14×10^{-3}	0.37	
	k_h/s^{-1}	$k_{-h}/M^{-1}s^{-1}$	k_t/s^{-1} [a]	k_{-t}/s^{-1}	k_i/s^{-1}	k_{-i}/s^{-1}
HBA1	0.01	377	0.09	0.086	2×10^{-6}	5×10^{-7}
HBA2	0.12	145	0.08	0.23		
HBA3	0.35	43	0.12	0.33		

[a] The value of k_{-t} and by consequence k_t could be lower because of the acidic catalysis.

[b] The pK'_a values of were not determined because of decomposition.

In Table 2.1, the rate and equilibrium constants in the HBA series are shown. In the case of HBA2 and HBA3, the isomerization is slower than in common anthocyanins (in monoglucosides, it takes a few hours).[22] and some decomposition takes place preventing a precise study of the system.

In Scheme 2.3, the energy level diagram of the **AH$^+$**, **CB**, and **CB$^-$** species of HBA1 is presented. Note the difference on stability on both **A**, and **A$^-$** when compared with their respective **B** species. The quinoidal base is even more stable in **CB$^-$** than in **CB** (ΔG values

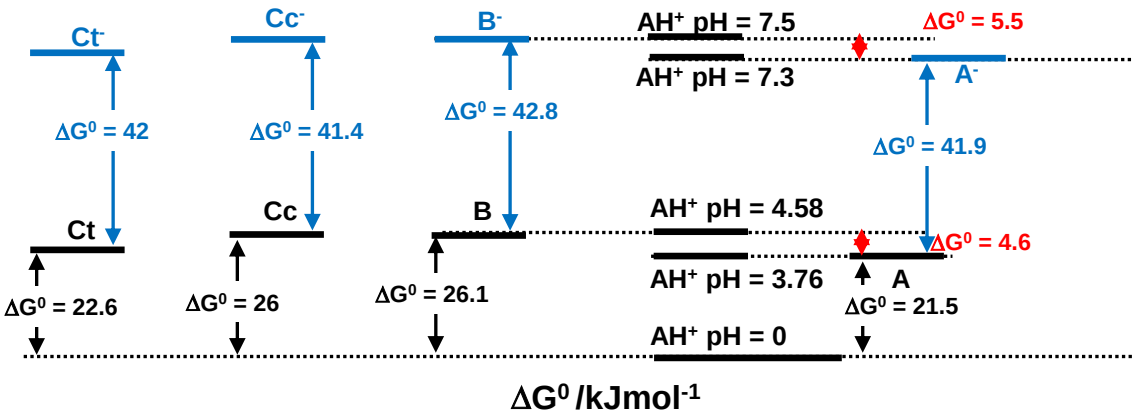

Scheme 2.3: Energy level diagram of the compound HBA1 in moderately acidic (**CB** black) and moderately alkaline conditions (**CB**$^-$ blue).

in red). In the case of the pigments reported by Dangles in Scheme 2.2[155], the more acylated units, the more unstable the hemiketal form (relative to the **AH**$^+$); the compound with two acylated units has the higher destabilization of **B**. The longer acylated sugar, the better protection against the hydration, these sugars can approach better to the electron-deficient C2, and C4 positions in the flavylium backbone. In the HBA series the hemiketal form is also more destabilized when the number of acylated units is increased; although in HBA1 there is an inversion in the level energy of the **A** species when compared with **B**, this makes the quinoidal base more stable than the hemiketal, see Scheme 2.4. Moreover, this effect is also observed in the deprotonated species, which permit the observation of the **A**$^-$ blue color. The reason for the peculiar behavior of HBA 1 has been attributed to an internal co-pigmentation.[91, 92, 146, 147, 148, 152] The acyl group's interaction with the flavylium backbone would create a hydrophobic environment protecting them from the water attack. At higher pH values, where the acyl groups deprotonate, this environment can be disrupted, leading to the anthocyanin's degradation. The tri-dimensional structure plays an essential role in the acyl unit protection against the hydration. Some works on genetic engineering have demonstrated that the blue colors are not observed in modified carnations varieties, where acylated delphinidins and acylated flavones acting as co-pigments, are not enough to produce blue flower colors, producing mauve-violet colors instead.[158]

2.2 The peculiar aggregation process of an acylated anthocyanin in water

The presence and content of different anthocyanin types in the grape varieties, as well as their degradation and formation of other chemical compounds during the winemaking process, contribute to the color in red wine. One of the most abundant anthocyanins in some grape varieties commonly used to produce wine is the Malvidin 3-O-(6-O-*p*-coumaroyl) glucoside (Mv3Coum),[159, 160] Scheme 2.5. This acylated anthocyanin has an interesting

behavior when is isolated and dissolved in acidified water, unlike other glucosyl-acylated anthocyanins and with its parent compound the Oenin, the Mv3Coum is poorly water-soluble.[161, 162] Despite a few works regarding this compound that have clarified some aspects of this behavior in aqueous solutions,[161, 162, 163] the complete understanding of its behavior was not fully achieved. The study of this compound regarding the other species of the multi-state formed in moderately acidic pH values has not been published because of the lack of reproducibility in the results. Other authors previously reported the dramatic effect of the glucosyl-acylated groups on the physical-chemical properties of polyacylated anthocyanins,[35, 164] and was the focus of discussion in the previous subsection.

It was reported that Mv3Coum does not show color enhancement due to self-association, as happens in Oenin, therefore the presence of the *p*-coumaroyl prevents anthocyanin aggregation.[162] However, the intermolecular association in flavylium species of Mv3Coum has been proven by NMR and molecular dynamics simulations.[161] Considering that the unique difference between the Oenin and the Mv3Coum is the coumaric acyl group (Scheme 2.5), all the differences in physical-chemical properties must be attributed to the effect of this acylation. In this section, the study of both anthocyanins about the aggregation and the thermodynamic constants is addressed.

2.2.1 The aggregation study by circular dichroism, NMR and theoretical calculations

After the extraction and isolation, the preparation of stock Mv3Coum solutions at different concentrations resulted in absorption UV-Vis spectra with differences in the molar absorptivity. This effect is typical during the aggregation in anthocyanins and is a common behavior in many flavylium-based compounds. The peculiarity of the Mv3Coum lies in the aggregation at very low concentrations, in the appearance of a new absorption band around 600 nm in the aggregated solutions, and the precipitation of a poorly water-soluble bluish solid.

The circular dichroism (CD) spectra of a Mv3Coum solution 2.5×10^{-4}M is presented in

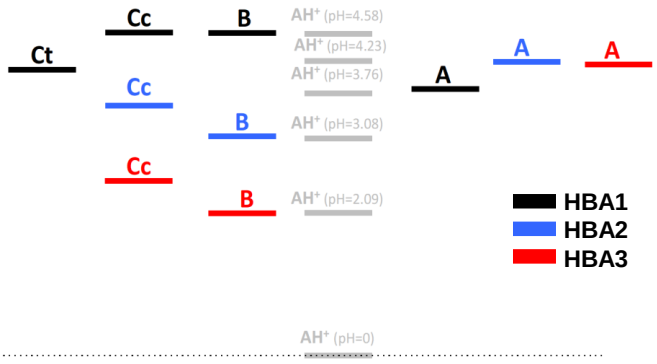

Scheme 2.4: Energy level diagram of HBA1 (black) compared with HBA2 (blue) and HBA3 (red).

Figure 2.8a showing two different signals in the visible region when the solution is at 20°C, one of these signals disappears when the solution is gradually heated to 70°C. In Figure 2.8b the UV-Vis absorption spectra of the same solution are presented. At 20°C, some small particles in suspension, visible at the naked eye, are responsible for the characteristic raise of baseline due to light scattering and the appearance of the absorption band around 600 nm. The data presented in Figure 2.8 can be interpreted by the presence of two kinds of molecular interactions in the solutions at lower temperatures; inter and intramolecular. As expected, heating the solution the characteristic negative Cotton effect CD signal is disrupted, this because this kind of signal is typical in the anthocyanin aggregation relative to the π-π anti-clockwise molecular staking.[101] An anomalous negative signal remains at 70°C and is observed in all the spectra in the visible region. As the sugar does not absorb in the visible region and the flavylium backbone has no chiral centers, this signal can be interpreted as an induced circular dichroism,[165, 166, 167] given by the intermolecular interaction between the chromophore and the acylated sugar that posses chiral centers. Moreover, Figure 2.8c shows the CD spectra of Mv3Coum at 70°C in three different concentrations (5×10^{-5}M; 1.2×10^{-4}M and 2.5×10^{-4}M) upon normalization. As observed, the signals do not change, supporting the absence of intermolecular interactions under this temperature. It is well known that intermolecular interactions can be reduced by decreasing the anthocyanin concentration, while intramolecular ones are not affected.

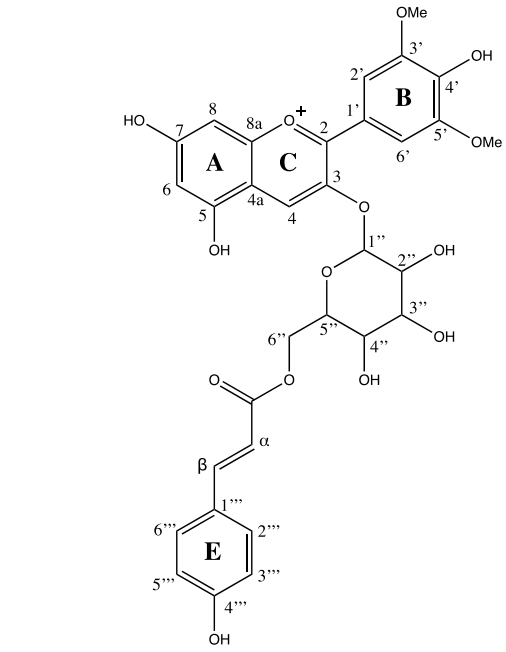

Malvidin 3-*O*-(6-*O*-coumaroyl) glucoside (Mv3Coum)

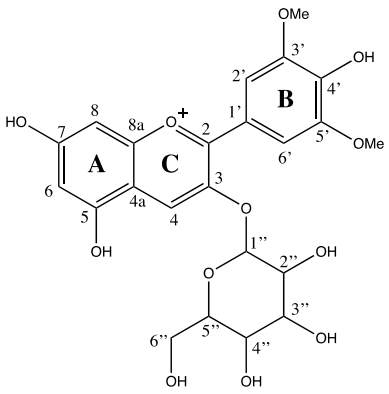

Malvidin 3-*O*-glucoside (Oenin)

Scheme 2.5: Structures of the Malvidin 3-O-(6-O-*p*-coumaroyl) glucoside (Mv3Coum) and Malvidin 3-O-glucoside (Oenin) in their cation flavylium from.

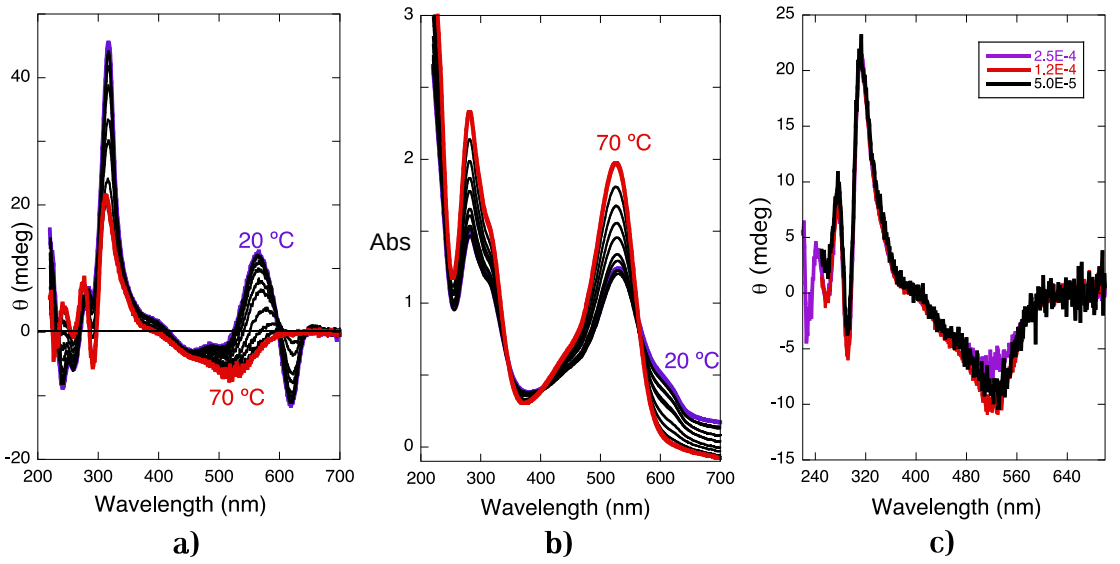

Figure 2.8: a) circular dichroism spectra of a 2.5×10^{-4}M Mv3Coum solution in water at pH=1, as a function of temperature. b) Absorption spectra of the same solution in a). c) CD spectra of Mv3Coum solutions at 70°C with different concentrations upon normalization (5×10^{-5}M; 1.2×10^{-4}M;2.5×10^{-4}M).

The CD spectra of anthocyanins with 3-O-mono-glucosides, including the Oenin, are already published.[100, 101, 148, 162, 168, 169]. As the Oenin lacks the coumaroyl group, the negative signal observed in Mv3Coum at 70°C is not expected when the solution is heated.[101] Figure 2.9a shows the typical Cotton effect of the aggregated Oenin; when the solution is heated, no visible signal remains. Figure 2.9c shows a comparison of the CD

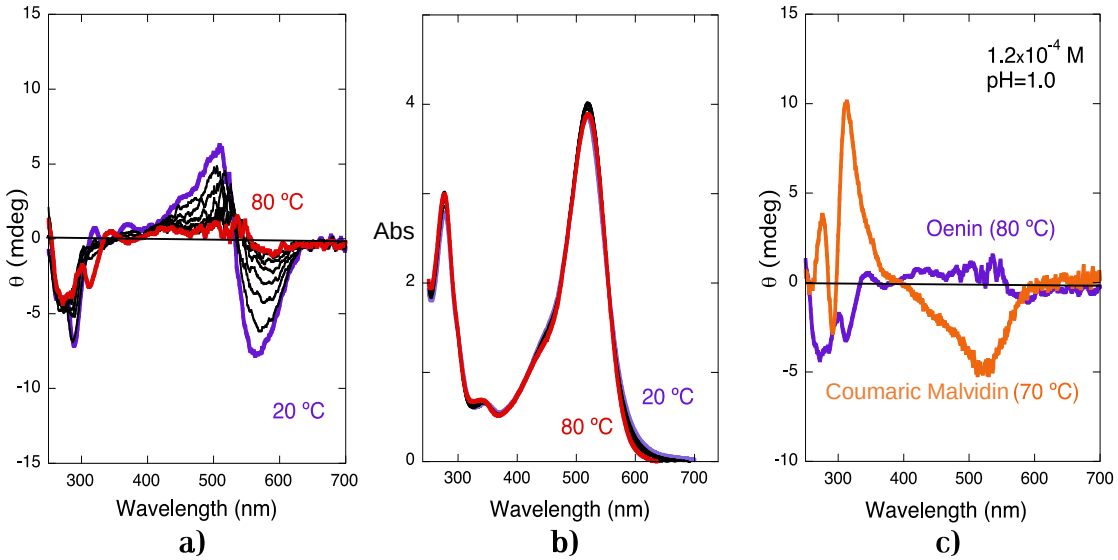

Figure 2.9: a) circular dichroism spectra of a 1.2×10^{-4}M Oenin solution in water at pH=1, as a function of temperature. b) Absorption spectra of the same solution in a). c) Comparison of the CD spectra of Mv3Coum and Oenin in the same conditions.

spectra of the Oenin and Mv3Coum; it is possible to observe the difference.

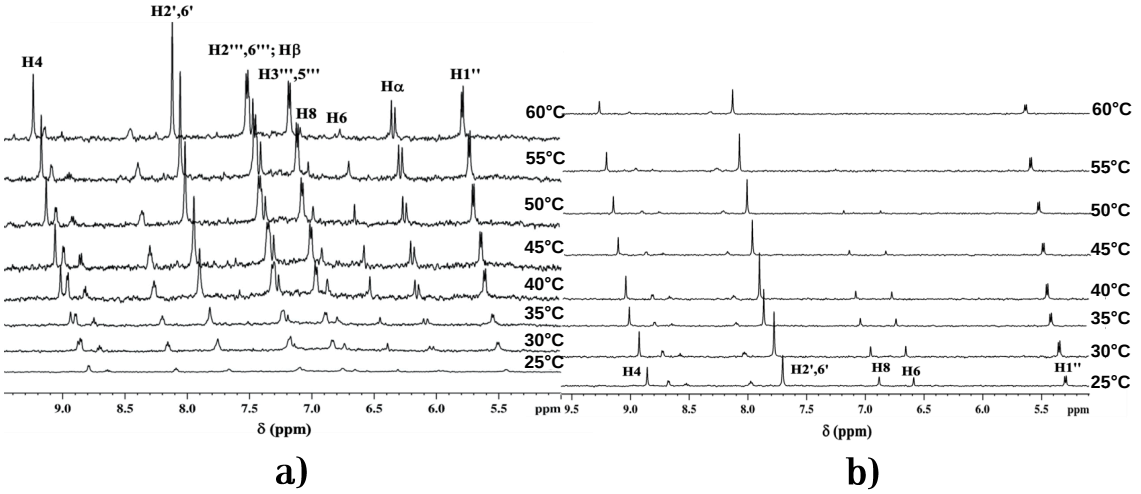

Figure 2.10: ^{1}H NMR spectra in the aromatic region of a) a 2.5×10^{-4}M Mv3Coum solution and b) a 2.5×10^{-4}M Oenin solution in D_2O at pD=1 as function of the temperature (Data provided by Joana Oliveira, University of Porto).

The ^{1}H NMR spectra of Mv3Coum and Oenin solutions (2.5×10^{-4}M) were measured at different temperatures by some colleagues in the University of Porto. Figure 2.10a shows the aromatic region signals. At 25°C the Mv3Coum protons signals are broadened and with a small resolution, something not observed in Oenin (2.10b), this is indicative of the intermolecular interaction in Mv3Coum and their poor solubility in water, the sharpening of the peaks is observed when the solution was heated, increasing the solubility of the compound, and all the signals shifted to lower fields. Figure 2.11a shows the difference between the chemical shifts of the phenylbenzopyrylium core protons at different temperatures of the Mv3Coum and Oenin. The difference of the signals would be zero in case of the absence of any interaction between the flavylium backbone and the coumaroyl moiety or if the coumaroyl's proximity does not affect the signals in the flavylium backbone. Figure 2.11a shows very significant differences in the chemical shifts in some protons; such differences are maintained with the temperature. While protons H2', H6', and H4 are less affected (chemical shifts differences close to zero), protons H6 and H8 have a negative shift, and the protons of the methoxyl groups and H1" of the sugar moiety are positively shifted when the coumaroyl is present. The same procedure was applied to construct the Figure 2.11b, with a comparison between the coumaroyl residue signals in Mv3Coum and Methyl-*p-trans*-coumarate (MeCoum). In this case, the H3''' and H5''' chemical shifts are similar ($\Delta\sigma \approx 0$) while the rest are up-field shifted. These data confirm the coumaroyl moiety's effect over the ^{1}H NMR signals in the flavylium backbone when no intermolecular interactions are involved.

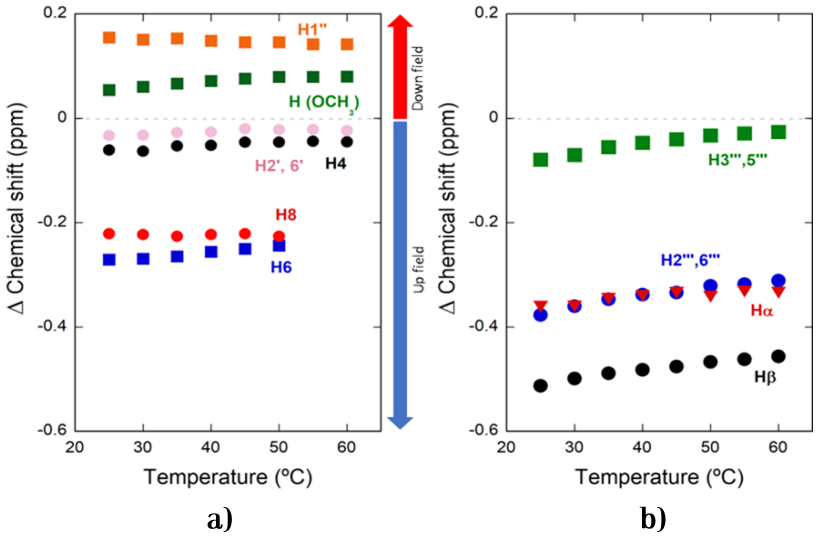

Figure 2.11: Chemical difference between a) the phenylbenzopyrylium core protons of Mv3Coum and Oenin and b) the coumaroyl protons of Mv3Coum and methyl-*p-trans*-coumarate at different temperatures. NMR data provided by Joana Oliveira, University of Porto

Theoretical calculations support the previous experiences. The optimized and most stable geometries of Mv3Coum and Oenin are represented in Figure 2.12. These structures are similar to other acylated anthocyanins reported previously using the same DFT (Density Functional Theory) method.[170] The electrostatic potential maps of the most stable structures were also calculated (Figure 2.12). It was observed that the main difference between the two stable conformers in Mv3Coum is the π-stacking between the flavylium and the *p*-coumaroyl units. According to Figure 2.12, the ground state electronic density of the p-coumaric acid moiety and the A and C rings of the flavylium backbone are overlapped (red circle) in the conformer B. However, this particular π-stacking is absent in conformer A. This latter agrees with the molecular structure reported previously for the Mv3Coum.[161] The Mv3Coum conformer A has only a moderate interaction between H4 and the oxygen of the carbonyl group. In contrast, conformer B has four weak intramolecular interactions: i) a C=O-π interaction of the O in the carbonyl group with the C ring, ii) a C=O–H interaction between the carbonyl group and the H1''' of the sugar, iii) a C-H-π interaction between the Hα and the A ring, and iv) a C-O-H interaction from O-2" to OMe-5', see Figure 2.13 and Table 2.2. As observed in Figure 2.12, no intermolecular interactions are possible in Oenin. Still, the interactions observed in the Mv3Coum conformer B explain the data reported in Figure 2.11 where the $\Delta\sigma$ is positive for H1" and the methoxy protons, being these protons deshielded and their ^{1}H NMR signals moved downfield, as has been described for a typical intramolecular hydrogen bonding.[171] In Figure 2.13 two intramolecular interactions through hydrogen bonding can be observed (green dotted line) between i) the carbonyl in the coumaroyl residue that acts as an acceptor and the anomeric proton of the glucose H1"

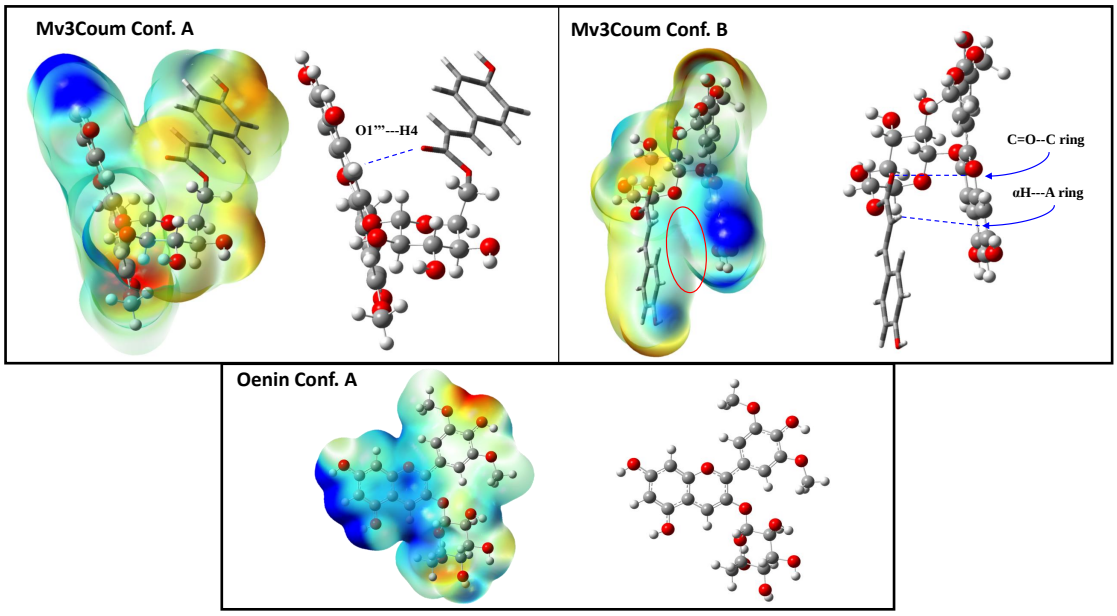

Figure 2.12: The optimized DFT:B3P86/6-31G** and most stable molecular structures of Mv3Coum and Oenin and their electronic density maps, including the main electrostatic/dispersion forces between the flavylium backbone and the coumaroyl moiety (Optimized structures were provided by Dr. Natercia Bras from the university of Porto).

acting as a donor; and ii) the hydroxyl group in C2' (the acceptor) and the methoxyl hydrogens (donors) from the B ring.

Table 2.2: Main electrostatic/dispersion forces between the flavylium backbone and the *p*-coumaroyl moiety observed in the most stable conformers at the DFT:B3P86/6-31G** level in water.

Interaction type	**Atom1**	**Atom 2**	**Distance (Å)**
Conformer A			
C=O—H	O carbonyl	H4	3.08
Conformer B			
C=O—π	O carbonyl	C ring	3.62
C-H—π	αH	A ring	3.83
C-OH—O	HMeO3'(5')	O2"	2.40

On the other side, as can be observed in Figures 2.11 and 2.13, the signals of H6 and H8 are shielded in Mv3Coum when compared with Oenin and move up-field in the NMR spectra. H3'"5'", H2'"6'", Hα and Hβ signals in the coumaroyl residue are also shielded and the $\Delta\sigma$ is negative. The H3'"5'" signals are less affected because they are far from the flavylium core (Figure 2.13). The electronic density is increased around these atoms because of the non-covalent forces between the coumaroyl residue, and the A and C rings from the

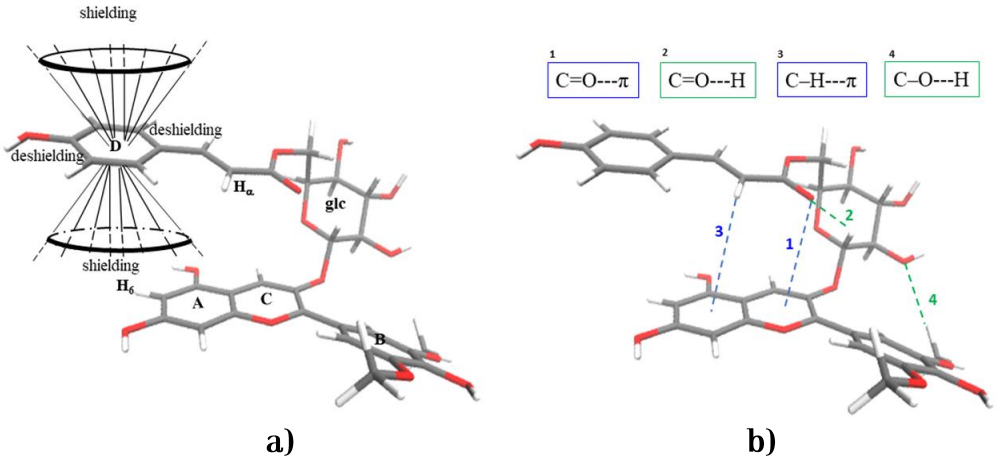

a) b)

Figure 2.13: Mv3Coum (conformer B) model at the B3P86/6-31G** level of theory in water representing a) the effect of the coumaroyl moiety on the ^{1}H NMR chemical shifts on the flavylium backbone and b) the main electrostatic/dispersion forces between the flavylium and the coumaroyl moiety.

flavylium.[172]

2.2.2 The reaction network

As previously described, the Mv3Coum solutions at pH=1 tend to aggregate even at low concentrations. In solutions, up to 2×10^{-5}M, some precipitation is visible after a few hours of preparation. After raising the pH of the solution, the kinetic of aggregation is faster, making impossible to study this system in water at room temperature. Figure 2.14a shows the kinetic of precipitation of the quinoidal base at room temperature; this effect is observable even at low concentrations. However, up to 50°C the system is sufficiently soluble, and the aggregation is disrupted allowing to carry out a series of direct and reverse pH jumps to calculate the kinetic and the equilibrium constants, which rule the typical transformation between the **AH$^+$** and the **CB** species in a similar way as previously described for the Oenin in Scheme 1.2. Once again, the differences in these constants are attributed to the presence of the coumaroyl moiety.

2.2.3 Equilibrium and rate constants

As is well known, the reaction rates are temperature-dependent, this because the rate constant increases according to the Arrhenius Equation, becoming faster when the temperature is raised. As expected, after the direct pH jumps, the pseudo-equilibrium is achieved rapidly in those solutions at 50°C. Representation of the absorption spectra of Mv3Coum solutions at different pH values at the pseudo-equilibrium and the equilibrium is shown in Figures 2.14b and 2.14c, respectively. As observed in Figure 2.14c, not a considerable amount of quinoidal base remains in the equilibrium, but it is certainly more than the one found for

the Oenin at room temperature (detailed information will be described in Chapter 3).

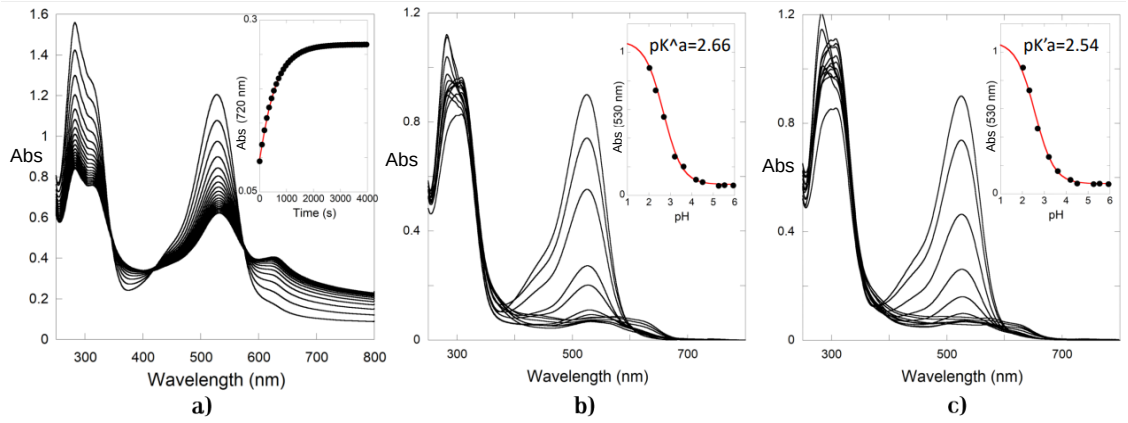

Figure 2.14: a) Aggregation process after a pH jump from pH=1 to pH=2.63 in a 5×10^{-4}M Mv3Coum solution at 25°C, inset shows the increase of the baseline during the time. b) Absorption spectra of Mv3Coum, 3.5×10^{-4}M at the pseudo-equilibrium upon a direct pH jump from pH=1.0 to higher pH values at 50°C and c) the same as b) at the equilibrium.

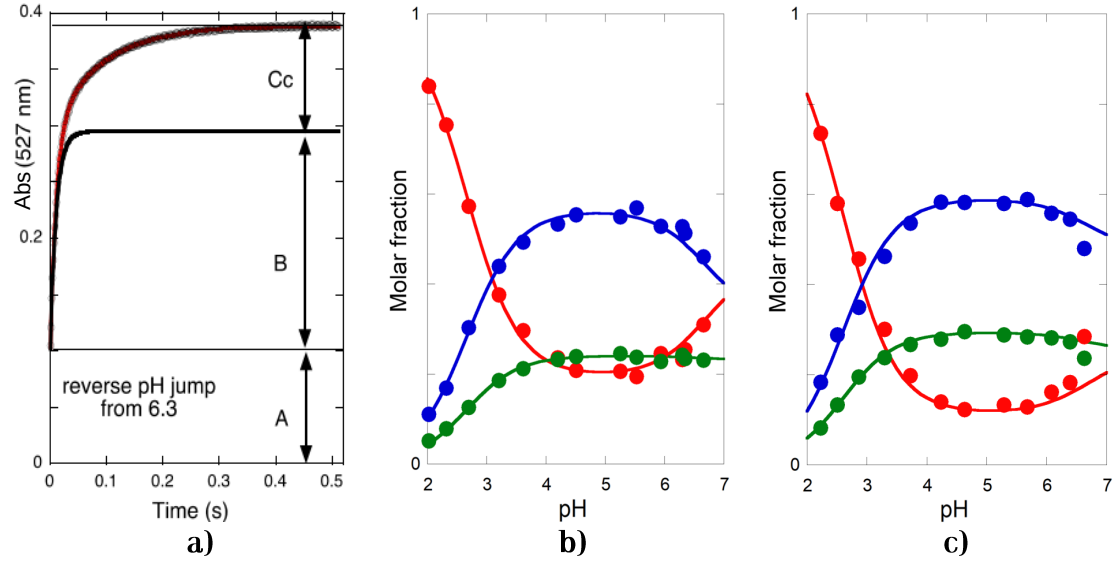

Figure 2.15: a) Reverse pH jump of Mv3Coum, 3.15×10^{-5}M from pH=6.3 to pH=1 at 50°C, followed by stopped-flow; b) Representation of the mole fraction distribution at the pseudo-equilibrium of the species flavylium cation plus quinoidal base and anionic quinoidal base (red), hemiketal and anionic hemiketal (blue) and *cis*-chalcone and anionic *cis*-chalcone (green) of Mv3Coum; c) the same for the Oenin.

Once in the pseudo-equilibrium the reverse pH jumps were performed to obtain the molar fractions of the $\mathbf{AH^+}$, **A**, **B**, and **Cc** species of the flavylium multi-state. Figure 2.15a shows a reverse pH jump from a pseudo-equilibrated solution of Mv3Coum from pH=6.3 to pH=1 at 50°C. Representation of the molar fractions of all the species in the pseudo-equilibrium along the pH scale is presented in Figure 2.15b and 2.15c for the Mv3Coum and

Oenin, respectively. A comparison of the Mv3Coum and Oenin's mole fraction distributions indicates that the concentration of the quinoidal base is circa 2-folds higher in the former. Considering that at 50°C and this specific concentration, only the intermolecular interactions occur, this is another consequence of the coumaroyl residue. Table 2.3 summarizes the equilibrium constants calculated for the Mv3Coum and Oenin at 50°C, in addition to those calculated for Oenin at 25°C.

Table 2.3: Equilibrium constants of Mv3Coum (50°C) and Oenin (50°C and 25°C).

Compound	pK'_a	$pK^{\wedge}_a$	pK_a	K_h/M	K_t	K_i
Mv3Coum (50°C)	2.54	2.66	3.37	1.23×10^{-3}	0.43	0.7
Oenin (50°C)		2.6	3.56	1.41×10^{-3}	0.50	
Oenin (25°C)		2.5	3.70	1.99×10^{-3}	0.42	

The $CB^{\wedge\wedge}$ and CB'' constants are not reported because of their inaccuracy.

2.3 Materials and Methods

The HBA series of compounds were provided by Prof. Kumi Yoshida from the University of Nagoya (JP). The HBA1 was extracted and purified from frozen petals of morning glory (*Ipomoea tricolor* cv. Heavenly Blue)[173], while HBA2 and HBA3 were obtained by mild alkaline hydrolysis.[174] Oenin chloride (≥ 95%) was obtained from Extrasynthese (Lyon, FR). Malvidin 3-O-(6-O-*p*-coumaroyl) glucoside was provided by Dr. Joana Oliveira from the University of Porto (PT).[175]

Stock HBA and Malvidin derivatives solutions were prepared in 0.1 M HCl with Millipore water. Reverse and direct pH jumps were achieved by the addition of HCl, NaOH, or Theorell and Stenhagen's universal buffer as needed, and pH was recorded on a Radiometer Copenhagen PHM240 pH/ion meter (Brønshøj, Denmark). UV-Vis spectra were recorded on a Varian-Cary 100 or 5000 spectrophotometers (Palo Alto, CA, US). The stopped-flow experiments were performed on a SX20 (Applied photophysics; Surrey, UK) spectrometer equipped with a PDA.1/UV photodiode array detector. For the Malvidin compounds, the kinetic were always monitored at 50°C, and a cut-off filter of 435 nm was used to prevent photodegradation in the stopped-flow experiments.

Circular dichroism absorption and UV-Vis spectra were recorded on a Chirascan qCD spectrometer equipped with a CS/JS recirculating cooler (Applied Photophysics; Surrey, UK) set with a temperature ramp between 0 and 80°C under constant nitrogen flush, acquisitions were made every 5°C with a stabilization time of 5 min between measurements. Quartz cells of 1 and 0.5 cm pathlength were used in a range of 220-700 nm with an interval of 1nm.

The averaged spectra of two scans with baseline correction were reported.

For theoretical calculations, the Malvidin 3-O-(6-O-*p*-coumaroyl) glucoside pre-optimized structures by molecular dynamics and DFT: B3P86/6-31+G(d,p)[176, 177] were received from Dr. Natercia Bras from the University of Porto (PT). The electrostatic potential surface over the Mv3Coum was calculated through a DFT: B3P86/6-31+G(d,p) single-point energy calculations.

2.4 Conclusions

The anthocyanins' physical-chemical properties are modified not only by the type and position of the substituents in the flavylium backbone, but also by the spatial distribution of them. In the two cases reviewed along this Chapter, the role played by the acylated sugars by the interaction with the flavylium core, and in general, the interaction of the molecular structure with other molecules has demonstrated a huge influence in the color preservation along the pH scale, and also in the water solubility of the flavylium multi-state species.

After studying the kinetic and thermodynamic constants of any anthocyanin, some properties as the color of the solution can be understood, mainly based on the study of the amount of colored species in the equilibrium. The fact that the hydration rate constant decreases and the dehydration increases will rise the equilibrium constant, making unstable the uncolored **B** form. This is the case observed in HBA1, where the hemiketal is even less stable than the quinoidal base at the equilibrium, leading to the blue color's appearance in slightly basic solutions and at higher pH values before degradation. In this manner, it is interesting how Nature uses intramolecular interactions in polyacylated anthocyanins to create stable colors in plant tissues.

Simultaneously, the intermolecular interactions in the mono-acylated Malvidin derivative promote the formation of water-insoluble aggregates, even at low concentrations. These aggregates have a low water solubility, but a change in the color of the solution is observed at room temperature before precipitation. This effect is due to the unique packaging after the $\pi - \pi$ stacking in Mv3Coum. These interactions can be disrupted at high temperatures, where only the intra-molecular interactions remain, and the solubility is increased. The system's study without intermolecular interactions shows that the color expression in the equilibrium is improved in mildly acidic solutions, something typical in mono-acylated anthocyanins. The study of mono and poly-acylated anthocyanins in aqueous solutions brings the opportunity to apply new knowledge in the development of more stable anthocyanin-based matrices in food and cosmetic industries.

Publications associated with this chapter:

- J. Mendoza, N. Basílio, F. Pina, T. Kondo, and K. Yoshida. "Rationalizing the color in heavenly blue anthocyanin: A complete kinetic and thermodynamic study."In: *The Journal of Physical Chemistry B*, 122.19 (2018), pp. 4982-4992.DOI: https://doi.org/10.1021/acs.jpcb.8b01136

- J. Mendoza, J. Oliveira, P. Araújo, N. Basílio, N. Teixeira, N.F. Brás, F. Pina, K. Yoshida and V. de Freitas. "The peculiarity of malvidin 3-O-(6-Op-coumaroyl) glucoside aggregation. Intra and intermolecular interactions."In: *Dyes and Pigments*, 180 (2020), pp. 108382. DOI: https://doi.org/10.1016/j.dyepig.2020.108382

CHAPTER 3

Anthocyanins color stabilization by intermolecular interactions.

The vast number of colors in the plant Kingdom results from the huge structural diversity of natural pigments and the intermolecular interactions between them and some other molecules acting as co-pigments and stabilizers.[35, 91, 178] Molecular complexation between the dyes and other colorless compounds (co-pigments) occurs inside the plant cell's vacuoles. In the anthocyanins behavior, this is no different. Once the natural pigments are extracted and isolated, many intermolecular interactions disappear, causing destabilization of the colors in the new medium or different shades that the ones observed in Nature. Despite of this, and as has been mention previously in Chapter 2, the study of the color properties in the flavylium multi-state can be dramatically simplified working in a environment where only one type of molecule is involved, focusing on the flavylium backbone substituents and the intra and intermolecular interactions between molecules of the same type. The study of the anthocyanins behavior in solutions with more than one type of molecule is essential from the point of view of mimicking the natural pigments stability in the Natural environment. This study can also be simplified if only one or even two different types of molecules are included in a controlled way.

There are two key points to prevent the color lost process in flavylium-based compounds, the control in the hydration rate reaction, and subsequently, the thermodynamic equilibria between the species. Therefore, any method able to avoid degradation, prevent or retard the hydration reaction, and in other words, stabilize the colored forms from the flavylium multi-state will help to preserve color.

In addition to the natural co-pigments that can be found in the same plat tissue interacting with the dye, the interaction with other molecules acting as stabilizers has been tested

to preserve the anthocyanins color, mainly with compounds that can be used as food additives. Some polysaccharides or polymers, such a β-cyclodextrins, denatured proteins, gums, pectins, among others, have resulted promising in the anthocyanins protection against their degradation at pH values higher than 3.2.[179] On the other hand some techniques as the host-guest complexation through the use of macrocycles as curcubit[n]urils (CBn) and calix[n]arenes (Cn) as host and flavylium-based compounds as guest molecules have been used to shield the colored forms of the flavylium-based compounds and protect them from the water attack stabilizing the colored forms against the uncolored ones.[129, 136, 180] Other techniques as micro-encapsulation, freeze and spray-drying are commonly used creating diverse types of interactions between different molecules with anthocyanin derivatives.[179].

Throughout this chapter, the stabilization of the species on the flavylium multi-state will be studied when the flavylium-based compounds (including anthocyanins) interact with other type molecules in aqueous solutions. Fist of all, the caffeine co-pigmentation effect will be addressed using a novel method developed by our teamwork, and later, the impact of the interaction of ionic surfactants in lipophilic anthocyanin derivatives will be the object of study. Finally, the interaction with two different water-soluble hosts as the CBn-type molecular clips and sulfonated calix[n]arenes, with different cavity sizes, will be explored.

3.1 Color stabilization in anthocyanins and other flavylium compounds by intermolecular co-pigmentation with caffeine

.

The co-pigmentation effect in anthocyanins is one of their most remarkable properties. The ability to develop π-stacking interactions, caused mainly by dispersion forces between the participant molecules and the solvent, produce a favorable release of water molecules from the solvation shell (hydrophobic effect).[24] In some cases, the formation of hydrogen bonds between the molecules is also the mechanism followed by the co-pigmentation. This effect seems to protect the flavylium cation from the hydration reaction. Besides the self-association reviewed previously in Chapter 2, the anthocyanins' ability to bind with other phenols and natural molecules by π-π stacking creates another way of protection used by Nature against the color lost. Despite numerous and well-documented research works regarding the co-pigmentation effects in anthocyanins, the complete understanding of this phenomenon over the equilibrium constants in the flavylium multi-state is not fully described. The anthocyanin co-pigmentation has been extensively studied, many mathematical models that explain this phenomenon have been reported.[96, 181, 182, 183] As the flavylium cation is the only stable species at pH=1, the co-pigmentation is relatively easy to study. However, when higher pH values are studied, the system turns complex due to the

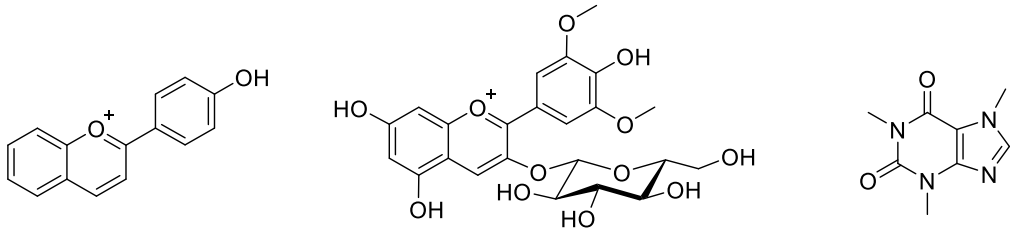

Scheme 3.1: Molecular structures of the 4'-hydroxyflavylium (4'OH) and Malvidin-3-glucoside (Oenin) in their flavylium cation form and caffeine.

other species' existence in the flavylium multi-state. A co-pigmentation model that considers the interaction of the co-pigment with $\mathbf{AH^+}$ and **A** was recently published by Petrov et al.,[184] but not an extension to the other species was included because the high number of variables to be fitted. The developed method for calculating all the equilibrium constants through the application of reverse pH jumps from equilibrated or pseudo-equilibrated solutions containing flavylium-based compounds, which mathematical model is presented in Appendix B, can be applied to obtain the equilibrium constants in the complex flavylium multi-state easily. An extension of this model can be used to the co-pigmentation effect (Appendix C). In this section, the application of both mathematical models is presented. The co-pigmentation protective effect over the colored forms of the flavylium multi-state at the pseudo-equilibrium and equilibrium is studied.

Caffeine is found together some anthocyanins in plant tissues as cacao seeds,[185] red tea leaves[186] and has been proposed to be introduced by means of genetic engineering into the blue roses breeding.[187] Caffeine co-pigmentation in anthocyanins increase the concentrations of the colored species in the equilibrium at moderate acidic pH values, producing a hyperchromic effect and a bathochromic shift on the maximum absorption band. It was found that the caffeine molecule preferentially stabilize the quinoidal base.[187] The co-pigmentation effect of caffeine with malvin,[188, 189] cyanidin-3-glucoside[190] and other synthetic flavylium-based compounds has been extensively studied.[191, 192] An strong hyperchromism is observed in the co-pigmentation of natural glycosilated anthocyanins by caffeine, this effect is not observed with other flavylium-based synthetic compounds, therefore the hyperchromism has been associated to the formation of stronger hydrogen bonds with the anthocyanin glycosil residues.[188]

3.1.1 The equilibrium in the absence of the co-pigment

Two different flavylium-based compounds were studied to prove the efficiency of the method described in Appendix B, the 4'-hydroxyflavylium (4'OH) representing the synthetic flavylium compounds and the Malvidin-3-glucoside (Oenin) representing the anthocyanins, see Scheme 3.1. In acidic medium the 4'OH takes a long time to reach the equilibrium, and the **A**, **B**

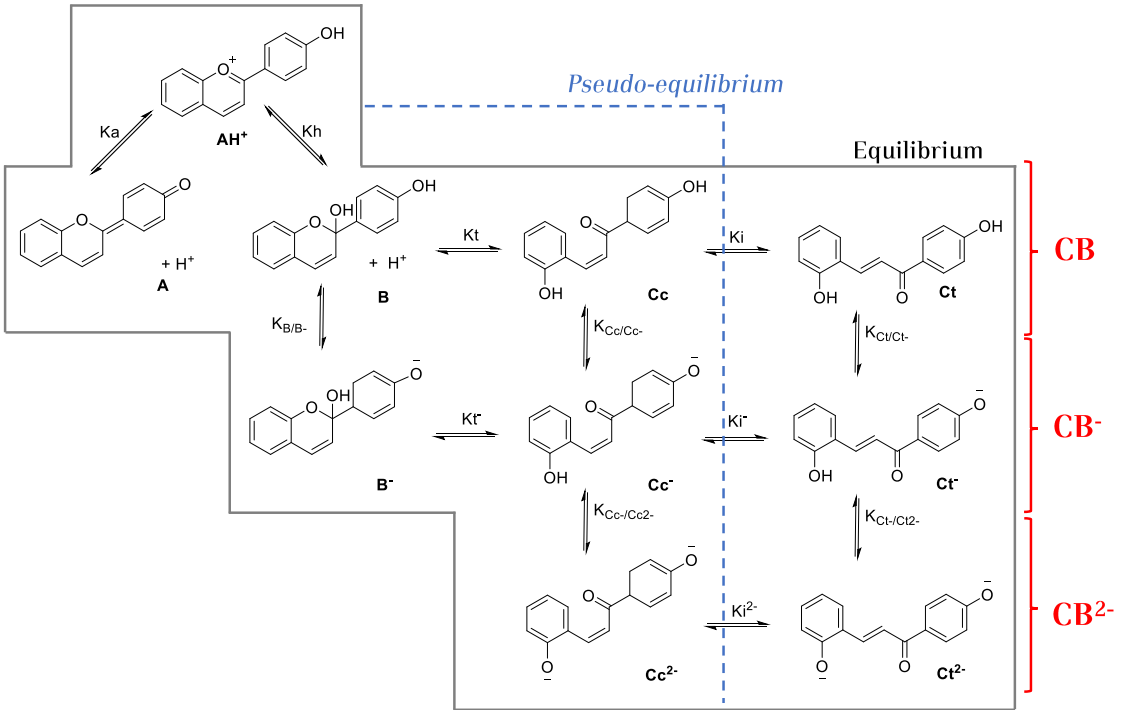

Scheme 3.2: Species in the flavylium multi-state of the model compound 4'hydroxyflavylium.

and **Cc** species have a similar mole fraction distribution at the pseudo-equilibrium, and therefore at the equilibrium.[72] The species obtained at different pH values for the 4'OH are represented in Scheme 3.2, as other flavylium-based compounds the set of equations described in Appendix A describes the entire formation process of the **AH⁺**, **CB**, **CB⁻** and **CB²⁻** species until the equilibrium in solutions at different pH values.

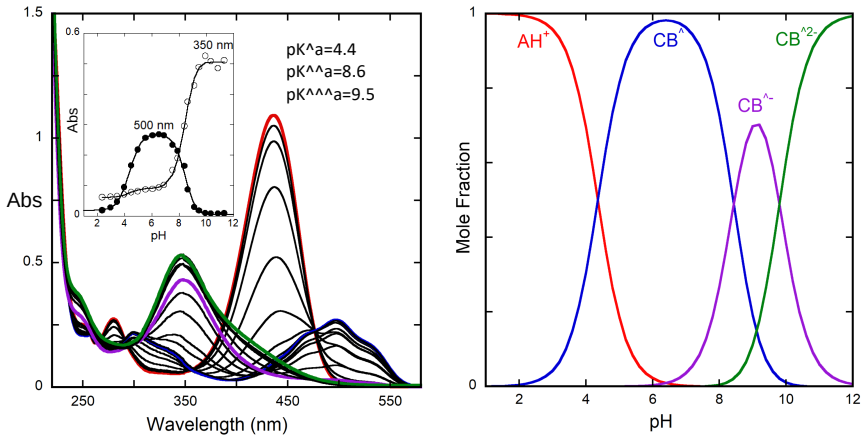

Figure 3.1: a) Spectral variation of 4'OH (2×10^{-5}M) at the pseudo-equilibrium, fitting in inset was achieved for $pK_a^{\wedge} = 4.4$, $pK_a^{\wedge\wedge} = 8.6$ and $pK_a^{\wedge\wedge\wedge} = 9.5$. b) Mole fraction distribution of the species **AH⁺**, **CB^**, **CB^−** and **CB^2−** at the pseudo-equilibrium.

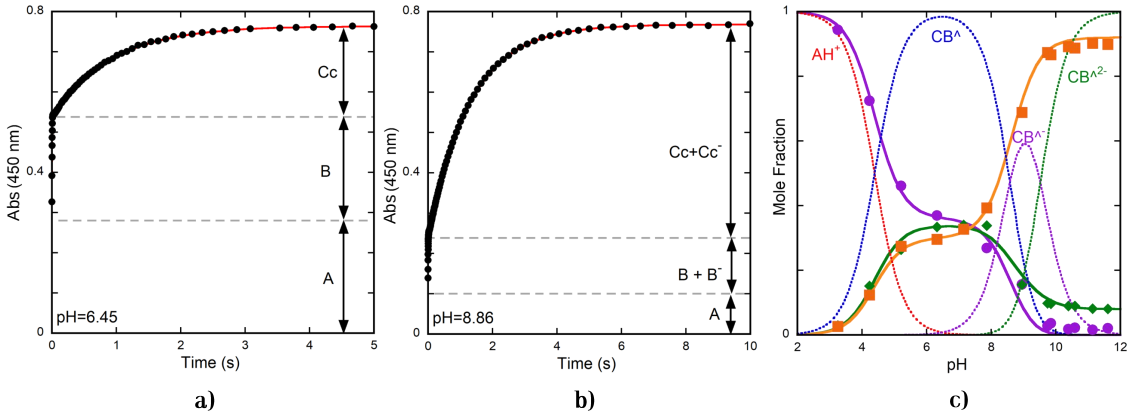

Figure 3.2: a) Reverse pH jump from pH=6.45 to pH=1 and b) the same from pH=8.86. The amplitudes of the traces should be normalized in order to have **A+B+Cc=1** and **A+ (B+B$^-$) + (Cc+Cc$^-$)=1**. c) Mole fraction distribution of the species in 4'OH at pseudo-equilibrium; **AH$^+$** plus **A** (violet), **B** and **B$^-$** (green), and **Cc**, **Cc$^-$** and **Cc^{2-}** species (orange). Fitting achieved with $a_0 = 0.36$, $b_0 = 0.34$, $b_1 = 0.15$, $b_2 = 0.08$, $c_0 = 0.3$, $c_1 = 0.85$, and $c_2 = 0.92$.

Table 3.1: Equilibrium Constants of 4'OH (2×10^{-5} M).

pK_a'	pK_a''	pK_a'''	$pK_a^{\wedge}$	$pK_a^{\wedge\wedge}$	$pK_a^{\wedge\wedge\wedge}$	pK_a	$K_h(M)$
3.3[b]	8.1	9.25	4.4	8.6	9.5	4.8	1.4×10^{-5}M
K_t	K_i	pK_{B/B^-}	$pK_{B^-/B^{-2}}$	pK_{Cc/Cc^-}	$pK_{Cc^-/Cc^{-2}}$	pK_{Ct/Ct^-}	$pK_{Ct^-/Ct^{-2}}$
0.88	37[b]	8.95	9.8	8.1	9.5	8.1	9.5

[a] Estimated error 10%. [b] Approximated values.

The pH-dependent absorption spectra of the model compound 4'-OH at the pseudo-equilibrium is shown in Figure 3.1a with the calculation of the $pK_a^{\wedge}$, $pK_a^{\wedge\wedge}$ and $pK_a^{\wedge\wedge\wedge}$ values. The absorption spectra in Figure 3.1a extended to high pH values shows the characteristic absorption spectrum of the flavylium cation (red line) at pH=1, the mixture of the neutral species in **CB$^{\wedge}$** is represented at pH=6.2 (blue line), with a huge absorption of the quinoidal base. The spectrum close to pH=9 represent a mixture of the neutral, mono deprotonated and di-deprotonated species (purple line), while at pH=12 (green line), the absorption is attributed mainly to **Ct^{2-}** with a small contribution of **B^{2-}** the unique species in the **CB$^{\wedge 2-}$**, see Scheme 3.2. The mole fraction distribution of the **AH$^+$**, **CB$^{\wedge}$**, **CB$^{\wedge -}$** and **CB$^{\wedge 2-}$** species shown in Figure 3.1b is obtained by the equations A.21, B.1, B.2, and B.3 respectively.

The mole fraction distribution can be obtained using the set of equations expressed in terms of equilibrium constants (from the kinetics tracking after a direct and reverse pH jumps),[22] or using the equations in Appendix B to obtain the mole fractions directly from the a_n, b_n, and c_n coefficients after a reverse pH jump from the pseudo-equilibrium. Not

only the equilibrium but also the kinetic constants are obtained from the first method. However, the second method is simpler, and the mole fractions are calculated with great accuracy. To obtain the specific amount of all the species, a series of reverse pH jumps to pH=1 are performed at different pH values once the pseudo-equilibrium is achieved. The kinetics must be followed in a stopped-flow apparatus due to the fast kinetics at this pH (see Chapter 1). Two examples of the traces obtained at pH=6.45 and pH=8.86 are shown in Figure 3.2. The first example shows the trace of the **AH⁺** formation kinetics after the jump, the amount of the species in **CB**$^{\wedge}$ can be then calculated obtaining the normalized amplitudes after every exponential process. The second example in Figure 3.2b represents the **AH⁺** formation kinetics as a result of the conversion of a mixture of the neutral, mono deprotonated and di-deprotonated species into it. In this last case, it is impossible to separate the deprotonated contribution from the neutral species; this because the proton transfer occurs in the microseconds time-scale. Nevertheless, it is possible to decompose the molar fractions of the species in the **CB**$^{\wedge}$, **CB**$^{\wedge-}$ and **CB**$^{\wedge 2-}$ using the already calculated $pK_a^{\wedge}$, $pK_a^{\wedge\wedge}$ and $pK_a^{\wedge\wedge\wedge}$ values and the set of equations included in the Appendix B. The fitting of the normalized data obtained from the reverse pH jumps at different pH values leads to calculate the coefficients a_n, b_n, and c_n (Figure 3.2c). These coefficients are the normalized amplitudes of the quinoidal base (and its deprotonated species), the hemiketal (and its deprotonated species), and *cis*-chalcone (and its deprotonated species), respectively. The normalized amplitudes are coincident with the mole fraction of the respective species. Once obtained the coefficients, all the equilibrium constants are accessible following the equations in Appendix B (See Table 3.1). The fitting in Figure 3.2c was achieved using $a_0 = 0.36$, $b_0 = 0.34$, $b_1 = 0.15$, $b_2 = 0.08$, $c_0 = 0.3$, $c_1 = 0.85$, and $c_2 = 0.92$.

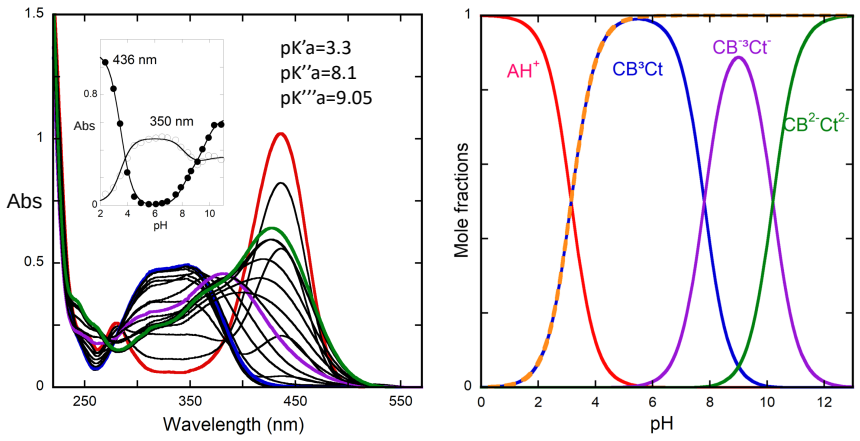

Figure 3.3: a) Equilibrium absorption spectra of the 4'OH (2×10^{-5}M) at different pH values. b) Mole fraction distribution of the species **AH⁺**, **CB**, **CB⁻** and **CB²⁻**, represented by the equilibrium between **AH⁺** and the *trans*-chalcone species.

The data obtained from the reverse pH jumps from the pseudo-equilibrium are equally

valid if some **Ct** was already formed, because the only effect is to reduce the amplitudes in the $\mathbf{AH^+}$ formation, but not their normalized values. When the true equilibrium is already achieved and the amount of **Ct** want to be calculated, a reverse pH jump followed by common spectrometer is performed. Similar to the pseudo-equilibrium, the mole fractions of the species $\mathbf{AH^+}$, **CB**, $\mathbf{CB^-}$ and $\mathbf{CB^{2-}}$ in the equilibrium can be obtained. Despite the equilibrium of 4'OH is extremely slow,[72, 193] the prediction that could take years was re-evaluated since the fact that the *cis-trans* isomerization is catalyzed in extremely acidic values.[193] Figure 3.3 shows absorption spectra of the 4'OH at the equilibrium; this state is mainly an equilibrium between the $\mathbf{AH^+}$ and the **Ct** species along all the pH scale. Due the extremely slow *cis-trans* isomerization at pH=1, the $pK'_a = 3.3$ value is an estimation. For higher pH values, the equilibrium is reached in several days for $pK''_a = 8.1$ and $pK'''_a = 9.25$. Once calculated these values, the $K_i = 37$ can be easily obtained from the expression $K'_a - K^{\wedge}_a = K_h K_t K_i$, for their part, the $K_{Ct/Ct^-} = 8.5 \times 10^{-9}$ and $K_{Ct^-/Ct^{2-}} = 5.7 \times 10^{-10}$ values were obtained following the equations in Appendix B.

3.1.2 Association between the chromophore with the co-pigment

A parameter to consider when the co-pigmentation is studied is the thermodynamic binding constant, which measures the affinity of each of the flavylium multi-state species with the co-pigment, the greatest the binding constant the higher affinity. The interaction of $\mathbf{AH^+}$ in 4'OH with the co-pigment (stoichiometry 1:1) can be calculated following the titration of equilibrated solutions with increasing concentrations of the co-pigment by UV-Vis spectroscopy at pH=1, where $\mathbf{AH^+}$ is the unique species (see Figure 3.4a). The obtained association constant $K_{AH^+CP} = 18M^{-1}$ was calculated through the fitting of A_f and K_{AH^+CP} with the data obtained from Figure 3.4a using the equation C.45 from Appendix C. The same procedure can be applied to calculate the association constant with **Ct** in equilibrated solutions at pH=6, where the chalcone is the unique species ($K_{Ct+CP} = 47M^{-1}$, see Figure 3.4b. This procedure is only applicable in **Ct** for compounds with high *cis-trans* isomerization barrier.

On the other hand, the titration of the $\mathbf{AH^+}$ in the Oenin was similarly performed, and its respective association constant calculated, see Figure 3.4c. All the calculations were made for 1:1 complexation, but in the case of the $\mathbf{AH^+}$-CP interaction in the Oenin, the system is not strictly 1:1, as can be observed in the inset of Figure 3.4c where the isosbestic point is lost at higher CP concentrations. Despite this, the 1:1 stoichiometry has a good fitting approximation with a constant of $134M^{-1}$. The association constants calculation for **A**, **B**, and **Cc** species is explained in the next subsection.

Table 3.2 summarizes the association constants of some anthocyanins with caffeine obtained in this work and reported in literature.[17, 35, 190, 194] The mathematical model described in Appendix C is deduced for a 1:1 assumed complexation, the co-pigmentation constant reported for the malvin in Table 3.2 was also calculated with this assumption.

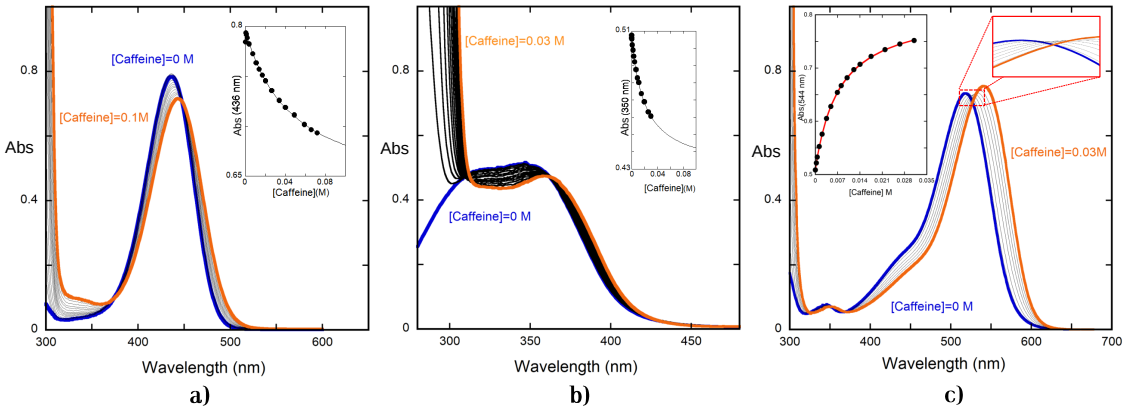

Figure 3.4: a) Spectral variation of the model compound 4'OH (1.8×10^{-5}M) in the consecutive increase in the concentration of caffeine (absorption in the UV zone) at pH=1; $K_{AH^+CP} = 18M^{-1}$. b) The same as in a) but at pH=6.0; $K_{CtCP} = 47M^{-1}$. c) Spectral variations of Oenin (1.7×10^{-5}M) at pH=1 as a function of caffeine addition; $K_{AH^+CP} = 134M^{-1}$.

Table 3.2: Co-pigmentation constants (M^{-1}) of some flavylium-based compounds with caffeine[a].

Compound	K_{AH^+CP}	K_{ACP}	K_{A^-CP}	K_{BCP}	K_{B^-CP}	K_{CcCP}	K_{Cc^-CP}	K_{CtCP}	K_{Ct^-CP}
4'OH	18	134		13	9	42	44	47	94
Oenin	134	303	43	0	0	17	0		
Malvin[188]	125	180							
Cyanidin-3G[190]	161[b]								
	21[c]								

[a] Estimated error 10%. [b] 1:1 stoichiometry. [c] 1:2 stoichiometry.

However, it is known from the literature that in anthocyanins, this requirement is not strictly observed.[17, 190] The mathematical approach described in Appendix C, just like other models published, does not take into account the self-association of the anthocyanin. However, this phenomenon is minimized by the low anthocyanin concentrations used.

As observed in Table 3.2, the higher association constants with caffeine are observed in anthocyanins. In the Oenin case, the caffeine affinity for the quinoidal base and the flavylium cation species is considerably higher than for the uncolored species, being the interaction with the last practically nil. For 4'OH, the same effect is observed over the quinoidal base, but the affinity to the uncolored species is higher than for the **AH$^+$**. The caffeine association constant is difficult to predict in flavylium-based compounds because it depends on different factors, as structure, spatial conformation, intermolecular interactions, etc.

3.1.3 Effect of the caffeine in the equilibrium constants

The pH-dependent absorption spectra of the 4'OH in the presence of caffeine at the pseudo-equilibrium are shown in Figure 3.5a, the fitting of the absorption at different wavelengths

along the pH scale defines $pK^{\wedge}_{a(CP)} = 4.1$, $pK^{\wedge\wedge}_{a(CP)} = 8.8$, and $pK^{\wedge\wedge\wedge}_{a(CP)} = 9.1$. The absorption spectra in Figure 3.5a is similar to those in Figure 3.1a, but the absorption of the quinoidal base is clearly higher in the presence of the caffeine. The mole fraction distribution of the **AH⁺**, **CB^**, **CB^⁻** and **CB^2⁻** species is represented in Figure 3.5b.

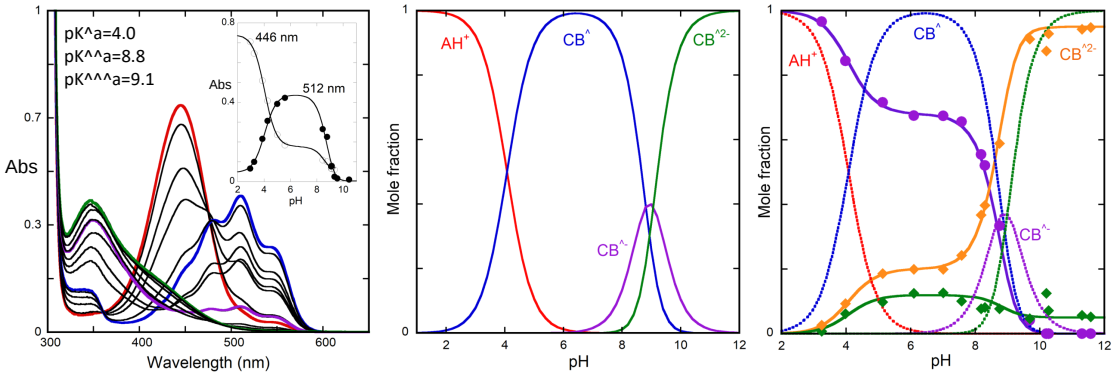

Figure 3.5: a) Spectral variation of 4'OH (1.8×10^{-5}M) at the pseudo-equilibrium in the presence of caffeine (0.058 M) extended to the entire pH range, fitting in inset was achieved for $pK^{\wedge}_{aCP} = 4.0$, $pK^{\wedge\wedge}_{aCP} = 8.8$ and $pK^{\wedge\wedge\wedge}_{aCP} = 9.1$. b) Mole fraction distribution of the species **AH⁺**, **CB^**, **CB^⁻** and **CB^2⁻** at the pseudo-equilibrium. c) Mole fraction distribution of the species in 4'OH in the presence of caffeine at pseudo-equilibrium; **AH⁺** plus **A** (violet), **B** and **B⁻** (green), and **Ct**, **Ct⁻** and **Ct²⁻** species (orange) Fitting was achieved with a_0=0.68, b_0=0.12, b_1=0.07, b_2=0.05, c_0=0.2, c_1=0.93, and c_2=0.95.

The reverse pH jumps of the solutions in Figure 3.5a were performed, the same procedure used before to calculate all the equilibrium constants was applied, but with the difference that the complexes formed between each flavylium multi-state species, and the co-pigment are included in the system. The mathematical model that provides for these complexes is presented in Appendix C. The representation of the three amplitudes obtained at different pH values after the reverse pH jumps is shown in Figure 3.5c, and the respective equilibrium constants presented in Table 3.3. It is worth to note that the experimentally obtained association constant $K_{AH^+CP} = 18$ and the equilibrium constants of this compound in the absence of caffeine were used to calculate the association constant with **A** ($K_{A^+CP} = 134$) using the equation C.25. Regarding the association constants for the other flavylium multi-state species, the rest of the equations from Appendix C were applied. In this way, the association and co-pigmentation equilibrium constants of the system except those of *trans*-chalcone can be calculated, see Tables 3.2 and 3.3. Comparing the molar fractions in the pseudo-equilibrium for the 4'OH in the absence and presence of caffeine in Figure 3.2c and 3.5c respectively shows a clear high interaction of the quinoidal base with the co-pigment, which is stabilized.

The equilibrium of 4'OH in presence of caffeine absorption spectra at representative

Table 3.3: Equilibrium Constants of 4'OH (1.8×10^{-5} M) in the presence of caffeine (0.058 M)[a].

pK'_{aCP}	pK''_{aCP}	pK'''_{aCP}	$pK^{\wedge}_{aCP}$	$pK^{\wedge\wedge}_{aCP}$	$pK^{\wedge\wedge\wedge}_{aCP}$
3.15[b]	7.8	10.2	4.0	8.8	10.5
pK_{aCP}	$K_{hCP}(M)$	K_{tCP}	K_{iCP}	pK_{BCP/B^-CP}	pK_{CcCP/Cc^-CP}
4.2	1.2×10^{-5}	1.66	37[b]	9.1	8.1

[a] Estimated error 10%. [b] Estimated value.

pH values, together with the respective mole fraction distribution of the species **AH$^+$**, **CB**, **CB$^-$** and **CB^{2-}** species is represented in Figure 3.6. The three inflection points when the absorbance is represented as function of pH give the equilibrium constants $pK'_a = 3.15$, $pK''_a = 7.8$, and $pK'''_a = 10.2$. Comparing the data in Figure 3.3 with Figure 3.6, **CB**, **CB$^-$** and **CB^{2-}** are practically equal to the mole fraction of the **Ct** species, but in the presence of caffeine there is a significant amount of **A**. This effect demonstrate that the K_{A^+CP} value is sufficiently strong to shift the equilibrium from **Ct** to **A**.

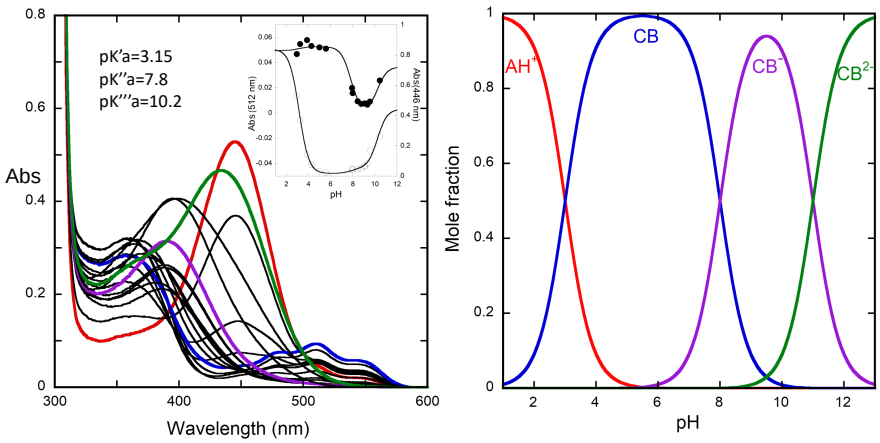

a) **b)**

Figure 3.6: a) Spectral variation of 4'OH (1.8×10^{-5}M) in the presence of caffeine (0.058 M) at the equilibrium, fitting in inset was achieved for $pK'_{aCP} = 3.15$, $pK''_{aCP} = 7.8$ and $pK'''_{aCP} = 10.2$. b) Mole fraction distribution of the species **AH$^+$**, **CB**, **CB$^-$** and **CB^{2-}** at the equilibrium.

The generalization of the method described in Appendix C to the equilibrium, including **Ct** species, is straightforward with:

$$K_{a(CP)} = \frac{K'_a(CP)}{1 + K_{AH^+CP}[CP]} \tag{3.1}$$

and

$$K'_a(CP) = K'_a + (K_{ACP}K_a + K_{BCP}K_h + K_{CcCP}K_hK_t + K_{CtCP}K_hK_tK_i)[CP]$$
$$K'_a(CP) = K^{\wedge}_a + (K_{ACP}K_a + K_{BCP}K_h + K_{CcCP}K_hK_t)[CP] + K_hK_tK_i + K_{CtCP}K_hK_tK_i)[CP] \quad (3.2)$$

$$K'_a(CP) = K^{\wedge}_a(CP) + K_hK_tK_i(1 + K_{CtCP})[CP] \quad (3.3)$$

considering that $K'_a(CP)$ is an experimental value, and the parameter $K^{\wedge}_a(CP)$ is obtained because all the association constants of the species in the pseudo-equilibrium was previously calculated in Figure 3.4 and applying the set of equations in Appendix C, eq. 3.3 permits the calculation of K_{CtCP} included in Table 3.2.

The Oenin molar fraction distribution in the presence of caffeine was also calculated in the pseudo-equilibrium. The results are shown in Figure 3.7b. Comparison of the molar fractions in the presence and absence of caffeine in Figure 3.7, shows as for the 4'OH a stabilization of the quinoidal base, these results are supported by the high association constant of the **A** with the co-pigment, that is higher than the other species, see Table 3.2. The interaction of caffeine with the ionized species is negligible except for the ionized quinoidal base. Since there is no competition of the ionized quinoidal base in this pH range for the interaction with caffeine, the complex of the ionized quinoidal base is the dominant species, and the color of the solution around neutrality is essentially blue.

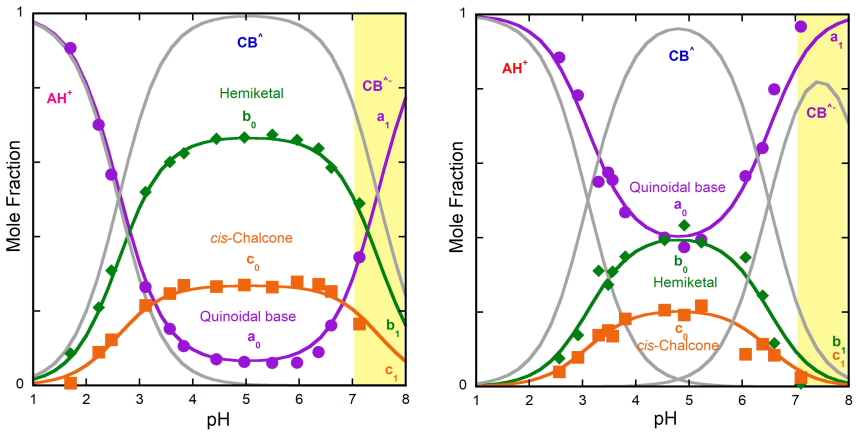

Figure 3.7: a) Mole fraction distribution of Oenin in the absence of caffeine obtained by reverse pH jumps from the pseudo-equilibrium. Fitting was achieved for a_0 = 0.06, b_0 = 0.67, and c_0 = 0.27 for the neutral species and a_1 = 1, b_1 = 0, and c_1 = 0. This last set of parameters regarding the ionized species is an estimation because of the slow decomposition processes. b) The same as in a) but with in the presence of the co-pigment (0.058 M), a_0 = 0.42, b_0 = 0.38, and c_0 = 0.2 for the neutral species and a_1 = 1, b_1 = 0, and c_1 = 0.

Table 3.4: Equilibrium Constants of Oenin (1.8×10^{-5} M) in the presence and absence of caffeine (0.053 M)[a].

Sample	pK'_a	pK''_a	$pK^{\wedge}_a$	$pK^{\wedge\wedge}_a$	pK_a	$K_h(M)$	K_t	K_i
Oenin	2.38[b]	6.4	2.6	7.5	3.8	1.7×10^{-3}	0.4	0.45[b]
Oenin-Caff	3.0[b]	6.4	3.1	6.4	3.5	3×10^{-4}	0.5	1.5[b]

[a] Estimated error 10%. [b] Estimated value.

In the case of the anthocyanin compound, the Oenin, the same method applied for the caffeine co-pigmentation with the 4'OH, was used. Like other natural anthocyanins as cyanidin-3-glucoside, the hydration rate is slower than the isomerization in the range between pH=7-9,[190] and the kinetics are represented by a mono-exponential (hydration control, see Chapter 1). Moreover, for equilibrated solutions up to pH=7, the molar fractions could not be calculated because some decomposition occurs. In solutions down pH=6, the kinetics are described by a bi-exponential process. The equilibrium constants were determined following the well-established procedure [22, 75] and for comparison purposes using the method of the reverse pH jumps used before for the 4'OH (see Figure 3.7)a. The fitting in Figure 3.7a was achieved using a_0=0.06, b_0=0.67, c_0=0.27 for the neutral species and a_1=1, b_1=0, c_1=0 (with a high error because of the decomposition of the anthocyanin at these pH values). The calculated equilibrium constants are reported in Table 3.4. These values are in good agreement with those previously reported except for the K_t, that in case of the Oenin and other monoglucosides has some uncertainly.[17] The value reported in Table 3.4 was obtained after 13 different measurements in the pH range of the **CB** species.

The interaction of some anthocyanins with caffeine was previously reported in the literature. Table 3.2 shows these data and the constants obtained for the Oenin using the method in Appendix C. According to Figure 3.7 and Table 3.2, the colored species of Oenin are those interacting strongly with caffeine, and the more significant co-pigmentation effect takes place mainly with the quinoidal base, as also observed for the 4'OH. The caffeine interaction with the other flavylium multi-state species is negligible except for the ionized quinoidal base. The stabilization effect of the co-pigment with the $\mathbf{A^-}$ species at pH values higher than pH=7 produces a stable blue colored solution until the degradation occurs. On the other hand, the **A** species is also stabilized, and the solutions with pH values close to neutrality keep their violet color at the equilibrium.

3.2 Anthocyanin color stabilization by intermolecular interactions in SDS micelles

.

Natural dyes for industrial applications, namely as in food and cosmetic products, have been very attractive in the last decade. This is because of their association with favorable

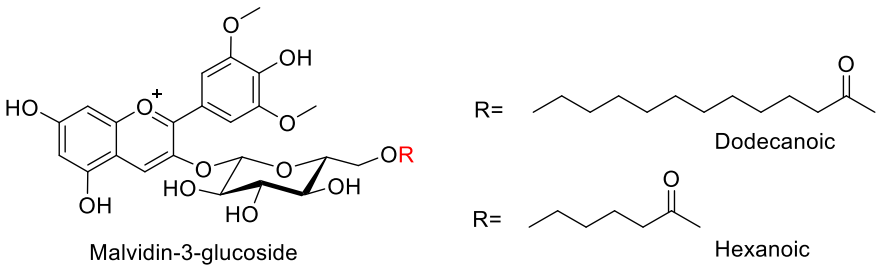

Scheme 3.3: Molecular structure of the Malvidin-3-glucoside (Oenin) fatty acid conjugates. Derived from the dodecanoic (1) and hexanoic (2) acids.

organoleptic properties and health-promoting effects in foods. However, in anthocyanins, the pH-dependence color variation and hydrophilic character constitute a major drawback for applications mainly in lipophilic matrices. To overcome the incorporation of some flavonoids into lipophilic mediums, their functionalization by alkylation and acylation of carbons and hydroxyl groups with hydrophobic molecules such as fatty acids has been reported.[195] Specifically, a series of anthocyanin-fatty acid conjugates with a variable chain length from C4 to C16 have been already synthesized.[196] Some of these compounds have already demonstrated superior antioxidant activity and lipophilic properties rather than their anthocyanin precursors, without altering their chromatic features.[196, 197] The incorporation of the anthocyanin-fatty acid conjugates in cosmetic formulations becomes an interesting activity because of these results. For future technological applications in cosmetics, the study of the color stability, and the possibility to obtain different attractive colors from the flavylium cation and quinoidal base species along the pH scale becomes very important. It is well known that the anthocyanins colors are generally unstable at moderate to neutral pH values, this because the proportion of quinoidal base in the equilibrium is low.

The solubility of the anthocyanin-fatty acid derivatives is limited in pure water, but they can be studied in aqueous solutions of sodium dodecyl sulfate (SDS) micelles, which also mimics potential lipophilic formulations. Moreover, the fatty acid residues could allow co-micellization with SDS because of their affinity to the hydrophobic core in SDS micelles. The SDS micelles has been used to extend the solubility and the pH stability of the anthocyanin $\mathbf{AH^+}$ form.[106, 108] The results obtained from these publications demonstrate an extension domain of the red flavylium cation along the pH scale, the mole fraction of the quinoidal base in moderately acidic to neutral pH values is also increased up to 20%.

The stability of two anthocyanin-fatty acid conjugates, derived from the Oenin and the dodecanoic and hexanoic fatty acids (Scheme 3.3) was studied in the presence of SDS micelles along the pH scale. The flavylium multi-state equilibrium and kinetic constants were calculated, and the co-micellization effect over properties of the malvidin-3-glucoside multi-state is also addressed in this subsection.

3.2.1 Water solubility of anthocyanin-fatty acid conjugates

Both compounds **1** and **2**, Scheme 3.3, are moderately water-soluble, but they are readily solubilized in micro heterogeneous systems as SDS micelles. The fully soluble pigment solutions were achieved for SDS concentrations in the millimolar range, while for more diluted surfactant solutions, complete solubilization was not observed (even after sonication). The UV-Vis spectra of solutions with compounds **1** and **2** and different SDS concentrations were obtained after 18h of incubation in the dark at room temperature are showed in Figure 3.8. An abrupt increase in the absorption intensity is observed at concentrations above 2×10^{-4} M of SDS. The critical micelle concentration (CMC) of SDS in the dye presence can be taken from the inflection point of the absorption intensity (538 nm) versus SDS concentration plots. The CMC of SDS in the presence of the dyes (7×10^{-4} M for compound **1** and 8×10^{-4} M for compound **2**) are one order of magnitude lower than the value obtained for SDS in pure water (8×10^{-3} M), this effect can be attributed to the presence of 0.1 M HCl because it is known that electrolytes in the solutions decrease the CMC of ionic surfactants.[198]. However, it is worth to note that the oppositely charged lipophilic pigments can also contribute to the formation of micelles at lower concentrations (co-micellization).[199] Compounds **1** and **2** are completely solubilized in 0.01 M of SDS (Figure 3.8).

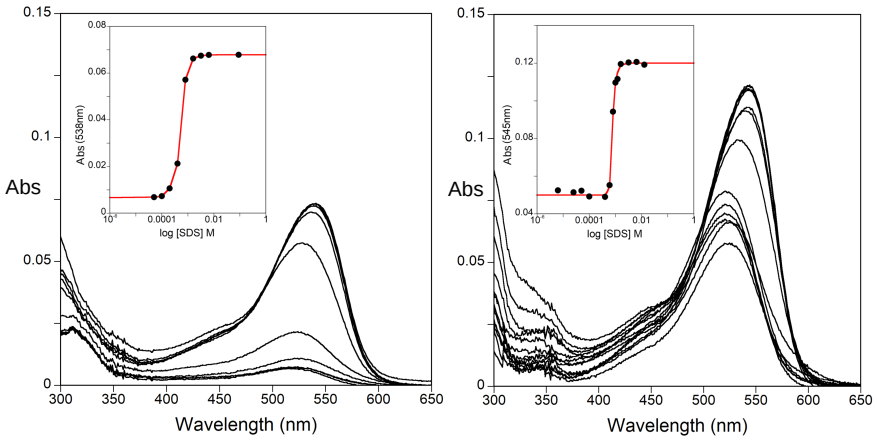

a) **b)**

Figure 3.8: Absorption spectra of a) compound **1** (4.5×10^{-6} M) and b) compound **2** (4.7×10^{-6} M) in water at pH=1.0 with increasing concentrations of SDS. The anthocyanin derivative is not fully soluble at low SDS concentrations which solubilize close to the surfactant CMC.

3.2.2 Equilibrium and kinetic constants

After a direct pH jump from pH=1 to higher pH values, the reaction network is similar to the one described for the Oenin in Scheme 1.2. The pH-dependant reaction networks of both compounds were completely characterized in 0.1 M SDS. The spectral variations observed immediately 10 ms after the direct pH jump observed by stopped flow for compound **1** are

reported in Figure 3.9a, the fitting observed in the inset indicates a $pK_a = 6.0$. The pseudo-equilibrium and the equilibrium absorption spectra are shown in Figures 3.9b and 3.9c with $pK_a^{\wedge} = 5.75$ and $pK_a' = 5.65$ respectively. In the same vein, the $pK_a = 6.1$, $pK_a^{\wedge} = 5.9$ and $pK_a' = 5.7$ values for compound **2** are reported in Figure 3.10.

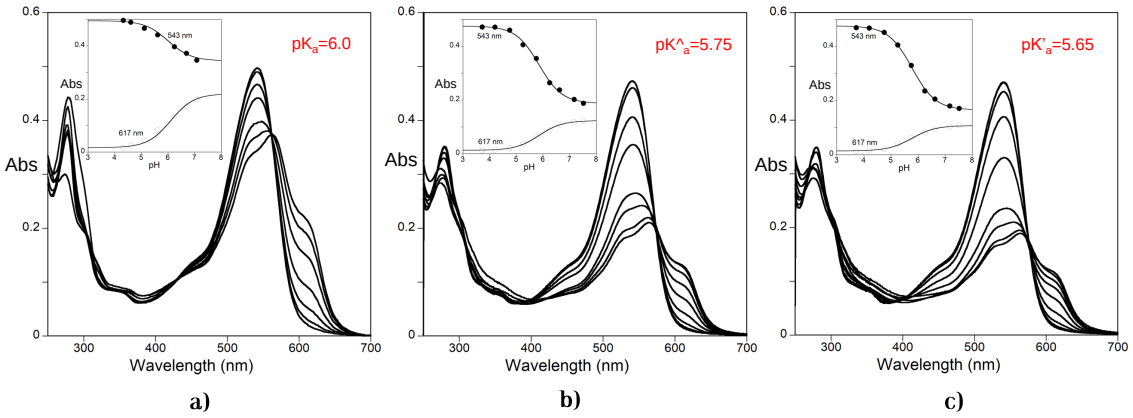

Figure 3.9: a) Spectral variations of compound **1** (3.1×10^{-5} M) in the presence of SDS micelles (0.1M) taken 10 ms after a direct pH jump to different pH values, b) the same at the pseudo-equilibrium, c) the same at the equilibrium.

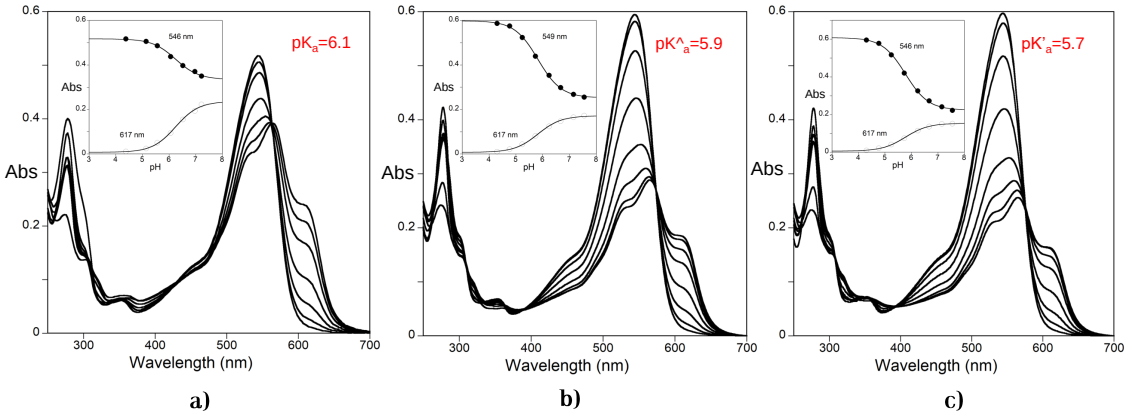

Figure 3.10: a) Spectral variations of compound **2** (2.2×10^{-5} M) in the presence of SDS micelles (0.1M) taken 10 ms after a direct pH jump to different pH values, b) the same at the pseudo-equilibrium, c) the same at the equilibrium.

A typical kinetic bi-exponential process (hydration and isomerization controlled) of a direct pH jump to pH=7.5 in compound **1** is shown in Figure 3.11a. The slowest step is represented at different pH values in Figure 3.11b and Figure 3.11c for the compound **1** and **2** respectively. Fitting was achieved using the equation 1.16 with $K_h K_t k_i = 1.7 \times 10^{-11}$ Ms^{-1}, $pK_a^{\wedge} = 5.75$ and $k_{-i} = 3.5 \times 10^{-5}$ s^{-1} for compound **1** and $K_h K_t k_i = 2.8 \times 10^{-11}$ Ms^{-1}, $pK_a^{\wedge} = 5.9$ and $k_{-i} = 2.7 \times 10^{-5}$ s^{-1} for compound **2**.

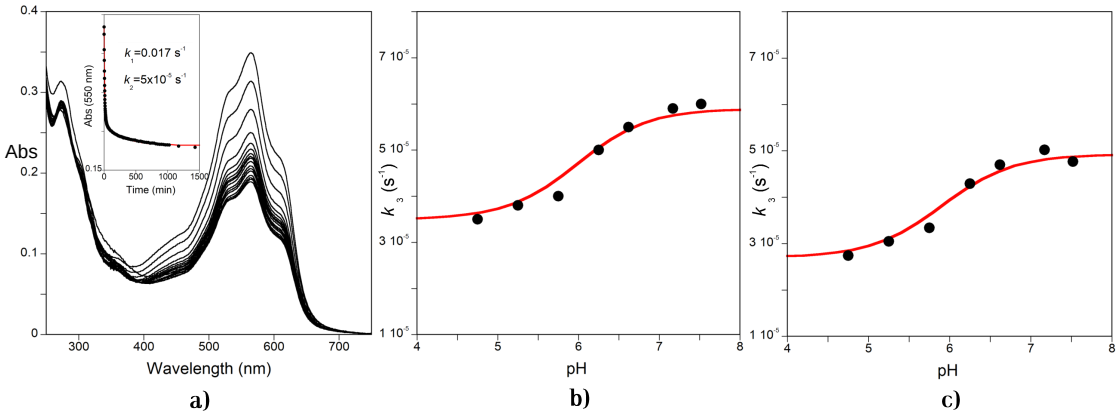

Figure 3.11: a) Spectral variations of compound **1** (3.1×10^{-5} M) in the presence of SDS micelles (0.1M) after a direct pH jump to pH=7.5. Representation of the isomerization constants along the pH scale in b) compound 1 and c) compound 2.

A series of reverse pH jumps monitored by stopped flow from equilibrated solutions was carried out, a typical trace after the reverse pH jump from pH=4.2 to 7.2 followed by stopped flow at 542nm is shown in Figure 3.12a. Figures 3.12b and 3.12c represents the hydration and tautomerization (inset) processes to different pH values for compound **1** and **2** respectively. These data are obtained from the first and second exponential processes in the reverse pH jumps. Fitting was achieved with equation 1.18 for the hydration and with equation 1.19 for the tautomerization process. The hydration process was fitted for $pK_a = 6.0$, $k_h = 0.02s^{-1}$ and $k{-}h = 4 \times 10^4 M^{-1}s^{-1}$ in compound **1** and $pK_a = 6.1$, $k_h = 0.02s^{-1}$ and $k{-}h = 6 \times 10^4 M^{-1}s^{-1}$ in compound **2**. The tautomerization was fitted with $k_{-t} = 0.016$ and $k^H_{-t} = 4000 M^{-1}s^{-1}$ for compound **1** and $k_{-t} = 0.002$ and $k^H_{-t} = 4000 M^{-1}s^{-1}$ for compound **2**.

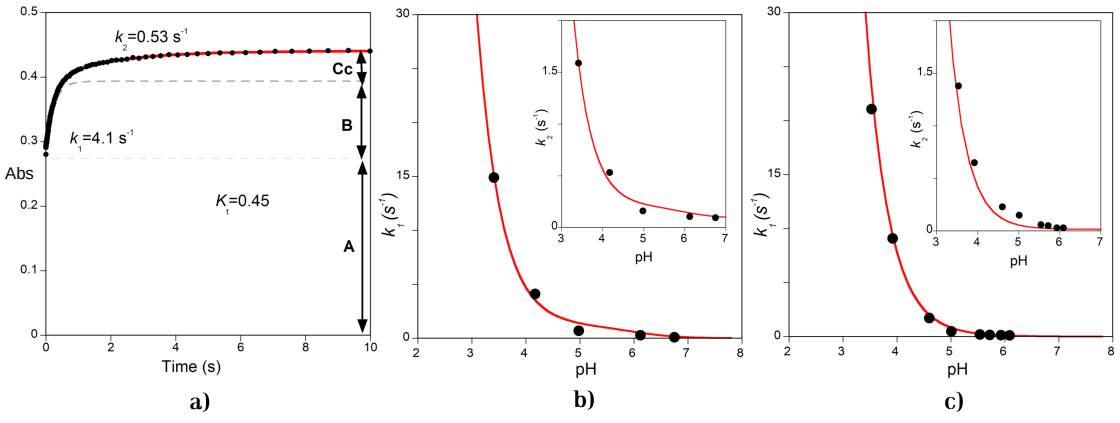

Figure 3.12: a) Kinetic trace of compound **1** after a reverse pH jump from pH=7.2 to 4.2 (0.1 M SDS) monitored by stopped flow, b) representation of hydration and tautomerization (inset) constants for compound **1**, c) the same for compound **2**.

The equilibrium and rate constants are reported in Table 3.5. Comparing the obtained

Table 3.5: Equilibrium and rate constants of compound **1** and **2** obtained from pH jumps in the presence of SDS 0.1 M.[a]

Compound	pK'_a	pK_a	$pK^{\wedge}_a$	$K_h(M)$	K_t	K_i
1	5.65	6.0	5.75	5×10^{-7}	0.5	2
2	5.7	6.1	5.9	3.3×10^{-7}	0.6	4
Oenin[82]	2.3	3.8	2.4	3.4×10^{-3}	0.12	
	$k_h(s^{-1})$	$k_{-h}(M^{-1}s^{-1})$	$k_t(s^{-1})$	$k_{-t}(s^{-1})$	$k_i(s^{-1})$	$k_{-i}(s^{-1})$
1	0.02	4×10^4	0.008	0.016	6.8×10^{-5}	3.5×10^{-5}
2	0.02	6×10^4	0.012	0.02	1.1×10^{-4}	2.9×10^{-5}
Oenin[82]	0.12	35	0.06	0.5		

[a] Estimated error 10%.

constants for compounds **1** and **2** with the Oenin in the absence of SDS micelles[82] puts in evidence that the flavylium species is greatly stabilized in the presence of the anionic self-assembled aggregates as previously reported.[82, 108]. This behavior can be attributed to the micellar interface anionic nature with attractive interactions with the cationic flavylium and/or to the increase in the local concentrations of H^+ at the same interface, with an increase in the local acidity on the micelle surface.[200] The most remarkable differences in the kinetic parameters in Table 3.5 concerning Oenin in water is found for the hydration reaction. While k_h is about 6 times lower for compound **1** in SDS micelles compared with the Oenin in water (0.02 vs 0.12 s^{-1}), the k_{-h} is larger by 3 orders of magnitude (4×10^4 vs 35 $M^{-1}s^{-1}$). The stabilization of $\mathbf{AH^+}$ in SDS micelles is reflected by the equilibrium constant K_h lower by four orders of magnitude (5×10^{-7} vs $3.4\times10^{-3}M$). Thus, assuming the same transition state for hydration and de-hydration elemental reaction, it would be difficult to explain the observed difference only based on the destabilization of the hemiketal in SDS micelles. The most likely explanation for this apparent k_{-h} lies in a significant increase in the local concentration of H^+ at the micelle surface (see Scheme3.4) which greatly differs from the bulk pH values used to obtain k_{-h} and suggests that this effect dominates the stabilization of flavylium species in this medium.

The mole fraction distribution of the Oenin in the absence of SDS micelles[82] is compared in Figure 3.13 with the Oenin in the presence of SDS (0.1 M) and compound **1** in SDS micelles (0.1 M). SDS has a huge effect on the stabilization of the flavylium cation following the order $pK'_a = 2.3$; 5.4 and 5.65 respectively for Figures 3.13a, b, and c. When Oenin and compound **1** are compared, there is a significant increase in the mole fraction of **A** in the neutral region with a concomitant increase of the purple color. The mole fraction of the quinoidal base present at the equilibrium depends on the ratio of K_a/K'_a. If the quinoidal base is stabilized, the K_a increases, or if the other species are destabilized, the K'_a decreases. Noteworthy, the apparent increase in the mole fraction of **A** in compounds **1** and **2** not arise from an improved stabilization of this species because pK_a is practically the same for Oenin

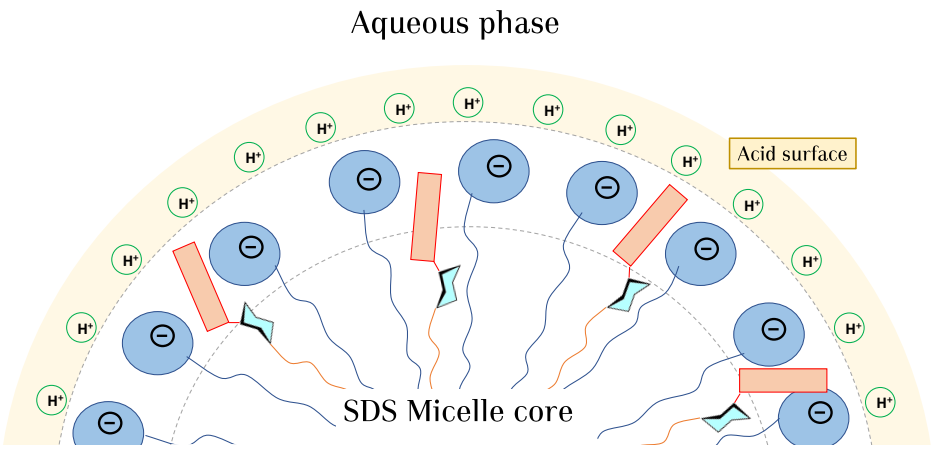

Scheme 3.4: Representation for the SDS micellar stabilization of the **AH⁺** form in compounds **1** and **2** by the increasing concentration of H^+ in the surface.

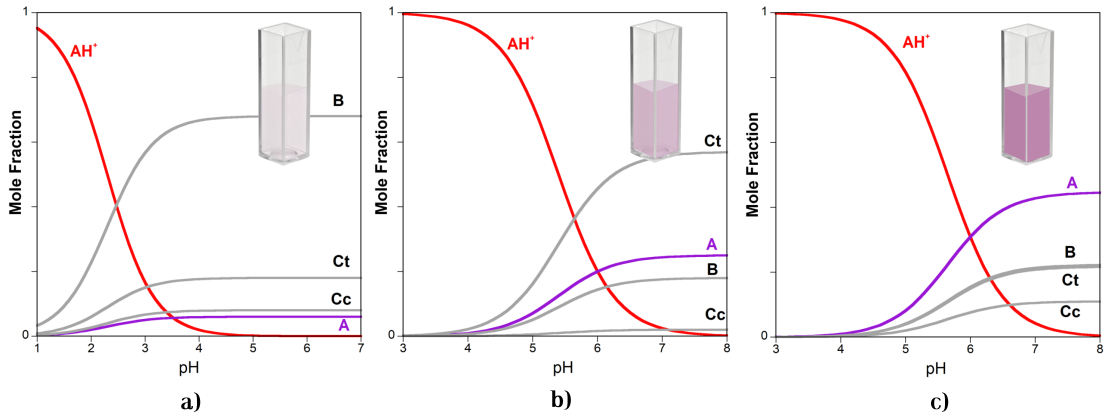

Figure 3.13: a) Mole fraction distribution of Oenin (2×10^{-5}) in the absence of SDS; b) the same in the presence of SDS 0.1 M; c) the same for the compound **1** (1.2×10^{-5}) in the presence of SDS 0.1 M.

in SDS micelles (pK_a=6).[106, 108] Conversely, in comparison with Oenin, the fatty acid chain affects the stability of **A** with respect to **AH⁺**. As seen in Figure 3.13, the **Ct** species is more stable in the Oenin than in the Oenin-fatty acids conjugates, and thus the high stability of the quinoidal base arises from a decrease in the stability of the **Ct** for the lipophilic pigments.

3.3 CB*n*-type molecular clips complexation for color stabilization

As has been described in subsection 1.6.3 the CB*n* molecules have high affinities (K_{ass} up to 10^{17} M^{-1}) and selectivity for cationic guests.[124] Also, some of them show high affinities for the complexation with flavylium derivatives with association constants of K_{ass}=10^6 to 10^7 M^{-1}.[180] The toxicity of CB[n] macrocycles and derivatives have been proven to be very

low in *in vivo* and *in vitro* tests.[201] Therefore, they are commonly used to encapsulate and protect water-insoluble pharmaceutical products.[202, 203, 204] Among the inconveniences in the use of CB*n* macrocycles are their low water solubility; only CB5 and CB7 have a considerable solubility in concentrations not higher than 30mM.[205] Their structural rigidity is also a disadvantage, limiting the size of the guest able to fit inside the cavity.[204] Although CB7 has a high affinity for the flavylium form in some derivatives,[129, 180] it is not a good alternative to host large compounds like the anthocyanins, exhibiting low association constants. To overcome the cavity limitations, specific acyclic CB*n*-type molecular clip receptors have been used for the complexation of organic compounds whose flexibility and high degrees of freedom allow to recognize large organic guests, mainly electron acceptor molecules.[204, 206, 207, 208]

Some functionalized belt-type and dimethylene-bridged molecular clips have been already tested in complexation with flavylium-based compounds.[143] These water-soluble clips formed stable complexes with the guests with large binding constants in methanol, but the complexes have a low solubility in water and therefore are not suitable for anthocyanins complexation. In this section, two water-soluble CB*n*-type molecular clips, CP1 and CP2, are tested as receptors for the flavylium-base compound 4',7 dihydroxiflavylium, and the Oenin (Figure 3.14). The association constants with the colored forms were calculated and the stability along the pH scale evaluated.

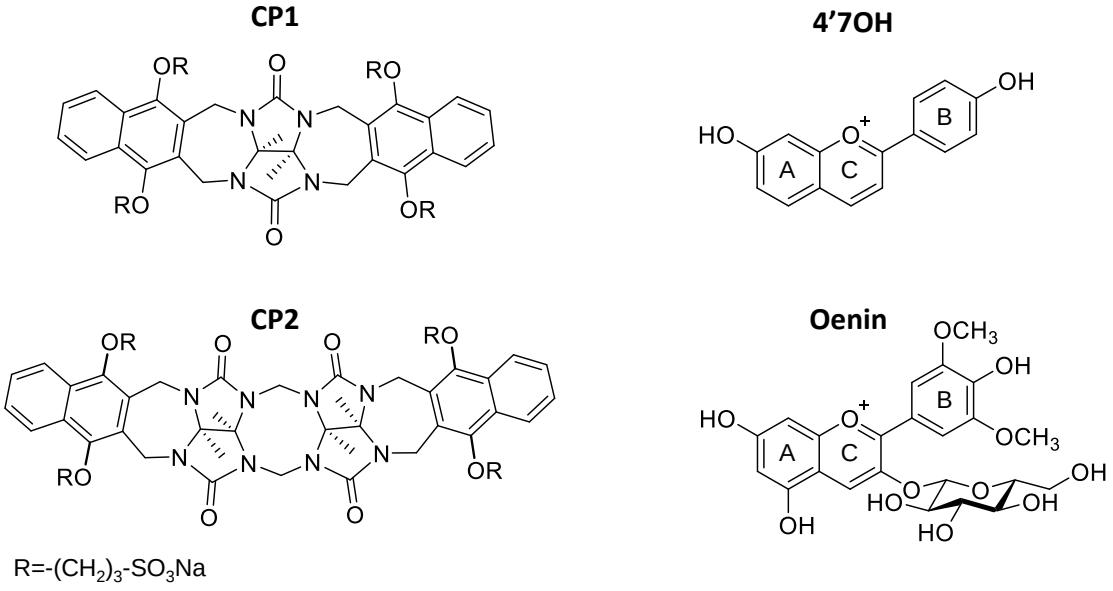

Figure 3.14: Structures of the CB*n*-type molecular clips **CP1** and **CP2** and the flavylium-base compounds 4',7 dihydroxiflavylium (4'7OH) and Oenin.

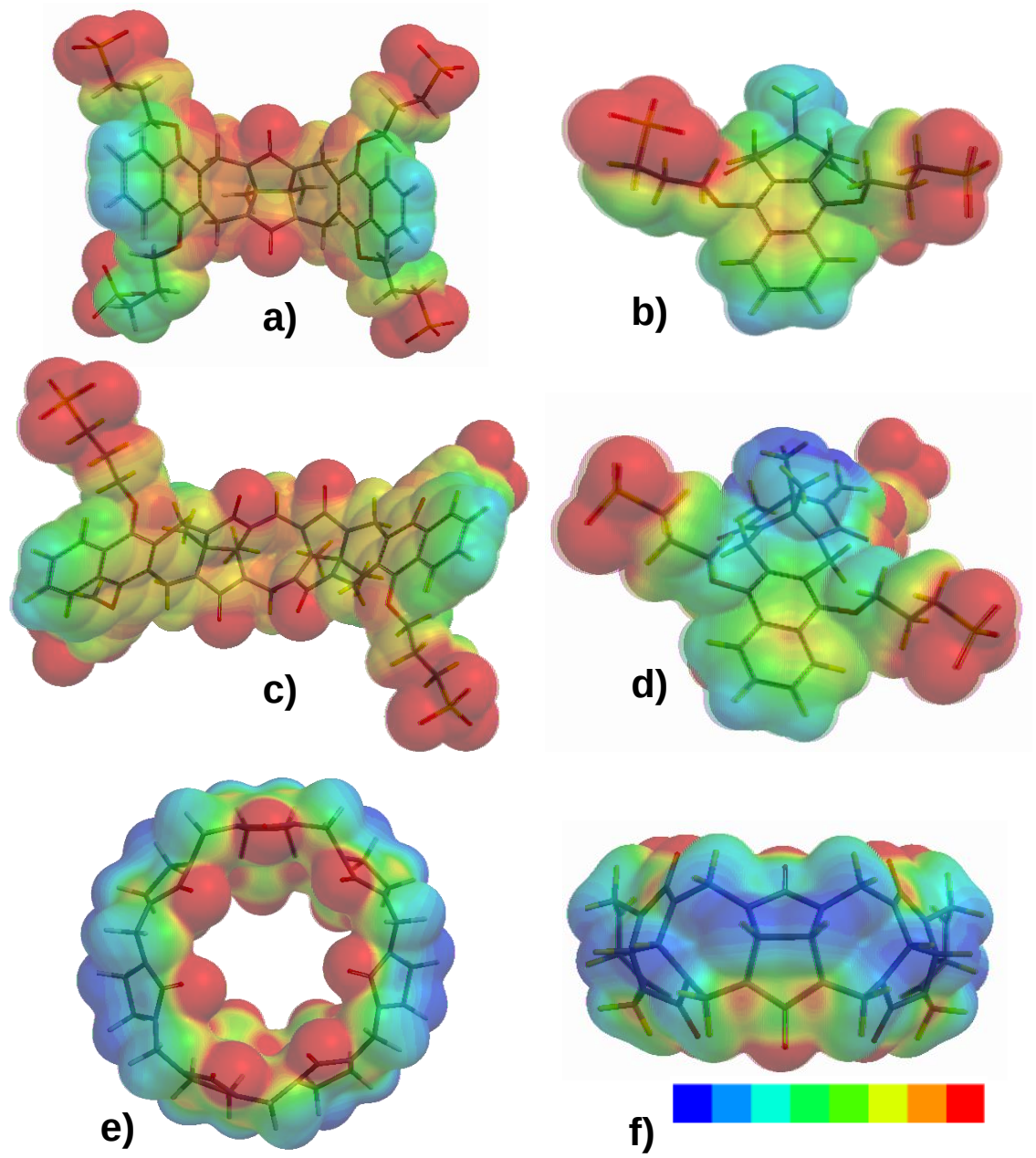

Figure 3.15: Representation of the three dimensional structure and Electrostatic Potential Surface (EPS) of the CB*n*-type molecular clips CP1 (a and b) and CP2 (c and d) and CB7 (e and f).

3.3.1 Description of the host and guest molecules

CP1 and CP2 molecular clips in Figure 3.14 comprise a central monomer, and a C-shaped methylene-bridged glycoluril dimer, respectively; this feature provides some of the characteristics of the CB[n] family. The dimethylglycoluril was the first alkyl-substituted glycoluril used for the synthesis of alkyl CB[n].[209] The methylene-bridged glycoluril dimer structure is the fundamental building block of the CB[n] family oligomers including the precursor

of the CP2. The general reaction mechanism for the formation of the dimer, oligomerization, and further formation of the Behrend's polymer to form the macrocycles and their derivatives was extensively studied by the groups of Issacs and Day[210, 211] and is always important to study after the synthesis of any CB*n*-type molecule. The reaction time, temperature, solvents, and concentration of reactants influence the formation of the dimer and its oligomerization. This dimer is produced after the condensation reaction between glycoluril and paraformaldehyde in concentrated HCl (see below).

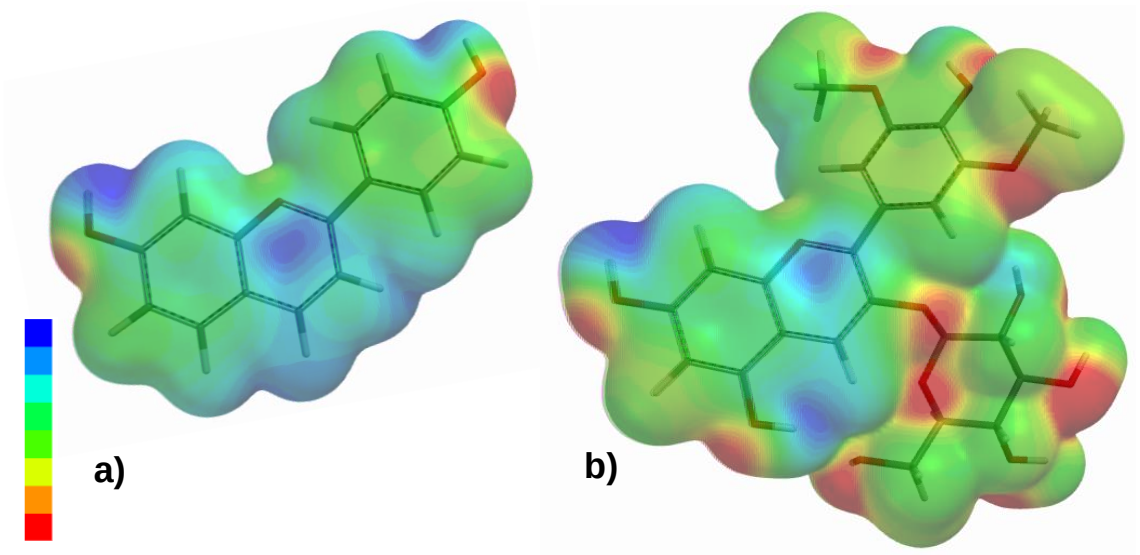

Figure 3.16: Representation of the three dimensional structure and Electrostatic Potential Surface (EPS) of the flavylium-based compounds 4'7OH and Oenin.

Both clips are also constructed with two dialkoxynaphtalene sidewalls and four sodium sulfonate groups to provide water solubility. The naphthalene sidewall molecular clips have demonstrated high degrees of association with cationic guests.[212] Figure 3.15 shows two views of the electrostatic potential surface of CP1 and CP2 in an AM1 model. Of course, the negative regions are centered in the four SO_3^- and on the ureidyl C=O groups. In contrast, the positive region is located in the clips' concave side (around the area of the CH_3 groups). Interestingly, the inner part of the sidewalls is provided by significantly higher negative electrostatic potential than the outer side (see Figure 3.15); these observations have been found in other clips with naphthalene sidewalls.[206, 212, 213] The study of some molecular clips based in glycoluril dimers have shown that they tend to undergo dimerization in both organic solvents and water.[214] However, the self-association of CP2 was already investigated, and it undergoes weak dimerization in water (K_s=6 M^{-1}); this because the unfavorable electrostatic interactions between the sulfonate groups.[208]

All the characteristics previously mentioned make both molecular clips suitable for their complexation with electron-poor cationic molecules. As can be observed in Figure 3.14,

the colored flavylium backbone structure comprises a cationic heterocyclic ring, commonly designed as C ring and other two aromatic rings (A and B). This electron-poor structure is suitable for complexation with both molecular clips. Figure 3.16 shows the electrostatic potential surface of the guest molecules; the electron-poor zones are distributed mainly around the C ring in both guests. Hence this part of the molecule is a candidate to be linked to the clip cavity.

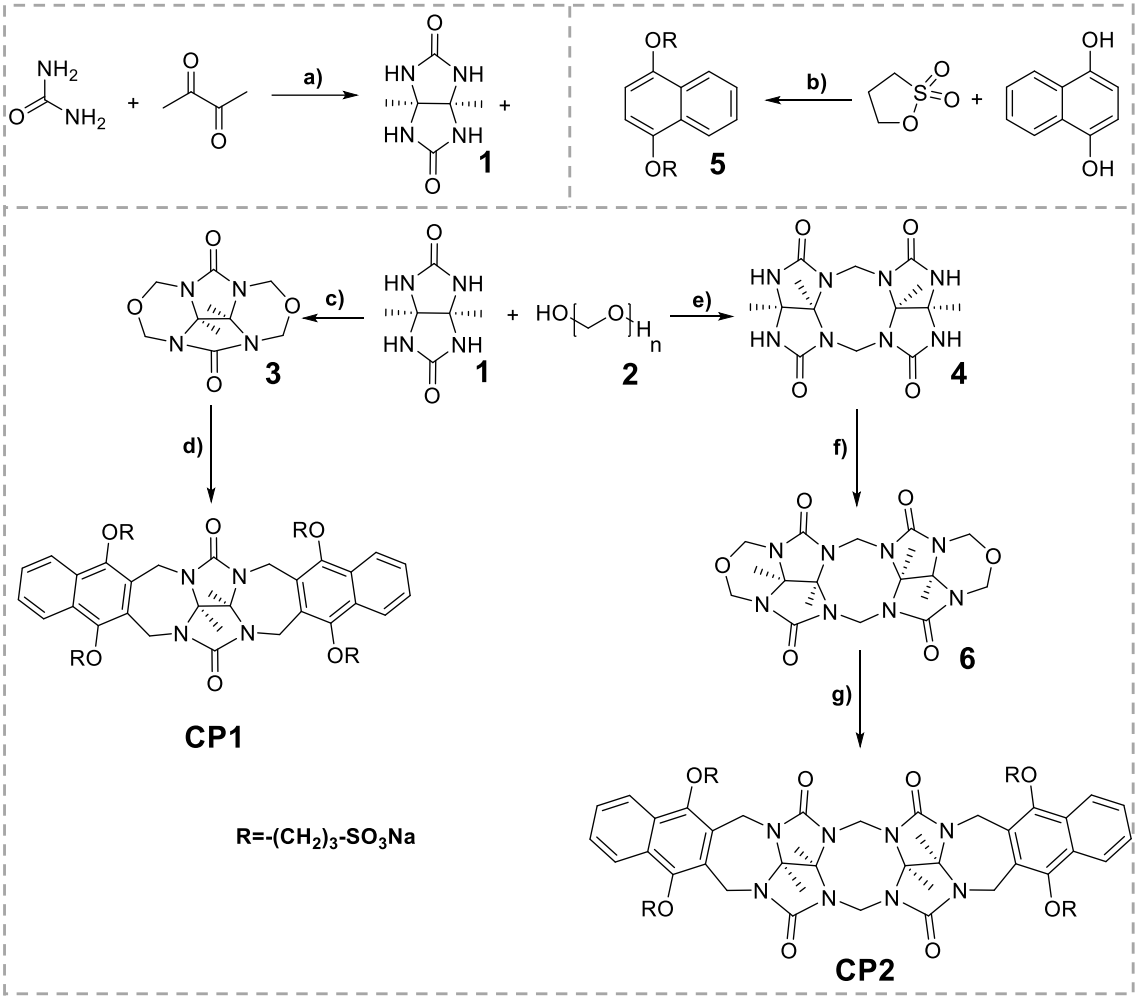

Scheme 3.5: Synthesis of the molecular clips **CP1** and **CP2**. a) HCl 0.3M, 12h, RT, b) NaOH (10 wt%)-1,4-dioxane (4:6) 12h, RT, c) HCl 9M, 24h, RT, d) **5**, TFA, 3h, 70°C, e) HCl 8M, 48h, 50°C, f) TFA, 20h, 80°C, g) **5**, TFA-AC_2O (1:1), 3h, 80°C.

3.3.2 Synthesis of the molecular clips

The synthetic route followed to get the molecular clips CP1 and CP2 is shown in Scheme 3.5, their synthesis was previously published elsewhere.[204, 206, 208] The procedure was followed to synthesize CP1, where a mixture of the glycoluril bis(cyclic ether), **3**, and the dialkoxyaromatic compound **5** in TFA-Ac_2O at 70°C produces the clip with a high yield.[204,

215] By the same manner, to prepare CP2 the glycoluril bis(cyclic ether) dimer, **6** was treated with **5** in TFA-Ac_2O at 70°C (See experimental section for details).

3.3.3 Association constants with the guests

The host-guest interactions between the molecular clips and the flavylium-based compounds were studied calculating the association constants. The UV-Vis spectra obtained after titration of the 4'7OH at pH=1, with increasing concentrations of **CP1** and **CP2** are shown in Figures 3.17a and b respectively. The spectral changes suggest the formation of the complexes, the variation of absorbance can be fitted to a 1:1 host-guest binding model (described in Appendix C) or following eq. C.45, where [CP] is now the molecular clip concentration, and K_{AH^+CP} is the association constant with the flavylium form. The association constants of $K_{ass} = 9.7 \times 10^4 M^{-1}$ with **CP1** and $K_{ass} = 5 \times 10^4 M^{-1}$ with **CP2** were obtained. The association constant of the 4'7OH with CB7 is included in Figure 3.17c for comparative purposes ($K_{ass} = 5.6 \times 10^5 M^{-1}$). The high association constant of CB7 with some flavylium compounds, including 4'7OH was already published.[180]

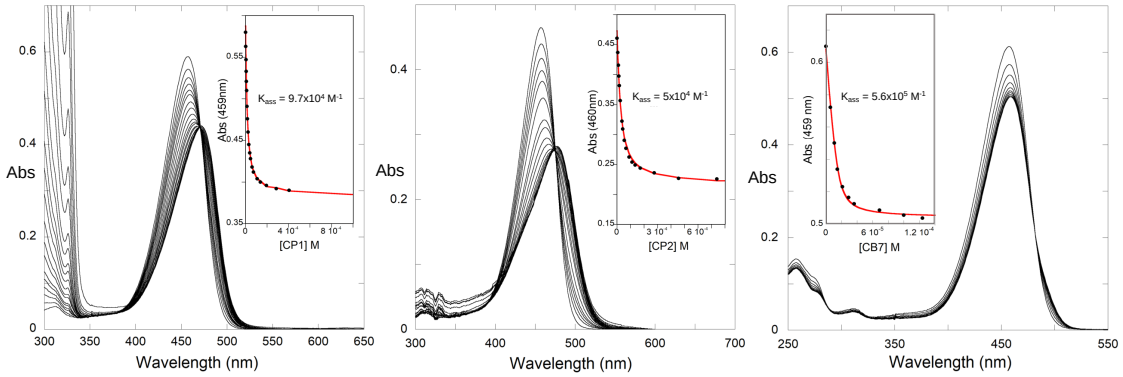

Figure 3.17: UV-Vis spectral variations of a solution with 4'7OH at pH 1 upon addition of increasing concentrations of a) **CP1** (4'7OH=1.12×10^{-5}M), b) **CP2** (4'7OH=8.8×10^{-6}M) and c) **CB7** (4'7OH=1.15×10^{-5}M). The inset in each graph shows the fitting for the calculation of the association constant with a 1:1 H-G model.

The complex formation is confirmed by the pronounced shifts of the flavylium ^{1}H NMR signals in the presence of the host clip. Figure 3.18 shows the obtained ^{1}H NMR spectra with different stoichiometries in the complex between 4'7OH and CP1. As shown in Figure 3.18 many 4'7OH protons present massive up-field shifts in the NMR spectra when the concentration of CP1 is increased. The protons with higher $\Delta\delta$ are the H4, H3, and H8, while others as H2'6', H3 and H5 are just slightly affected. Therefore this implies a higher interaction of the protons in the C ring of the flavylium cation, as expected since the poor electron zone is located around the C ring in Figure 3.16. Also, these variations in the chemical shifts allow the calculation of the 4'7OH-CP1 association constant. In Figure 3.19,

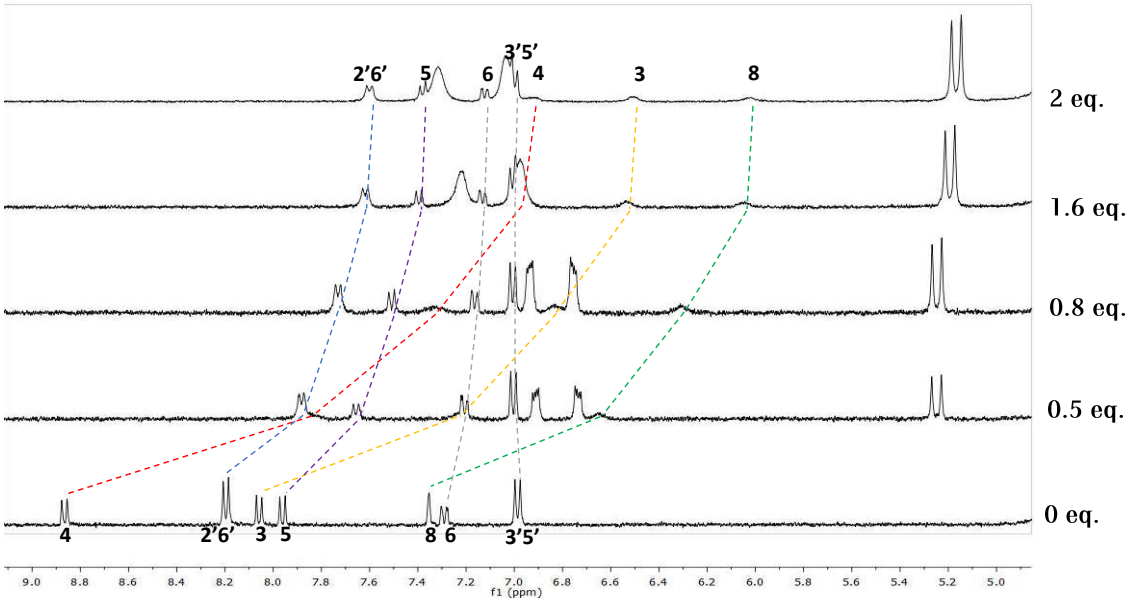

Figure 3.18: ^{1}H NMR spectra of 4'7OH (6×10^{-4}M) with increasing concentrations of CP1: 0, 0.5, 0.8, 1.6 and 2 equivalents. All spectra were acquired in D_2O with 0.1M of DCl.

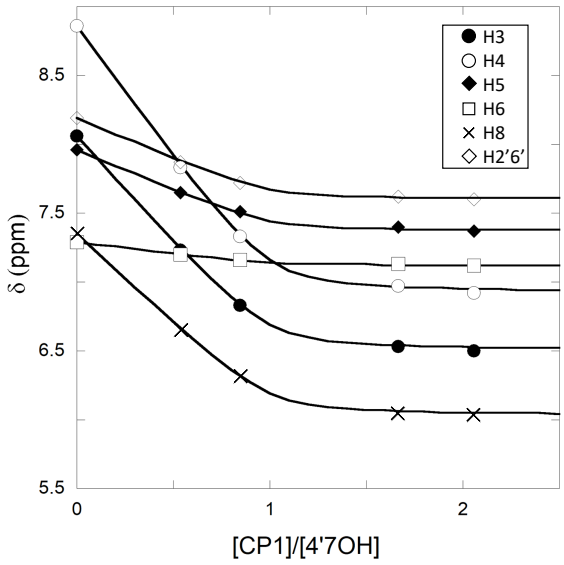

Figure 3.19: Plot of the change in chemical shift of the flavylium proton signals as a function of [CP1]/[4'7OH] obtained from Figure 3.18. The solid line is the best non-linear fitting of the data to a 1:1 binding model with $K_{ass} = 9.7 \times 10^4 M^{-1}$.

the proton signals with higher shifts are presented versus the molar ratio [CP1]/[4'7OH]. Equation C.45 fitted all the data series, where the A_0 and A_f are, in this case, the chemical shift of the proton in the absence of the clip and the final displacement when all the flavylium is complexed. The same value of $K_{ass} = 9.7 \times 10^4 M^{-1}$ obtained from the UV-Vis titration was obtained by ^{1}H NMR titration.

The same procedure was applied to calculate the association constants with the anthocyanin Oenin, Figure 3.20 shows the obtained constants. The presence of isosbestic points in Figures 3.17 and 3.20 confirm the formation of 1:1 complexes.

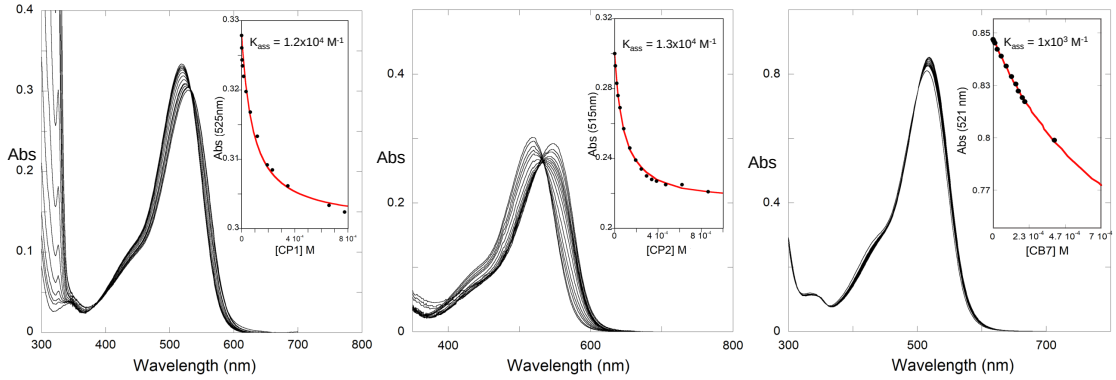

a) b) c)

Figure 3.20: UV-Vis spectral variations of a solution with Oenin at pH 1 upon addition of increasing concentrations of a) **CP1** (Oenin=9.5×10^{-6}M), b) **CP2** (Oenin=8.3×10^{-6}M) and c) **CB7** (Oenin=2.5×10^{-5}M). The inset in each graph shows the fitting for the calculation of the association constant for a 1:1 H-G model.

The Oenin titration with CP1 followed by NMR spectroscopy does not show strong evidence to know the binding site with the CP1. As observed in Figure 3.21 despite some proton signals as H8 and H2'6' are up-field shifted, the maximum shift is not attained. A representation and fitting of the chemical shifts of the H8 and H2'6' signals after the NMR titration results in a very low association constant, lower than the one calculated by UV-Vis titration. These results have two possible explanations, i) it is well known that the high concentration of the Oenin causes its self-association,[82, 161] the aggregates in the NMR samples could decrease the interaction with the CP1 molecule lowering the association constant, and ii) the anthocyanins self-association results in the up-field shifts of the protons,[82] while the interaction with the clip can produce by one side the disaggregation of the anthocyanins and consequently a down-field shift of the proton signals, but by the other side and as observed for the 47'OH, the complexation with the clip reflects an up-field shift, these opposite effects over the chemical shifts may result in a non-observable signal change. Table 3.6 summarizes the association constants obtained from Figures 3.18, 3.19, and 3.20.

The stabilization of the **AH$^+$** form in the Oenin after the titration with CP1, CP2 and CB7 was evaluated in a pH value above its $pK_a^{\wedge}$. Figure 3.22 shows a clear increment in the absorption band of the flavylium after the addition of the clips and the CB7 in a pseudo-equilibrated solution at pH≈3.2.

The association constants reported in Figure 3.20 were confirmed by the use of the co-pigmentation model published by Oliveira et. al.[216] The fitting of the variation in the

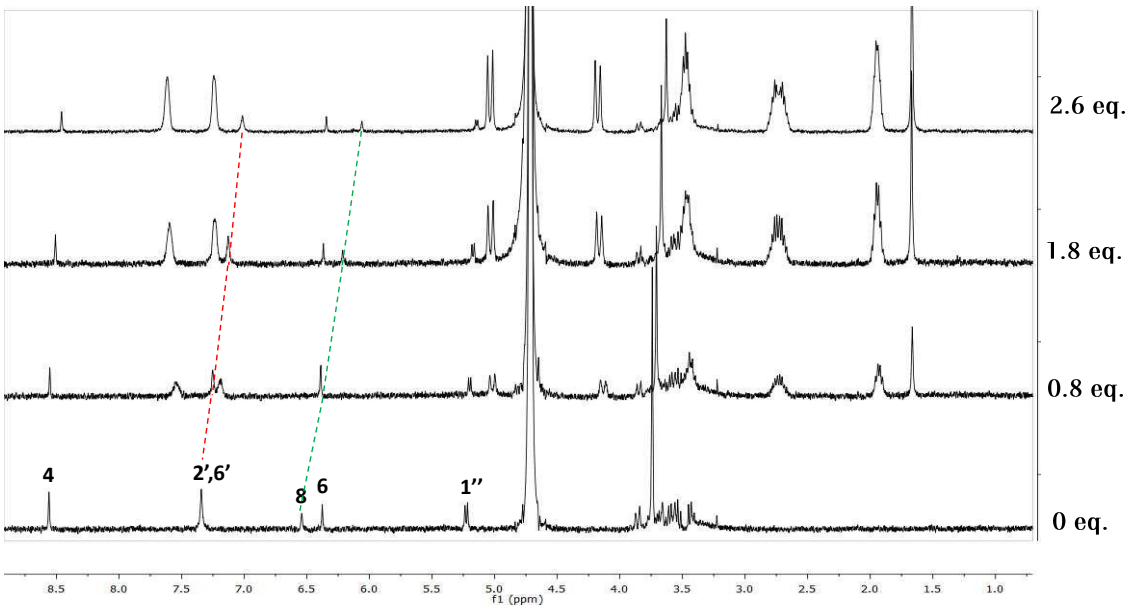

Figure 3.21: ^{1}H NMR spectra of Oenin (6×10^{-4}M) with increasing concentrations of CP1: 0, 0.8, 1.8, and 2.6 equivalents. All spectra were acquired in D_2O with 0.1M of DCl.

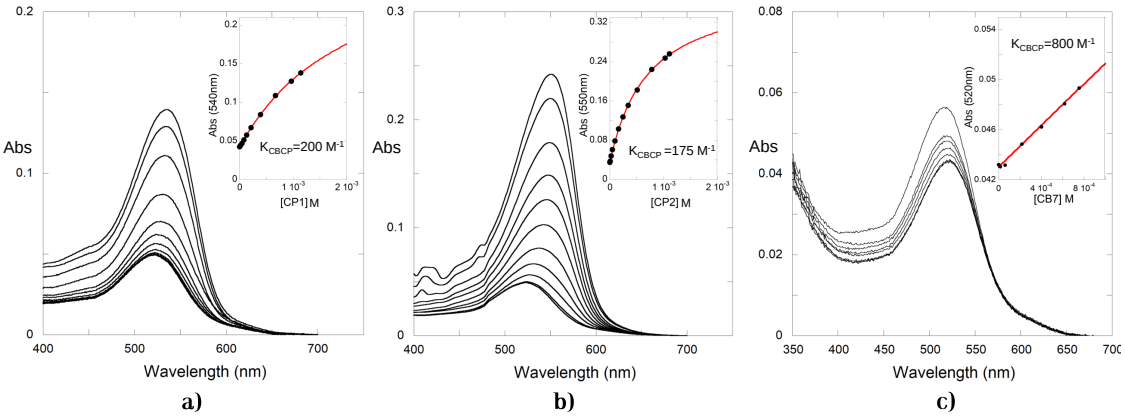

Figure 3.22: UV-Vis spectral variations of a solution with Oenin (1.8×10^{-5}M) upon addition of increasing concentrations of a) **CP1** at pH 3.12, b) **CP2** at pH 3.15 and c) **CB7** at pH 3.23. The inset shows the fitting for the calculation of the average association constant of all the species in the pseudo-equilibrium, using Equation 3.5.

absorbance after the addition of the guest was addressed by Equation 3.4:

$$A_\lambda = \frac{A_0([H^+](1 + r_{AH^+CP}K_{AH^+CP})[CP])}{(1 + K_{AH^+CP}[CP])[H^+] + K'_a} \tag{3.4}$$

where A_λ is the absorption measured at a specific wavelength (observed), A_0 is the absorption at that wavelength when **AH$^+$** is the only species in the system, and the fitted values of r_{AH^+CP} and K_{AH^+CP} represent the ratio of the $\epsilon_{AH^+CP}/\epsilon_{AH^+}$ and the association constant of the **AH$^+$** with the host/co-pigment respectively.

Table 3.6: Association constants K_{ass} for the formation of host-guest complexes between CB*n*-type molecular clips, CB7 and flavylium-based compounds.

Flavylium	**CP1**	**CP2**	**CB7**
4'7OH	9.7×10^4 M^{-1}[a]	5×10^4 M^{-1}	5.6×10^5 M^{-1}
Oenin	1.2×10^4 M^{-1}	1.3×10^4 M^{-1}	1×10^3 M^{-1}

[a] Obtained from the variation in the UV-Vis spectra and the $\Delta\delta$ in ^{1}H NMR.

The values of the previously calculated r_{AH^+CP} and K_{AH^+CP} were used in Equation 3.5[216] to calculate an average of the association constants with the species of the multi-state at pH≈3.2 (K_{CBCP}), mainly **A**, **B** and **Cc** by the fitting of the data obtained in the insets in Figure 3.22.

$$A_\lambda = \frac{A_0((1 + r_{AH^+CP}K_{AH^+CP}[CP])[H^+] + r_{CB} + r_{CBCP}[CP])}{(1 + K_{AH^+CP}[CP])[H^+] + (1 + K_{CBCP}[CP])K'_a} \tag{3.5}$$

Adjusting the K_{CBCP}, as well as the r_{CBCP} values in Equation 3.5 let the calculation of $K_{CBCP} = 200M^{-1}$ in the presence of CP1, and 175 M^{-1} and 800 M^{-1} in the presence of CP2 and CB7 respectively. The r_{CB}, that represents $K_a\epsilon_A/\epsilon_{AH^+} + K_h\epsilon_B/\epsilon_{AH^+} + K_hK_t\epsilon_{Cc}/\epsilon_{AH^+} + K_hK_tK_i\epsilon_{Ct}/\epsilon_{AH^+}$, can be calculated from Equation 3.6, where $A_{\lambda(CP=0)}$ is the absorption when the concentration of the co-pigment is zero. The calculation of the K_{CBCP} values by Equation 3.5 lacks of sensitivity, at least following the wavelength where only the flavylium species absorb, this is because the r_{CBCP} values are close to be zero. Nevertheless, the lower K_{CBCP} constants compared with the K_{AH^+CP} in all the cases, indicate a higher stabilization of the **AH$^+$** over the **CB** species.

$$A_{\lambda(CP=0)} = \frac{A_0([H^+] + r_{CB}}{[H^+] + K'_a} \tag{3.6}$$

The flavylium cation stabilization was also studied along the pH scale. A series of pH jumps from pH=1 to higher pH values was performed for the complex CP1-Oenin, CP2-Oenin, and CB7-Oenin. The results are shown in Figure 3.23; in the absence of the host, the anthocyanin exhibits a $pK'_a = 2.38$ and the complexation with CP1 and CP2 increase the flavylium domain over the pH scale, with pK'_a values of 3.12 and 3.51 respectively. As the association constant of the Oenin with CB7 are low, for the flavylium cation and equally its conjugated base, does not change the pK'_a value. The higher shift in the pK'_a was obtained with the CP2 even when the calculation was made in lower concentrations, this results are in accordance with the K_{CBCP} and K_{AH^+CP} constants previously calculated, the difference between these two constants is higher for the CP2 than the CP1, then the **AH$^+$** species are more stabilized by the CP2 with a higher K_{AH^+CP} and a lower K_{CBCP} constant.

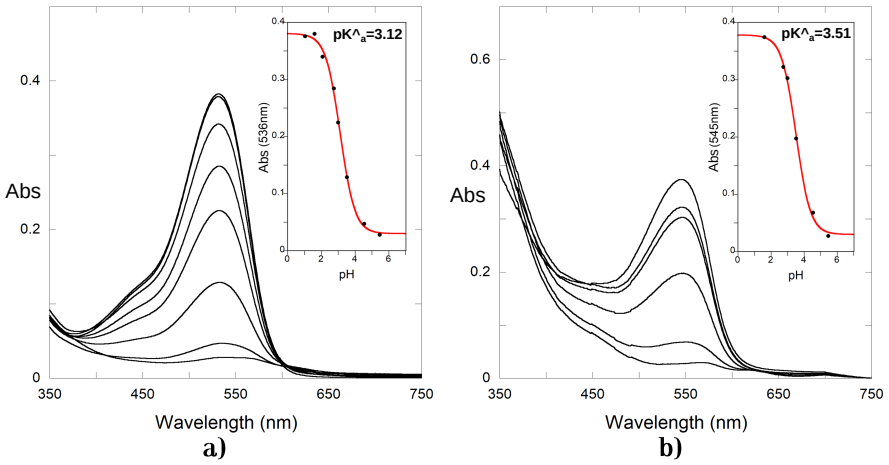

Figure 3.23: UV-Vis spectral variations of a solution with Oenin (1.2×10^{-5}M) at the pseudo-equilibrium after direct pH jumps from pH=1 to different pH values in the presence of a) CP1 (1×10^{-3}M) and b) CP2 (5.1×10^{-4}M).

3.4 Complexation with sulfonated calix[n]arenes: extending the flavylium cation domain in the pH scale

In Chapter 1 some characteristics of the Calix[*n*]arene (C*n*) macrocycles were described and their use to hosts organic cations was addressed. C*n* compounds are typically water-insoluble, and their functionalization to improve their solubility is of great interest to apply them in biological systems. Some sulfonate, amino, nitro, carboxyl, and phosphonate groups have been included in their structures to increase their water solubility. Sulfonate groups have shown the maximum increase in solubility with concentrations up to 0.1 M.[130]

Commonly, the C*n* are compared with the cyclodextrins, reviewed in subsection 1.6.2, because both macrocycles are cage-like molecules with a hydrophobic cavity, although the sulfonated calix[n]arenes (SC*n*) do not provide just hydrophobic properties because of their hydrophilic heads (SO_3^-) in the upper rim, they exhibit molecular selectivity to different guests by π-stacking, CH-π and electrostatic interactions.[217, 218] However, the cyclodextrins are relatively rigid molecules, while the SC*n* are highly flexible, with more degrees of freedom in their structures, possessing the ability to produce ring inversions. The SC*n* structure has variable conformations due to the free phenols groups rotation between the methylene bridges. Thus SC*4* has four different conformations, while SC*6* and SC*8* have eight and sixteen different conformers respectively.[130, 131] Due to their symmetrical structures SC*n* with 4, 6, and 8 units have similar properties, with cylindrical shapes and, of course, different cavity sizes, with 3, 7.6, and 11.7Årespectively.[130]

Previous studies revealed that the SC*n* are not cytotoxic or carcinogenic,[130, 219, 220] thus, they can be used as host receptors for anthocyanins in food, pharmaceutical, and

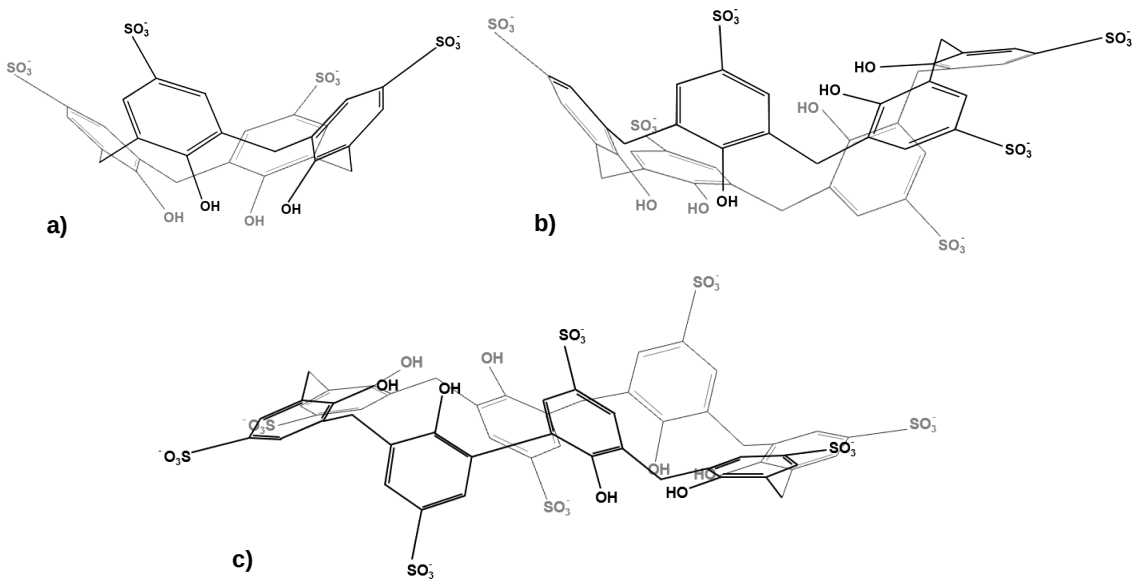

Figure 3.24: Chemical structures of the *p*-sulfonated calix[*n*]arenes. a) SC*4* in its cone conformer, b) the double partial cone conformation (1,2,3-alternate) of SC*6* and c) the pleated loop conformation (1,2,3,4-alternate) of SC*8*.

cosmetic formulations. As a background in their complexation with flavylium-based compounds, the high association constants (10^4 M^{-1}) of the SC*4* with different synthetic guests were already published.[136] High affinities with the guest is commonly associated with an increase of their pKa values,[218] turning the guest into a stronger base than its free form. However, the effect of the host-guest complexation between SC*n* and flavylium-based compounds over the equilibrium constants that lead to the formation of uncolored species has not been proved. To ensure the hypothetical total inclusion of larger organic flavylium-based compounds as anthocyanins inside the SC*n* cavity, the SC*4*, SC*6* and SC*8* were tested, avoiding the cavity size as a limitation. In Figure 3.24, the general structure of the SC*n* is presented, the guest molecules are the 4'7OH, and Oenin represented before in Figure 3.16.

3.4.1 Conformational isomers of the hosts

The flexibility of the SC*n* is an important feature for the association constants with guest molecules. These macrocycles can reorganize their molecular structure depending on the host-guest complex formed. The typical conformation observed in solid-state complexes with SC*4* is the cone form.[130, 221] The variety of conformers in SC*n* with 6 and 8 units are even more complex, and dynamic NMR experiments demonstrated the fast interconversion between their conformers in aqueous solution.[130] However, their most common structures have been identified in solid state by X-ray diffraction.[222]

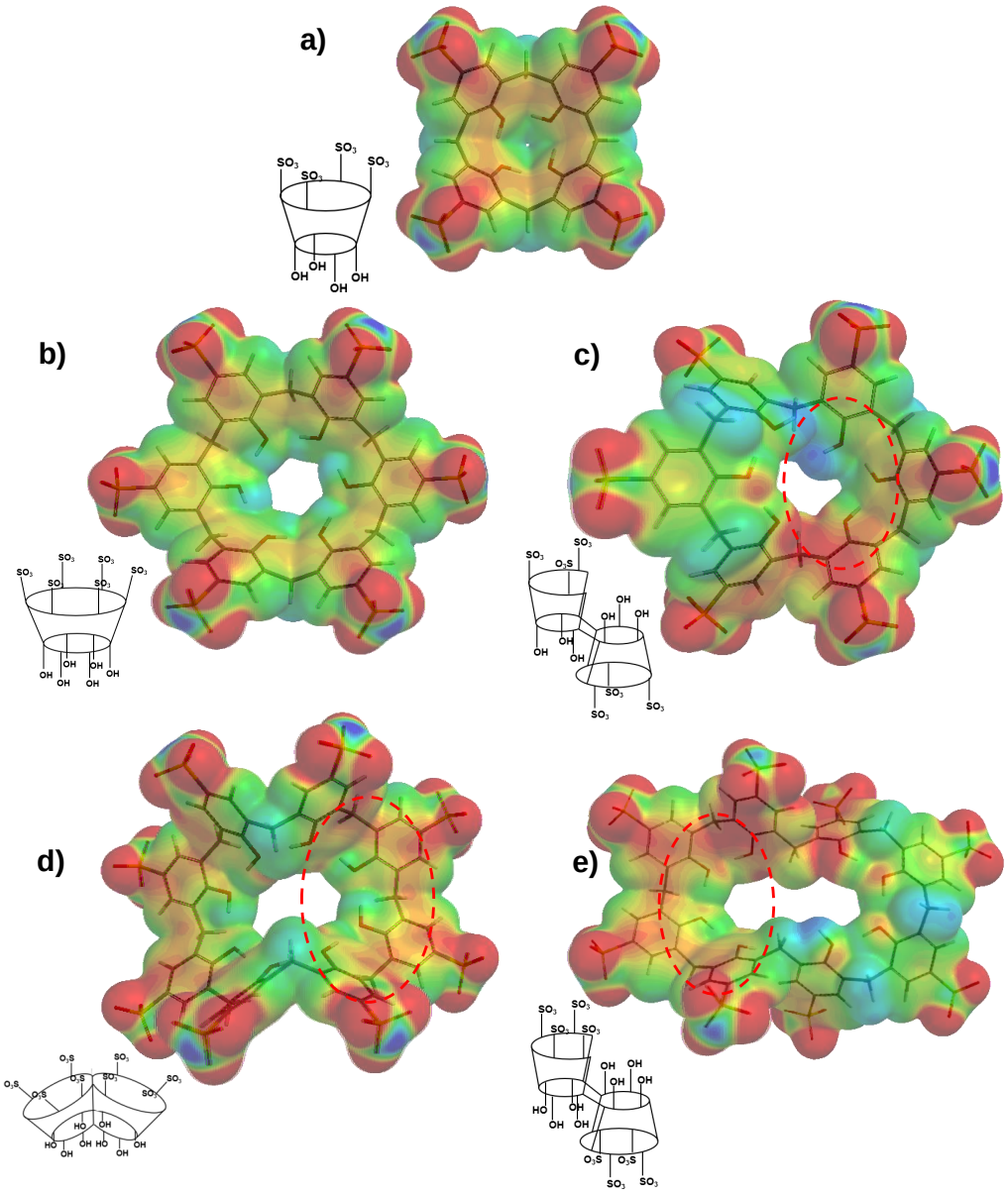

Figure 3.25: Three dimensional structures and AM1 Electrostatic Potential Surface (EPS) of the main SC*n* conformers. a) cone conformation in SC*4*, SC*6* in its b) cone conformation and c) double partial cone conformation and SC*8* in its d) cone and e) pleated loop conformations. The red dotted circles indicate partial cone electron-rich zones.

Similarly, as the CB*n*-type molecular clips were studied in subsection 3.3.1. The electronic properties of the most common SC*n* conformers are described by the electronic potential surface in Figure 3.25. Whichever the case, all the structures shown in Figure 3.25 have an electron-rich zone in the inner face of the phenolic units. In the cone conformations (Figure 3.25a, c, and d) where all the sulfonate groups are pointing out from the cavity, a clear electron-rich region is extended around the entire cycle. The SC*6* double partial cone and the SC*8* pleated loop conformations in form two partial cones up and down the molecule

(red dotted circles in Figure 3.25). These structures have been associated with host-guest interactions with 2:1 stoichiometries with small cationic guests.[221, 222, 223] The zone in the inner face of the cones will serve as the primary site of cleavage for the electron-deficient zones in the guests (see Figure 3.16)

3.4.2 Synthesis of sulfonated calix[n]arenes

The synthesis of the SC*n* follows the simple general pathway reported in Scheme 3.6, where the respective benzenoid substrate bearing *p-tert*-butyl groups is sulfonated by the addition of concentrated H_2SO_4, the formation of cyclohexadienyl cation has been identified as a reversible reaction.[224] The formation of butene makes the reaction irreversible. This single step describes a *ipso*-substitution to yield *p*-sulfonated calixarenes with yields of 60-70%.

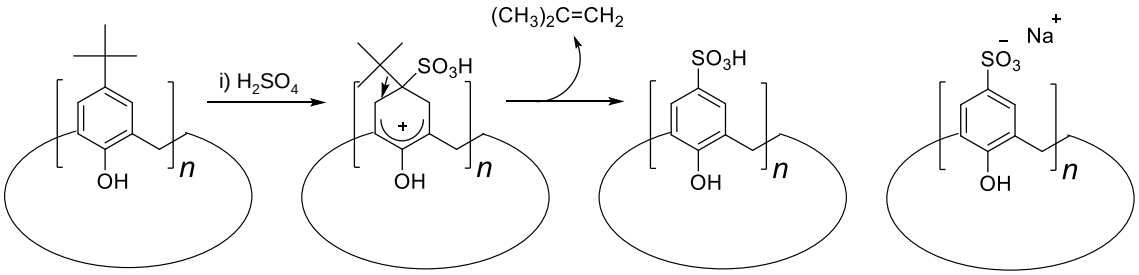

Scheme 3.6: General pathway for the synthesis of the *p*-sulfonated calixarenes.

3.4.3 Association constants with the guests

As observed in other complex formation in previous Chapters, the absorption UV-Vis spectrum of the guest changed with the addition of different amounts of SC*n*. This allows us to calculate the association constants between the host and the guest. Figure 3.26 shows the variation in the absorbance spectra after titration of 4'7OH solutions with increasing amounts of SC*4*, SC*6* and SC*8*. The bathochromic and hypochromic effects are observed after the gradual addition of the host. The inset in Figure 3.26 plots the variation of a single wavelength after increasing concentrations of the hosts. In all cases, the formation of stable stoichiometric host-guest 1:1 complexes was defined by fitting the data using Equation C.45.

The same procedure was applied for the association constants with the anthocyanin Oenin. The UV-Vis spectra results obtained after titration with the different SC*n* are presented in Figure 3.27. The association constants obtained from both Figures 3.27 and 3.26 is summarized in Table 3.7. While in 4'7OH, the higher association constant is achieved in the complex with SC*4*, Oenin association constant with the SC*n* increases with the number of phenolic units. The constants to link the synthetic guest are around 10x higher than those observed for the Oenin. The size of the 4'7OH makes it easy to fit inside the cavity of all the SC*n*. However, it is interesting to note that the higher association constant was obtained

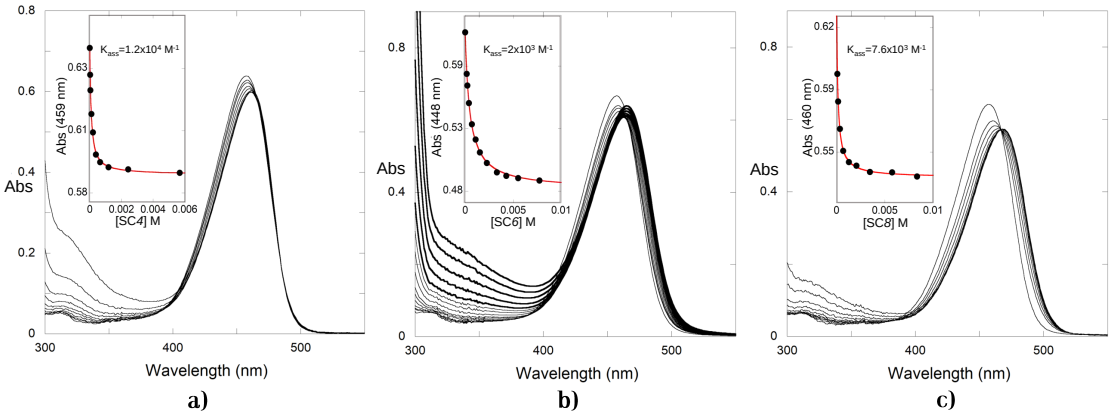

Figure 3.26: UV-Vis spectral variations of a solution with 4'7OH at pH 1 upon addition of increasing concentrations of a) SC*4* (4'7OH=1.2×10^{-5}M), b) SC*6* (4'7OH=1.3×10^{-5}M) and c) SC*8* (4'7OH=1.2×10^{-5}M). The inset shows the fitting for the calculation of the association constant with a 1:1 H-G model.

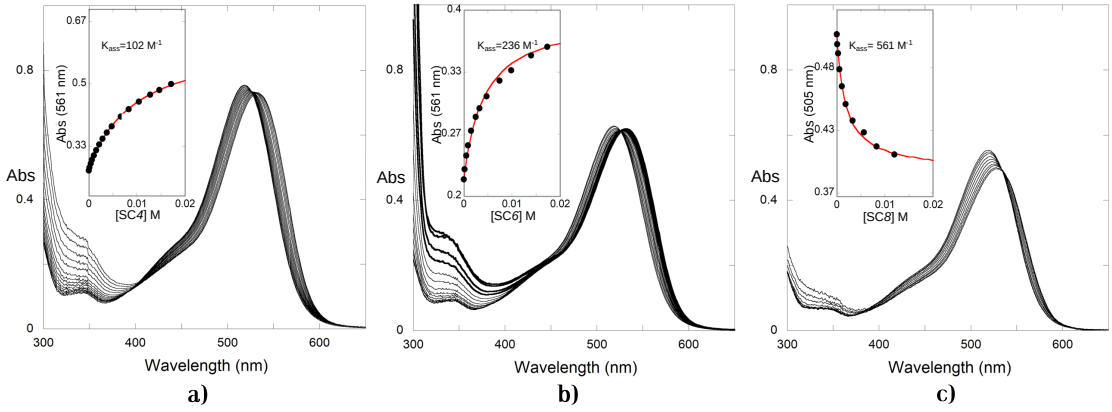

Figure 3.27: UV-Vis spectral variations of a solution with Oenin at pH 1 upon addition of increasing concentrations of a) SC*4* (Oenin=2.2×10^{-5}M), b) SC*6* (Oenin=1.8×10^{-5}M) and c) SC*8* (Oenin=1.6×10^{-5}M). The inset shows the fitting for the calculation of the association constant with a 1:1 H-G model.

for the complex with SC*4* (1.2×10^4 M^{-1}). This particular result is in complete concordance with the association constants reported previously for similar guests.[136] The small cavity and the proximity of the sulfonate groups in the host and the small size of the guest can be responsible for the higher constant. The flexibility in SC*8* is higher than in SC*6*, this can be enough to increase the association constant with the 4'7OH, especially if the SC*8* double cone conformation is favored during the interaction, where two SC*4* similar linking sites are formed. On the other hand, the cavity size of the SC*n* seems to be a determining factor in the association constants with the Oenin. The small cavity in SC*4* limits the interaction with the anthocyanin. Thus, the high flexibility and the numerous possibilities for the recognition sites in the SC*8* hosting the Oenin make a stronger interaction.

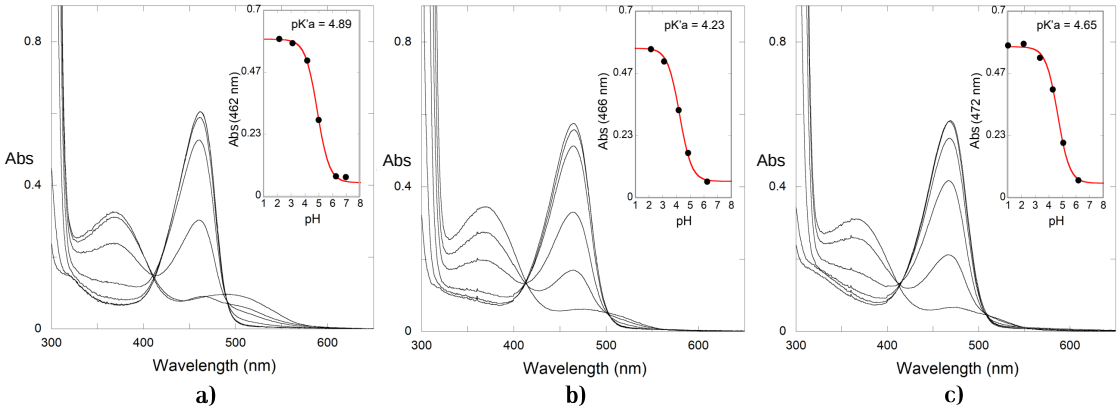

Figure 3.28: UV-Vis spectral variations of a 4'7OH (1.15×10^{-5}M) solutions after direct pH jumps from pH=1 to higher pH values (citrate buffer 0.01M) in the presence of a) SC*4* (3×10^{-3}M), b) SC*6* (5×10^{-3}M) and c) SC*8* (2×10^{-3}M). The inset shows the fitting for the calculation of pK'_a.

Table 3.7: Association constants K_{ass} for the formation of 1:1 host-guest complexes between *p*-sulfonated calix[n]arenes and flavylium-based compounds.

Flavylium	**SC*4***	**SC*6***	**SC*8***
4'7OH	1.2×10^4 M^{-1}	2×10^3 M^{-1}	7.6×10^3 M^{-1}
Oenin	102 M^{-1}	236 M^{-1}	561 M^{-1}

The effect of the SC*n*-flavylium association for stabilizing the colored forms over the pH scale was evaluated. The equilibrium UV-Vis spectral variations of the guest spectrum, obtained after direct pH jumps from pH=1 to higher pH values, in the presence of the SC*n* as host molecules are presented in Figure 3.28 for the 4'7OH and in Figure 3.29 for the Oenin. The inset in each graph shows the pK_a calculation. In Table 3.8 the pK_a shifts in the presence of the SC*n* hosting the 4'7OH and the Oenin are represented.

Table 3.8: Flavylium pK'_a/pK_a shifts after SC*n* complexation.

Flavylium	**Without Host**	**SC*4***	**SC*6***	**SC*8***
4'7OH	3.05	4.89	4.23	4.65
Oenin	2.6	3.46	3.45	3.57

The complexation of the 4'7OH with the SC*n* exhibits a pK'_a shift between one and two pH units. This in accordance with the association constants, where the higher pK'_a shift is observed for those complexes with higher association constants. Nevertheless, in the Oenin, the pK_a shifts after the complexation are not higher than one pH unit, as the association constants for the anthocyanins are lower than those observed for the synthetic flavylium without the sugar moiety; this result was expected. However higher pK_a shifts were observed in the hosts with larger cavities (SC*8*>SC*6*>SC*4*).

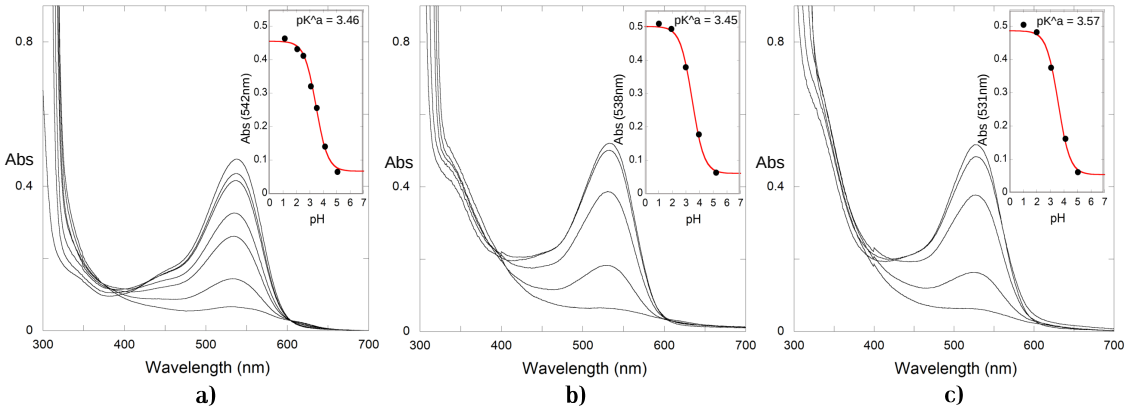

Figure 3.29: UV-Vis spectral variations of a Oenin (1.5×10^{-5}M) solutions after direct pH jumps from pH=1 to higher pH values (citrate buffer 0.01M) in the presence of a) SC*4* (1×10^{-2}M), b) SC*6* (3×10^{-2}M) and c) SC*8* (1×10^{-2}M). The inset shows the fitting for the calculation of pK_a.

3.5 Materials and Methods

The synthetic flavylium-based compound 4'-hydroxyflavylium was obtained from the flavylium compounds bank from the Prof. Fernando Pina's research group and was previously synthesized as described elsewhere.[72] Prof. Victor de Freitas and Dr. Luis Cruz from the University of Porto (PT) provided the Malvidin-3-glucoside (Oenin)[197] and the Malvidin-3-glucoside-fatty acid derivatives.[196] Caffeine was purchased from Alfa Aesar Co. Ltd. Starting materials for the synthesis of the CB*n*-type molecular clips and the sulfonated calix[n]arenes were purchased from commercial suppliers and were used without further purification. Compounds CP1 and CP2 were prepared according to literature procedures[204, 206, 208] (See Annex I for characterization data). Cucurbit[7]uril (CB7) was obtained from previous studies in the research group.[180]

Stock solutions of all the Oenin and 4'OH were prepared in 0.1 M HCl using Millipore water. Stock solutions of the Malvidin-3-glucoside-fatty acid derivatives were prepared in aqueous SDS solution (0.1M) at pH=3 (0.001 M HCl). For the caffeine experiments, a caffeine 0.1 M stock solution was prepared in both Millipore water and Theorell and Stenhagen's universal buffer pH=7.

Direct pH and reverse pH jumps in the caffeine and micelle experiments were performed always keeping the caffeine or SDS concentrations as a constant. The solutions pH was adjusted by the addition of HCl, NaOH, or Theorell and Stenhagen's universal buffer as needed. For the solutions containing CB*n*-type molecular clips and the sulfonated calix[n]arenes citrate buffer was used instead to ensure pH values between 3 and 6.

All pH changes were measured by a Radiometer Copenhagen PHM240 pH/ion meter

(Brønshøj, Denmark). The UV-Vis spectra were recorded on a Varian-Cary 100 or 5000 spectrophotometers (Palo Alto, CA, US). The reverse pH jumps from the pseudo-equilibrium were monitored on an SX20 (Applied photophysics; Surrey, UK) stopped-flow spectrometer equipped with a PDA.1/UV photodiode array detector. A 435 nm cut-off filter was used to prevent any photochemical reaction that could take place from **Cc** to **B**, or photodegradation.

NMR spectra were obtained using a Bruker AMX 400 (Billerica, MA, US) instrument operating at 400.13 MHz (^1H). All the sample solutions were prepared in D_2O and pH was set to pH=1 with DCl. The hosts and guests 3D structures and the electronic potential surfaces (EPS) were designed and calculated at the AM1 level of theory using the Wavefunction Spartan 09 software package.

The CMC and the full dissolution of the Malvidin-3-glucoside-fatty acid derivatives in SDS were calculated as follows: A stock solution in methanol:water (9:1, 0.1 M HCl) was prepared, and aliquots of this solution were placed in different cuvettes, the solvent was allowed to evaporate under a gentle flow of nitrogen, and aqueous solutions of SDS at different concentrations (containing HCl 0.1 M to stabilize the flavylium form) were added to the cuvettes.

The synthesis of the compounds associated to this chapter was performed as follows:

Compound 1. 2,3-butanedione (7g, 81 mmol) was added to a solution of urea (16g, 266 mmol) dissolved in HCl (0.3M, 40mL). The solution was stirred for 12h at RT. The mixture was filtered, and the solid washed twice with water (40mL) an later with ethanol (40mL) to yield 10.5g (76%) of dimethyl glycoluril as a white solid. ^{1}H NMR (400 MHz, DMSO-d_6) δ (ppm): 7.1 (s, 4H), 1.3 (s, 6H).

Compound 3. Dimethyl glycoluril (7g, 41 mmol) was mixed with **2** (6g, 200 mmol) in 35mL of HCl 9M, and the mixture was stirred for 24h at RT. 120mL of water were added to the mixture and was stirred for other 12h. The mixture was filtered and washed with water (150 mL) and ethanol (150 mL) to yield 6.7g (65%) of **3** as a white solid. ^{1}H NMR (400 MHz, DMSO-d_6) δ (ppm): 5.2 (d, J=11.6, 4H), 5.0 (d, J=11.4, 4H) 1.8 (s, 6H).

Compound 4. A mixture of **1** (13g, 76 mmol) and **2** (2.29g, 76 mmol) and 8M HCl (18 mL) was stirred and heated at 50°C for 48h. The precipitate was collected by filtration and washed with water to give 7.23g of **4** (62%) as a white solid. ^{1}H NMR (400 MHz, DMSO-d_6) δ (ppm): 7.57 (s, 4H), 5.46 (d, 2H), 3.96 (d, 2H), 1.54 (s, 6H), 1.32 (s, 6H).

Compound 5. A solution of 1,4-dihydroxynaphthalene (0.5g, 3 mmol) in NaOH (10 wt%, 4 mL) was treated with another solution of propanesultone (0.95g, 7.7 mmol) in 1,4-dioxane (6 mL). The mixture was stirred at RT for 12h. After filtration, the solid was dissolved in

water (3 mL) and precipitated with MeCN (20 mL) to yield 375 mg (27%) of **5** as a blue solid. ^{1}H NMR (400 MHz, D_2O) δ (ppm): 8.01 (m, 2H), 7.43 (m, 2H), 6.63 (s, 2H), 4.02 (t, 4H), 3.02 (t, 4H), 2.16 (m, 4H).

Compound 6. A solution of **4** (1.45g, 5.8 mmol) in TFA (40 mL) was treated with **2** (0.6g, 20 mmol). The mixture was stirred and heated at 80°C for 20h. The mixture was poured in MeOH (250 mL) and the precipitate was filtered and washed with MeOH to yield 0.7 g of **5** (40%) as a white solid. ^{1}H NMR (400 MHz, DMSO-d_6) δ (ppm): 5.47 (d, J=15.8, 2H), 5.15 (d, J=11.0, 4H), 4.87 (d, J=11.0, 4H), 4.33 (d, J=15.8, 2H), 1.83 (s, 6H), 1.65 (s, 6H).

CP1. A solution of **2** (43mg, 0.17 mmol) in TFA (0.5 mL) was mixed with **3** (0.3g, 0.67 mmol). The mixture was heated at 70°C for 3h and then was poured into MeOH (5 mL). The precipitate was collected by filtration and dried. The crude was recrystallized twice with a mixture of water and acetone (1:2, v/v, 5 mL). The solid was redissolved in water (2 mL) and the pH adjusted to 7 with NaOH. The solvent was removed by rotary evaporation, the solid dried under high vacuum to yield 172 mg of **CP1**(91%) as a white solid. ^{1}H NMR (400 MHz, D_2O) δ (ppm): 7.98 (m, 4H), 7.55 (m, 4H), 5.20 (d, J=16.2, 4H), 4.39 (d, J=16.2, 4H), 3.60 (m, 8H), 2.9 (m, 8H), 2.1 (m, 8H), 1.81 (s, 6H).

CP2. A mixture of **4** (0.45g, 1 mmol) was dissolved in TFA-AC_2O (1:1, v/v, 6.5 mL) and **5** (1.79g, 4 mmol) was stirred and heated at 80°C for 3h and then was poured into MeOH (75 mL) and filtered. The residue was redissolved in water (10 mL) and then acetone was added (50 mL). The precipitate was obtained by filtration and the solid redissolved in water, the pH was adjusted to 7 with NaOH and the solvent removed by rotary evaporation, the solid was dried obtaining 0.75g of **CP2**(57%) as a white solid. ^{1}H NMR (400 MHz, D_2O) δ (ppm): 7.80 (m, 8H), 5.35 (d, J=16.3, 2H), 5.18 (d, J=16.2, 4H), 4.34 (d, J=16.3, 2H), 4.23 (d, J=16.2, 4H), 3.70 (m, 4H), 3.25 (m, 4H), 3.10 (m, 4H), 2.95 (m, 4H), 2.00 (m, 4H), 1.85 (m, 4H), 1.75 (s, 6H), 1.70 (s, 6H).

The SC*n* macrocycles were obtained by *ipso*-sulfonation of their respective *p-tert* butylcalix[*n*]arenes in sulfuric acid.[131, 224] 15mL of H_2SO_4 were mixed with 0.5 g of the respective *p-tert* butylcalix[*n*]arene. The reaction mixture was stirred for 6-18h at 70-80°C. The reaction was monitored by taking an aliquot of reaction and placed in water; it is complete when no water-insoluble material was detected. The reaction was added to 100 mL, and the SC*n*Na salt obtained by neutralizing the mixture with Na_2CO_3 in H_2O and further filtration. The powder was redissolved in water and treated with activated charcoal for its decoloration; the solution was filtered through Celite. The sodium salts were purified by recrystallization from water/methanol mixtures (See Annex I for the ^{1}H NMR characterization data).

SC*4*. Following the general procedure this calixarene was obtained in 66% yield. ^{1}H

NMR (400 MHz, D_2O) δ (ppm): 3.9 (s, 8H, $ArCH_2Ar$), 7.45 (s, 8H, ArH).

SC*6*. Following the general procedure this calixarene was obtained in 59% yield. ^{1}H NMR (400 MHz, D_2O) δ (ppm): 3.88 (s, 12H, $ArCH_2Ar$), 7.41 (s, 12H, ArH).

SC*8*. Following the general procedure this calixarene was obtained in 63% yield. ^{1}H NMR (400 MHz, D_2O) δ (ppm): 4.11 (s, 16H, $ArCH_2Ar$), 7.64 (s, 16H, ArH).

3.6 Conclusions

The study of the intermolecular interactions of all the species obtained at different pH values in flavylium-based compounds is essential when we try to stabilize a particular species. In this case, the colored flavylium cation and quinoidal base species are the point of interest, however, the interaction of these and the uncolored species with other molecules as co-pigments and stabilizers also plays an important role in the color expression of flavylium solutions. The equilibrium and association constants calculation involving all the species with their respective complexes could be a daunting and challenging task.

The new method to calculate all the equilibrium constants through the application of reverse pH jumps and its use to the co-pigmentation obtaining the association constants makes a more accessible study of complicated systems involving the flavylium-base compounds, the co-pigments and their complexes, including for the first time the interaction with all the flavylium multi-state species. The caffeine interacts preferentially with the quinoidal base species and, in particular, has negligible interaction with the hemiketal in anthocyanins, something important from the point of view of mole fractions, because hemiketal form is the most abundant in equilibrated anthocyanin solutions in moderately acidic medium. The sugar moiety in mono glycosylated anthocyanins plays an important role in associating the co-pigment, increasing the association constant. The study of the interaction of flavylium-based compounds with other molecules in solution by the method described along with this Chapter contribute to clarify the color stability of anthocyanins in aqueous solutions and to understanding the physical-chemical mechanisms behind the effects of co-pigmentation present in many natural systems that are responsible for the stabilization of color in plant tissues and food derived from them such as jams, red fruits drinks, wines and so on.

On the other hand, some systems are still more complicated, as the micellar environment. This supramolecular assembly involves more than two molecules, creating a molecular aggregate and, at the same time, a microenvironment with different physical-chemical characteristics both within and on the surface of the micelle. The anthocyanin-fatty acid conjugates allow us to obtain co-micellization with SDS and increase the mole fraction of **A**

at moderately acidic and neutral conditions. This is the first time that a significant stabilization of the quinoidal base at higher pH of an anthocyanin monoglucoside derivative is reported. It seems that the longer fatty acid chain improves the amount of quinoidal base in the equilibrium being around 45% in compound **1** and 37% in compound **2**. This tend is coherent with Oenin data in SDS micelles, where *ca* 25% of the quinoidal base is observed.

The interaction of the flavylium-based compounds with host molecules acting as stabilizers as the water-soluble CB*n*-type molecular clips and the sulfonated calix[n]arenes is a good alternative to extend the pH domain of the positively charged **AH$^+$** species, since these compounds tend to form complexes with higher association constants than the ones with the **CB** species. The most remarkable features in the CB*n*-type molecular clips as well as in the SC*6* and SC*8* sulfonated calix[n]arenes are their high water solubility provided by the sulfonate groups, and their big size cavity able to complex large molecules as the anthocyanins.

The synthesized C-shaped CB*n*-type molecular clips CP1 and CP2 are good host receptors for the flavylium-based compounds in their **AH$^+$** form, since the dialkoxynaphtalene sidewalls are able to form strong complexes with cationic molecules. In this case, the cavity size is not a problem for the complexation with larger compounds as anthocyanins, has happen with cucurbit[n]urils, because the clips have the possibility to extend or shorten the distance between the walls. Although the association constants with the 4'7OH are higher that the ones with the Oenin, they are in the same order of magnitude (10^4). The NMR experiments confirmed the linking of the 4'7OH with the CP1 with a stronger interaction of the A and C rings. The use of mathematical models to estimate the association constants of the clips with the **AH$^+$** (K_{AH^+CP}) and the uncolored species (K_{CBCP}) proved the higher interaction with the first. The higher difference between these two constants in the interaction of CP2 and the Oenin makes of this clip a better host for the extension of the pH domain of the colored species when compared with CP1, increasing the pK'_a in at least one unit of pH.

The association constants of the SC*n* for smaller molecules as the 4'7OH are high following the order SC*4*>SC*8*>SC*6*, whereas for the Oenin they are lower but slightly increased when the cavity size is extended (SC*8*>SC*6*>SC*4*). The cavity size as well as the conformational changes of the hosts seems to be important for the complexation of flavylium-based compounds. The stabilization of the **AH$^+$** along the pH scale is in accordance with the association constants, the higher the association with the cation, the higher pK'_a shifts. The best results showed a 4'7OH pK'_a shift of almost two units in the presence of SC*4* and a Oenin pK'_a shift of one unit in presence of SC*8*.

Publications associated with this chapter:

- J. Mendoza, N. Basílio, V. de Freitas, and F. Pina. "New procedure to calculate all equilibrium constants in flavylium compounds: application to the copigmentation of anthocyanins."In: *ACS omega*, 4.7 (2019), pp. 12058-12070. DOI: https://doi.org/10.1021/acsomega.9b01066
- J. Mendoza, F. Pina, N. Basílio, M. Guimarães, V. de Freitas, and L. Cruz. "Extending the stability of red and blue colors of malvidin-3-glucoside-lipophilic derivatives in the presence of SDS micelles."In: *Dyes and Pigments*, 151 (2018), pp. 321-326. DOI: https://doi.org/10.1016/j.dyepig.2018.01.007

CHAPTER 4

Applications for the flavylium multi-state: response to external stimuli

All multi-state systems based in molecules that can be inter-converted by an external stimulus are interesting from the point of view of the design of molecular switches and devices.[225, 226, 227, 228, 229, 230] The term *molecular switch* was first used in the 80's and typically refers to any kind of molecule that can exist in two or more stable (or meta stable) states, the conversion between these states can be induced by external stimuli as temperature, chemical modifications, redox reactions, light and electric fields.[231] The sensibility of the multi-state to an external stimuli and the interconversion between the different molecules as a response to these stimuli, allows the application in advanced molecular devices modeling as molecular keypad locks and memory effects.[232, 233, 234, 235] The most used molecular switches are light[236] and pH[237] sensitive, based on the photochemical transformations and in the acid-base equilibria between the species.

The flavylium multi-state is not the exception, the conversion between different molecules in aqueous solutions responding to variations of the pH of the solutions and light inputs. Some anthocyanins synthetic flavylium derivatives,[71] deoxyanthocyanins,[238] styrylflavylium,[239] naphtoflavyliums,[240] are just some examples of switchable systems. Flavylium based multi-states have been applied as models for optical memories and in the mimesis of natural events as the mechanism of the neuronal network.[88, 241]

In this Chapter, the study of the multi-state of different flavylium-based compounds induced by changes in the pH and light exposure is addressed. First, the inclusion of the flavanone species in the flavylium system, allows the construction of a molecular timer with a reset controlled by the pH. The effect of the host-guest interactions of the flavylium

multi-state species with macrocycles over the photochemical transformations, equilibrium and rate constants is also included. And finally, the light and pH control over the covalent bonding between the diol groups in some flavylium-multistate species and phenylboronic acids is described.

4.1 2'-hydroxyflavylium-flavanone system as a molecular timer with a reset

The synthetic 2'-hydroxyflavylium derivatives have a similar behavior to the anthocyanins and other flavylium-derived compounds when they are dissolved in aqueous acidic solutions (see Chapter 1). In basic solutions 2'-hydroxyflavylium derivatives leads to the formation of flavanones from the deprotonated *trans*-chalcone.[242, 243] This mechanism is already well described in the literature for the synthetic 2-hydroxy chalcones. The mechanism involves the chalcone isomerization and cyclization in alkaline medium.[244]

In Nature is well known that flavanones are found as part of the flavonoid biosynthesis pathways, and normally are formed by enzymatic cyclization of chalcones.[245] In the last years, flavanones have received large attention because of been identified as compounds with high antioxidant[246, 247], antimicrobial[248, 249] and cytotoxic[250] activity.

On the other hand, a molecular timer involves a group of molecules that are interconnected, commonly the timer is activated by external stimuli followed by a kinetic process that controls an specific event. Molecular timers have important roles in chemical and biological processes by regulating events with temporal order.[251, 252] In this case, the inclusion of the flavanone species in the flavylium multi-state let the construction of a molecular timer model including a reset feature controlled by the changes in the pH of the solution.

4.1.1 The reaction network

As other flavylium-based compounds, the $\mathbf{AH^+}$ form of the 2'-hydroxy-5'-methylflavylium (2'OH-5'Me) is stable in aqueous solutions at pH=1.0. After a change of the pH towards high values, not only the formation of **A**, **B**, **Cc**, **Ct**, and their deprotonated species, but also the inclusion of the flavanone species to the system is achieved. Scheme 4.1 shows the entire multi-state system for 2'OH-5'Me, as a result of the generalized three acid-base equilibria, where the formation of all species is controlled through the specific rate and equilibrium constants for this compound. Here is important to note that the only way to access to the flavanone species is through the deprotonated *trans*-chalcones which, in a first step is in equilibrium with the flavanone phenoxide ion that produces the flavanone (**Flv**), second step is conducted through the medium alkalization to the conversion into ionized flavanone ($\mathbf{Flv^-}$), see the blue square in Scheme 4.1. The set of equations extended to the basic region presented in Appendix A was used to entirely describe the 2'OH-5'Me multi-state system.

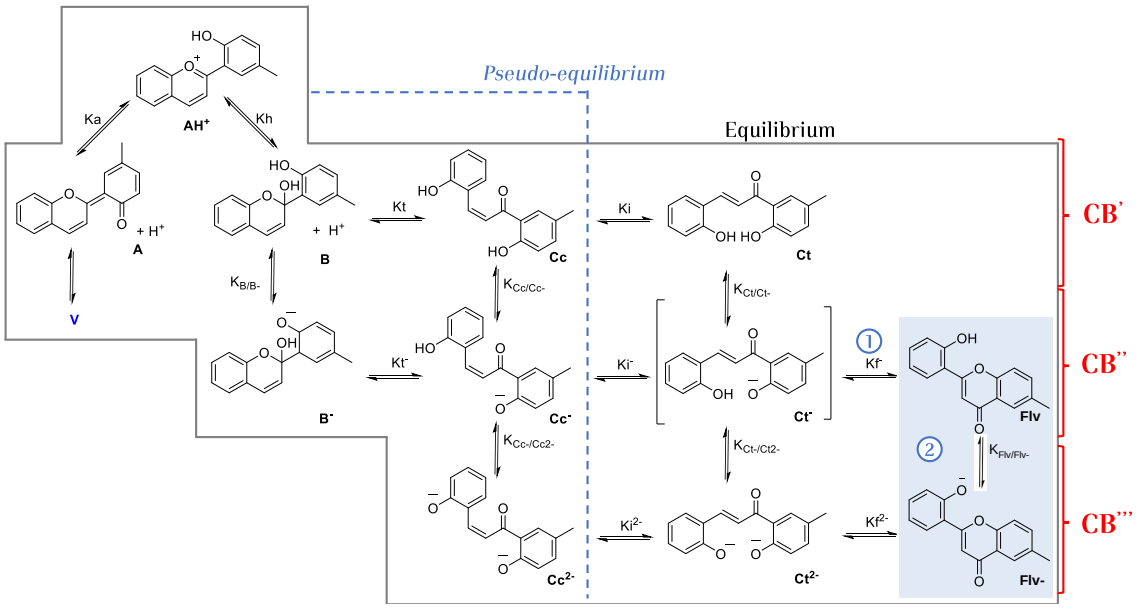

Scheme 4.1: 2'-hydroxy-5'-methylflavylium (2'OH-5'Me) multi-state species formed after the first, second and third acid-base equilibria (CB, CB^- and CB^{2-}).

As can be seen in Scheme 4.1 the **A**$^-$ cannot be formed, and although **B**$^{2-}$ can, it was not observed in any kinetic process. Therefore and as other flavylium-based compounds, the system can be described as a triprotic acid: **AH**$^+$ with the conjugated bases **CB**, **CB**$^-$ and **CB**$^{2-}$ (Eqs. A.1, A.15 and A.16).

The results observed after the performance of the direct pH jumps to different pH values, let to highlight the presence of another species, designed as V, that is a transient species formed from the quinoidal base and only appears at the pseudo-equilibrium, the really small concentrations of this compound made not possible to characterize it. Equation 4.1 represents this not identified process.

$$\mathrm{A} \overset{K_v}{\rightleftharpoons} \mathrm{V} \tag{4.1}$$

The 2'OH-5'Me compound has a high *cis-trans* isomerization barrier and therefore $[\boldsymbol{CB}^{\wedge}] = [\boldsymbol{A}]+[\boldsymbol{V}]+[\boldsymbol{B}]+[\boldsymbol{Cc}]$; $[\boldsymbol{CB}^{\wedge\wedge}] = [\boldsymbol{B}^-]+[\boldsymbol{Cc}^-]$ and $[\boldsymbol{CB}^{\wedge\wedge\wedge}] = [\boldsymbol{Cc}^{2-}]$. While at the equilibrium the **Ct** species are included.

Due the presence of the **V** species, Equations A.6 and A.40 must be rewritten as:

$$K'_a = K_a + K_h + K_a K_v + K_h K_t + K_h K_t K_i \tag{4.2}$$

$$K^{\wedge}_a = K_a + K_h + K_a K_v + K_h K_t \tag{4.3}$$

and the **V** molar fraction obtained by Equation 4.4.

$$\chi_V = \frac{K_v[H^+]^2}{D} = \frac{e_0 K^{\wedge}_a [H^+]^2}{D} \tag{4.4}$$

where $D = [H^+]^3 + K_a^{\wedge}[H^+]^2 + K_a^{\wedge}K_a^{\wedge\wedge}[H^+] + K_a^{\wedge}K_a^{\wedge\wedge}K_a^{\wedge\wedge\wedge}$ and e_0 is the percentage assigned to **V** at the pH of **CB** during the reverse pH jumps experiments (see Appendix B).

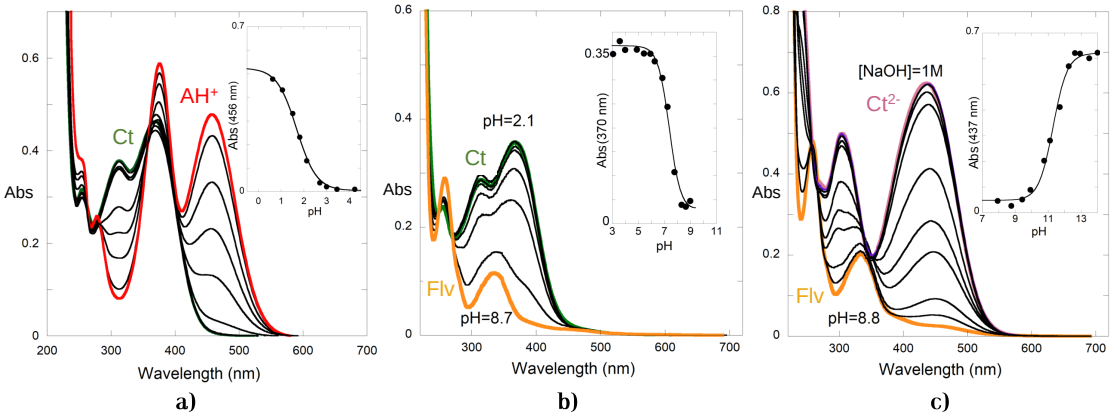

Figure 4.1: pH dependent UV-Vis spectral variations of the 2'OH-5'Me flavylium based compound at the equilibrium, a) ($3.5 \times 10^{-5} M$) involving the **AH⁺** (red line) and the **Ct** (green line) $pK'_a = 1.7$, b) ($2.8 \times 10^{-5} M$) the equilibrium between **Ct** and **Flv** (orange line) $pK''_a = 7.4$ and c) ($3.5 \times 10^{-5} M$) the equilibrium between the **Flv** and the **Ct²⁻** (pink line) $pK'''_a = 11.3$.

As the formation of the flavanone species is conducted only by the amount of **Ct⁻** and **Ct²⁻** by a slow rate constant (even slower than the isomerization), the system can be studied at the beginning without those species, but at the end, the series of reversible reactions included by the flavanone species let to create a system that works as a pH-dependent molecular timer as will be demonstrated below.

4.1.2 The 2'OH-5'Me equilibrium constants

After the direct pH jumps the absorption spectra of the 2'OH-5'Me equilibrated solutions at different pH values are presented in Figure 4.1. These spectra confirm the presence of three inflection points at distinct pH values, a normal behavior in a triprotic acid with $pK'_a = 1.7$, Fig. 4.1a, $pK''_a = 7.4$, Fig. 4.1b and $pK'''_a = 11.3$, Fig. 4.1c. The shape and position of the absorption bands suggest a final equilibrium between **AH⁺** ($\epsilon_{373} = 16{,}970$), **Ct** ($\epsilon_{365} = 12{,}960$), **Flv** ($\epsilon_{243} = 10{,}460$), and the di-deprotonated **Ct²⁻** ($\epsilon_{443} = 17{,}650$).

The fist deprotonation constant $pK_a = 5.35$, which represents the equilibrium between **AH⁺** and **A**, was calculated from the immediate UV-Vis spectra registered after a direct pH jump (Figure 4.2a). The pseudo-equilibrium transient state constants were also obtained when no significant amount of **Ct** species are formed. Figure 4.2b and c show the spectral variation along the pH scale at the pseudo-equilibrium permitting to obtain the acidity constants $pK_a^{\wedge} = 3.5$, $pK_a^{\wedge\wedge} = 7.5$ and $pK_a^{\wedge\wedge\wedge} = 11.5$.

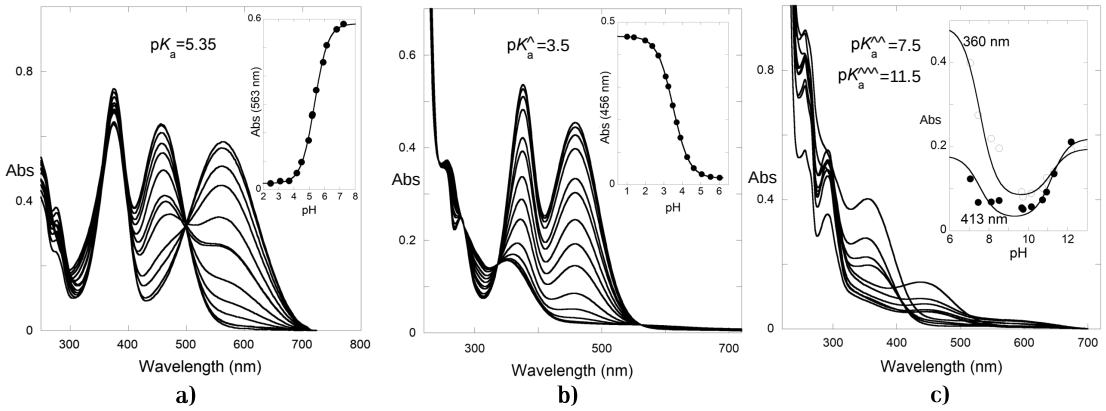

Figure 4.2: pH dependent UV-Vis spectral variations of the 2'OH-5'Me flavylium based compound a)($4.5 \times 10^{-5} M$) 10 ms after a pH jump followed by stopped-flow, $pK_a = 5.35$; b) ($3 \times 10^{-5} M$) after reaching the pseudo-equilibrium followed by common spectrophotometer; c)($1 \times 10^{-4} M$) the same as b for alkaline solutions, $pK_a^{\wedge\wedge} = 7.5$ and $pK_a^{\wedge\wedge\wedge} = 11.5$.

The data obtained from Figures 4.1 and 4.2 allow the calculation of the mole fraction distribution of $\mathbf{AH^+}$, **CB**, $\mathbf{CB^-}$ and $\mathbf{CB^{2-}}$ in the equilibrium and the pseudo-equilibrium respectively, as shown in Figure 4.3b (dotted lines) and Figure 4.3c. The reverse pH jumps from pseudo-equilibrated solutions to pH=1 and the series of equations presented in Appendix B were used to calculate the molar fractions of each species at a specific pH (Figure 4.3b). Figure 4.3a shows a typical trace observed after a reverse pH jump from a pseudo-equilibrated solution followed at 490 nm. Commonly the initial absorption is due to the fast transformation of the quinoidal base species in flavylium cation during the mixing time of the stopped-flow, that in this case should be very small considering a low quinoidal absorption band at pH=4.85 in the pseudo-equilibrium (Figure 4.2b), however, the reverse pH jumps experiments results showed a non negligible absorbance at t=0 in the pH range of the $\mathbf{CB^{\wedge}}$, suggesting the existence of another species (**V**) that is in equilibrium with the other species and is quickly transformed into the flavylium cation, in a similar way as **A**. The reverse pH jump experiments from pH values in the range of $\mathbf{CB^{\wedge -}}$ and $\mathbf{CB^{\wedge 2-}}$ showed no initial absorbance, indicating the lack of **V** or **A** species. Further evidence for the inclusion of **V** are the results of the hydration kinetics, studied deeply below. The faster kinetic step in Figure 4.3a represents the conversion of hemiketal, and the slower the transformation of *cis*-chalcone into more flavylium cation. Once obtained the mole fractions for each species at the pseudo-equilibrium and plotted in Figure 4.3b its not strange to note that the $\mathbf{CB^{\wedge 2-}}$ mole fraction coincides with the $\mathbf{Cc^{2-}}$ mole fraction because this is the sole species after the second deprotonation. After all, it is not possible to obtain the deprotonated quinoidal bases and the di-deprotonated hemiketal, the same in the equilibrium with $\mathbf{CB^{2-}}$=$\mathbf{Ct^{2-}}$. Comparing the difference from pK_a' and $pK_a^{\wedge}$ is enough to calculate $K_h K_t K_i = 1.96 \times 10^{-2}$ and after the reverse pH jumps experiments get $K_i = 89$, see Table 4.1.

Since at pH=11 the 2'OH-5'Me solution at the equilibrium has $\mathbf{Ct^{2-}}$ as major species,

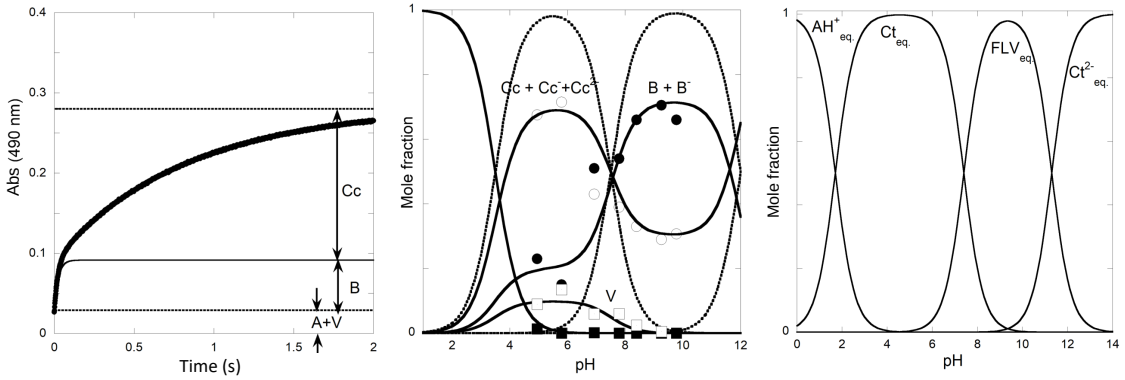

Figure 4.3: a) Trace of reverse pH jump (pH=4.85 to 2.1) from pseudo-equilibrated solution of 2'OH-5'Me, $2.8 \times 10^{-5} M$. The amplitudes of the traces should be normalized to have (A+V)+B+Cc=1; b) fitting of the mole fraction distribution at the pseudo-equilibrium including the data obtained from the reverse pH jumps and c) fitting of the mole fraction distribution at the equilibrium using the data obtained from Fig. 4.1.

Table 4.1: Equilibrium constants of the 2'OH-5'Me flavylium based compound.

pK_a'	pK_a''	pK_a'''	$pK_a^{\wedge}$	$pK_a^{\wedge\wedge}$	$pK_a^{\wedge\wedge\wedge}$	pK_a	$pK_{Ct/Ct-}$
1.7 ± 0.1	7.4 ± 0.1	11.3 ± 0.1	3.5 ± 0.1	7.5 ± 0.1	11.5 ± 0.1	5.36 ± 0.1	8.7 ± 0.1
$pK_{Ct-/Ct2-}$	$K_h M^{-1}$	K_t	K_i	$pK_{B/B-}$	$pK_{Cc/Cc-}$	$pK_{Cc-/Cc2-}$	
12.1 ± 0.1	$6.3 \times 10^{-5} \pm 0.5$	3.5 ± 0.5	89 ± 10	6.9 ± 0.1	7.9 ± 0.1	11.5 ± 0.1	

[a] pK_a''' regards basically the equilibrium between Flv/Ct^{2-}, while $pK_{Ct-/Ct2-}$ concerns the equilibrium constant between Ct^{2-}/Ct^{-}, only obtained from the equilibrium of **Ct** species.

its titration through reverse pH jumps let the calculation of the **Ct** equilibrium constants with their protonated species. The equilibrium between **Ct^{2-}** and **Ct^{-}** is observed in Figure 4.4a with a $pK_{Ct-/Ct2-} = 12.1$, while the equilibrium of **Ct^{-}** and **Ct** observed in Figure 4.4b let to calculate $pK_{Ct/Ct-} = 8.7$. When the spectra obtained in Figure 4.1 is compared with the **Ct** species obtained in Figure 4.4 is clear that the spectra of **Ct^{-}** does not appear in the equilibrium, thus it is responsible for the formation of the flavanone species.

The formation of the flavanone species, blue square in Scheme 4.1, from deprotonated **Ct** species, was confirmed by ^{1}H NMR experiments (see Figure 4.5). The equilibrium at pD=5.5 in D_2O:CD_3OD shows a typical spectrum for the **Ct** as major species, identified by the pair of doublets appearing at lower field with a coupling constant of $J = 16Hz$. The spectra obtained ca. 5 min after a pD jump from pD=5.5 to pD=8.7, over a yellow solution, shows once again the signals for the **Ct^{-}**, where the chemical shifts observed in Figure 4.5b can be assigned to the ionization of this species that is in fast equilibrium with **Ct**. After 14h in the dark, the spectrum shows new signals (around 37% of formation) increased after 72h, these signals attributed to the **Flv** species.

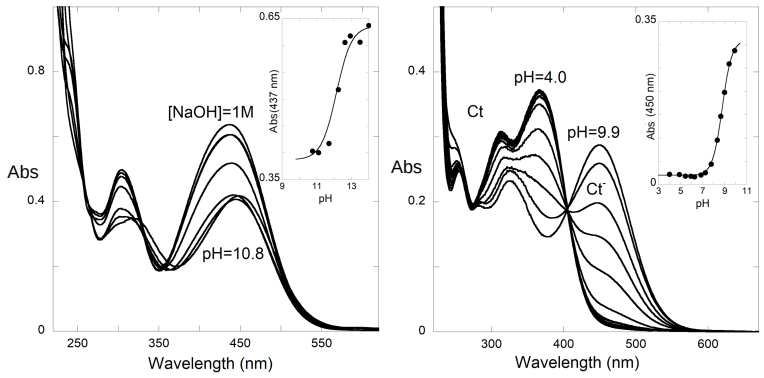

a) b)

Figure 4.4: UV-Vis spectra obtained immediately after a reverse pH jump titration of the *trans*-chalcones of the 2'OH-5'Me flavylium based compound a) ($4 \times 10^{-5} M$) from NaOH=1M to pH=10.8, $pK_{Ct-/Ct2-} = 12.1$ and b) ($2.8 \times 10^{-5} M$) from pH=9.9 to pH=4.0, $pK_{Ct/Ct-} = 8.7$.

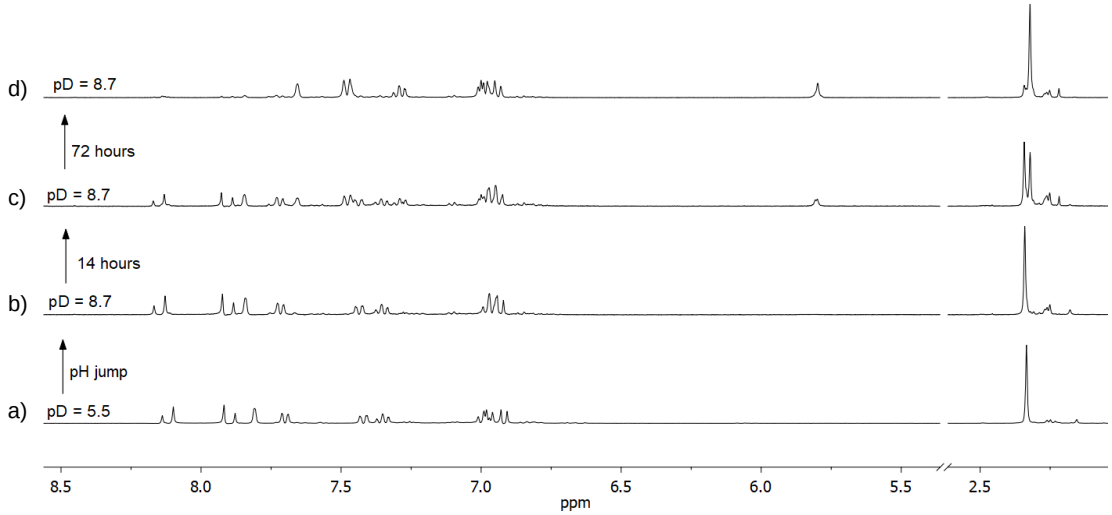

Figure 4.5: ^{1}H NMR of the 2'OH-5'Me flavylium based compound ($1 \times 10^{-3} M$) in D_2O:CD_3OD at a) pD=5.5 (equilibrated solution), b) immediately after a pD jump 5.5 to 8.7 (borate buffer); after 14h and c) after 72h.

4.1.3 Kinetics of the 2'OH-5'Me flavylium system

As already observed in the previous section, the only species in the equilibrium are **AH$^+$**, **Ct**, **Flv**, and **Ct^{2-}**. The mole fraction of these species at the equilibrium is presented in Figure 4.3c. The fact that the access to the flavanone species is only through **Ct$^-$**, makes this system a good candidate to set a molecular timer with a reset controlled by the pH of the solution. Firstly, it is important to characterize the kinetics that control the conversion between the species. The rate constants can be obtained following the kinetics by UV-Vis spectrophotometry after a direct pH jump or a reverse pH jump (from pseudo-equilibrated solutions) and applying the set of equations already studied in Chapter 1. By demonstrative purposes, the spectral variations after a direct pH jump from pH=1.0 to pH=4.96 followed by

stopped-flow is shown in Figure 4.6a, where an observable kinetic constant can be calculated following a specific wavelength during the time (see inset). Once the k values obtained from the direct (black circles) and reverse pH jumps (open circles) along the pH scale, the plot in Figure 4.6b can be constructed representing the hydration rate constant.

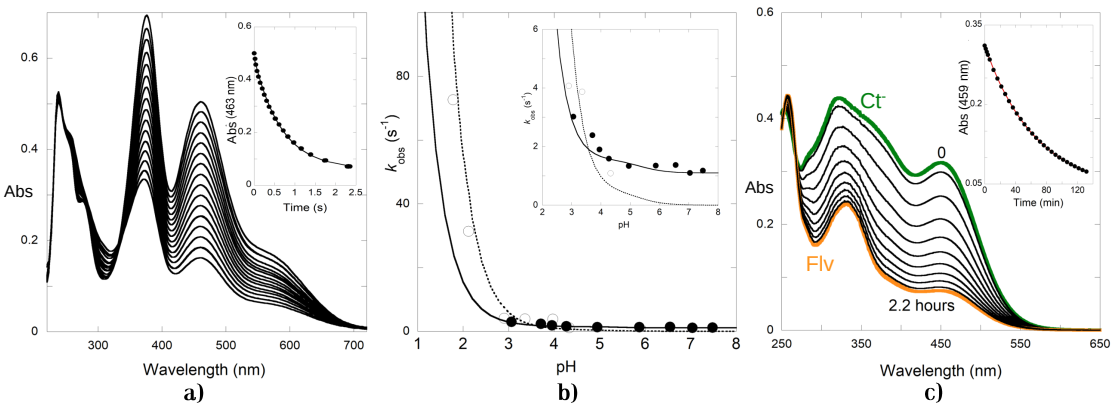

Figure 4.6: a) UV-Vis spectral variations of 2'OH-5'Me $3.5 \times 10^{-5} M$, after a direct pH jump from pH=1.0 to pH=4.96. The decay is mono-exponential with a $k_{obs} = 1.65 s^{-1}$; b) Rate constants obtained from the direct (●) and the reverse (○) pH jumps followed by stopped-flow, fitting achieved for $q = 1590 M^{-1} s^{-1}$; $p = 0.45 s^{-1}$; c) UV-Vis spectral variations of 2'OH-5'Me $3.5 \times 10^{-5} M$, after a direct pH jump from pH=12 to pH=8.3, $k_{obs} = 2.5 \times 10^{-4} s^{-1}$.

The inset in Figure 4.6b shows that the pH-dependent observed rate constant does not tend to zero, as commonly occurs in the flavylium based compounds. The black points are compatible with the reaction of **A** and not only from **AH⁺** as conventional systems, that tends to zero after the inflection point at pK_a. These results are evidence of the existence of **V** species. The fitting of the direct pH jumps represented in Figure 4.6b is achieved using Equation 4.5, that is formally equal to Equation 1.17 (Chapter 1 plus a constant r that accounts for the observed reaction of **A**.

$$k_{obs} = \frac{[H^+]}{[H^+] + K_a} p + q[H^+] + r \tag{4.5}$$

where p is equal to $k_h = 0.45 s^{-1}$ and q to $k_{-h}/(1+K_t)$ (fitting with $K_t = 3.5$, $k_{-h} = 7140 M^{-1} s^{-1}$).

During a direct pH jump to a pH value in the **Ct⁻** domain, two consecutive kinetic steps are observed, Figure 4.7. Immediately after the pH jump the quinoidal base is formed (not observed), disappearing fast to form the species in the pseudo-equilibrium (**B⁻** and **Cc⁻**). The fist process observed is the formation of **Ct⁻** (Figure 4.7a), followed by the appearance of **Flv** in a second and slower process (Figure 4.7b). The kinetic of the two processes is presented in Figure 4.7c, fitted with rate constants $k_{obs1} = 7.7 \times 10^{-4} s^{-1}$ and $k_{obs2} = 2.3 \times 10^{-4} s^{-1}$. This series of kinetic steps indicates that the isomerization process to form **Ct⁻** is required to form **Flv**. At pH=12 the system is isomerized to **Ct²⁻** ($pK_a''' = 11.3$) without the formation of the

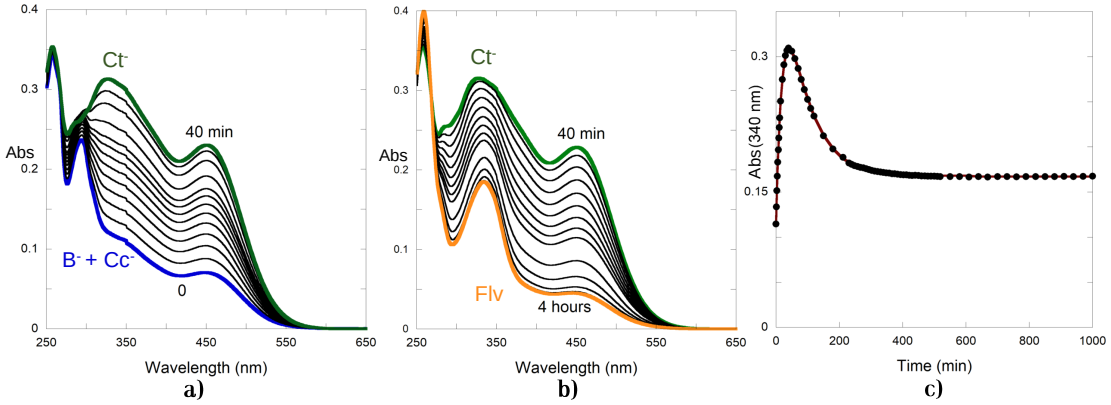

Figure 4.7: UV-Vis spectral variation upon a direct pH jump (pH=1 to pH=8.1) of a $4.4 \times 10^{-5} M$ 2'OH-5'Me solution corresponding to the first kinetic process from the pseudo-equilibrium to Ct^-; b) the second kinetic process from the Ct^- to Flv: c) trace of the global process followed at 340nm, $k_{obs1} = 7.7 \times 10^{-4} s^{-1}$ and $k_{obs2} = 2.3 \times 10^{-4} s^{-1}$.

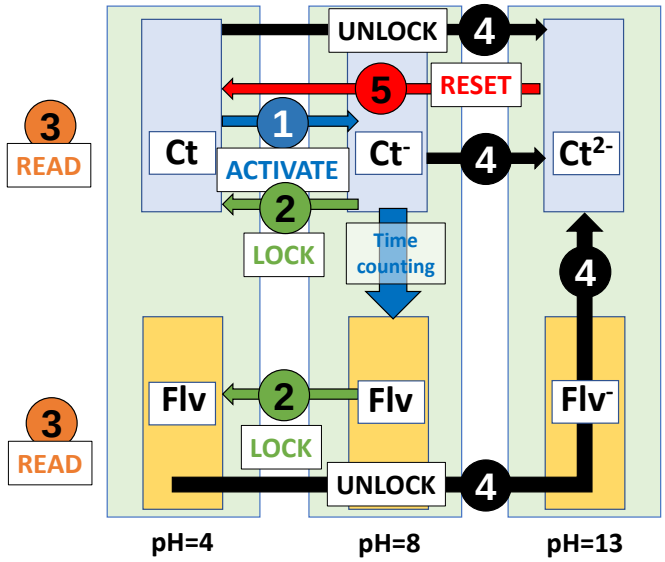

Scheme 4.2: The concept of timer with reset at molecular level from the *trans*-chalcone/flavanone system. Steps 1, 2, 4 and 5 take place in the ms time scale.

flavanone species. As previously reported in Figure 4.4 reverse pH jump gives immediately the protonated **Ct** species, and only **Ct**$^-$ evolves to **Flv**, see Figure 4.6c.

4.1.4 A model for a timer with a reset including the flavanone species

The cycle to define the molecular timer starts with **Ct** and its deprotonated species, Scheme 4.2. The timer is activated upon a direct pH jump from an equilibrated solution pH=4 to pH=8 (**Ct** to **Ct**$^-$), where **Flv** is slowly formed. At this point, the system can be locked decreasing the pH back to pH=4 that converts the remaining **Ct**$^-$ into **Ct**. The ratio **Ct**/**Flv** is dependent on the time spent between the activation and the lock. The unlock can be

activated by increasing the pH to pH=13 converting both **Ct** and **Flv** into $\mathbf{Ct^{2-}}$. Finally, the system reset is applied by a reverse pH jump to pH=4. All the reactions in the model are completed in the mixing time of the stopped-flow (ms time scale), except for the reaction that serves to count the time $\mathbf{Ct^{-}}$ to **Flv**. The conversion of **Ct** species into $\mathbf{AH^{+}}$ is useless to include in the timer model, because the isomerization reaction at acidic pH values is extremely slow and is not achieved photochemically.

4.2 Host-guest stabilization of the species of the 7-β-D-Glucopyranosyloxy-4'-hydroxyflavylium by a Cyclodextrin

3-Deoxyanthocyanidins (3-DAs) and their *O*-glycosides are natural flavylium derivatives that can be found in many plant tissues, especially in black sorghum and some ferns[253, 254, 255]. These compounds are considered the chemical ancestors of anthocyanins but oppositely to them, 3-DAs lacks a hydroxyl or sugar substituent in position C3.[22, 256] This feature provides the 3-DAs unique physicochemical properties, and maybe the most important is the great resistance to color bleaching and higher stability than common anthocyanins.[253, 256, 257]. Hydroxyl groups in positions C4' and C7 are common in natural 3-DAs and, as all the hydroxyl groups, are important for the expression of different color shades through hydroxyl proton lost, that leads to the formation of the quinoidal bases. Unlike the typical anthocyanins the molar fraction of **Ct** in 3-DAs is high at mildly acidic media. Being the **Ct** the main species able to react with a light stimulus for the chemical inter conversions into the other species in the flavylium multi-sate system, the 3-DAs become interesting compounds to study the photochemical transformation between the species.

The time-consuming and low-yielding in the extraction of natural 3-DAs makes their synthesis a relevant alternative to obtain pure compounds, these synthetic compounds could also be modified to increase their photochromic properties. Recently, an efficient method for the synthesis of 3-DAs with glucosyl substituents in different positions was published,[258] promoting the glycosylation of C4' and C7 as a large influence in the resulting color and their stability.[258, 259]. The 7-β-D-Glucopyranosyloxy-4'-hydroxyflavylium flavylium cation (GHF) shown in Figure 4.8 is a synthetic 3-DA with a high *cis-trans* isomerization barrier that has shown photochromism by means of the photoisomerization reaction of **Ct** to **Cc** and the rest of the species in the pseudo-equilibrium.[259] Some macrocycles as the Cyclodextrins (CDs) form inclusion complexes or host-guest associations, which are intermolecular arrangements where a guest molecule interacts through non-covalent forces with the cyclodextrin host. Once the complex has been formed the solubility and stability of some guest compounds can be improved. Even the stabilization of different dyes have been tested by means of their encapsulation.[260, 261, 262] The use of native CDs (Figure 4.8 where R=H) is limited by their water solubility, therefore the charge and hydrophobicity of the macrocycles have been modified by their derivatization.[263] Despite many available

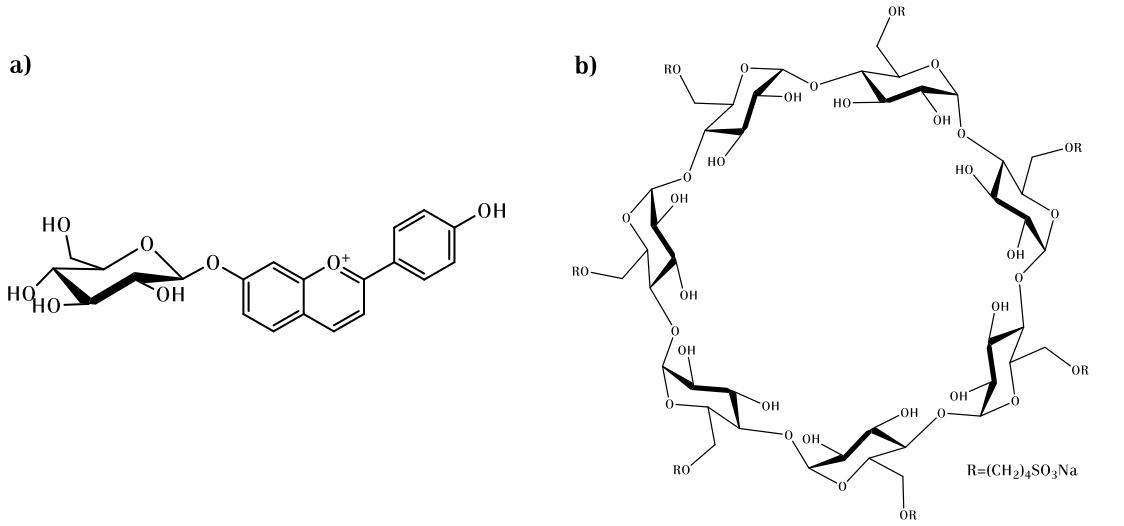

Figure 4.8: Structure representation of a) the 7-β-D-Glucopyranosyloxy-4'-hydroxyflavylium flavylium cation (GHF) and the b) Sulfobutylether-β-Cyclodextrin (SBE-β-CD).

derivatives, the Sulfobutylether-β-Cyclodextrin (SBE-β-CD) has shown higher water solubility and strong complexing ability with natural phenolic compounds as curcuminoids,[113, 114] carotenoids[115, 116] and flavonoids.[117, 118]

Relatively to the flavylium-based compounds, Roewer reported that the storage stability in the color of some anthocyanins is enhanced by interaction with SBE-β-CD[119], these findings could result also in the stabilization of $\mathbf{AH^+}$ form even in 3-DAs and anthocyanins. Despite β-cyclodextrins have an anti co-pigmentation effect over the colored forms in the flavylium-based compounds[122, 123], the high association constants with the chalcones causes their stabilization and, there is an important increment in the photoisomerization reaction in some synthetic 3-DAs as the 3',4',7-trihydroxy-flavylium or the 4',7-dihydroxy-flavylium.[123, 264].

As reviewed in Chapter1 many external factors affect directly the equilibrium between the flavylium multi-state species, and the stability of each one is important to consider a specific observable property of the system. Some factors alter the equilibrium in a reversible way, as a light pulse, whereas other factors as the pH or the complexation with other molecules are irreversible. Consequently, the equilibrium and kinetic constants of the synthetic 3-DA compound GHF were compared in the absence and the presence of the commercial SBE-β-CD *"Captisol"* as host. This knowledge could help to define new strategies of color stabilization in flavylium-based compounds and/or find more efficient photochromic systems.

4.2.1 The reaction network

After raising the pH of an acid solution containing GHF, the species shown in Scheme 4.3 are formed, following the typical flavylium multi-state set of equations. As have been reported previously the GHF presents a high *cis-trans* isomerization barrier and therefore, it is possible to define a pseudo-equilibrium. This let the possibility to observe three distinct kinetic processes: (i) formation of the quinoidal base, (ii) hydration (rate-determining step) followed immediately by the tautomerization and the *cis-trans* isomerization. The equilibrium and rate constants of the GHF also were previously reported.[259]

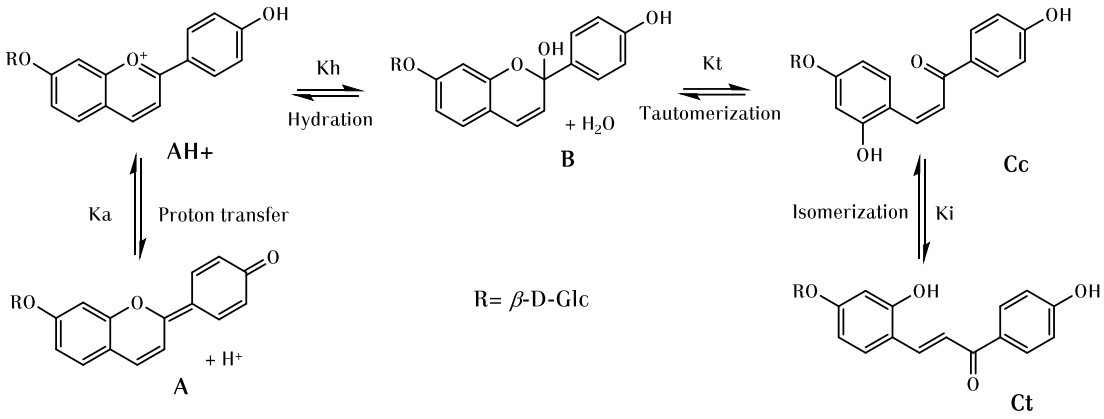

Scheme 4.3: 7-β-D-Glucopyranosyloxy-4'-hydroxyflavylium flavylium cation (GHF) flavylium multi-state species formed after the first acid-base equilibrium ($AH^+ \rightleftharpoons CB'$).

4.2.2 Host-guest association constants

The association constants of some GHF species with Captisol as a host can be calculated experimentally by different techniques. Being **AH⁺** and **Ct** stable species at the equilibrium in acidic and mildly acidic solutions respectively, their association constants with the host can be calculated by UV-Vis titration, see Figure 4.9. The **AH⁺**-Captisol binding constant was estimated from the spectra collected a few seconds after increasing the concentration of the macrocycle at pH=1.0. On the other hand, the **A**-Captisol binding constant was calculated collecting the absorption spectra after a pH jump to pH=7.7 where **A** is the major species at the very begging of the jump (the spectra must be recorded in the first 10 ms). In both cases, Captisol brought about significant spectral differences, leading the calculation of their corresponding binding constants, using a specific wavelength absorbance versus Captisol concentration plots. The resulting **AH⁺**-Captisol binding constant, 200 M^{-1}, is much higher than those reported in native β-CDs in similar compounds.[123, 264] A possible explanation for this effect is the additional electrostatic attraction of the sulfobutyl units negative charges in the host and the flavylium cation, in the same manner, it happens in some anthocyanidins.[119] Conversely, the **A**-Captisol binding constant results close to

the one reported with β-CD.[123]

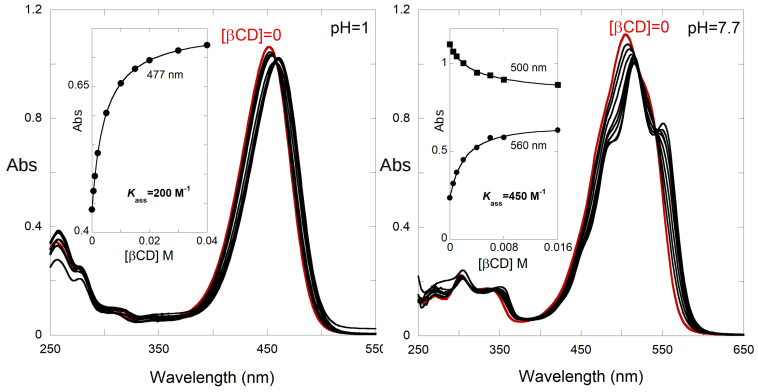

Figure 4.9: a) UV-Vis spectral variation of GHF as function of added Captisol, a) GHF (3.33×10^{-5}M) at pH=1.0 b) GHF (4×10^{-5}M) at pH=7.7 followed by stopped-flow.

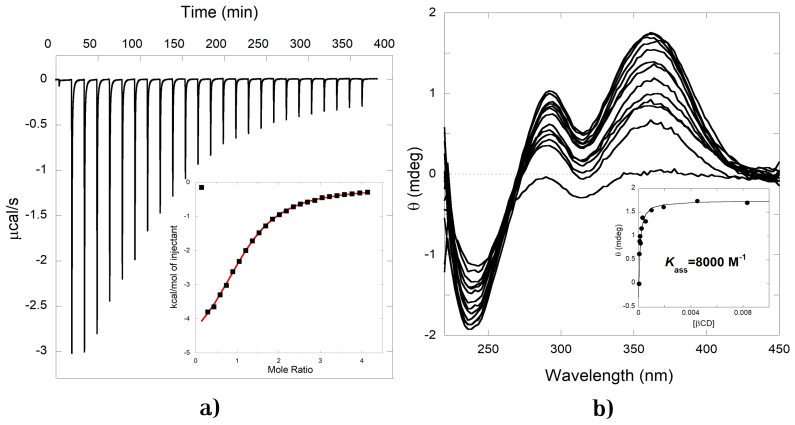

Figure 4.10: a) Isotermal titration calorimetry of GHF (0.288 mM) by captisol (4 mM) at pH=6.18 and b) circular dichroism spectra of GHF (6.93×10^{-5}M) as a function of captisol concentration (0-8.33×10^{-3}M) at pH=6.0.

To obtain the **Ct**-Captisol binding constant, an equilibrated GHF solution pH=6.18 (where **Ct** is the sole species) was titrated with Captisol by isothermal titration calorimetry (ITC). The study of the results obtained from Figure 4.10, $K_b = 7700M^{-1}$, $\Delta H_b^0 = -21.6kJmol^{-1}$ and $\Delta S_b^0 = +4.83Jmol^{-1}K^{-1}$, leads to the differentiation between the types of non-covalent interactions between the host and the guest. In accordance with Bouchemal and Mazzaferro[265] the van der Waals interactions between cyclodextrins and their guest are enthalpy-driven processes with minor favorable or unfavorable entropies of interaction ($|\Delta H| > T|\Delta S|$); while hydrophobic interactions are entropy-driven, where the entropy is large and positive whereas the enthalpy is small ($|\Delta H| < T|\Delta S|$). In the case of the Captisol-GHF binding, a favorable (exothermic) enthalpy-driven binding process ($|\Delta H| > T|\Delta S|$) is

established, then prevailing van der Waals over hydrophobic interactions take place. Confirmation of the **Ct**-Captisol binding constant is possible by a titration followed by circular dichroism (CD). CD has been widely used with other inclusion complexes of **Ct** and β-CDs,[86, 266] where the induced circular dichroism signal in the **Ct** wavelength [167] resulting from the association with the host is plotted versus its concentration (Figure 4.10b). Assuming a 1:1 binding model, the **Ct**-Captisol binding constant is $K_b = 8000M^{-1}$ in agreement with the result obtained by ITC.

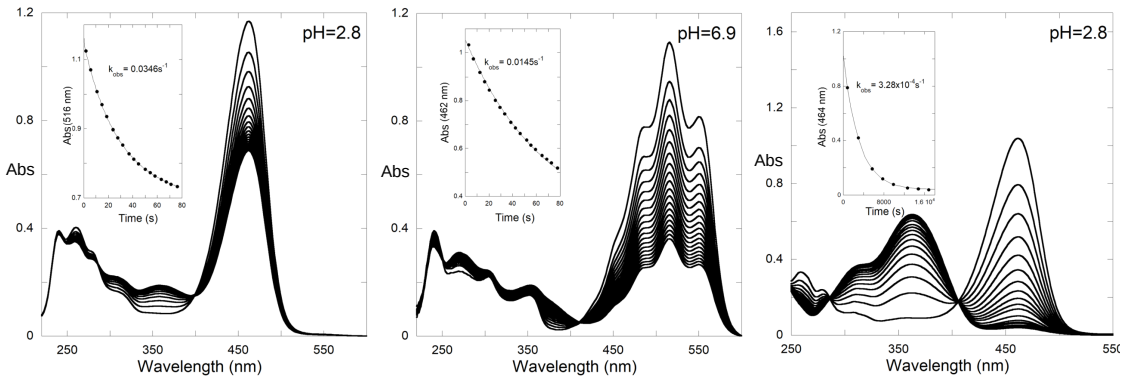

a) b) c)

Figure 4.11: a) UV-Vis spectra spectral variation of GHF (3.33×10^{-5}M) in the presence of Captisol (0.05M) after a pH jump from pH=1.0 to a) pH=2.35 and b) pH=6.9 followed by stopped-flow, and c) pH=2.8 until equilibrium is achieved.

4.2.3 Equilibrium and rate constants

To evaluate the effect of the CDs over the equilibrium and rate constants, a series of direct pH jumps (followed by stopped-flow) from equilibrated solutions at pH=1.0 to higher pH values, in the presence of Captisol, was carried out. Figure 4.11a represents the kinetics observed after a direct pH jump to pH=2.35, the $\mathbf{AH^+}$ disappears to give the **B** and **Cc** forms in a single process controlled by the hydration, the formation of **Ct** being much slower. At this pH, the **A** is negligible, unlike what happens at pH=6.9 (Figure 4.11b where no $\mathbf{AH^+}$ is observed and all of it is practically converted into **A**, and the spectral variation refers to the disappearance of this species leading to the pseudo-equilibrium. Once again, no significant amount of **Ct** is formed. The slowest process leads to the full equilibrium, where **Ct** is finally formed (Figure 4.11c).

Representation of the pH dependant hydration and isomerization rate constants is presented in Figure 4.12a and b respectively. Hydration in Figure 4.12a was fitted using Equation 1.14 for the direct pH jumps and Equation 1.17 for the reverse pH jumps from solution at the pseudo-equilibrium, while the isomerization rate constant was fitted by Equation 1.15. At high pH values, the fraction of electrophilic $\mathbf{AH^+}$ is weak and hydration is slower than tautomerization thus rate-determining. Conversely, the isomerization plot in 4.12b

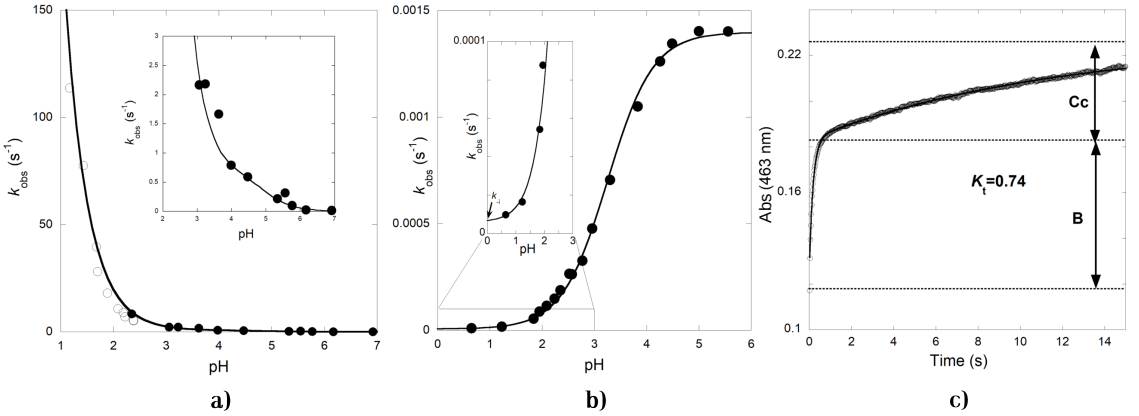

Figure 4.12: pH dependent constants representation of GHF in the presence of Captisol a) apparent hydration rate constant, ● direct pH jumps, ❍ reverse pH jumps from pseudo-equilibrium and b) apparent isomerization rate constant and c) reverse pH jump from a pseudo-equilibrated solution (pH=6.0) to pH=2.4 followed by stopped-flow.

gives the expected sigmoid curve, with an inflection point at $pK_a^{\wedge} = 3.2$. The limits of this curve at low and high pH represent the $k_{-i} = 6 \times 10^{-6} s^{-1}$ and $K_h K_t k_i / K_a^{\wedge} = 1.4 \times 10^{-3} s^{-1}$.

The absorption spectra obtained by the stopped-flow apparatus immediately after a direct pH jump to different pH values in solutions with GHF and the SBE-β-CD Captisol is represented in Figure 4.13a, from which the pK_a value can be easily calculated. In the same way, the $K_a^{\wedge}$ and K_a' can be obtained from the absorption spectra obtained, after following the kinetics, in the pseudo-equilibrium and the equilibrium (Figures 4.13b and c). Comparing the acid dissociation constant in the presence of Captisol, $K_a = 1.12 \times 10^{-5}$ ($pK_a = 4.95$), is higher than the one in the absence of the cyclodextrin, $K_a = 3.98 \times 10^{-6}$ ($pK_a = 5.4$), indicating that the quinoidal base binds Captisol more tightly than the flavylium cation does. The same occurs with the $K_a^{\wedge}$ values, where the higher $pK_a^{\wedge}$ value in the absence of Captisol (4.7) shows that the macrocycle has a higher affinity for the $CB^{\wedge}$ species (essentially, for **B** and **Cc**) than for $\mathbf{AH^+}$. Finally, the same trend is observed at full equilibrium where the pK_a' is reduced in 1.5 units in the presence of Captisol (pK_a'=0.8), indicating a preferential stabilization of the *trans*-chalcone over the flavylium cation, $\mathbf{AH^+}$. It is remarkable that in the presence of Captisol the compound GHF behaves as a stronger acid.

Considering that the value of $K_h(1+K_t)$ obtained from $K_a^{\wedge} - K_a$ is equal to the ratio between k_h and $k_{-h}/(1+K_t)$, the rate and equilibrium parameters obtained from Figures 4.11, 4.12 and 4.13 can be confirmed. When the flavylium multi-state has a high isomerization barrier, it is possible to study the reverse pH jumps from the pseudo-equilibrium to obtain more information related to the rate and equilibrium constants.[71, 72] When the final pH is sufficiently acidic, the hydration that is highly $[H^+]$ dependent, is faster than tautomerization (change of regime). This phenomenon is fitted by Equation 1.17 when **B** gives $\mathbf{AH^+}$ and 1.18 when **Cc** produces more flavylium cation. Figure 4.12c shows a typical representation

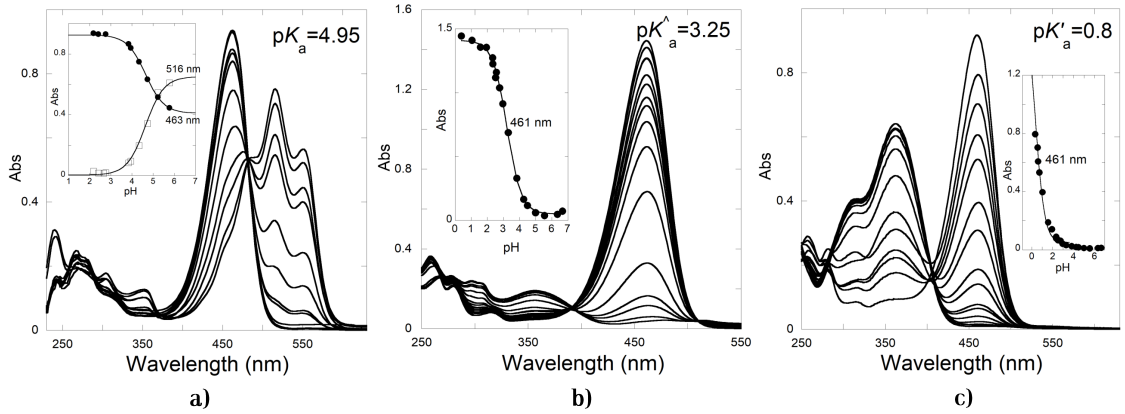

Figure 4.13: Spectral modifications observed for GHF (3.33×10^{-5}M) in the presence of 0.05M of Captisol after a direct pH jump a) 10 ms b) at the pseudo-equilibrium and c) at the equilibrium.

of a reverse pH jump of a pseudo-equilibrated solution of GHF in the presence of Captisol at pH=6.0. The $K_t = 0.74$ results from the ratio between the molar fraction of **Cc** and **B**.

4.2.4 Photochemistry

In the flash photolysis experiments, the *trans*-chalcone is photoisomerized into *cis*-chalcone during the flash lifetime (≈ 2.4ms). The initial bleaching at 362nm observed in Figure 4.14a is representative of this event, because **Cc** has a lower absorption coefficient than **Ct**.[22, 72] Later, in a second process, **Cc** disappears exponentially through the tautomerization reaction, the k_{obs} of this second step is represented in Figure 4.14b for different pH values. Irradiation of **Cc** during a prolonged time leads to the formation of $\mathbf{AH^+}$ reaching the pseudo-equilibrium as shown in Fig. 4.14c, once the light source is turned off the solution goes back to **Cc** until the equilibrium (data not shown). This photochromic system operates in acidic pH, with a quantum yield three times higher ($\Phi = 0.3$) than in the absence of the host ($\Phi = 0.1$).

Table 4.2: Equilibrium and rate constants of GHF in the absence and presence of Captisol.

Compound	pK'_a	$pK^{\wedge}_a$	pK_a	K_h/M	K_t	K_i
GHF	2.30 ± 0.05	4.70 ± 0.05	5.40 ± 0.05	8.9×10^{-6}	0.60	935
GHF-Captisol	0.83 ± 0.05	3.25 ± 0.05	4.95 ± 0.05	3.5×10^{-4}	0.74	567
	k_h/s^{-1}	$k_{-h}/M^{-1}s^{-1}$	k_t/s^{-1}	k_{-t}/s^{-1} [a]	k_i/s^{-1} [a]	k_{-i}/s^{-1} [a]
GHF	0.08	9×10^3	0.36	0.60	5.5×10^{-3}	5.9×10^{-6}
GHF-Captisol	0.67	1.9×10^3	0.019	0.025	3.4×10^{-3}	6×10^{-6}

[a] Estimated error: 10%

The data reported in Table 4.2 shows the equilibrium and rate constants obtained from Fig. 4.12 to 4.14 after the fittings with Equ. 1.14, 1.15 and 1.18. In the presence of Captisol,

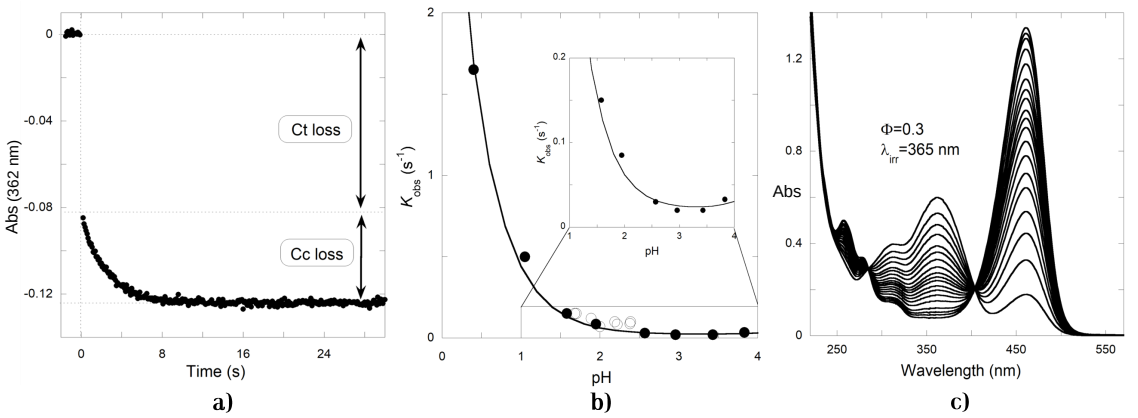

Figure 4.14: a) Time dependence of the max. absorption wavelength in chalcones after a flash light at pH=1.0. b) pH dependent tautomerization plot, with the experimental data obtained from the slowest process in reverse pH jumps ❍ and from the flash photolysis experiments ●, fitting obtained by Equation 1.18 and c) spectral modifications of GHF in the presence of Captisol upon irradiation.

the hydration equilibrium constant increases ca. 39 times due to the increase and decrease of the hydration and dehydration rates respectively. The tautomerization process is also affected by Captisol, making it more difficult to open or close the C ring, this effect can be attributed to the geometric constraints inside the host cavity.

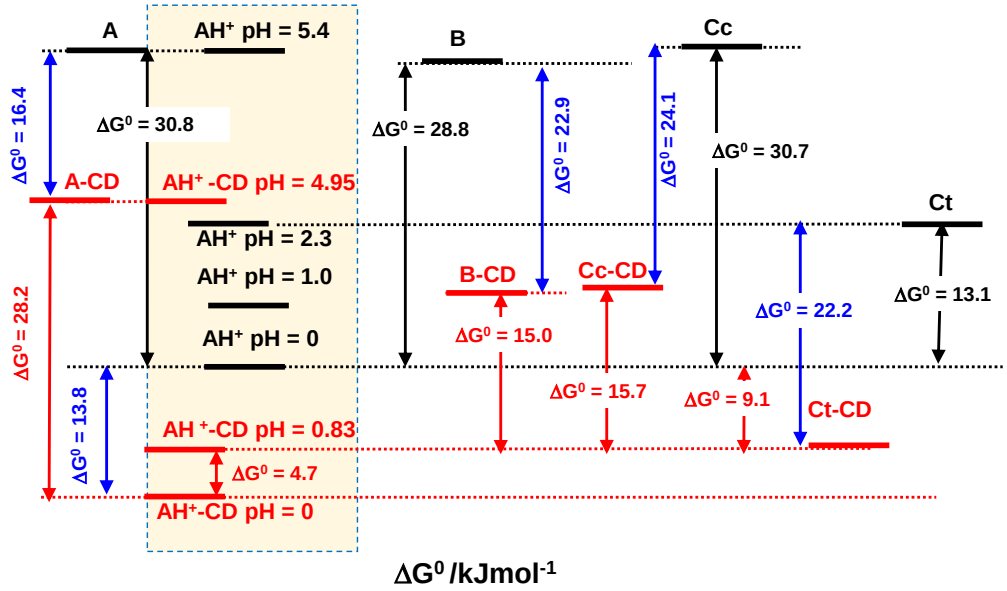

Figure 4.15: Energy level diagram of GHF in the absence (black) and presence of Captisol 0.05 M(red). Superposition of the two diagrams using the *trans*-chalcone-Captisol binding constant allows the calculation of the other binding constants (blue color).

Taking into account the equilibrium constants of Table 4.2 is possible to construct an

Table 4.3: Binding constants of GHF with Captisol [a].

	AH^+	A	B	Cc	Ct
$K_b(M^{-1})$ [b]	200	450	(10300)	(17000)	8000 [c]
ΔG^0 [b] $(kJmol^{-1})$	13.1 (13.8)	15.1 (16.4)	(22.9)	(24.1)	22.2 [c]

[a] Estimated error: 10%

[b] Experimental values, in brackets the calculated values

[c] Used to calibrate the energy level diagram (determined by CD and ITC)

energy level diagram of GHF in the absence (black) and the presence (red) of Captisol represented in Figure 4.15. The two independent diagrams can be merged by using the binding constants of **Ct**, **A** and **AH$^+$** with Captisol previously calculated. The binding constants with the host of all other species can be obtained by calculating the corresponding ΔG^0 values (blue). The theoretical **B**-Captisol=$10300M^{-1}$ and **Cc**-Captisol=$17000M^{-1}$ binding constants (K_b) were obtained. The experimental binding constants obtained in Figures 4.9 and 4.10 are in complete agreement with the theoretical values calculated from the diagram. The K_b values presented in Table 4.3 show that the flavylium cation and the quinoidal base have a low affinity for the host, while the hemiketal and *cis*-chalcone strengthen the binding by two orders of magnitude.

4.3 pH and photo responsive covalent bonding between flavylium compounds and boronic acids

The condensation reaction between boronic acids, $RB(OH)_2$ and dihydric alcohols, H_2L, have been studied in various fields of chemistry and biochemistry. The equilibria among the species in aqueous solution and the mechanism of boronate esters formation is still debatable and is under constant discussion. Many different mechanisms are documented,[267, 268] among them the one published by Furikado et. al.[269] seems to be the most complete including the complexation with bidentate ligands. Monodentate boronate esters are formed only at very alkaline solutions and with ligands with high pK_a values. Conversely, the reaction of the boronic acids with bidentate ligands with lower pK_a values is favored in neutral or slightly acidic solutions. This mechanism is presented in Scheme 4.4 for the complexation between a boronic acid and catechol representing a diol, where the four different paths can be identified depending on the species involved in the reaction. The reactivity of the boronic species is $RB(OH)_2$>$RB(OH)_3^-$, while in the case of the ligands H_2L>HL^->L^{2-}, therefore the paths 1 and 2 from the Scheme 4.4 are favored. Once the BL^- is formed, this is in fast equilibrium with its BL form.[270]

Due the reactivity of the species involved in the boronate esters formation, it is clear that the reaction is pH-dependant. Therefore, an optimal pH for the association constant must be associated with the pK_a values of the boronic acid and its ligand. The prediction

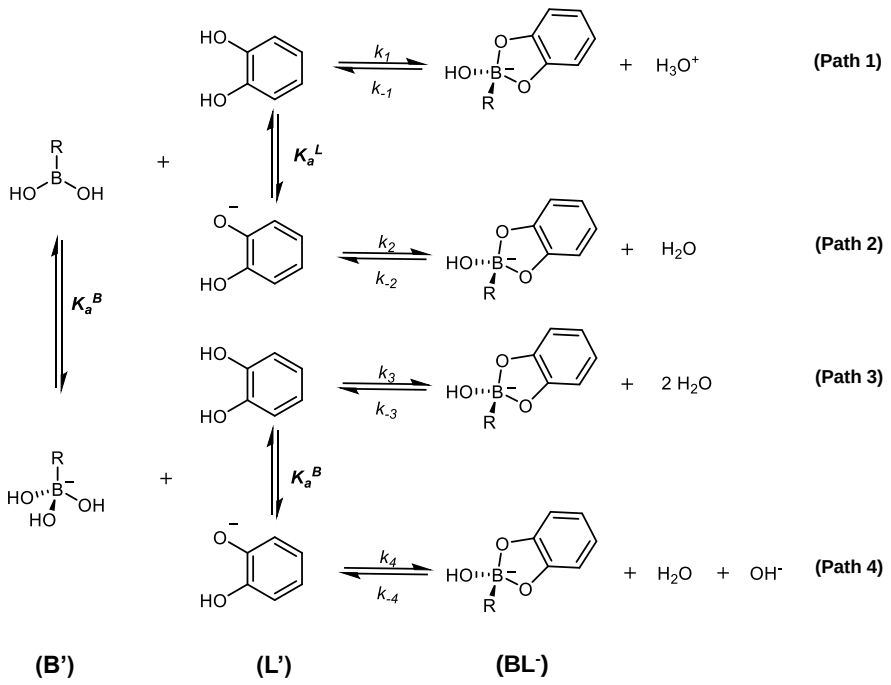

Scheme 4.4: Different reaction pathways for the bidentate condensation of a boronic acid and a diol (catechol).

of the optimal pH was previously reported for the Wang's group[271] for a series of boronic acids and diols. The optimal pH with the higher association constant can be calculated as an approximate of an average of the pK_a values of the boronic acid and the ligand.

The typical pK_a' values of the flavylium-based compounds are between the slightly acidic and the neutral pH range.[22] This is an advantage if the interaction with a boronic acid with a higher pK_a value takes place, ensuring the presence of the most reactive species $RB(OH)_2$ and H_2L.

8-hydroxyflavylium compounds can form boronate esters in a selective way through the chalcone species. The boronic acid (BA) interact only with the *trans* or *cis*-chalcone bearing a catechol group. This association can be disrupted after the formation of the the flavylium cation (**AH$^+$**), achieved by acidification of the medium or in some cases by the

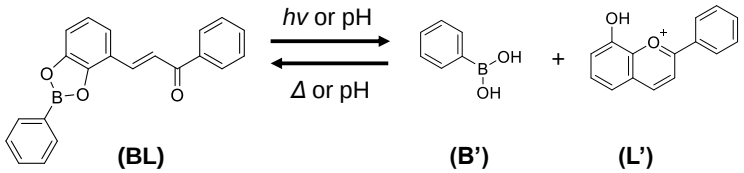

Scheme 4.5: General pH and photo induced disruption of the boronic ester formed between a chalcone from the 8 hydroxyflavylium family and phenylboronic acid.

cis-trans photoisomerization of the **Ct**, see Scheme 4.5. In this section the design of a 8-hydroxyflavylium derivative compound able to react selectively through the chalcones with phenylboronic acid to form a boronate ester and their dissociation using light as an external stimulus.

4.3.1 Design of the ligand and its interaction with the boronic acid

In a preliminary stage, the synthesis of the 8,4'-dihydroxyflavylium (8,4'OH) compound and its interaction with the phenylboronic acid (PBA) was performed. The low water-solubility of the 8,4'OH and the low response to the light stimulus for the *cis-trans* photoisomerization in acidic media led to the design of a higher soluble 8-hydroxyflavylium compound. As most of the flavylium compounds have low pK'_a values, this force to work in acidic medium, far from the optimal pH to the formation of the boronate esters with the PBA. This problem can be overcome including a host molecule as the curcubit[7]uryl (CB7), that have demonstrated to increase both, the pK'_a and also in the quantum yield for the photoisomerization in many flavylium systems.[180, 272]

The new compound was designed thinking not only in increasing its water solubility, but also in a high association constant with the host CB7. Flavylium compounds with ammonium groups have shown high association constants with CB7[180, 237] and of course higher water solubility because of their ionic properties. Scheme 4.6 shows the structure of the flavylium dication 8OH4'TMA and its conjugate base species (CB) formed in aqueous solution at different pH values.

Once synthesized, the 8OH4'TMA pK'_a was calculated registering the variation in the absorption UV-Vis spectra of equilibrated solutions at different pH values. Figure 4.16a shows the spectra of these solutions, inset shows the inflection point for the calculation of a low $pK'_a = 1.73$. The equilibrium in 8OH4'TMA is attained only between the **AH⁺** and **Ct** species. As the phenylboronic acid has a $pK_a = 8.8$, thus the $RB(OH)_2$ form, that is more reactive, is always present in solutions with pH values lower than 7. On the other hand, the pK_a value of the chalcones can not be calculated because of their degradation up to pH 7, but at pH lower than pH 6 no spectral variations can be observed, then the neutral form

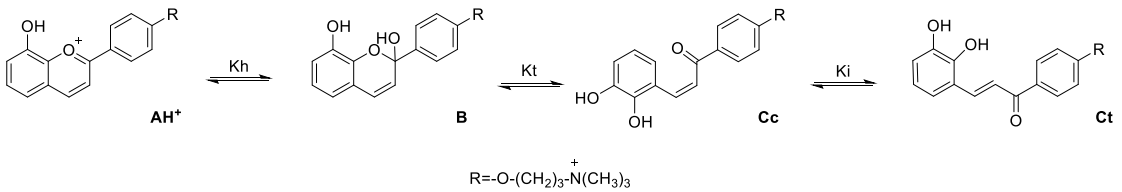

Scheme 4.6: Species in the flavylium multi-state of the compound 8OH4'TMA as a result of its first deprotonation (CB).

is ensured between pH 1 to 6. The association constant between the PBA and the *trans*-chalcone was calculated at different pH values following the UV-Vis spectra after titration of equilibrated solutions of 8OH4'TMA with increasing concentrations of PBA. Figure 4.16b shows the UV-Vis spectra variations at pH=6.26, while in Figure 4.16c the pH-dependence association constants in the formation of the boronate esters are represented (no higher pH values were explored because some 8OH4'TMA degradation is observed). It is well known that buffer conjugate bases from phosphate and citrate react with the boronic acids [267] but in this case all the buffer concentrations were kept as low as 0.01 M. The optimal pH prediction for the boronate esters formation, using the method applied by the Wang's group,[271] was impossible to calculate because the **Ct** pK_a was neither possible to obtain due to its degradation at pH above pH=7. However, this method does not take in account the intermolecular interactions, buffer and solvent effects, and other external factors that could affect the association constants, therefore is considered imprecise. As seen in Figure 4.16c the optimal pH for the formation of 8OH4'TMA-PBA boronate esters is clearly higher than pH=5.26.

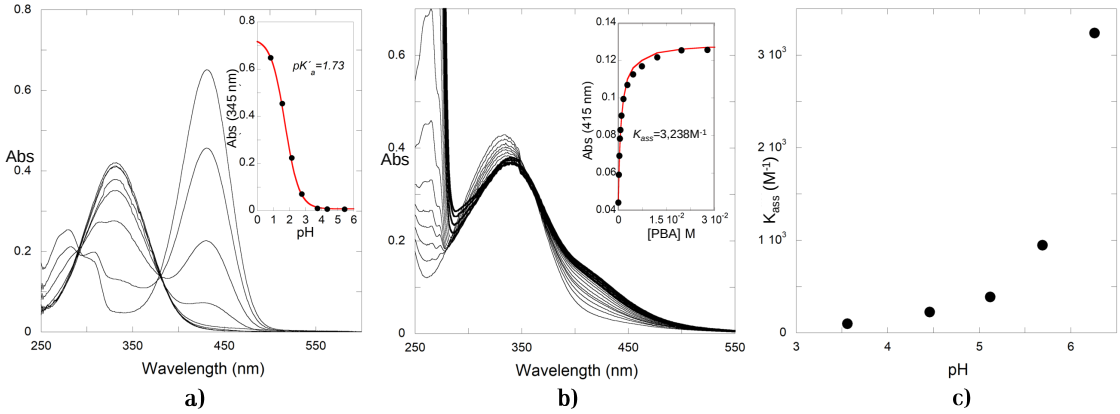

Figure 4.16: a) UV-Vis absorption spectra of equilibrated solutions of 8OH4'TMA(2.7×10^{-5}) obtained after direct pH jumps from pH=1 to different pH values; b) UV-Vis absorption spectra of an equilibrated solution of 8OH4'TMA(1.8×10^{-5}) at pH=6.34 obtained after its titration with increasing concentrations of phenylboronic acid (PBA), fitting was achieved for a 1:1 stoichiometry with $K_{ass} = 3,238 M^{-1}$; c) association constants of the 8OH4'TMA **Ct** and PBA at different pH values.

As the optimal pH for the 8OH4'TMA-PBA boronate esters formation is far from the pH where some $\mathbf{AH^+}$ can be transformed after photoisomerization of the **Ct**, the complexation with CB7 seems to be an alternative to increase the 8OH4'TMA pK'_a. Figure 4.17a shows the UV-Vis spectra variations after titration of $\mathbf{AH^+}$ with CB7 at pH=1. The association constants were obtained by the 2:1 host-guest model fitting of the experimental data for a $K_{1:1} = 1.6 \times 10^5 M^{-1}$ and $K_{2:1} = 1.4 \times 10^5 M^{-1}$, see inset. Similarly, the CB7 interaction with **Ct** was studied at pH=4.06, obtaining $K_{1:1} = 1 \times 10^5 M^{-1}$ and $K_{2:1} = 500 M^{-1}$, see Figure Figure 4.17b. These results are in complete agreement with those reported for the CB7 association with similar flavylium compounds.[237] The molar fractions obtained with the

constants from Figure 4.17b are represented in Figure 4.17c, where a maximum of CB7-Ct (1:1) complex is obtained with 0.1 mM of the host. The higher association constants between CB7 and **AH⁺** compared with those with **Ct** results in the increase of the stabilization of the first. This stabilization increases the pK'_a value of the 8OH4'TMA to 4.62 in the presence of CB7 0.1 mM, increasing the pH domain of the **AH⁺** as shown below in Figure 4.19a.

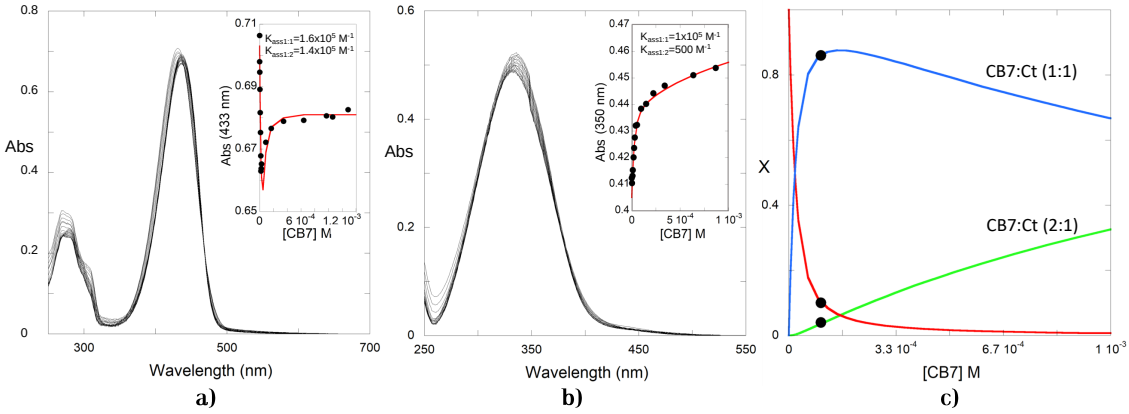

Figure 4.17: a) UV-Vis absorption spectra of a solution of 8OH4'TMA (**AH⁺**)(1.8×10^{-5} M) at pH=1 obtained after its titration with increasing concentrations of cucurbit[7]uril (CB7), fitting was achieved for a 2:1 host-guest stoichiometry with $K_{1:1} = 1.6 \times 10^5 M^{-1}$ and $K_{2:1} = 1.4 \times 10^5 M^{-1}$; b) the same but at pH=4.06 (**Ct**) fitting was achieved for a 2:1 host-guest stoichiometry with $K_{1:1} = 1 \times 10^5 M^{-1}$ and $K_{2:1} = 5 \times 10^2 M^{-1}$; c) molar fractions of the complexes between **Ct** (1.8×10^{-5} M) and CB7 at different concentrations of CB7.

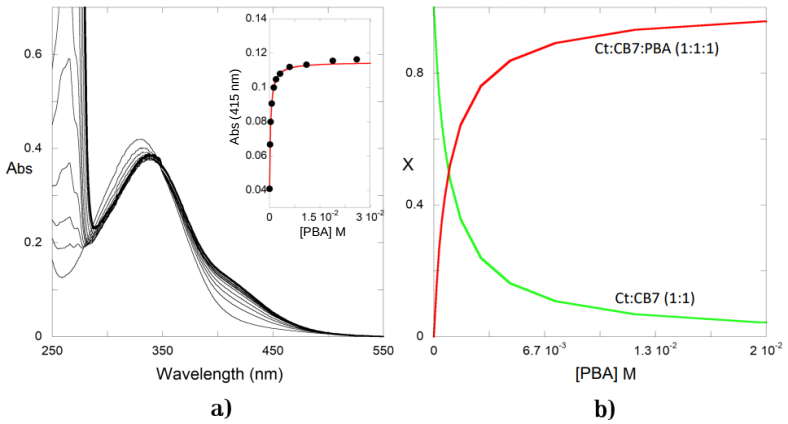

Figure 4.18: a) UV-Vis absorption spectra of a solution containing 8OH4'TMA (**Ct**)(1.8×10^{-5} M) and CB7 (1×10^{-4} M) at pH=6.28 obtained after its titration with increasing concentrations of PBA, fitting was achieved for a 1:1 stoichiometry with $K_{ass} = 1.13 \times 10^3 M^{-1}$ (K_{BL}); b) molar fractions of the complexes between **Ct**(1.8×10^{-5} M), CB7 (1×10^{-4} M) and PBA at different concentrations of PBA.

By the same way as the association constant between **Ct** and PBA was previously calculated, this constant was recalculated but in the presence of 0.1 mM of CB7 at pH=6.12,

where **Ct** is the only flavylium multi-state species in solution. Figure 4.18a shows the UV-Vis absorption spectra after the titration. The obtained association constant in the presence of the host is lower than in the absence, two different reasons can be responsible for this behavior; i) the optimal pH for the formation of the boronate esters is shifted to higher pH values since the 8OH4'TMA pK'_a increases with the presence of CB7 or ii) the interaction of the host with the flavylium species hinders the interaction with the PBA.

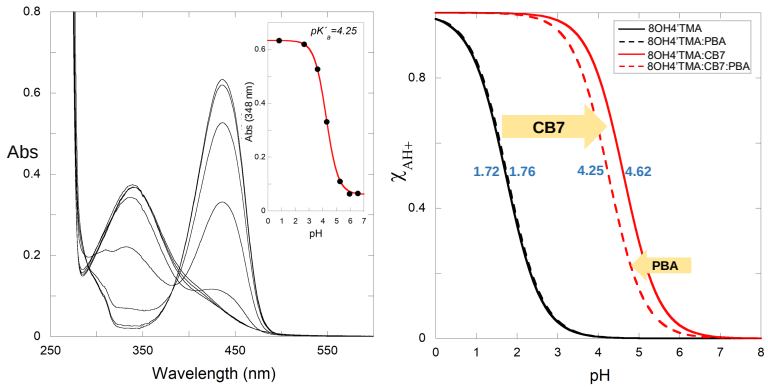

a) b)

Figure 4.19: a) UV-Vis absorption spectra of 8OH4'TMA (2.7×10^{-5} M) equilibrated solutions containing CB7 (1×10^{-4} M) and PBA (6×10^{-3} M) obtained after direct pH jumps from pH=1 to different pH values; b) pK'_a shifts in solutions with 8OH4'TMA (black line), in the presence of PBA (6×10^{-3} M; black dotted line), in the presence of CB7 (1×10^{-4} M; red line) and in the presence of CB7 (1×10^{-4} M) and PBA (6×10^{-3} M; red dotted line).

The affinity of the PBA for the chalcones can decrease the pK'_a value due to the stabilization of the chalcones, for this reason a $pK'_a = 1.76$ was calculated in the presence of PBA 6 mM. In the same way the pK'_a was calculated in the presence of CB7 0.1 mM and PBA 6 mM ($pK'_a = 4.25$). The representation of the pK'_a shifts in the presence and absence of PBA and CB7 appears in Figure 4.19b. Interestingly, the acidic dissociation constant remains practically unchanged in the presence of the PBA and the absence of CB7, whereas in the presence of CB7 a decrease from $pK'_a = 4.62$ to 4.25 is observed. The formation of boronate esters at acidic pH values has a low constant, therefore the pK'_a remains unchanged because non species is stabilized. Around pH=6 the Ct-PBA association constant is higher and some stabilization of the chalcones take place lowering the pK'_a value. The interaction between the PBA and a ligand with slightly acidic pK_a value as alizarin red S ($pK_a = 5.33$) has been already reported,[269] after the boronate ester formation, a decrease in the pK_a value of the complex to 2.36 was observed.

4.3.2 Photochemical dissociation of the boronate esters

In Chapter 1 the photochemical properties of flavylium-based compounds were introduced. Some flavylium derivatives possess the quality to react to a light stimulus, interconverting

the chalcone species between their *cis* and *trans* isomers. As the 8-hydroxyflavylium compounds only form bidentate boronate esters with their chalcone form, and these are formed by means of a reversible reaction, irradiation of equilibrated solutions with **Ct**-PBA in the presence of CB7 can disrupt the boronate esters by formation of **B** and **AH⁺**. Three different equilibrated solutions at pH≈6 containing 8OH4'TMA (**Ct**), CB7 0.1 mM and different concentrations of PBA (1, 2 and 5 mM) were irradiated at 365 nm, the UV-Vis spectra of the solution was monitored and the results are shown in Figure 4.20.

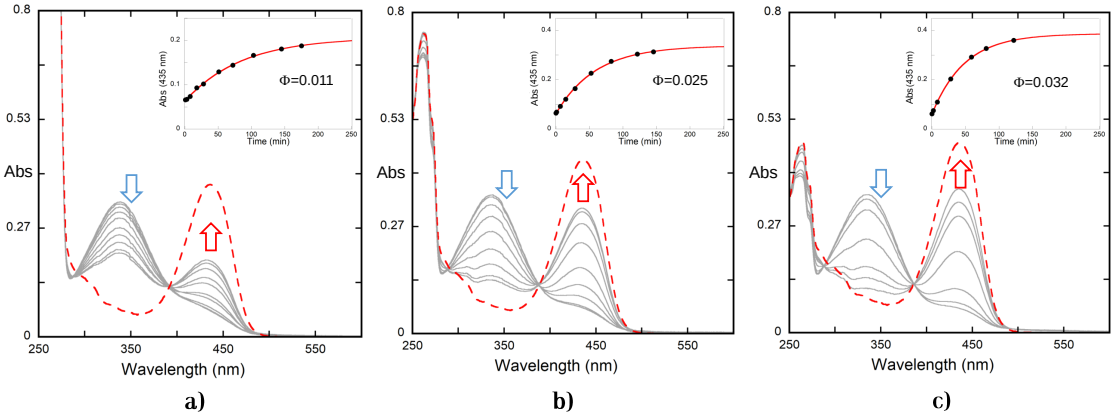

Figure 4.20: a) Spectral UV-Vis absorption variations observed upon irradiation (365 nm) of 8OH4'TMA (2.7×10^{-5} M) in the presence of CB7 (1×10^{-4} M) and PBA=5×10^{-3} M; b) the same with PBA=2×10^{-3} M, and c) the same with PBA=1×10^{-3} M. Red dotted line represents the absorption spectrum at the pseudo-equilibrium.

As observed in Figure 4.20, after irradiation of the solutions at 365 nm, the chalcones absorption band centered at 338 nm decreases progressively, while the band of the flavylium cation at 435 nm is increased. The higher the concentration of PBA, the less formation of **AH⁺** after irradiation. With a PBA vs **Ct**-CB7 association constant (K_{BL}) of 1.1×10^3

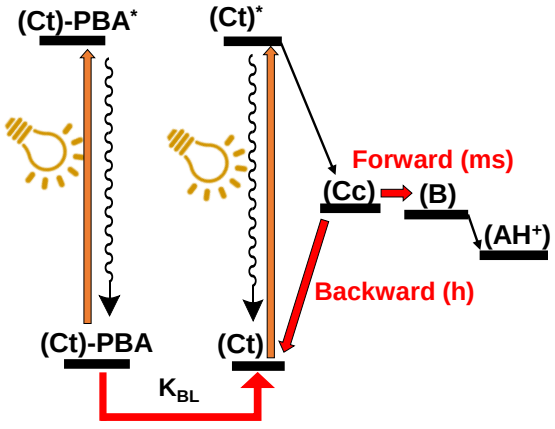

Scheme 4.7: Proposed mechanism for the disruption of **Ct**-PBA boronate esters through photo-isomerization of **Ct** to **Cc**.

M^{-1} (Figure 4.19) the molar fraction of boronate esters would be 0.53, 0.69 and 0.85, this represents the 47, 31 and 25% of free **Ct** in the equilibrated solutions with 1, 2 and 5 mM of PBA respectively. The red dotted line in Figure 4.20 represents the spectra at the pseudo-equilibrium for each solution, thus are the expected after total conversion of the **Ct** species into **Cc** upon irradiation. After the light exposure a fraction of free **Ct** is isomerized into **Cc**, at the same time **Cc** is quickly converted into **B** and $\mathbf{AH^+}$ because they are in fast equilibrium. The less $\mathbf{AH^+}$ formation in those solutions with higher PBA concentrations indicate that the fraction of **Ct** forming a boronate ester is not available to photo-isomerize and only the free **Ct** reacts to the light stimulus. This results are confirmed with the calculation of the quantum yield of reaction (ϕ), which is lower in those solutions with higher concentrations of PBA. As the **Ct**-PBA complexes absorb light at the irradiation wavelength, and they are not photoisomerized, the quantum yield decreases. Once a fraction of free **Ct** is converted into **Cc**, a new equilibrium between **Ct**/**Ct**-PBA is set ruled by the equilibrium constant K_{BL}, see Scheme 4.7.

The chalcones *cis-trans* photo isomerization by itself can be described as a photochromic system.[273] Commonly, both chalcones absorb light in the same range, close to the UV zone but **Ct** is red-shifted and its molar absorption coefficient is higher. An equilibrated solution containing only **Ct** can be photo-isomerized into **Cc**, then **Ct** can be recovered if the solution is irradiated at the wavelength of absorption of **Cc**. This effect was confirmed in solutions irradiated at 335 nm, the maximum absorbance in **Ct**/**Ct**-PBA boronate esters, where less $\mathbf{AH^+}$ is formed, this is because the fraction of **Cc** converted during the photo-isomerization of **Ct** also absorbs the incident light at 335 nm, and therefore it isomerizes back to **Ct**, this phenomenon stops when the equilibrium is reached in a photo-stationary state.

4.4 Materials and Methods

The 2'-hydroxy-5'-methylflavylium (2'OH-5'Me) was provided by Prof. Vesselin Petrov from the University of Sofia (BG) and was prepared by similar methods reported by Petrov et. al.[242] for 2'-hydroxyflavylium salt. Compound GHF was provided by Prof. Olivier Dangles from the University of Avignon (FR), it was prepared and characterized as published elsewhere.[258] Cucurbit[7]uril (CB7) was obtained from previous studies in the research group.[180] Commercial β-Cyclodextrin Captisol and phenylboronic acid (PBA) were purchased from Cydex pharmaceuticals (Lenexa, KS, US) and Sigma Aldrich (St. Louis, MO, US) respectively. Compounds 8,4'OH and 8OH4'TMA were prepared according to literature procedures.[274] Starting materials for the synthesis were purchased from commercial suppliers; 2,3-Dihydroxybenzaldehyde from Sigma Aldrich and 4'-hydroxyacetophenone from Alpha Aesar. The 3-(4-acetylphenoxy) -N,N,N-trimethylpropane-1-ammonium chloride was synthesised by other members of the research group following the procedures reported in the literature.[237]

Compound 8,4'OH. A mixture of 2,3-Dihydroxybenzaldehyde (0.14g, 1mmol) and 4'-hydroxyacetophenone (0.14g, 1mmol) were solubilized in the minimum of acetic acid, an excess of hexafluorophosphoric acid, 60% in H_2O. The mixture becomes immediately dark red and is stirred at room temperature during 48h. The solution was poured into 20 mL of diethyl ether and a colored solid precipitated. The solid was filtered and washed with diethyl ether to yield 0.37g (84%) of the flavylium hexafluoro-phosphate salt. ^{1}H NMR (400 MHz, CD_3OD-d_4) δ (ppm): 9.21 (d, J=9.2, 1H), 8.65 (d, J=9.2, 1H), 8.61 (d, J=8.9, 2H), 7.7 (m, 3H), 7.19 (d, J=9.0, 2H).

Compound 8OH4'TMA. A mixture of 2,3-Dihydroxybenzaldehyde (210 mg, 1.5mmol) and 3-(4-acetylphenoxy) -N,N,N-trimethylpropane-1-ammonium chloride (107mg, 0.4mmol) were solubilized in 4 mL of acetic acid, 1 mL of H_2SO_4 was added to the mixture. The solution was stirred at room temperature during 72h, diluted $HClO_4$ was added. The mixture was poured into diethyl ether and a colored solid precipitated. The solid was filtered and washed with diethyl ether to yield 147 mg (86%) of the flavylium salt. ^{1}H NMR (400 MHz, D_2O) δ (ppm): 9.01 (d, J=9.0, 1H), 8.33 (d, J=9.0, 1H), 7.54 (m, 3H), 7.05 (d, J=8.7, 2H), 4.16 (t, 2H), 3.46 (t, 2H), 3.06 (s, 9H), 2.24 (m, 2H).

All solutions were prepared in Millipore water, the flavylium stock solutions prepared in 0.1 M HCl. Any pH was adjusted by addition of HCl, NaOH, and/or Theorell and Stenhagen's universal buffer, for the experiments involving boronate esters 0.01 M citrate buffer was used. Direct pH jumps were carried out mixing stock flavylium solutions, neutralized with NaOH, and buffer (desired pH). Reverse pH jumps were achieved by the addition of concentrated HCl to equilibrated solutions prepared as a direct pH jump.

For the host-guest and chalcone-boronic acid constant calculations, a series of titrations were carried out in 1 cm pathlength quartz cells as follows: two solutions were prepared, A and B, both equilibrated solutions containing the same concentration of the flavylium-based compound at desired pH. Solution B contains a known concentration of the guest/boronic acid in excess, small aliquots of B are placed and mixed with solution A. After every addition an UV-Vis absorption spectra was registered. Using this method, the concentration of the compounds placed in A solution remain constant, while the concentration of the guest/boronic acid is increased until no more spectral variations are observed. The fittings of the host-guest and ligand-receptor interactions were achieved using the mathematical models for 1:1 or 2:1 interactions (See Appendix B).

pH was recorded on a Radiometer Copenhagen PHM240 pH/ion meter (Brønshøj, Denmark). UV-Vis spectra were recorded on a Varian-Cary 100 or 5000 spectrophotometer (Palo Alto, CA, US). The stopped-flow experiments were conducted on an SX20 (Applied photophysics; Surrey, UK) spectrometer equipped with a PDA.1/UV photodiode array detector. Flash photolysis experiments were performed on a Varian Cary 5000 spectrophotometer

with a Harrick fiber-mate (Pleasantville, NY, US). The compartment is isolated from daylight and a commercially Achiever 630AF camera flash (Hong Kong China) was used as a pulsed white light source (≈ 2.4ms lifetime). Quantum yields were calculated based on the total absorbed light. The **Ct**-PBA boronate esters solutions were irradiated in a 1 cm pathlength quartz cell under stirring with a xenon lamp and a monochromator was used to set the desired wavelength.

Circular dichroism absorption spectra experiments in Section 4.2 were recorded on a Chirascan qCD spectrometer (Applied Photophysics; Surrey, UK) at 25°C under constant N_2 flush. As other titrations, the flavylium-based compound was kept constant (6.93×10^{-5}) and the concentration of the Captisol was increased from 0 to 8.33×10^{-3}. A 1cm quartz cell was used for scans between 220-550 nm. The spectra was replicated and an average was applied.

Isothermal Titration Calorimetry (ITC) measurements were performed on a Nano ITC (TA instruments; New Castle, DE, US) with standard volumes. The solutions were degassed by stirring under vacuum, the sample cell was loaded with a 0.288 mM of the flavylium-based compound (equilibrated at pH=6) and 250 μM autopipette was filled with Captisol (4 mM). GHF was titrated by 25 injections of 10 μl aliquots until achieve the stability.

NMR spectra were collected using a Bruker AMX 400 (Billerica, MA, US) instrument operating at 400.13 MHz (^1H). Solutions were prepared in D_2O and any pH adjustment was performed by addition of DCl, NaOD and Borate buffer if necessary.

4.5 Conclusions

Cyclodextrins can modify the pH-dependent mole fractions of the species in the flavylium multi-state of the DAs. In GHF the Captisol cyclodextrin shifts the pH domain of hemiketal and *cis*-chalcone in the pseudo-equilibrium toward low pH values, while at the equilibrium the *trans*-chalcone domain was shifted towards lower pH values being together the flavylium cation the sole species. The quantum yield was 3-fold increased in the presence of the host. The superimposition of the energy level diagrams in the presence and absence of the host allows the calculation of the binding constants of all the multi-state species binds particularly the **B** and **Cc** species.

The flavylium multi-state chemical reactions are inspired in natural anthocyanins illustrating the complexity of the biological process. Synthetic flavylium based compounds can play a role in artificial systems able to mimic some biological process. The 2'-hydroxyflavylium family compounds are an example of the versatility of these multi-state systems. The *trans*-chalcone/flavanone cycle that works as a molecular timer with a reset responds to external

stimuli, in this case, the pH. This function together with those previously reported regarding optical memories shows potential uses for these bio-inspired systems.

The photochemical properties of the flavylium multi-state can be exploited to generate a system able to control the formation and disruption of boronate esters in compounds from the 8-hydroxyflavylium family. The association constant for the formation of the boronate esters is pH-dependent with an optimal pH between the pK_a values of the boronic acid and the diol. As the pK'_a of the 8-hydroxyflavylium compounds is low, it can be shifted by their complexation with macrocycles as CB7 to a pH value where both, the equilibrium constant for the boronic esters formation is higher, and the formation of $\mathbf{AH^+}$ through photoisomerization of **Ct** be viable. Even though the 8OH4'TMA **Ct** species linked to the phenylboronic acid do not react to the light stimulus, the photo-isomerization of the free **Ct** species shifts the equilibrium and the boronate esters are disrupted.

Publications associated with this chapter:

- S. Slavcheva, J. Mendoza, S. Stanimirov, I. Petkov, N. Basílio, F. Pina, and V. Petrov. "On the multistate of 2*I*-hydroxyflavylium-flavanone system. Illustrating the concept of a timer with reset at the molecular level."In: *Dyes and Pigments*, 158 (2018), pp. 465-473. DOI: https://doi.org/10.1016/j.dyepig.2018.05.066
- J. Mendoza, N. Basílio, O. Dangles, N. Mora, S. Al Bittar, and F. Pina. "Binding of the five multistate species of the anthocyanin analog 7-β-D-glucopyranosyloxy-4′-hydroxyflavylium to the β-cyclodextrin derivative captisol."*Dyes and Pigments*, 143 (2017), pp. 479-487. DOI: https://doi.org/10.1016/j.dyepig.2017.04.061

5

General conclusions and future perspectives.

The inter and intramolecular interactions found in natural anthocyanins as self-association, aggregation, and co-pigmentation affect in different manner the flavylium multi-state species distribution. Other intermolecular associations as host-guest interactions with macrocycles as cucurbiturils, cyclodextrins, and calixarenes, and molecular clips and micelle inclusion also affect the stability of the species in the multi-state.

The spatial distribution of the substituents in natural anthocyanins, mainly the long poly-acylated sugar chains, is important for the stabilization of the colored species. The interaction of the acylated moieties with the chromophore has demonstrated a big influence on color preservation and the hydrophobicity of the anthocyanins and their aggregates. The effective protection of the long poly-acylated residues was confirmed in the Heavenly Blue Anthocyanin (HBA1), where the intramolecular interactions between these residues with the flavylium core made the anthocyanin resistant to the hydration reaction, which leads to the production of the uncolored species. Therefore the **B** form is destabilized not only at the first deprotonation but also at the second and the third. The same effect was also observed in mono-acylated anthocyanins, but the destabilization of the uncolored species is not enough to be less stable than the quinoidal base species. The spatial distribution of the acylated moieties in natural anthocyanins must be studied in the future to study the physical protective effect over the reactive sites, sensible for water attack, in the flavylium backbone. This can be achieved by NMR techniques supported by the use of theoretical calculations. Another point that must be in consideration is the effect of external factors over the tri-dimensional structure of the acylated anthocyanins, which could affect the protection for color loss. Finally, apply the knowledge in the development of more stable anthocyanin-based matrices in food and cosmetic industries.

Some uncolored compounds can act as co-pigments increasing the expression of the colored species; the flavylium cation, and the quinoidal base. Other compounds can have an anti-co pigmentation effect stabilizing the uncolored species. Calculation of all the equilibrium and association constants in the presence of any molecule that can form complexes with the flavylium multi-state species is important to evaluate the effect of such interactions over the multi-state properties. Some co-pigments as caffeine, can increase significantly the molar fraction of the quinoidal base at the equilibrium not only in synthetic flavylium derivatives but also in natural anthocyanins. Caffeine is a stable co-pigment that has not an acid-base equilibrium between pH 1 and 7 as many other natural compounds that can act as co-pigments such as flavonols or hydroxycinnamic acids, for this reason, the association with the deprotonated forms of those compounds with the flavylium multi-state species must be also evaluated in the future. Other molecules as the water-soluble macrocycles: cucurbiturils and calixarenes or the cucurbituril-type molecular clips can act also as co-pigments, increasing the stability of the colored forms, in this case, the flavylium cation. The flavylium stabilization has been studied extensively, but the stabilization of quinoidal base could be more interesting in terms of color stability because they are extended along the pH scale after deprotonation of the flavylium cation, that is already stable at very acidic conditions. Other macrocycles as the cyclodextrins have more affinity for the uncolored species in synthetic flavylium derivatives acting as an anti-copigment, but increase the response to light during the photoisomerization reaction, the properties of the complexes can be used to construct light-responsive systems.

The stabilizing effect over the quinoidal base form was also observed in a higher level of complexity environment, the micelle inclusion, where more than two molecules interact in a supramolecular assembly. The co-micellization effect was observed when some anthocyanin-fatty acid conjugates were tested in a micelle, increasing, even more, the stability of the quinoidal base species. Stabilization of anthocyanin-based compounds in amphiphilic environments is important for the formulation of cosmetics.

The introduction of flavanones in the flavylium multi-state system opens an interesting research area. A pH-responsive system can be created in 2'-hydroxyflavylium family compounds, which can form flavanones through the ionized trans chalcones in an alkaline medium. In this case, it was possible to create a molecular timer equipped with a reset and controlled by pH changes. The photo sensibility of the flavylium multi-state can be also exploited to generate a system able to control the formation and disruption of boronate esters in compounds from the 8-hydroxyflavylium family. In the future, this photochemical reaction could be optimized by changing the flavylium compound and/or the boronic acid and exploring different pH conditions. Also, the associative/dissociative constants for the covalent bonding can be studied in the excited state to evaluate the possibility to break the bond directly by applying light.

Bibliography

[1] B. Janine. “Echoing Nature.” In: *Biomimicry: Innovation inspired by nature*. New York: Harper Collins Publishers, 2002. Chap. 1, pp. 1–10.

[2] Y. H. Cohen and Y. Reich. “The biomimicry discipline: boundaries, definitions, drivers, promises and limits.” In: *Biomimetic Design Method for Innovation and Sustainability*. Switzerland: Springer, 2016. Chap. 1, pp. 3–16.

[3] C. L. Merrill. “Biomimicry of the dioxygen active site in the copper proteins hemocyanin and cytochrome oxidase: Part I: Copper (I) complexes which react reversibly with dioxygen and serve to mimic the active site function of hemocyanin. Part II: Mu-imidazolato binuclear metalloporphyrin complexes of iron and copper as models for the active site structure in cytochrome oxidase.” Doctoral dissertation. Rice University, 1982.

[4] B. J. Brown, M. E. Hanson, D. M. Liverman, and R. W. Merideth. “Global sustainability: toward definition.” In: *Environmental Management* 11.6 (1987), pp. 713–719. DOI: http://doi.acm.org/10.1007/BF01867238.

[5] P. Glavič and R. Lukman. “Review of sustainability terms and their definitions.” In: *Journal of Cleaner Production* 15.18 (2007), pp. 1875–1885. DOI: http://doi.acm.org/10.1016/j.jclepro.2006.12.006.

[6] B. Bhushan. “Biomimetics: lessons from nature–an overview.” In: *Philosophical Transactions of the Royal Society A* 367.28 (2009), pp. 1445–1486. DOI: https://doi.org/10.1098/rsta.2009.0011.

[7] A. Gürses, M. Açıkyıldız, K. Güneş, and M. S. Gürses. “Historical development of colorants.” In: *Dyes and Pigments*. Switzerland: Springer, 2016. Chap. 1, pp. 1–9.

[8] A. Abel. “The history of dyes and pigments: From natural dyes to high performance pigments.” In: *Colour Design*. Ed. by J. Best. Textiles. Cambridge, UK: Woodhead publishing, 2012. Chap. 16, pp. 433–468.

[9] A. Siegel. “Sir Robert Robinson’s “Anthocyanin Period”: 1922–1934—A Case Study of an Early Twentieth-Century Natural Products Synthesis.” In: *Ambix* 55.1 (2008), pp. 62–82. DOI: https://doi.org/10.1179/174582308X255406.

[10] S. L. Glashow. “Immanuel Kant versus the princes of serendip: Does science evolve through blind chance or intelligent design?” In: *Contributions to Science* 2.2 (2002), pp. 251–255.

[11] G. J. Nohynek, E. Antignac, T. Re, and H. Toutain. “Safety assessment of personal care products/cosmetics and their ingredients.” In: *Toxicology and Applied Pharmacology* 243.2 (2010), pp. 239–259. DOI: https://doi.org/10.1016/j.taap.2009.12.001.

[12] D. Cardon, M. J. Melo, and H. E. Ahmed. “Historical aspects.” In: *Handbook of Natural Colorants*. Ed. by T. Bechtold and R. Mussak. West Sussex, UK: John Wiley & Sons, 2009. Chap. 1, pp. 3–36.

[13] H. Kanekar and A. Khale. “Coloring agents: Current regulatory perspective for coloring agents intended for pharmaceutical & cosmetic use.” In: *International Journal of Pharmaceutical and Phytopharmacological Research* 3.5 (2014), pp. 365–73.

[14] S. Saxena and A. Raja. “Natural dyes: sources, chemistry, application and sustainability issues.” In: *Roadmap for Sustainable Textiles and Clothing*. Ed. by S. Muthu. Hong Kong, CN: Springer, 2014. Chap. 2, pp. 37–80.

[15] S. Ali. “Biomimicry in solar energy conversion with natural dye-sensitized nanocrystalline photovoltaic cells.” Doctoral dissertation. Obelin College, Ohio, 2007.

[16] A. Smeriglio, D. Barreca, E. Bellocco, and D. Trombetta. “Chemistry, pharmacology and health benefits of anthocyanins.” In: *Phytotherapy Research* 30.8 (2016), pp. 1265–1286. DOI: http://doi.org/10.1002/ptr.5642.

[17] F. Pina. “Chemical applications of anthocyanins and related compounds. A source of bioinspiration.” In: *Journal of Agricultural and Food Chemistry* 62.29 (2014), pp. 6885–6897. DOI: https://doi.org/10.1021/jf404869m.

[18] C. Santos-Bulega and A. M. Gonzalez-Paramas. “Anthocyanins.” In: *Encyclopedia of Food Chemistry*. Ed. by P. Varelis, L. Melton, and F. Shahidi. Amsterdam, Netherlands: Elsevier, 2018. Chap. 2, pp. 10–21.

[19] R. Brouillard and O. Dangles. “Flavonoids and flower colors.” In: *The Flavonoids: Advances in Research Since 1986*. Ed. by J. Harborne. Boca Raton, FL: Chapman & Hall, 1994. Chap. 13, pp. 565–588.

[20] O. M. Andersen and M. Jordheim. “The anthocyanins.” In: *Flavonoids: chemistry, biochemistry and applications*. Ed. by O. M. Andersen and K. R. Markham. Boca Raton, FL: CRC press, 2005. Chap. 10, pp. 471–551.

[21] A. Castañeda-Ovando, M. L. Pacheco-Hernandez, M. E. Páez-Hernández, J. A. Rodriguez, and C. A. Galán-Vidal. “Chemical studies of anthocyanins: A review.” In: *Food Chemistry* 113.4 (2009), pp. 859–871. DOI: https://doi.org/10.1016/j.foodchem.2008.09.001.

[22] F. Pina, M. J. Melo, C. A. Laia, A. J. Parola, and J. C. Lima. "Chemistry and applications of flavylium compounds: a handful of colours." In: *Chemical Society Reviews* 41.2 (2012), pp. 869–908. DOI: https://doi.org/10.1039/C1CS15126F.

[23] R. Brouillard, S. Chassaing, G. Isorez, M. Kueny-Stotz, and P. Figueiredo. "The visible flavonoids or anthocyanins: From research to applications." In: *Recent Advances in Polyphenol Research, Volume 2*. Ed. by C. Santos-Buelga, M. T. Escribano-Bailon, and V. Lattanzio. West Sussex, UK: Wiley-Blackwell, 2010. Chap. 1, pp. 1–22.

[24] O. Dangles and J.-A. Fenger. "The chemical reactivity of anthocyanins and its consequences in food science and nutrition." In: *Molecules* 23.8 (2018), p. 1970. DOI: https://doi.org/10.3390/molecules23081970.

[25] P. Furtado, P. Figueiredo, H. C. das Neves, and F. Pina. "Photochemical and thermal degradation of anthocyanidins." In: *Journal of Photochemistry and Photobiology A: Chemistry* 75.2 (1993), pp. 113–118. DOI: https://doi.org/10.1016/1010-6030(93)80191-B.

[26] G Hrazdina, A. Borzell, and W. Robinson. "Studies on the Stability of the Anthocyanidin-3, 5-Digucosides." In: *American Journal of Enology and Viticulture* 21.4 (1970), pp. 201–204. DOI: https://doi.org/10.1021/acs.jafc.5b03471.

[27] T. Goto and T. Kondo. "Structure and molecular stacking of anthocyanins—flower color variation." In: *Angewandte Chemie International Edition in English* 30.1 (1991), pp. 17–33. DOI: https://doi.org/10.1002/anie.199100171.

[28] V. de Freitas and N. Mateus. "Formation of pyranoanthocyanins in red wines: a new and diverse class of anthocyanin derivatives." In: *Analytical and Bioanalytical Chemistry* 401.5 (2011), pp. 1463–1473. DOI: https://doi.org/10.1007/s00216-010-4479-9.

[29] L. Ojwang and J. M. Awika. "Effect of pyruvic acid and ascorbic acid on stability of 3-deoxyanthocyanidins." In: *Journal of the Science of Food and Agriculture* 88.11 (2008), pp. 1987–1996. DOI: https://doi.org/10.1002/jsfa.3308.

[30] L. Yang, L. Dykes, and J. M. Awika. "Thermal stability of 3-deoxyanthocyanidin pigments." In: *Food Chemistry* 160 (2014), pp. 246–254. DOI: https://doi.org/10.1016/j.foodchem.2014.03.105.

[31] F. Akogou, A. Kayodé, H. den Besten, A. Linnemann, and V Fogliano. "Effects of processing and storage on the stability of the red biocolorant apigeninidin from sorghum." In: *LWT* 90 (2018), pp. 592–597. DOI: https://doi.org/10.1016/j.lwt.2017.12.071.

[32] F. Pina, J. Parola, M. J. Melo, J. C. Lima, and V. de Freitas. "Chemistry of anthocyanins." In: *Anthocyanins From Natural Sources: Exploiting Targeted Delivery for Improved Health*. Ed. by M. S.-L. Brooks and G. B. Celli. Croydon, UK: Royal Society of Chemistry, 2019. Chap. 2, pp. 34–74.

[33] M. S. Sharara. "Copigmentation effect of some phenolic acids on stabilization of roselle (*Hibiscus sabdariffa*) anthocyanin extract." In: *American Journal of Food Science and Technology* 5.2 (2017), pp. 45–52. DOI: http://doi.org/10.12691/ajfst-5-2-3.

[34] A. El Hassane, J. Gierschner, J.-L. Duroux, and P. Trouillas. "UV/Visible spectra of natural polyphenols: A time-dependent density functional theory study." In: *Food Chemistry* 131.1 (2012), pp. 79–89. DOI: https://doi.org/10.1016/j.foodchem.2011.08.034.

[35] P. Trouillas, J. C. Sancho-Garcia, V. De Freitas, J. Gierschner, M. Otyepka, and O. Dangles. "Stabilizing and modulating color by copigmentation: insights from theory and experiment." In: *Chemical Reviews* 116.9 (2016), pp. 4937–4982. DOI: https://doi.org/10.1021/acs.chemrev.5b00507.

[36] F. C. Stintzing and R. Carle. "Functional properties of anthocyanins and betalains in plants, food, and in human nutrition." In: *Trends in Food Science & Technology* 15.1 (2004), pp. 19–38. DOI: https://doi.org/10.1016/j.tifs.2003.07.004.

[37] Ø. M. Andersen and M. Jordheim. "Basic anthocyanin chemistry and dietary sources." In: *Anthocyanins in Health and Disease*. Ed. by T. C. Wallace and M. M. Giusti. Boca Raton, FL: CRC Press, 2014. Chap. 2, pp. 14–72.

[38] R. E. Wrolstad, R. W. Durst, M. M. Giusti, and L. E. Rodriguez-Saona. "Analysis of anthocyanins in nutraceuticals." In: *Quality Management of Nutraceuticals*. Ed. by C.-T. Ho and Q. Y. Zheng. Washington, DC: ACS Publications, 2002. Chap. 4, pp. 42–62.

[39] H. E. Khoo, A. Azlan, S. T. Tang, and S. M. Lim. "Anthocyanidins and anthocyanins: colored pigments as food, pharmaceutical ingredients, and the potential health benefits." In: *Food & Nutrition Research* 61.1 (2017), p. 1361779. DOI: https://doi.org/10.1080/16546628.2017.1361779.

[40] V. Gowd, Z. Jia, and W. Chen. "Anthocyanins as promising molecules and dietary bioactive components against diabetes–A review of recent advances." In: *Trends in Food Science & Technology* 68 (2017), pp. 1–13. DOI: https://doi.org/10.1016/j.tifs.2017.07.015.

[41] B.-W. Lin, C.-C. Gong, H.-F. Song, and Y.-Y. Cui. "Effects of anthocyanins on the prevention and treatment of cancer." In: *British Journal of Pharmacology* 174.11 (2017), pp. 1226–1243. DOI: https://doi.org/10.1111/bph.13627.

[42] N. Roewer and J. Broscheit. "Use of delphinidin against *Staphylococcus aureus*." Pat. US Patent App. 14/389,492. 2015.

[43] S. Miyake, N. Takahashi, M. Sasaki, S. Kobayashi, K. Tsubota, and Y. Ozawa. "Vision preservation during retinal inflammation by anthocyanin-rich bilberry extract: cellular and molecular mechanism." In: *Laboratory Investigation* 92.1 (2012), pp. 102–109. DOI: https://doi.org/10.1038/labinvest.2011.132.

[44] C.-F. Chan, C.-Y. Lien, Y.-C. Lai, C.-L. Huang, and W. C. Liao. "Influence of purple sweet potato extracts on the UV absorption properties of a cosmetic cream." In: *Journal of Cosmetic Science* 61.5 (2010), pp. 333–341.

[45] A. Westfall and M. Giusti. "Color profiles and stability of acylated and nonacylated anthocyanins as novel pigment sources in a lipstick model: A viable alternative to synthetic colorants." In: *Journal of Cosmetic Science* 68.3 (2017), pp. 233–244.

[46] L. E. Rojo, D. E. Roopchand, B. Graf, D. M. Cheng, D. Ribnicky, B. Fridlender, and I. Raskin. "Role of anthocyanins in skin aging and UV-induced skin damage." In: *Anthocyanins in Health and Disease*. Ed. by T. C. Wallace and M. M. Giusti. Boca Raton, FL: CRC Press, 2013. Chap. 11, pp. 309–318.

[47] N Plundrich, M. Grace, I. Raskin, and M Ann Lila. "Bioactive polyphenols from muscadine grape and blackcurrant stably concentrated onto protein-rich matrices for topical applications." In: *International Journal of Cosmetic Science* 35.4 (2013), pp. 394–401. DOI: https://doi.org/10.1111/ics.12057.

[48] S. Zolghadri, A. Bahrami, M. T. Hassan Khan, J Munoz-Munoz, F. Garcia-Molina, F Garcia-Canovas, and A. A. Saboury. "A comprehensive review on tyrosinase inhibitors." In: *Journal of Enzyme Inhibition and Medicinal Chemistry* 34.1 (2019), pp. 279–309. DOI: https://doi.org/10.1080/14756366.2018.1545767.

[49] G. Calogero and G. Di Marco. "Red Sicilian orange and purple eggplant fruits as natural sensitizers for dye-sensitized solar cells." In: *Solar Energy Materials and Solar Cells* 92.11 (2008), pp. 1341–1346. DOI: https://doi.org/10.1016/j.solmat.2008.05.007.

[50] N. J. Cherepy, G. P. Smestad, M. Grätzel, and J. Z. Zhang. "Ultrafast electron injection: implications for a photoelectrochemical cell utilizing an anthocyanin dye-sensitized TiO2 nanocrystalline electrode." In: *The Journal of Physical Chemistry B* 101.45 (1997), pp. 9342–9351. DOI: https://doi.org/10.1021/jp972197w.

[51] I. Lacatusu, N. Badea, D. Bojin, S. Iosub, and A. Meghea. "Novel fluorescence nanostructured materials obtained by entrapment of an ornamental bush extract in hybrid silica glass." In: *Journal of Sol-gel Science and Technology* 51.1 (2009), pp. 84–91. DOI: https://doi.org/10.1007/s10971-009-1925-2.

[52] I. Iosub, F. Kajzar, M. Makowska-Janusik, A. Meghea, A. Tane, and I. Rau. "Electronic structure and optical properties of some anthocyanins extracted from grapes." In: *Optical Materials* 34.10 (2012), pp. 1644–1650. DOI: https://doi.org/10.1016/j.optmat.2012.03.020.

[53] F. Galindo, J. C. Lima, S. V. Luis, M. J. Melo, A. J. Parola, and F. Pina. "Water/humidity and ammonia sensor, based on a polymer hydrogel matrix containing a fluorescent flavylium compound." In: *Journal of Materials Chemistry* 15.27-28 (2005), pp. 2840–2847. DOI: https://doi.org/10.1039/B500512D.

[54] G. Calogero, A. Sinopoli, I. Citro, G. Di Marco, V. Petrov, A. M. Diniz, A. J. Parola, and F. Pina. "Synthetic analogues of anthocyanins as sensitizers for dye-sensitized solar cells." In: *Photochemical & Photobiological Sciences* 12.5 (2013), pp. 883–894. DOI: https://doi.org/10.1039/C3PP25347C.

[55] F. Pina, A. J. Parola, R. Gomes, M. Maestri, and V. Balzani. "Multistate/multifunctional molecular-level systems: Photochromic flavylium compounds." In: *Molecular Switches* 1 (2011), pp. 181–226. DOI: https://doi.org/10.1080/14756366.2018.1545767.

[56] S. Gago, N. Basílio, A. J. Moro, and F. Pina. "Flavylium based dual photochromism: addressing cis–trans isomerization and ring opening-closure by different light inputs." In: *Chemical Communications* 51.34 (2015), pp. 7349–7351. DOI: https://doi.org/10.1039/C5CC01677K.

[57] N. Basílio and U. Pischel. "Drug delivery by controlling a supramolecular host–guest assembly with a reversible photoswitch." In: *Chemistry–A European Journal* 22.43 (2016), pp. 15208–15211. DOI: https://doi.org/10.1002/chem.201603331.

[58] N. Basílio and F. Pina. "Chemistry and photochemistry of anthocyanins and related compounds: a thermodynamic and kinetic approach." In: *Molecules* 21.11 (2016), p. 1502. DOI: https://doi.org/10.3390/molecules21111502.

[59] C Büllow and H Wagner. "Derivatives of 1, 4-benzopyranol, the mother substance of a new class of pigments. II." In: *Berichte der Deutschen Chemischen Gesellschaft* 34 (1901), pp. 1782–1804.

[60] E. H. Huntress. "The chemistry of the red and blue pigments of flowers and fruits. Part I." In: *Journal of Chemical Education* 5.11 (1928), p. 1392. DOI: http://doi.org/10.1021/ed005p1392.

[61] E. H. Huntress. "The chemistry of the red and blue pigments of flowers and fruits. Part II." In: *Journal of Chemical Education* 5.12 (1928), p. 1615. DOI: http://doi.org/10.1021/ed005p1615.

[62] R. Willstätter and A. E. Everest. "Untersuchungen über die Anthocyane. I. Über den Farbstoff der Kornblume." In: *Justus Liebigs Annalen der Chemie* 401.2 (1913), pp. 189–232. DOI: https://doi.org/10.1002/jlac.19134010205.

[63] D. Trauner. "Richard Willstätter and the 1915 Nobel Prize in Chemistry." In: *Angewandte Chemie International Edition* 54.41 (2015), pp. 11910–11916. DOI: https://doi.org/10.1002/anie.201505507.

[64] R. Willstätter, L. Zechmeister, and W. Kindler. "Synthese des Pelargonidins und Cyanidins." In: *Berichte der deutschen chemischen Gesellschaft (A and B Series)* 57.10 (1924), pp. 1938–1944. DOI: https://doi.org/10.1002/cber.19240571031.

[65] D. R. Kammerer. "Anthocyanins." In: *Handbook on Natural Pigments in Food and Beverages*. Ed. by R. Carle and R. Schweiggert. Amsterdam, NL: Elsevier, 2016. Chap. 3, pp. 61–78.

[66] D. D. Pratt and R. Robinson. "XXV.—A synthesis of pyrylium salts of anthocyanidin type. Part III. A new synthesis of pelargonidin chloride." In: *Journal of the Chemical Society, Transactions* 125 (1924), pp. 188–199. DOI: https://doi.org/10.1039/JR9280001537.

[67] G. M. Robinson and R. Robinson. "A survey of anthocyanins. I." In: *Biochemical Journal* 25.5 (1931), pp. 1687–1705. DOI: https://doi.org/10.1042/bj0251687.

[68] E. Sondheimer. "On the relation between spectral changes and pH of the anthocyanin pelargonidin 3-monoglucoside." In: *Journal of the American Chemical Society* 75.6 (1953), pp. 1507–1508. DOI: http://doi.org/10.1021/ja01102a528.

[69] C. Timberlake and P Bridle. "Spectral studies of anthocyanin and anthocyanidin equilibria in aqueous solution." In: *Nature* 212.5058 (1966), pp. 158–159. DOI: https://doi.org/10.1038/212158a0.

[70] L Jurd. "Anthocyanidins and related compounds—XV: The effects of sunlight on flavylium salt-chalcone equilibrium in acid solutions." In: *Tetrahedron* 25.11 (1969), pp. 2367–2380. DOI: https://doi.org/10.1016/S0040-4020(01)82785-X.

[71] R. A. McClelland and S. Gedge. "Hydration of the flavylium ion." In: *Journal of the American Chemical Society* 102.18 (1980), pp. 5838–5848. DOI: http://doi.org/10.1021/ja00538a024.

[72] R. A. McClelland and G. H. McGall. "Hydration of the flavylium ion. 2. The 4'-hydroxyflavylium ion." In: *The Journal of Organic Chemistry* 47.19 (1982), pp. 3730–3736. DOI: http://doi.org/10.1021/jo00140a027.

[73] R. Brouillard and B. Delaporte. "Chemistry of anthocyanin pigments. 2. Kinetic and thermodynamic study of proton transfer, hydration, and tautomeric reactions of malvidin 3-glucoside." In: *Journal of the American Chemical Society* 99.26 (1977), pp. 8461–8468. DOI: http://doi.org/10.1021/ja00468a015.

[74] R. Brouillard and J.-E. Dubois. "Mechanism of the structural transformations of anthocyanins in acidic media." In: *Journal of the American Chemical Society* 99.5 (1977), pp. 1359–1364. DOI: http://doi.org/10.1021/ja00447a012.

[75] R. Brouillard and J. Lang. "The hemiacetal–cis-chalcone equilibrium of malvin, a natural anthocyanin." In: *Canadian Journal of Chemistry* 68.5 (1990), pp. 755–761. DOI: https://doi.org/10.1139/v90-119.

[76] H. Santos, D. L. Turner, J. C. Lima, P. Figueiredo, F. S. Pina, et al. "Elucidation of the multiple equilibria of malvin in aqueous solution by one-and two-dimensional NMR." In: *Phytochemistry* 33.5 (1993), pp. 1227–1232. DOI: https://doi.org/10.1016/0031-9422(93)85054-U.

[77] A. L. Maçanita, P. F. Moreira, J. C. Lima, F. H. Quina, C. Yihwa, and C. Vautier-Giongo. "Proton transfer in anthocyanins and related flavylium salts. Determination of ground-state rate constants with nanosecond laser flash photolysis." In: *The Journal of Physical Chemistry A* 106.7 (2002), pp. 1248–1255. DOI: https://doi.org/10.1021/jp0140421.

[78] P. F. Moreira, L. Giestas, C. Yihwa, C. Vautier-Giongo, F. H. Quina, A. L. Maçanita, and J. C. Lima. "Ground-and excited-state proton transfer in anthocyanins: From weak acids to superphotoacids." In: *The Journal of Physical Chemistry A* 107.21 (2003), pp. 4203–4210. DOI: https://doi.org/10.1021/jp027260i.

[79] P. Ferreira da Silva, J. C. Lima, F. H. Quina, and A. L. Maçanita. "Excited-state electron transfer in anthocyanins and related flavylium salts." In: *The Journal of Physical Chemistry A* 108.46 (2004), pp. 10133–10140. DOI: https://doi.org/10.1021/jp047300d.

[80] V. Petrov and F. Pina. "Complete resolution of the reaction Rates of flavylium Networks. The role played by 2-phenyl-2H-chromen-4-ol and the hydroxyl attack to the quinoidal Base." In: *Journal of Mathematical Chemistry* 50.4 (2012), pp. 1003–1019. DOI: https://doi.org/10.1007/s10910-011-9948-7.

[81] V. Petrov and F. Pina. "Analytical resolution of the reaction rates of flavylium network by Laplace transform." In: *Journal of mathematical chemistry* 47.3 (2010), pp. 1005–1026. DOI: https://doi.org/10.1007/s10910-009-9621-6.

[82] Y. Leydet, R. Gavara, V. Petrov, A. M. Diniz, A. J. Parola, J. C. Lima, and F. Pina. "The effect of self-aggregation on the determination of the kinetic and thermodynamic constants of the network of chemical reactions in 3-glucoside anthocyanins." In: *Phytochemistry* 83 (2012), pp. 125–135. DOI: https://doi.org/10.1016/j.phytochem.2012.06.022.

[83] F. Pina. "Anthocyanins and related compounds and their bio-inspired applications." In: *Recent Advanced in Polyphenols Research, Volume 4*. Ed. by A. Romani, V. Lattanzio, and Q. Stephane. West Sussex, UK: Wiley-Blackwell, 2014. Chap. 11, pp. 341–370.

[84] F. Pina, M. J. Melo, M. Maestri, R. Ballardini, and V. Balzani. "Photochromism of 4 '-Methoxyflavylium Perchlorate. A "Write- Lock- Read- Unlock- Erase" Molecular Switching System." In: *Journal of the American Chemical Society* 119.24 (1997), pp. 5556–5561. DOI: https://doi.org/10.1021/ja9704646.

[85] M. Montalti, A. Credi, L. Prodi, and M. T. Gandolfi. "Chemical actinometry." In: *Handbook of Photochemistry*. Boca Raton, FL: CRC press, 2006. Chap. 12, pp. 601–611.

[86] S. Gago, N. Basílio, A. Fernandes, V. Freitas, A. Quintas, and F. Pina. "Photochromism of the complex between 4′-(2-hydroxyethoxy)-7-hydroxyflavylium and β-cyclodextrin, studied by ^{1}H NMR, UV–Vis, continuous irradiation and circular dichroism." In: *Dyes and Pigments* 110 (2014), pp. 106–112. DOI: https://doi.org/10.1016/j.dyepig.2014.04.038.

[87] F. Pina, M. Maestri, and V. Balzani. "Photochromic flavylium compounds as multistate/multifunction molecular-level systems." In: *Chemical Communications* 2 (1999), pp. 107–114. DOI: https://doi.org/10.1039/A805522J.

[88] F. Pina, V. Petrov, and C. A. Laia. "Photochromism of flavylium systems. An overview of a versatile multistate system." In: *Dyes and Pigments* 92.2 (2012), pp. 877–889. DOI: https://doi.org/10.1016/j.dyepig.2011.03.033.

[89] J. Lehn. "From molecular to supramolecular chemistry." In: *Supramolecular Chemistry, Concept and Perspectives*. Weinheim, DE: VCH, 1995. Chap. 1, pp. 1–4.

[90] S Asen, R. Stewart, and K. Norris. "Co-pigmentation of anthocyanins in plant tissues and its effect on color." In: *Phytochemistry* 11.3 (1972), pp. 1139–1144. DOI: https://doi.org/10.1016/S0031-9422(00)88467-8.

[91] K. Yoshida, M. Mori, and T. Kondo. "Blue flower color development by anthocyanins: from chemical structure to cell physiology." In: *Natural Product Reports* 26.7 (2009), pp. 884–915. DOI: https://doi.org/10.1039/B800165K.

[92] K. Yoshida, T. Kondo, Y. Okazaki, and K. Katou. "Cause of blue petal colour." In: *Nature* 373.6512 (1995), pp. 291–291. DOI: https://doi.org/10.1038/373291a0.

[93] T. Hondo, K. Yoshida, A. Nakagawa, T. Kawai, H. Tamura, and T. Goto. "Structural basis of blue-colour development in flower petals from Commelina communis." In: *Nature* 358.6386 (1992), pp. 515–518. DOI: https://doi.org/10.1038/358515a0.

[94] T. Kondo, K.-i. Oyama, and K. Yoshida. "Chiral molecular recognition on formation of a metalloanthocyanin: a supramolecular metal complex pigment from blue flowers of Salvia patens." In: *Angewandte Chemie International Edition* 40.5 (2001), pp. 894–897. DOI: https://doi.org/10.1002/1521-3773(20010302)40:5<894::AID-ANIE894>3.0.CO;2-8.

[95] R. Brouillard. "Chemical structure of anthocyanins." In: *Anthocyanins as Food Colors*. Ed. by P. Markakis. London, UK: Academic press, 1982. Chap. 1, pp. 1–38.

[96] R. Brouillard, M.-C. Wigand, O. Dangles, and A. Cheminat. "pH and solvent effects on the copigmentation reaction of malvin with polyphenols, purine and pyrimidine derivatives." In: *Journal of the Chemical Society, Perkin Transactions 2* 8 (1991), pp. 1235–1241. DOI: https://doi.org/10.1039/P29910001235.

[97] J. M. Baranac, N. A. Petranović, and J. M. Dimitrić-Marković. "Spectrophotometric study of anthocyan copigmentation reactions. 2. Malvin and the nonglycosidized flavone quercetin." In: *Journal of Agricultural and Food Chemistry* 45.5 (1997), pp. 1694–1697. DOI: https://doi.org/10.1021/jf9606114.

[98] T. Honda and N. Saito. "Recent progress in the chemistry of polyacylated anthocyanins as flower color pigments." In: *Heterocycles* 56.1 (2002), pp. 633–692. DOI: http://doi.org/10.3987/REV-01-SR(K)2.

[99] T. Hoshino. "An approximate estimate of self-association constants and the self-stacking conformation of Malvin quinonoidal bases studied by ^{1}H NMR." In: *Phytochemistry* 30.6 (1991), pp. 2049–2055. DOI: https://doi.org/10.1016/0031-9422(91)85065-8.

[100] T. Hoshino. "Self-association of flavylium cations of anthocyanidin 3, 5-diglucosides studied by circular dichroism and ^{1}H NMR." In: *Phytochemistry* 31.2 (1992), pp. 647–653. DOI: https://doi.org/10.1016/0031-9422(92)90053-S.

[101] R. Gavara, V. Petrov, A. Quintas, and F. Pina. "Circular dichroism of anthocyanidin 3-glucoside self-aggregates." In: *Phytochemistry* 88 (2013), pp. 92–98. DOI: https://doi.org/10.1016/j.phytochem.2012.12.011.

[102] G. Sigurdson, R. Robbins, T. Collins, and M. Giusti. "Evaluating the role of metal ions in the bathochromic and hyperchromic responses of cyanidin derivatives in acidic and alkaline pH." In: *Food Chemistry* 208 (2016), pp. 26–34. DOI: https://doi.org/10.1016/j.foodchem.2016.03.109.

[103] V. S. Fedenko, S. A. Shemet, and M. Landi. "UV–vis spectroscopy and colorimetric models for detecting anthocyanin-metal complexes in plants: An overview of in vitro and in vivo techniques." In: *Journal of Plant Physiology* 212 (2017), pp. 13–28. DOI: https://doi.org/10.1016/j.jplph.2017.02.001.

[104] K. Shibata, Y. Shibata, and I. Kasiwagi. "Studies on anthocyanins: color variation in anthocyanins." In: *Journal of the American Chemical Society* 41.2 (1919), pp. 208–220. DOI: https://doi.org/10.1021/ja01459a008.

[105] P. Figueiredo and F. Pina. "Formation of anthocyanin ion-pairs. A co-pigmentation effect." In: *Journal of the Chemical Society, Perkin Transactions 2* 4 (1994), pp. 775–778. DOI: https://doi.org/10.1039/P29940000775.

[106] N. Mulinacci, A. Romani, P. Pinelli, S. Gallori, C. Giaccherini, and F. F. Vincieri. "Stabilisation of natural anthocyanins by micellar systems." In: *International Journal of Pharmaceutics* 216.1-2 (2001), pp. 23–31. DOI: https://doi.org/10.1016/S0378-5173(00)00685-2.

[107] C. Vautier-Giongo, C. Yihwa, P. F. Moreira, J. C. Lima, A. A. Freitas, M. Alves, F. H. Quina, and A. L. Maçanita. "Manipulation of the reactivity of a synthetic anthocyanin analogue in aqueous micellar media." In: *Langmuir* 18.26 (2002), pp. 10109–10115. DOI: https://doi.org/10.1021/la026336z.

[108] J. C. Lima, C. Vautier-Giongo, A. Lopes, E. Melo, F. H. Quina, and A. L. Maçanita. "Color stabilization of anthocyanins: effect of SDS micelles on the acid- base and hydration kinetics of malvidin 3-glucoside (oenin)." In: *The Journal of Physical Chemistry A* 106.24 (2002), pp. 5851–5859. DOI: https://doi.org/10.1021/jp014081c.

[109] L. Giestas, C. Yihwa, J. C. Lima, C. Vautier-Giongo, A. Lopes, A. L. Maçanita, and F. H. Quina. "The dynamics of ultrafast excited state proton transfer in anionic micelles." In: *The Journal of Physical Chemistry A* 107.18 (2003), pp. 3263–3269. DOI: https://doi.org/10.1021/jp0265900.

[110] A. J. Parola, P. Pereira, F. Pina, and M. Maestri. "Effect of SDS micelles on the reactivity of 4-methoxyflavylium ion: A stopped-flow and photochemical study." In: *Journal of Photochemistry and Photobiology A: Chemistry* 185.2-3 (2007), pp. 383–390. DOI: https://doi.org/10.1016/j.jphotochem.2006.07.001.

[111] C. Aramă, C. Nicolescu, A. Nedelcu, and C.-M. Monciu. "Synthesis and characterization of the inclusion complex between repaglinide and sulfobutylether-β-cyclodextrin (Captisol®)." In: *Journal of Inclusion Phenomena and Macrocyclic Chemistry* 70.3-4 (2011), pp. 421–428. DOI: https://doi.org/10.1007/s10847-010-9911-4.

[112] J. Szejtli. "Introduction and general overview of cyclodextrin chemistry." In: *Chemical Reviews* 98.5 (1998), pp. 1743–1754. DOI: http://doi.org/10.1021/cr970022c.

[113] T. Al Hagbani and S. Nazzal. "Curcumin complexation with cyclodextrins by the autoclave process: Method development and characterization of complex formation." In: *International Journal of Pharmaceutics* 520.1-2 (2017), pp. 173–180. DOI: https://doi.org/10.1016/j.ijpharm.2017.01.063.

[114] H. H. Tønnesen, M. Másson, and T. Loftsson. "Studies of curcumin and curcuminoids. XXVII. Cyclodextrin complexation: solubility, chemical and photochemical stability." In: *International Journal of Pharmaceutics* 244.1-2 (2002), pp. 127–135. DOI: https://doi.org/10.1016/S0378-5173(02)00323-X.

[115] S. F. Lockwood, S. O'Malley, and G. L. Mosher. "Improved aqueous solubility of crystalline astaxanthin (3, 3′-dihydroxy-β, β-carotene-4, 4′-dione) by Captisol®(sulfobutyl ether β-cyclodextrin)." In: *Journal of Pharmaceutical Sciences* 92.4 (2003), pp. 922–926. DOI: https://doi.org/10.1002/jps.10359.

[116] M. Háda, V. Nagy, J. Deli, and A. Agócs. "Hydrophilic carotenoids: recent progress." In: *Molecules* 17.5 (2012), pp. 5003–5012. DOI: https://doi.org/10.3390/molecules17055003.

[117] C. Jullian, L. Moyano, C. Yanez, and C. Olea-Azar. "Complexation of quercetin with three kinds of cyclodextrins: an antioxidant study." In: *Spectrochimica Acta Part A: Molecular and Biomolecular Spectroscopy* 67.1 (2007), pp. 230–234. DOI: https://doi.org/10.1016/j.saa.2006.07.006.

[118] A. D. Kulkarni and V. S. Belgamwar. "Inclusion complex of chrysin with sulfobutyl ether-β-cyclodextrin (Captisol®): Preparation, characterization, molecular modelling and in vitro anticancer activity." In: *Journal of Molecular Structure* 1128 (2017), pp. 563–571. DOI: https://doi.org/10.1016/j.molstruc.2016.09.025.

[119] N. Roewer and J. Broscheit. "Anthocyanidin complex for the treatment of multiple myeloma." Pat. US Patent App. 14/432,654. 2015.

[120] I. Mourtzinos, D. P. Makris, K. Yannakopoulou, N. Kalogeropoulos, I. Michali, and V. T. Karathanos. "Thermal stability of anthocyanin extract of *Hibiscus sabdariffa* L. in the presence of β-cyclodextrin." In: *Journal of Agricultural and Food Chemistry* 56.21 (2008), pp. 10303–10310. DOI: https://doi.org/10.1021/jf801389j.

[121] A. Fernandes, M. A. Rocha, L. M. Santos, J. Brás, J. Oliveira, N. Mateus, and V. de Freitas. "Blackberry anthocyanins: β-Cyclodextrin fortification for thermal and gastrointestinal stabilization." In: *Food Chemistry* 245 (2018), pp. 426–431. DOI: https://doi.org/10.1016/j.foodchem.2017.10.109.

[122] A. Fernandes, A. Sousa, J. Azevedo, N. Mateus, and V. de Freitas. "Effect of cyclodextrins on the thermodynamic and kinetic properties of cyanidin-3-O-glucoside." In: *Food Research International* 51.2 (2013), pp. 748–755. DOI: https://doi.org/10.1016/j.foodres.2013.01.037.

[123] N. Basílio, A. Fernandes, V. de Freitas, S. Gago, and F. Pina. "Effect of β-cyclodextrin on the chemistry of $3',4',7-trihydroxyflavylium$." In: *New Journal of Chemistry* 37.10 (2013), pp. 3166–3173. DOI: https://doi.org/10.1039/C3NJ00588G.

[124] S. Liu, C. Ruspic, P. Mukhopadhyay, S. Chakrabarti, P. Y. Zavalij, and L. Isaacs. "The cucurbit [n] uril family: prime components for self-sorting systems." In: *Journal of the American Chemical Society* 127.45 (2005), pp. 15959–15967. DOI: https://doi.org/10.1021/ja055013x.

[125] S. J. Barrow, S. Kasera, M. J. Rowland, J. del Barrio, and O. A. Scherman. "Cucurbituril-based molecular recognition." In: *Chemical Reviews* 115.22 (2015), pp. 12320–12406. DOI: https://doi.org/10.1021/acs.chemrev.5b00341.

[126] Y. J. Jeon, H. Kim, S. Jon, N. Selvapalam, D. H. Oh, I. Seo, C.-S. Park, S. R. Jung, D.-S. Koh, and K. Kim. "Artificial ion channel formed by cucurbit [n] uril derivatives with a carbonyl group fringed portal reminiscent of the selectivity filter of K+ channels." In: *Journal of the American Chemical Society* 126.49 (2004), pp. 15944–15945. DOI: https://doi.org/10.1021/ja044748j.

[127] N. Basílio, C. A. Laia, and F. Pina. "Excited-state proton transfer in confined medium. 4-Methyl-7-hydroxyflavylium and β-naphthol incorporated in cucurbit [7] uril." In: *The Journal of Physical Chemistry B* 119.6 (2015), pp. 2749–2757. DOI: https://doi.org/10.1021/jp511351w.

[128] N. Basílio, V. Petrov, and F. Pina. "Corrigendum: Host–guest complexes of flavylium cations and cucurbit [7] uril: The influence of flavylium substituents on the structure and stability of the complex." In: *ChemPlusChem* 81.11 (2016), pp. 1136–1136. DOI: https://doi.org/10.1002/cplu.201600486.

[129] N. Basílio, L. Cabrita, and F. Pina. "Mimicking positive and negative copigmentation effects in anthocyanin analogues by host–guest interaction with cucurbit [7] uril and β-cyclodextrins." In: *Journal of Agricultural and Food Chemistry* 63.35 (2015), pp. 7624–7629. DOI: https://doi.org/10.1021/acs.jafc.5b00765.

[130] C. D. Gutsche. "From resinous tar to molecular baskets." In: *Calixarenes: An introduction*. Cambrigde, UK: RSC Publishing, 2004. Chap. 1, pp. 1–25.

[131] N. Basilio, V. Francisco, and L. Garcia-Rio. "Aggregation of p-sulfonatocalixarene-based amphiphiles and supra-amphiphiles." In: *International Journal of Molecular Sciences* 14.2 (2013), pp. 3140–3157. DOI: https://doi.org/10.3390/ijms14023140.

[132] L. Baldini, A. Casnati, F. Sansone, and R. Ungaro. "Calixarene-based multivalent ligands." In: *Chemical Society Reviews* 36.2 (2007), pp. 254–266. DOI: https://doi.org/10.1039/B603082N.

[133] R. Ludwig. "Calixarenes for biochemical recognition and separation." In: *Microchimica Acta* 152.1-2 (2005), pp. 1–19. DOI: https://doi.org/10.1007/s00604-005-0422-8.

[134] W. M. Nau, G. Ghale, A. Hennig, H. Bakirci, and D. M. Bailey. "Substrate-selective supramolecular tandem assays: monitoring enzyme inhibition of arginase and diamine oxidase by fluorescent dye displacement from calixarene and cucurbituril macrocycles." In: *Journal of the American Chemical Society* 131.32 (2009), pp. 11558–11570. DOI: https://doi.org/10.1021/ja904165c.

[135] D.-S. Guo, V. D. Uzunova, X. Su, Y. Liu, and W. M. Nau. "Operational calixarene-based fluorescent sensing systems for choline and acetylcholine and their application to enzymatic reactions." In: *Chemical Science* 2.9 (2011), pp. 1722–1734. DOI: https://doi.org/10.1039/C1SC00231G.

[136] M. A. Romero, P. Mateus, B. Matos, A. Acuna, L. García-Río, J. F. Arteaga, U. Pischel, and N. Basílio. "Binding of flavylium ions to sulfonatocalix [4] arene and implication in the photorelease of biologically relevant guests in water." In: *The Journal of Organic Chemistry* 84.17 (2019), pp. 10852–10859. DOI: https://doi.org/10.1021/acs.joc.9b01420.

[137] R. Brahma, M. P. Singh, and J. B. Baruah. "Stacking among the clips of the polyaromatic rings of phenazine with hydroxy-aromatics and photophysical properties." In: *RSC Advances* 9.57 (2019), pp. 33403–33412. DOI: https://doi.org/10.1039/C9RA07602F.

[138] J. Leblond and A. Petitjean. "Molecular tweezers: concepts and applications." In: *ChemPhysChem* 12.6 (2011), pp. 1043–1051. DOI: https://doi.org/10.1002/cphc.201001050.

[139] S. C. Zimmerman, Z. Zeng, W. Wu, and D. E. Reichert. "Synthesis and structure of molecular tweezers containing active site functionality." In: *Journal of the American Chemical Society* 113.1 (1991), pp. 183–196. DOI: https://doi.org/10.1021/ja00001a027.

[140] J. Polkowska, F. Bastkowski, T. Schrader, F.-G. Klärner, J. Zienau, F. Koziol, and C. Ochsenfeld. "A combined experimental and theoretical study of the pH-dependent binding mode of NAD+ by water-soluble molecular clips." In: *Journal of Physical Organic Chemistry* 22.8 (2009), pp. 779–790. DOI: https://doi.org/10.1002/poc.1519.

[141] C. Jasper, T. Schrader, J. Panitzky, and F.-G. Klärner. "Selective Complexation of N-Alkylpyridinium Salts: Recognition of NAD+ in Water." In: *Angewandte Chemie International Edition* 41.8 (2002), pp. 1355–1358.

[142] M. Kirsch, P. Talbiersky, J. Polkowska, F. Bastkowski, T. Schaller, H. de Groot, F.-G. Klärner, and T. Schrader. "A mechanism of efficient G6PD inhibition by a molecular clip." In: *Angewandte Chemie International Edition* 48.16 (2009), pp. 2886–2890. DOI: https://doi.org/10.1002/ange.200806175.

[143] R. Gomes, A. J. Parola, F. Bastkowski, J. Polkowska, and F.-G. Klarner. "Host- guest interactions between molecular clips and multistate systems based on flavylium salts." In: *Journal of the American Chemical Society* 131.25 (2009), pp. 8922–8938. DOI: https://doi.org/10.1021/ja9019098.

[144] K. Yonekura-Sakakibara, T. Nakayama, and M. Yamazaki. "Modification and stabilization of anthocyanins." In: *Anthocyanins: Biosynthesis, Functions, and Applications*. Ed. by K. Gould, K. M. Davies, and C. Winefield. New York, NY: Springer, 2009. Chap. 6, pp. 169–190.

[145] E. Echeverria, J. Burns, and H. Felle. "Compartmentation and cellular conditions controlling sucrose breakdown in mature acid lime fruits." In: *Phytochemistry* 31.12 (1992), pp. 4091–4095. DOI: https://doi.org/10.1016/0031-9422(92)80420-J.

[146] K. Yoshitama. "Blue and purple anthocyanins isolated from the flowers of *Tradescantia reflexa*." In: *The Botanical Magazine= Shokubutsu-gaku-zasshi* 91.3 (1978), pp. 207–212. DOI: https://doi.org/10.1007/BF02489357.

[147] T. Goto, T. Hoshino, and S. Takase. "A proposed structure of commelinin, a sky-blue anthocyanin complex obtained from the flower petals of commelina." In: *Tetrahedron Letters* 20.31 (1979), pp. 2905–2908. DOI: https://doi.org/10.1016/S0040-4039(01)86447-9.

[148] T. Hoshino, U. Matsumoto, and T. Goto. "Evidences of the self-association of anthocyanins I. Circular dichroism of cyanin anhydrobase." In: *Tetrahedron Letters* 21.18 (1980), pp. 1751–1754. DOI: https://doi.org/10.1016/S0040-4039(00)77827-0.

[149] R. Brouillard. "The in vivo expression of anthocyanin colour in plants." In: *Phytochemistry* 22.6 (1983), pp. 1311–1323. DOI: https://doi.org/10.1016/S0031-9422(00)84008-X.

[150] K. Yoshida, T. Kondo, and T. Goto. "Unusually stable monoacylated anthocyanin from purple yam *Dioscorea alata*." In: *Tetrahedron letters* 32.40 (1991), pp. 5579–5580. DOI: https://doi.org/10.1016/0040-4039(91)80088-N.

[151] W. Nerdal and Ø. M. Andersen. "Intermolecular aromatic acid association of an anthocyanin (petanin) evidenced by two-dimensional nuclear overhauser enhancement nuclear magnetic resonance experiments and distance geometry calculations." In: *Phytochemical Analysis* 3.4 (1992), pp. 182–189. DOI: https://doi.org/10.1002/pca.2800030408.

[152] K. Yoshida, K.-i. Oyama, and T. Kondo. "Structure of polyacylated anthocyanins and their UV protective effect." In: *Recent Advances in Polyphenol Research, Volume 5*. Ed. by K. Yoshida, V. Cheynier, and S. Quideau. West Sussex, UK: Wiley-Blackwell, 2017. Chap. 8, pp. 171–192.

[153] H. Matsufuji, T. Otsuki, T. Takeda, M. Chino, and M. Takeda. "Identification of reaction products of acylated anthocyanins from red radish with peroxyl radicals." In: *Journal of Agricultural and Food Chemistry* 51.10 (2003), pp. 3157–3161. DOI: https://doi.org/10.1021/jf0210122.

[154] K. Yoshida, M. Kawachi, M. Mori, M. Maeshima, M. Kondo, M. Nishimura, and T. Kondo. "The involvement of tonoplast proton pumps and Na+ (K+)/H+ exchangers in the change of petal color during flower opening of morning glory, *Ipomoea tricolor* cv. heavenly blue." In: *Plant and Cell Physiology* 46.3 (2005), pp. 407–415. DOI: https://doi.org/10.1093/pcp/pci057.

[155] O. Dangles, N. Saito, and R. Brouillard. "Kinetic and thermodynamic control of flavylium hydration in the pelargonidin-cinnamic acid complexation. Origin of the extraordinary flower color diversity of Pharbitis nil." In: *Journal of the American Chemical Society* 115.8 (1993), pp. 3125–3132. DOI: https://doi.org/10.1021/ja00061a011.

[156] F. Pina, A. Roque, M. J. Melo, M. Maestri, L. Belladelli, and V. Balzani. "Multistate/multifunctional molecular-level systems: Light and pH switching between the various forms of a synthetic flavylium salt." In: *Chemistry–A European Journal* 4.7 (1998), pp. 1184–1191. DOI: https://doi.org/10.1002/(SICI)1521-3765(19980710)4:7<1184::AID-CHEM1184>3.0.CO;2-6.

[157] A. Roque, C. Lodeiro, F. Pina, M. Maestri, S. Dumas, P. Passaniti, and V. Balzani. "Multistate/multifunctional systems. A thermodynamic, kinetic, and photochemical investigation of the 4′-dimethylaminoflavylium compound." In: *Journal of the American Chemical Society* 125.4 (2003), pp. 987–994. DOI: https://doi.org/10.1021/ja0287276.

[158] Y. Fukui, Y. Tanaka, T. Kusumi, T. Iwashita, and K. Nomoto. "A rationale for the shift in colour towards blue in transgenic carnation flowers expressing the flavonoid 3′, 5′-hydroxylase gene." In: *Phytochemistry* 63.1 (2003), pp. 15–23. DOI: https://doi.org/10.1016/S0031-9422(02)00684-2.

[159] N. Mateus, S Proença, P Ribeiro, J. Machado, and V. De Freitas. "Grape and wine polyphenolic composition of red vitis vinifera varieties concerning vineyard altitude." In: *CYTA-Journal of Food* 3.2 (2001), pp. 102–110. DOI: https://doi.org/10.1080/11358120109487653.

[160] J. Oliveira, M. Alhinho da Silva, N. Teixeira, V. De Freitas, and E. Salas. "Screening of anthocyanins and anthocyanin-derived pigments in red wine grape pomace using LC-DAD/MS and MALDI-TOF techniques." In: *Journal of Agricultural and Food Chemistry* 63.35 (2015), pp. 7636–7644. DOI: https://doi.org/10.1021/acs.jafc.5b00256.

[161] A. Fernandes, N. F. Brás, N. Mateus, and V. de Freitas. "A study of anthocyanin self-association by NMR spectroscopy." In: *New Journal of Chemistry* 39.4 (2015), pp. 2602–2611. DOI: https://doi.org/10.1039/C4NJ02339K.

[162] S. G. Lambert, R. E. Asenstorfer, N. M. Williamson, P. G. Iland, and G. P. Jones. "Copigmentation between malvidin-3-glucoside and some wine constituents and its importance to colour expression in red wine." In: *Food Chemistry* 125.1 (2011), pp. 106–115. DOI: https://doi.org/10.1016/j.foodchem.2010.08.045.

[163] M. Moloney, R. J. Robbins, T. M. Collins, T. Kondo, K. Yoshida, and O. Dangles. "Red cabbage anthocyanins: The influence of d-glucose acylation by hydroxycinnamic acids on their structural transformations in acidic to mildly alkaline conditions and on the resulting color." In: *Dyes and Pigments* 158 (2018), pp. 342–352. DOI: https://doi.org/10.1016/j.dyepig.2018.05.057.

[164] O. Dangles, N. Saito, and R. Brouillard. "Anthocyanin intramolecular copigment effect." In: *Phytochemistry* 34.1 (1993), pp. 119–124. DOI: https://doi.org/10.1016/S0031-9422(00)90792-1.

[165] S. Mason. "Induced circular dichroism." In: *Chemical Physics Letters* 32.2 (1975), pp. 201–203. DOI: https://doi.org/10.1016/0009-2614(75)85103-7.

[166] J. Gawronski and J. Grajewski. "The significance of induced circular dichroism." In: *Organic Letters* 5.18 (2003), pp. 3301–3303. DOI: https://doi.org/10.1021/ol0352456.

[167] S. Allenmark. "Induced circular dichroism by chiral molecular interaction." In: *Chirality: The Pharmacological, Biological, and Chemical Consequences of Molecular Asymmetry* 15.5 (2003), pp. 409–422. DOI: https://doi.org/10.1002/chir.10220.

[168] T. Hoshino and T. Goto. "Effects of pH and concentration on the self-association of malvin quinonoidal base—electronic and circular dichroic studies." In: *Tetrahedron letters* 31.11 (1990), pp. 1593–1596. DOI: https://doi.org/10.1016/0040-4039(90)80025-H.

[169] T. Hoshino, U. Matsumoto, and T. Goto. "Self-association of some anthocyanins in neutral aqueous solution." In: *Phytochemistry* 20.8 (1981), pp. 1971–1976. DOI: https://doi.org/10.1016/0031-9422(81)84047-2.

[170] J. He, X. Li, G. Silva, F. H. Quina, and A. J. Aquino. "Quantum chemical investigation of the intramolecular copigmentation complex of an acylated anthocyanin." In: *Journal of the Brazilian Chemical Society* 30.3 (2019), pp. 492–498. DOI: https://doi.org/10.21577/0103-5053.20180233.

[171] A. V. Afonin, I. A. Ushakov, A. V. Vashchenko, D. E. Simonenko, A. V. Ivanov, A. M. Vasil'tsov, A. I. Mikhaleva, and B. A. Trofimov. "C-H··· N and C- H··· O intramolecular hydrogen bonding effects in the 1H, 13C and 15 N NMR spectra of the configurational isomers of 1-vinylpyrrole-2-carbaldehyde oxime substantiated by DFT calculations." In: *Magnetic Resonance in Chemistry* 47.2 (2009), pp. 105–112. DOI: https://doi.org/10.1002/mrc.2358.

[172] K. Yoshida, T. Kondo, and T. Goto. "Intramolecular stacking conformation of gentiodelphin, a diacylated anthocyanin from *Gentiana makinoi*." In: *Tetrahedron* 48.21 (1992), pp. 4313–4326. DOI: https://doi.org/10.1016/S0040-4020(01)80442-7.

[173] T. Kondo, T. Kawai, H. Tamura, and T. Goto. "Structure determination of heavenly blue anthocyanin, a complex monomeric anthocyanin from the morning glory ipomea tricolor, by means of the negative NOE method." In: *Tetrahedron Letters* 28.20 (1987), pp. 2273–2276. DOI: https://doi.org/10.1016/S0040-4039(00)96099-4.

[174] T. Goto, H. Imagawa, T. Kondo, and I. Miura. "Heavenly blue anthocyanin III. Structure of bis-deacyl heavenly blue anthocyanin, a controlled alkaline hydrolysis product of heavenly blue anthocyanin." In: *Heterocycles* 17.1 (1982), pp. 355–358. DOI: https://doi.org/10.3987/S-1982-01-0355.

[175] J. Oliveira, V. Fernandes, C. Miranda, C. Santos-Buelga, A. Silva, V. de Freitas, and N. Mateus. "Color properties of four cyanidin-pyruvic acid adducts." In: *Journal of Agricultural and Food Chemistry* 54.18 (2006), pp. 6894–6903. DOI: https://doi.org/10.1021/jf061085b.

[176] H. Bahmann, A. Rodenberg, A. V. Arbuznikov, and M. Kaupp. "A thermochemically competitive local hybrid functional without gradient corrections." In: *The Journal of Chemical Physics* 126.1 (2007), p. 011103. DOI: https://doi.org/10.1063/1.2429058.

[177] G. Petersson and M. A. Al-Laham. "A complete basis set model chemistry. II. Open-shell systems and the total energies of the first-row atoms." In: *The Journal of Chemical Physics* 94.9 (1991), pp. 6081–6090. DOI: https://doi.org/10.1063/1.460447.

[178] V. O. Silva, A. A. Freitas, A. L. Maçanita, and F. H. Quina. "Chemistry and photochemistry of natural plant pigments: the anthocyanins." In: *Journal of Physical Organic Chemistry* 29.11 (2016), pp. 594–599. DOI: https://doi.org/10.1002/poc.3534.

[179] R. Cortez, D. A. Luna-Vital, D. Margulis, and E. Gonzalez de Mejia. "Natural pigments: stabilization methods of anthocyanins for food applications." In: *Comprehensive Reviews in Food Science and Food Safety* 16.1 (2017), pp. 180–198. DOI: https://doi.org/10.1111/1541-4337.12244.

[180] N. Basílio, V. Petrov, and F. Pina. "Host–guest complexes of flavylium cations and cucurbit [7] uril: the influence of flavylium substituents on the structure and stability of the complex." In: *ChemPlusChem* 80.12 (2015), pp. 1779–1785. DOI: https://doi.org/10.1002/cplu.201500304.

[181] S. Asen, R. N. Stewart, and K. H. Norris. "Anthocyanin, flavonol copigments, and pH responsible for larkspur flower color." In: *Phytochemistry* 14.12 (1975), pp. 2677–2682. DOI: https://doi.org/10.1016/0031-9422(75)85249-6.

[182] C. Malien-Aubert, O. Dangles, and M. J. Amiot. "Influence of procyanidins on the color stability of oenin solutions." In: *Journal of Agricultural and Food Chemistry* 50.11 (2002), pp. 3299–3305. DOI: https://doi.org/10.1021/jf011392b.

[183] O. Dangles and H. Elhajji. "Synthesis of 3-Methoxy-and 3-(β-D-Glucopyranosyloxy) flavylium Ions. Influence of the flavylium substitution pattern on the reactivity of anthocyanins in aqueous solution." In: *Helvetica Chimica Acta* 77.6 (1994), pp. 1595–1610. DOI: https://doi.org/10.1002/hlca.19940770616.

[184] V. Petrov, S. Slavcheva, S. Stanimirov, and F. Pina. "Origin of the metastable stability in flavylium multistate systems." In: *The Journal of Physical Chemistry A* 119.12 (2015), pp. 2908–2918. DOI: https://doi.org/10.1021/acs.jpca.5b01473.

[185] M. Bordiga, M. Locatelli, F. Travaglia, J. D. Coïsson, G. Mazza, and M. Arlorio. "Evaluation of the effect of processing on cocoa polyphenols: antiradical activity, anthocyanins and procyanidins profiling from raw beans to chocolate." In: *International Journal of Food Science & Technology* 50.3 (2015), pp. 840–848. DOI: https://doi.org/10.1111/ijfs.12760.

[186] M. Maeda-Yamamoto, T. Saito, A. Nesumi, Y. Tokuda, K. Ema, D. Honma, A. Ogino, M. Monobe, A. Murakami, A. Murakami, and H. Tachibana. "Chemical analysis and acetylcholinesterase inhibitory effect of anthocyanin-rich red leaf tea (cv. Sunrouge)." In: *Journal of the Science of Food and Agriculture* 92.11 (2012), pp. 2379–2386. DOI: https://doi.org/10.1002/jsfa.5644.

[187] E. Haslam. "Nature's palette." In: *Chemistry in Britain* 29.10 (1993), pp. 875–875.

[188] O. Dangles and R. Brouillard. "Polyphenol interactions. The copigmentation case: thermodynamic data from temperature variation and relaxation kinetics. Medium effect." In: *Canadian Journal of Chemistry* 70.8 (1992), pp. 2174–2189. DOI: https://doi.org/10.1139/v92-273.

[189] T. V. Mistry, Y. Cai, T. H. Lilley, and E. Haslam. "Polyphenol interactions. Part 5. Anthocyanin co-pigmentation." In: *Journal of the Chemical Society, Perkin Transactions 2* 8 (1991), pp. 1287–1296. DOI: https://doi.org/10.1039/P29910001287.

[190] P. M. Limon, R. Gavara, and F. Pina. "Thermodynamics and kinetics of cyanidin 3-glucoside and caffeine copigments." In: *Journal of Agricultural and Food Chemistry* 61.22 (2013), pp. 5245–5251. DOI: https://doi.org/10.1021/jf4006643.

[191] H. E. Hajji, O. Dangles, P. Figueiredo, and R. Brouillard. "3′-(β-D-Glycopyranosyloxy) flavylium Ions: Synthesis and investigation of their properties in aqueous solution. Hydrogen bonding as a mean of colour variation." In: *Helvetica Chimica Acta* 80.2 (1997), pp. 398–413. DOI: https://doi.org/10.1002/hlca.19970800206.

[192] F. Pina. "Caffeine interaction with synthetic flavylium salts. A flash photolysis study for the adduct involving 4′, 7-dihydroxyflavylium." In: *Journal of Photochemistry and Photobiology A: Chemistry* 117.1 (1998), pp. 51–59. DOI: https://doi.org/10.1016/S1010-6030(98)00306-2.

[193] M. Pessêgo, N. Basílio, J. Mendoza, J. Avó, L. Cunha-Silva, A. J. Parola, and F. Pina. "Exploring the diethylaminoflavylium derivatives multistate system of chemical reactions in the presence of CTAB micelles: thermodynamic reversibility achieved through different kinetic pathways." In: *RSC Advances* 7.48 (2017), pp. 30469–30480. DOI: https://doi.org/10.1039/C7RA04514J.

[194] A. J. Charlton, A. L. Davis, D. P. Jones, J. R. Lewis, A. P. Davies, E. Haslam, and M. P. Williamson. "The self-association of the black tea polyphenol thea flavin and its complexation with caffeine." In: *Journal of the Chemical Society, Perkin Transactions 2* 2 (2000), pp. 317–322. DOI: https://doi.org/10.1039/A906380C.

[195] L. Chebil, C. Humeau, A. Falcimaigne, J.-M. Engasser, and M. Ghoul. "Enzymatic acylation of flavonoids." In: *Process Biochemistry* 41.11 (2006), pp. 2237–2251. DOI: https://doi.org/10.1016/j.procbio.2006.05.027.

[196] L. Cruz, M. Guimaraes, P. Araujo, A. Evora, V. de Freitas, and N. Mateus. "Malvidin 3-glucoside–fatty acid conjugates: from hydrophilic toward novel lipophilic derivatives." In: *Journal of Agricultural and Food Chemistry* 65.31 (2017), pp. 6513–6518. DOI: https://doi.org/10.1021/acs.jafc.6b05461.

[197] L. Cruz, I. Fernandes, M. Guimarães, V. de Freitas, and N. Mateus. "Enzymatic synthesis, structural characterization and antioxidant capacity assessment of a new lipophilic malvidin-3-glucoside–oleic acid conjugate." In: *Food & Function* 7.6 (2016), pp. 2754–2762. DOI: https://doi.org/10.1039/C6FO00466K.

[198] P. Mukerjee, K. Mysels, and P. Kapauan. "Counterion specificity in the formation of ionic micelles-size, hydration, and hydrophobic bonding effects." In: *The Journal of Physical Chemistry* 71.13 (1967), pp. 4166–4175. DOI: https://doi.org/10.1021/j100872a702.

[199] W. Al-Soufi, L. Piñeiro, and M. Novo. "A model for monomer and micellar concentrations in surfactant solutions: Application to conductivity, NMR, diffusion, and surface tension data." In: *Journal of Colloid and Interface Science* 370.1 (2012), pp. 102–110. DOI: https://doi.org/10.1016/j.jcis.2011.12.037.

[200] C. A. Bunton, F. Nome, F. H. Quina, and L. S. Romsted. "Ion binding and reactivity at charged aqueous interfaces." In: *Accounts of Chemical Research* 24.12 (1991), pp. 357–364. DOI: https://doi.org/10.1021/ar00012a001.

[201] G. Hettiarachchi, D. Nguyen, J. Wu, D. Lucas, D. Ma, L. Isaacs, and V. Briken. "Toxicology and drug delivery by cucurbit [n] uril type molecular containers." In: *PLoS One* 5.5 (2010), e10514. DOI: https://doi.org/10.1371/journal.pone.0010514.

[202] A. I. Day and J. G. Collins. "Cucurbituril receptors and drug delivery." In: *Supramolecular Chemistry: From Molecules to Nanomaterials* (2012). DOI: https://doi.org/10.1002/9780470661345.smc056.

[203] J. A. Plumb, B. Venugopal, R. Oun, N. Gomez-Roman, Y. Kawazoe, N. S. Venkataramanan, and N. J. Wheate. "Cucurbit [7] uril encapsulated cisplatin overcomes cisplatin resistance via a pharmacokinetic effect." In: *Metallomics* 4.6 (2012), pp. 561–567. DOI: https://doi.org/10.1039/C2MT20054F.

[204] D. Ma, G. Hettiarachchi, D. Nguyen, B. Zhang, J. B. Wittenberg, P. Y. Zavalij, V. Briken, and L. Isaacs. "Acyclic cucurbit [n] uril molecular containers enhance the solubility and bioactivity of poorly soluble pharmaceuticals." In: *Nature Chemistry* 4.6 (2012), pp. 503–510. DOI: https://doi.org/10.1038/nchem.1326.

[205] J. W. Lee, S. Samal, N. Selvapalam, H.-J. Kim, and K. Kim. "Cucurbituril homologues and derivatives: new opportunities in supramolecular chemistry." In: *Accounts of Chemical Research* 36.8 (2003), pp. 621–630. DOI: https://doi.org/10.1021/ar020254k.

[206] D. Nengfang She, D. Moncelet, L. Gilberg, X. Lu, V. Sindelar, V. Briken, and L. Isaacs. "Glycoluril derived molecular clips are potent and selective receptors for cationic dyes in water." In: *Chemistry (Weinheim an der Bergstrasse, Germany)* 22.43 (2016), p. 15270. DOI: https://doi.org/10.1002/chem.201601796.

[207] P. Polavarapu, H. Melander, V. Langer, A. Gogoll, and H. Grennberg. "Modulation and binding properties of extended glycoluril molecular clips." In: *New Journal of Chemistry* 32.4 (2008), pp. 643–651. DOI: https://doi.org/10.1039/B715208F.

[208] L. Gilberg, B. Zhang, P. Y. Zavalij, V. Sindelar, and L. Isaacs. "Acyclic cucurbit [n] uril-type molecular containers: influence of glycoluril oligomer length on their function as solubilizing agents." In: *Organic & Biomolecular Chemistry* 13.13 (2015), pp. 4041–4050. DOI: https://doi.org/10.1039/C5OB00184F.

[209] H. Cong, X. L. Ni, X. Xiao, Y. Huang, Q.-J. Zhu, S.-F. Xue, Z. Tao, L. F. Lindoy, and G. Wei. "Synthesis and separation of cucurbit [n] urils and their derivatives." In: *Organic & Biomolecular Chemistry* 14.19 (2016), pp. 4335–4364. DOI: https://doi.org/10.1039/C6OB00268D.

[210] A. Chakraborty, A. Wu, D. Witt, J. Lagona, J. C. Fettinger, and L. Isaacs. "Diastereoselective formation of glycoluril dimers: Isomerization mechanism and implications for cucurbit [n] uril synthesis." In: *Journal of the American Chemical Society* 124.28 (2002), pp. 8297–8306. DOI: https://doi.org/10.1021/ja025876f.

[211] A. Day, A. P. Arnold, R. J. Blanch, and B. Snushall. "Controlling factors in the synthesis of cucurbituril and its homologues." In: *The Journal of Organic Chemistry* 66.24 (2001), pp. 8094–8100. DOI: https://doi.org/10.1021/jo015897c.

[212] F.-G. Klärner and B. Kahlert. "Molecular tweezers and clips as synthetic receptors. Molecular recognition and dynamics in receptor- substrate complexes." In: *Accounts of Chemical Research* 36.12 (2003), pp. 919–932. DOI: https://doi.org/10.1021/ar0200448.

[213] B. Branchi, V. Balzani, P. Ceroni, M. C. Kuchenbrandt, F.-G. Klarner, D. Blaser, and R. Boese. "Molecular clips with extended aromatic sidewalls as receptors for electron-acceptor molecules. Synthesis and NMR, photophysical, and electrochemical properties." In: *The Journal of Organic Chemistry* 73.15 (2008), pp. 5839–5851. DOI: https://doi.org/10.1021/jo8007513.

[214] A. Wu, A. Chakraborty, J. C. Fettinger, R. A. Flowers Ii, and L. Isaacs. "Molecular clips that undergo heterochiral aggregation and self-sorting." In: *Angewandte Chemie International Edition* 41.21 (2002), pp. 4028–4031. DOI: https://doi.org/10.1002/1521-3773(20021104)41:21<4028::AID-ANIE4028>3.0.CO;2-2.

[215] R. Sijbesma, A. Kentgens, E. Lutz, J. Van der Maas, and R. Nolte. "Binding features of molecular clips derived from diphenylglycoluril." In: *Journal of the American Chemical Society* 115.20 (1993), pp. 8999–9005. DOI: https://doi.org/10.1021/ja00073a015.

[216] J. Oliveira, J. Azevedo, N. Teixeira, P. Araujo, V. De Freitas, N. Basilio, and F. Pina. "On the limits of anthocyanins co-iigmentation models." In: *Journal of Agricultural and Food Chemistry* X.X (2020). DOI: http://.

[217] D.-S. Guo, K. Wang, and Y. Liu. "Selective binding behaviors of p-sulfonatocalixarenes in aqueous solution." In: *Journal of Inclusion Phenomena and Macrocyclic Chemistry* 62.1-2 (2008), pp. 1–21. DOI: https://doi.org/10.1007/s10847-008-9452-2.

[218] V. S. Kalyani and D. D. Malkhede. "p-Sulfonatocalix [8] arene and vitamin C complexation: assessment of photophysical, pKa and antioxidant property." In: *Journal of Inclusion Phenomena and Macrocyclic Chemistry* 87.1-2 (2017), pp. 179–189. DOI: https://doi.org/10.1007/s10847-016-0689-x.

[219] E. Da Silva, A. N. Lazar, and A. W. Coleman. "Biopharmaceutical applications of calixarenes." In: *Journal of Drug Delivery Science and Technology* 14.1 (2004), pp. 3–20. DOI: Biopharmaceuticalapplicationsofcal-ixarenes.

[220] E. Da Silva, P. Shahgaldian, and A. W. Coleman. "Haemolytic properties of some water-soluble para-sulphonato-calix-[n]-arenes." In: *International Journal of Pharmaceutics* 273.1-2 (2004), pp. 57–62. DOI: https://doi.org/10.1016/j.ijpharm.2003.12.008.

[221] S. J. Dalgarno, M. J. Hardie, J. L. Atwood, J. E. Warren, and C. L. Raston. "A complex 3D 'wavy brick wall' coordination polymer based on p-sulfonatocalix [8] arene." In: *New Journal of Chemistry* 29.5 (2005), pp. 649–652. DOI: https://doi.org/10.1039/B418352P.

[222] F. Perret, V. Bonnard, O. Danylyuk, K. Suwinska, and A. W. Coleman. "Conformational extremes in the supramolecular assemblies of para-sulfonato-calix [8] arene." In: *New Journal of Chemistry* 30.7 (2006), pp. 987–990. DOI: https://doi.org/10.1039/B604349F.

[223] N. Lavande, A. Acuña, N. Basílio, V. Francisco, D. D. Malkhede, and L. Garcia-Rio. "A journey from calix [4] arene to calix [6] and calix [8] arene reveals more than a matter of size. Receptor concentration affects the stability and stoichiometric nature of the complexes." In: *Physical Chemistry Chemical Physics* 19.21 (2017), pp. 13640–13649. DOI: https://doi.org/10.1039/C7CP01889D.

[224] S. Kumar, H. M. Chawla, and R Varadarajan. "A single step preparation of p-sulphonated calixarenes." In: *Indian Journal of Chemistry* 42B (2003), pp. 2863–2865.

[225] R. Rodríguez, E. Quiñoá, R. Riguera, and F. Freire. "Multistate chiroptical switch triggered by stimuli-responsive chiral teleinduction." In: *Chemistry of Materials* 30.8 (2018), pp. 2493–2497. DOI: https://doi.org/10.1021/acs.chemmater.8b00800.

[226] B. Doistau, L. Benda, J.-L. Cantin, L.-M. Chamoreau, E. Ruiz, V. Marvaud, B. Hasenknopf, and G. Vives. "Six states switching of redox-active molecular tweezers by three orthogonal stimuli." In: *Journal of the American Chemical Society* 139.27 (2017), pp. 9213–9220. DOI: https://doi.org/10.1021/jacs.7b02945.

[227] W. Zhao, B. Qiao, C.-H. Chen, and A. H. Flood. "High-fidelity multistate switching with anion–anion and acid–anion dimers of organophosphates in cyanostar complexes." In: *Angewandte Chemie International Edition* 56.42 (2017), pp. 13083–13087. DOI: https://doi.org/10.1002/ange.201707869.

[228] A. Petitjean, N. Kyritsakas, and J.-M. Lehn. "Ion-triggered multistate molecular switching device based on regioselective coordination-controlled ion binding." In: *Chemistry–A European Journal* 11.23 (2005), pp. 6818–6828. DOI: https://doi.org/10.1002/chem.200500625.

[229] N. Basíio, L. Cruz, V. de Freitas, and F. Pina. "A multistate molecular switch based on the 6, 8-rearrangement in bromo-apigeninidin operated with pH and host–guest inputs." In: *The Journal of Physical Chemistry B* 120.29 (2016), pp. 7053–7061. DOI: https://doi.org/10.1021/acs.jpcb.6b03694.

[230] Z. Tian, S. Cui, C. Zheng, and S. Pu. "A multi-state fluorescent switch based on a diarylethene with an acridine unit." In: *Spectrochimica Acta Part A: Molecular and Biomolecular Spectroscopy* 173 (2017), pp. 75–81. DOI: https://doi.org/10.1016/j.saa.2016.08.027.

[231] J. Bresien, T. Kröger-Badge, S. Lochbrunner, D. Michalik, H. Müller, A. Schulz, and E. Zander. "A chemical reaction controlled by light-activated molecular switches based on hetero-cyclopentanediyls." In: *Chemical science* 10.12 (2019), pp. 3486–3493. DOI: https://doi.org/10.1039/C8SC04893B.

[232] D. Margulies, C. E. Felder, G. Melman, and A. Shanzer. "A molecular keypad lock: a photochemical device capable of authorizing password entries." In: *Journal of the American Chemical Society* 129.2 (2007), pp. 347–354. DOI: https://doi.org/10.1021/ja065317z.

[233] G. Naren, C.-W. Hsu, S. Li, M. Morimoto, S. Tang, J. Hernando, G. Guirado, M. Irie, F. M. Raymo, H. Sundén, and J. Andréasson. "An all-photonic full color RGB system based on molecular photoswitches." In: *Nature Communications* 10.1 (2019), pp. 1–7. DOI: https://doi.org/10.1038/s41467-019-11885-4.

[234] J. Andréasson and U. Pischel. "Molecules for security measures: from keypad locks to advanced communication protocols." In: *Chemical Society Reviews* 47.7 (2018), pp. 2266–2279. DOI: https://doi.org/10.1039/C7CS00287D.

[235] F. M. Raymo, R. J. Alvarado, S. Giordani, and M. A. Cejas. "Memory effects based on intermolecular photoinduced proton transfer." In: *Journal of the American Chemical Society* 125.8 (2003), pp. 2361–2364. DOI: https://doi.org/10.1021/ja027977j.

[236] M. El Gemayel, K. Börjesson, M. Herder, D. T. Duong, J. A. Hutchison, C. Ruzié, G. Schweicher, A. Salleo, Y. Geerts, S. Hecht, E. Orgiu, and P. Samorí. "Optically switchable transistors by simple incorporation of photochromic systems into small-molecule semiconducting matrices." In: *Nature Communications* 6.1 (2015), pp. 1–8. DOI: https://doi.org/10.1038/ncomms7330.

[237] A. Zubillaga, P. Ferreira, A. J. Parola, S. Gago, and N. Basílio. "pH-Gated photoresponsive shuttling in a water-soluble pseudorotaxane." In: *Chemical Communications* 54.22 (2018), pp. 2743–2746. DOI: https://doi.org/10.1039/C8CC00688A.

[238] M. J. Melo, S. Moura, A. Roque, M. Maestri, and F. Pina. "Photochemistry of luteolinidin:"Write-lock-read-unlock-erase" with a natural compound." In: *Journal of Photochemistry and Photobiology A: Chemistry* 135.1 (2000), pp. 33–39. DOI: https://doi.org/10.1016/S1010-6030(00)00272-0.

[239] R. Gomes, A. M. Diniz, A. Jesus, A. J. Parola, and F. Pina. "The synthesis and reaction network of 2-styryl-1-benzopyrylium salts: An unexploited class of potential colorants." In: *Dyes and Pigments* 81.1 (2009), pp. 69–79. DOI: https://doi.org/10.1016/j.dyepig.2008.09.007.

[240] R. Gavara, V. Petrov, and F. Pina. "Characterization of the 4′-hydroxynaphthoflavylium network of chemical reactions." In: *Photochemical & Photobiological Sciences* 9.3 (2010), pp. 298–303. DOI: https://doi.org/10.1039/B9PP00035F.

[241] F. Pina, M. J. Melo, M. Maestri, P. Passaniti, and V. Balzani. "Artificial chemical systems capable of mimicking some elementary properties of neurons." In: *Journal of the American Chemical Society* 122.18 (2000), pp. 4496–4498. DOI: https://doi.org/10.1021/ja000190d.

[242] V. Petrov, R. Gomes, A. J. Parola, A. Jesus, C. A. Laia, and F. Pina. "2′-Hydroxyflavylium: introducing flavanones into the flavylium network of chemical reactions." In: *Tetrahedron* 64.4 (2008), pp. 714–720. DOI: https://doi.org/10.1016/j.tet.2007.11.007.

[243] V. Petrov, A. M. Diniz, L. Cunha-Silva, A. J. Parola, and F. Pina. "Kinetic and thermodynamic study of 2′-hydroxy-8-methoxyflavylium. Reaction network interconverting flavylium cation and flavanone." In: *RSC Advances* 3.27 (2013), pp. 10786–10794. DOI: https://doi.org/10.1039/C3RA40846A.

[244] O. A. Shareef, S. A. Said, and A. Y. Abdulrazaq. "Synthesis and kinetic investigations for the isomerization process of 2–hydroxy chalcone derivatives." In: *Journal of The Chemical Society of Pakistan* 41.06 (2019), p. 1046.

[245] J. M. Jez and J. P. Noel. "Reaction mechanism of chalcone isomerase pH dependence, diffusion control, and product binding differences." In: *Journal of Biological Chemistry* 277.2 (2002), pp. 1361–1369. DOI: https://doi.org/10.1074/jbc.M109224200.

[246] C. Brunetti, M. Di Ferdinando, A. Fini, S. Pollastri, and M. Tattini. "Flavonoids as antioxidants and developmental regulators: relative significance in plants and humans." In: *International Journal of Molecular Sciences* 14.2 (2013), pp. 3540–3555. DOI: https://doi.org/10.3390/ijms14023540.

[247] I. Trendafilova, J. Mihály, D. Momekova, R. Chimshirova, H. Lazarova, G. Momekov, and M. Popova. "Antioxidant activity and modified release profiles of morin and hesperetin flavonoids loaded in Mg-or Ag-modified SBA-16 carriers." In: *Materials Today Communications* (2020), p. 101198. DOI: https://doi.org/10.1016/j.mtcomm.2020.101198.

[248] L. Feng, M. M. Maddox, M. Z. Alam, L. S. Tsutsumi, G. Narula, D. F. Bruhn, X. Wu, S. Sandhaus, R. B. Lee, C. J. Simmons, et al. "Synthesis, structure–activity relationship studies, and antibacterial evaluation of 4-chromanones and chalcones, as well as olympicin A and derivatives." In: *Journal of Medicinal Chemistry* 57.20 (2014), pp. 8398–8420. DOI: https://doi.org/10.1021/jm500853v.

[249] C. Chen, C. Wan, X. Peng, and J. Chen. "A flavonone pinocembroside inhibits Penicillium italicum growth and blue mold development in 'Newhall'navel oranges by targeting membrane damage mechanism." In: *Pesticide Biochemistry and Physiology* (2019). DOI: https://doi.org/10.1016/j.pestbp.2019.11.025.

[250] S. A. Ahmed and E. M. Kamel. "Cytotoxic activities of flavonoids from *Centaurea scoparia*." In: *The Scientific World Journal* 2014 (2014). DOI: https://doi.org/10.1155/2014/274207.

[251] S. Serra, A. Alouane, T. Le Saux, S. Huvelle, R. Plasson, F. Schmidt, L. Jullien, and R. Labruère. "A chemically encoded timer for dual molecular delivery at tailored ranges and concentrations." In: *Chemical Communications* 54.49 (2018), pp. 6396–6399. DOI: https://doi.org/10.1039/C8CC03253J.

[252] A. Singh, Z. Vahdat, and Z. Xu. "Time-triggered stochastic hybrid systems with two timer-dependent resets." In: (2019). DOI: https://doi.org/10.31219/osf.io/u8fzg.

[253] A. Khalil, R. Baltenweck-Guyot, R. Ocampo-Torres, and P. Albrecht. "A novel symmetrical pyrano-3-deoxyanthocyanidin from a Sorghum species." In: *Phytochemistry Letters* 3.2 (2010), pp. 93–95. DOI: https://doi.org/10.1016/j.phytol.2010.02.003.

[254] C. Petti, R. Kushwaha, M. Tateno, A. E. Harman-Ware, M. Crocker, J. Awika, and S. DeBolt. "Mutagenesis breeding for increased 3-deoxyanthocyanidin accumulation in leaves of Sorghum bicolor (L.) Moench: A source of natural food pigment." In: *Journal of Agricultural and Food Chemistry* 62.6 (2014), pp. 1227–1232. DOI: https://doi.org/10.1021/jf405324j.

[255] T. Iwashina, J. Kitajima, S. Matsumoto, et al. "Luteolinidin 5-O-glucoside from Azolla as a stable taxonomic marker." In: *Bulletin of the National Museum of Nature and Science* 36 (2010), pp. 61–64.

[256] A Alejo-Armijo, J. Mendoza, A. J. Parola, and F. Pina. "Chemical evolution of the colour systems generated by riccionidin A, 3-deoxyanthocyanidins and anthocyanins." In: *Phytochemistry* 174 (2020), p. 112339. DOI: https://doi.org/10.1016/j.phytochem.2020.112339.

[257] A. Sousa, V. Petrov, P. Araujo, N. Mateus, F. Pina, and V. de Freitas. "Thermodynamics, kinetics, and photochromism of oaklins: A recent family of deoxyanthocyanidins." In: *The Journal of Physical Chemistry B* 117.6 (2013), pp. 1901–1910. DOI: https://doi.org/10.1021/jp3110216.

[258] S. Al Bittar, N. Mora, M. Loonis, and O. Dangles. "A simple synthesis of 3-deoxyanthocyanidins and their O-glucosides." In: *Tetrahedron* 72.29 (2016), pp. 4294–4302. DOI: https://doi.org/10.1016/j.tet.2016.05.076.

[259] N. Basílio, S. Al Bittar, N. Mora, O. Dangles, and F. Pina. "Analogs of natural 3-deoxyanthocyanins: O-glucosides of the 4′, 7-dihydroxyflavylium ion and the deep influence of glycosidation on color." In: *International Journal of Molecular Sciences* 17.10 (2016), p. 1751. DOI: https://doi.org/10.3390/ijms17101751.

[260] T. Harada, D.-T. Pham, M. H. Leung, H. T. Ngo, S. F. Lincoln, C. J. Easton, and T. W. Kee. "Cooperative binding and stabilization of the medicinal pigment curcumin by diamide linked γ-cyclodextrin dimers: a spectroscopic characterization." In: *The Journal of Physical Chemistry B* 115.5 (2011), pp. 1268–1274. DOI: https://doi.org/10.1021/jp1096025.

[261] S. Jeong, W. Y. Kang, C. K. Song, and J. S. Park. "Supramolecular cyclodextrin-dye complex exhibiting selective and efficient quenching by lead ions." In: *Dyes and Pigments* 93.1-3 (2012), pp. 1544–1548. DOI: https://doi.org/10.1016/j.dyepig.2011.08.011.

[262] M. K. Singh, H. Pal, A. S. R. Koti, and A. V. Sapre. "Photophysical properties and rotational relaxation dynamics of neutral red bound to β-cyclodextrin." In: *The Journal of Physical Chemistry A* 108.9 (2004), pp. 1465–1474. DOI: https://doi.org/10.1021/jp035075e.

[263] M. Budau, G. Hancu, Z. I. Szabó, H. Kelemen, A. Rusu, D. L. Muntean, and A. G. Cârje. "Captisol® as chiral selector in capillary electrophoresis of non-acidic drugs." In: *Journal of the Chilean Chemical Society* 62.3 (2017), pp. 3566–3571. DOI: http://dx.doi.org/10.4067/s0717-97072017000303566.

[264] V. Petrov, S. Stanimirov, I. K. Petrov, A. Fernandes, V. de Freitas, and F. Pina. "Emptying the β-cyclodextrin cavity by light: photochemical removal of the trans-chalcone of 4′, 7-dihydroxyflavylium." In: *The Journal of Physical Chemistry A* 117.41 (2013), pp. 10692–10701. DOI: https://doi.org/10.1021/jp4060582.

[265] K. Bouchemal and S. Mazzaferro. "How to conduct and interpret ITC experiments accurately for cyclodextrin–guest interactions." In: *Drug Discovery Today* 17.11-12 (2012), pp. 623–629. DOI: https://doi.org/10.1016/j.drudis.2012.01.023.

[266] X. Zhang, G. Gramlich, X. Wang, and W. M. Nau. "A joint structural, kinetic, and thermodynamic investigation of substituent effects on host- guest complexation of bicyclic azoalkanes by β-cyclodextrin." In: *Journal of the American Chemical Society* 124.2 (2002), pp. 254–263. DOI: https://doi.org/10.1021/ja011866n.

[267] L. I. Bosch, T. M. Fyles, and T. D. James. "Binary and ternary phenylboronic acid complexes with saccharides and Lewis bases." In: *Tetrahedron* 60.49 (2004), pp. 11175–11190. DOI: https://doi.org/10.1016/j.tet.2004.08.046.

[268] D. G. Hall. "Structure, properties, and preparation of boronic acid derivatives. Overview of their reactions and applications." In: *Boronic acids*. Ed. by D. G. Hall. Weinheim, DE: Wiley-VCH, 2005. Chap. 1, pp. 1–97.

[269] Y. Furikado, T. Nagahata, T. Okamoto, T. Sugaya, S. Iwatsuki, M. Inamo, H. D. Takagi, A. Odani, and K. Ishihara. "Universal reaction mechanism of boronic acids with diols in aqueous solution: kinetics and the basic concept of a conditional formation constant." In: *Chemistry–A European Journal* 20.41 (2014), pp. 13194–13202. DOI: https://doi.org/10.1002/chem.201403719.

[270] Y. Yamamoto, T. Matsumura, N. Takao, H. Yamagishi, M. Takahashi, S. Iwatsuki, and K. Ishihara. "Fast trigonal/tetragonal interconversion followed by slow chelate-ring closure in the complexation of boronic acids." In: *Inorganica Chimica Acta* 358.12 (2005), pp. 3355–3361. DOI: https://doi.org/10.1016/j.ica.2005.05.026.

[271] J. Yan, G. Springsteen, S. Deeter, and B. Wang. "The relationship among pKa, pH, and binding constants in the interactions between boronic acids and diols—it is not as simple as it appears." In: *Tetrahedron* 60.49 (2004), pp. 11205–11209. DOI: https://doi.org/10.1016/j.tet.2004.08.051.

[272] N. Basílio and F. Pina. "Flavylium Network of Chemical Reactions in Confined Media: Modulation of 3′, 4′, 7-Trihydroxyflavilium Reactions by Host–Guest Interactions with Cucurbit [7] uril." In: *ChemPhysChem* 15.11 (2014), pp. 2295–2302. DOI: https://doi.org/10.1002/cphc.201402051.

[273] Y. Leydet, P. Batat, G. Jonusauskas, S. Denisov, J. C. Lima, A. J. Parola, N. D. Mcclenaghan, and F. Pina. "Impact of water on the cis–trans photoisomerization of hydroxychalcones." In: *The Journal of Physical Chemistry A* 117.20 (2013), pp. 4167–4173. DOI: https://doi.org/10.1021/jp402761j.

[274] M. Kueny-Stotz, S. Chassaing, R. Brouillard, M. Nielsen, and M. Goeldner. "Flavylium salts as in vitro precursors of potent ligands to brain GABA-A receptors." In: *Bioorganic & Medicinal Chemistry Letters* 18.17 (2008), pp. 4864–4867. DOI: https://doi.org/10.1016/j.bmcl.2008.07.107.

APPENDIX A

Mathematical deduction of the flavylium multi-state molar fractions and equilibrium constants.

The flavylim multi-state can be expressed as a series of multiprotic acid-base reactons along the pH scale, depending on the number and acidity of the protons available, in the structure of each compound, to form oxonium ions when they are released. For illustration proposes, a triprotic acid is going to be used as example.

The first global acid-base equilibrium is obtained after the proton transfer of the **AH^+** leading to the formation of the other species.

In the equilibrium:

$$AH^+ + H_2O \overset{K'_a}{\rightleftharpoons} CB + H_3O^+ \tag{A.1}$$

with $[\boldsymbol{CB}] = [\boldsymbol{A}] + [\boldsymbol{B}] + [\boldsymbol{Cc}] + [\boldsymbol{Ct}]$
Formation of all the species of the multi-state takes place by different reactions:

Proton transfer

$$AH^+ + H_2O \overset{K_a}{\rightleftharpoons} A + H_3O^+ \tag{A.2}$$

Hydration

$$AH^+ + 2H_2O \overset{K_h}{\rightleftharpoons} B + H_3O^+ \tag{A.3}$$

Tautomerization

$$B \overset{K_t}{\rightleftharpoons} Cc \tag{A.4}$$

Isomerization

$$\mathrm{Cc} \overset{K_i}{\rightleftharpoons} \mathrm{Ct} \tag{A.5}$$

The equilibrium constant K'_a for Eq.A.1 is defined then as:

$$K'_a = K_a + K_h + K_h K_t + K_h K_t K_i \tag{A.6}$$

The second global acid-base equilibrium results from the proton transfer reaction from the neutral species of the flavylium multi-state to the mono-ionized species (Eqs. A.7 to A.10).

$$\mathrm{A} + \mathrm{H_2O} \overset{K_{A/A^-}}{\rightleftharpoons} \mathrm{A^-} + \mathrm{H_3O^+} \tag{A.7}$$

$$\mathrm{B} + \mathrm{H_2O} \overset{K_{B/B^-}}{\rightleftharpoons} \mathrm{B^-} + \mathrm{H_3O^+} \tag{A.8}$$

$$\mathrm{Cc} + \mathrm{H_2O} \overset{K_{Cc/Cc^-}}{\rightleftharpoons} \mathrm{Cc^-} + \mathrm{H_3O^+} \tag{A.9}$$

$$\mathrm{Ct} + \mathrm{H_2O} \overset{K_{Ct/Ct^-}}{\rightleftharpoons} \mathrm{Ct^-} + \mathrm{H_3O^+} \tag{A.10}$$

Finally the third global acid-base equilibrium is obtained after the proton transfer from the ionized species to the di-ionized species (Eqs. A.11 to A.14).

$$\mathrm{A^-} + \mathrm{H_2O} \overset{K_{A^-/A^{2-}}}{\rightleftharpoons} \mathrm{A^{2-}} + \mathrm{H_3O^+} \tag{A.11}$$

$$\mathrm{B^-} + \mathrm{H_2O} \overset{K_{B^-/B^{2-}}}{\rightleftharpoons} \mathrm{B^{2-}} + \mathrm{H_3O^+} \tag{A.12}$$

$$\mathrm{Cc^-} + \mathrm{H_2O} \overset{K_{Cc^-/Cc^{2-}}}{\rightleftharpoons} \mathrm{Cc^{2-}} + \mathrm{H_3O^+} \tag{A.13}$$

$$\mathrm{Ct^-} + \mathrm{H_2O} \overset{K_{Ct^-/Ct^{2-}}}{\rightleftharpoons} \mathrm{Ct^{2-}} + \mathrm{H_3O^+} \tag{A.14}$$

In the sense of an acid-base equilibrium between the species, the equations A.15 and A.16 are generalized from the group of equations A.7 to A.10 and A.11 to A.14 respectably.

$$\mathrm{CB} + \mathrm{H_2O} \overset{K''_a}{\rightleftharpoons} \mathrm{CB^-} + \mathrm{H_3O^+} \tag{A.15}$$

$$\mathrm{CB^-} + \mathrm{H_2O} \overset{K'''_a}{\rightleftharpoons} \mathrm{CB^{2-}} + \mathrm{H_3O^+} \tag{A.16}$$

with $[\boldsymbol{CB^-}] = [\boldsymbol{A^-}] + [\boldsymbol{B^-}] + [\boldsymbol{Cc^-}] + [\boldsymbol{Ct^-}]$ and $[\boldsymbol{CB^{2-}}] = [\boldsymbol{A^{2-}}] + [\boldsymbol{B^{2-}}] + [\boldsymbol{Cc^{2-}}] + [\boldsymbol{Ct^{2-}}]$
Thus the equilibrium constant K''_a for Eq.A.15 is defined then as:

$$K''_a = \frac{K_{A/A^-} K_a + K_{B/B^-} K_h + K_{Cc/Cc^-} K_h K_t + K_{Ct/Ct^-} K_h K_t K_i}{K'_a} \tag{A.17}$$

And the equilibrium constant K_a''' for Eq.A.16 as:

$$K_a''' = \frac{K_{A^-/A^{2-}} K_{A/A^-} K_a + K_{A^-/A^{2-}} K_{B/B^-} K_h + K_{A^-/A^{2-}} K_{Cc/Cc^-} K_h K_t + K_{A^-/A^{2-}} K_{Ct/Ct^-} K_h K_t K_i}{K_a' K_a''} \tag{A.18}$$

Mole fractions of all the species can be then straightforwardly calculated by a simple mass balance (Eqs. A.1 to A.14) analysis in function of $\mathbf{AH^+}$.

$$C_0 = [AH^+]+[A]+[B]+[Cc]+[Ct]+[A^-]+[B^-]+[Cc^-]+[Ct^-]+[A^{2-}]+[B^{2-}]+[Cc^{2-}]+[Ct^{2-}] \tag{A.19}$$

$$\begin{aligned} C_0 = [AH^+]\Bigg(1 &+ \frac{K_a}{[H^+]} + \frac{K_h}{[H^+]} + \frac{K_h K_t}{[H^+]} + \frac{K_h K_t K_i}{[H^+]} + \frac{K_{A/A^-} K_a}{[H^+]^2} + \frac{K_{B/B^-} K_h}{[H^+]^2} \\ &+ \frac{K_{Cc/Cc^-} K_h K_t}{[H^+]^2} + \frac{K_{Ct/Ct^-} K_h K_t K_i}{[H^+]^2} + \frac{K_{A^-/A^{2-}} K_{A/A^-} K_a}{[H^+]^3} + \frac{K_{B^-/B^{2-}} K_{B/B^-} K_h}{[H^+]^3} \\ &+ \frac{K_{Cc^-/Cc^{2-}} K_{Cc/Cc^-} K_h K_t}{[H^+]^3} + \frac{K_{Ct^-/Ct^{2-}} K_{Ct/Ct^-} K_h K_t K_i}{[H^+]^3}\Bigg) \end{aligned} \tag{A.20}$$

From eq.A.20 the mole fraction distribution can be calculated as:

$$\chi_{AH^+} = \frac{[AH^+]}{C_0} = \frac{[H^+]^3}{D} \tag{A.21}$$

where

$$\begin{aligned} D = [H^+]^3 &+ (K_a + K_h + K_h K_t + K_h K_t K_i)[H^+]^2 + (K_{A/A^-} K_a + K_{B/B^-} K_h + K_{Cc/Cc^-} K_h K_t \\ &+ K_{Ct/Ct^-} K_h K_t K_i)[H^+] + K_{A^-/A^{2-}} K_{A/A^-} K_a + K_{B^-/B^{2-}} K_{B/B^-} K_h \\ &+ K_{Cc^-/Cc^{2-}} K_{Cc/Cc^-} K_h K_t + K_{Ct^-/Ct^{2-}} K_{Ct/Ct^-} K_h K_t K_i \end{aligned}$$

or condensed as

$$D = [H^+]^3 + K_a'[H^+]^2 + K_a' K_a''[H^+] + K_a' K_a'' K_a'''$$

By this way, the molar fractions of all the species can be calculated:

$$\chi_A = \frac{K_a [H^+]^2}{D} \tag{A.22}$$

$$\chi_B = \frac{K_h [H^+]^2}{D} \tag{A.23}$$

$$\chi_{Cc} = \frac{K_h K_t [H^+]^2}{D} \tag{A.24}$$

$$\chi_{Ct} = \frac{K_h K_t K_i [H^+]^2}{D} \tag{A.25}$$

$$\chi_{A^-} = \frac{K_a K_{A/A^-} [H^+]}{D} \tag{A.26}$$

$$\chi_{B^-} = \frac{K_h K_{B/B^-}[H^+]}{D} \tag{A.27}$$

$$\chi_{Cc^-} = \frac{K_h K_t K_{Cc/Cc^-}[H^+]}{D} \tag{A.28}$$

$$\chi_{Ct^-} = \frac{K_h K_t K_i K_{Ct/Ct^-}[H^+]}{D} \tag{A.29}$$

$$\chi_{A^{2-}} = \frac{K_a K_{A/A^-} K_{A^-/A^{2-}}}{D} \tag{A.30}$$

$$\chi_{B^{2-}} = \frac{K_h K_{B/B^-} K_{B^-/B^{2-}}}{D} \tag{A.31}$$

$$\chi_{Cc^{2-}} = \frac{K_h K_t K_{Cc/Cc^-} K_{Cc^-/Cc^{2-}}}{D} \tag{A.32}$$

$$\chi_{Ct^{2-}} = \frac{K_h K_t K_i K_{Ct/Ct^-} K_{Ct^-/Ct^{2-}}}{D} \tag{A.33}$$

Also the molar fractions expressed in terms of a triprotic acid can be calculated:

$$\chi_{CB} = \frac{K'_a[H^+]^2}{D} \tag{A.34}$$

$$\chi_{CB^-} = \frac{K'_a K''_a[H^+]}{D} \tag{A.35}$$

$$\chi_{CB^{2-}} = \frac{K'_a K''_a K'''_a}{D} \tag{A.36}$$

The molar fraction of the **AH⁺** is always calculated by Equation A.21.

In the pseudo-equilibrium

All equations above described can be applied at the pseudo-equilibrium, reached when the flavylium base-compound has a high *cis-trans* isomerization barrier.

$$AH^+ + H_2O \overset{K_a^{\wedge}}{\rightleftharpoons} CB^{\wedge} + H_3O^+ \tag{A.37}$$

$$CB^{\wedge} + H_2O \overset{K_a^{\wedge\wedge}}{\rightleftharpoons} CB^{\wedge\wedge} + H_3O^+ \tag{A.38}$$

$$CB^{\wedge\wedge} + H_2O \overset{K_a^{\wedge\wedge\wedge}}{\rightleftharpoons} CB^{\wedge\wedge\wedge} + H_3O^+ \tag{A.39}$$

with

$[\boldsymbol{CB}^{\wedge}] = [\boldsymbol{A}] + [\boldsymbol{B}] + [\boldsymbol{Cc}]$

$[\boldsymbol{CB}^{\wedge\wedge}] = [\boldsymbol{A}^{-}] + [\boldsymbol{B}^{-}] + [\boldsymbol{Cc}^{-}]$
$[\boldsymbol{CB}^{\wedge\wedge\wedge}] = [\boldsymbol{A}^{\mathbf{2-}}] + [\boldsymbol{B}^{\mathbf{2-}}] + [\boldsymbol{Cc}^{\mathbf{2-}}]$

The equilibrium constants $K_a^{\wedge}$, $K_a^{\wedge\wedge}$ and $K_a^{\wedge\wedge\wedge}$ in Equations A.37 to A.39 can be expressed as:

$$K_a^{\wedge} = K_a + K_h + K_h K_t \tag{A.40}$$

$$K_a^{\wedge} K_a^{\wedge\wedge} = K_{A/A^-} K_a + K_{B/B^-} K_h + K_{Cc/Cc^-} K_h K_t \tag{A.41}$$

$$K_a^{\wedge} K^{\wedge\wedge} K_a^{\wedge\wedge\wedge} = K_{A^-/A^{2-}} K_{A/A^-} K_a + K_{B^-/B^{2-}} K_{B/B^-} K_h + K_{Cc^-/Cc^{2-}} K_{Cc/Cc^-} K_h K_t \tag{A.42}$$

and by consequence:

$$K_a^{\wedge\wedge} = \frac{K_{A/A^-} K_a + K_{B/B^-} K_h + K_{Cc/Cc^-} K_h K_t + K_{Ct/Ct^-} K_h K_t K_i}{K_a^{\wedge}} \tag{A.43}$$

$$K_a^{\wedge\wedge\wedge} = \frac{K_{A^-/A^{2-}} K_{A/A^-} K_a + K_{A^-/A^{2-}} K_{B/B^-} K_h + K_{A^-/A^{2-}} K_{Cc/Cc^-} K_h K_t + K_{A^-/A^{2-}} K_{Ct/Ct^-} K_h K_t K_i}{K_a^{\wedge} K_a^{\wedge\wedge}} \tag{A.44}$$

The mole fractions of each species in the pseudo-equilibrium are calculated in the same way as the ones in the equilibrium, except for the **Ct** species, and substituting the equilibrium constants K_a', K_a'' and K_a''' by $K_a^{\wedge}$, $K_a^{\wedge\wedge}$ and $K_a^{\wedge\wedge\wedge}$.

APPENDIX B

New method to calculate all the equilibrium constants in the flavylium multi-sate

The expressions described in Appendix A allows to calculate all the flavylium multi-state species molar fractions, in the equilibrium and in the pseudo-equilibrium, for those compounds with high *cis-trans* isomerization barrier. The normalized mole fractions of A, B and Cc can be easily calculated trough reverse pH jumps from pseudo-equilibrated or equilibrated solutions at different pH values. The mole fraction of the species in the first deprotonation of **AH⁺**, CB, can be written as described in Appendix A or expressing the normalized mole fractions of A (a_0), B (b_0) and Cc (c_0) as:

$$\chi_{CB^{\wedge}} = \frac{K_a^{\wedge}[H^+]^2}{D} = a_0\frac{K_a^{\wedge}[H^+]^2}{D} + b_0\frac{K_a^{\wedge}[H^+]^2}{D} + c_0\frac{K_a^{\wedge}[H^+]^2}{D} \tag{B.1}$$

$a_0 + b_0 + c_0 = 1$

By the same way, the mole normalized mole fraction of a, b and c in the $CB^{\wedge\wedge}$ and $CB^{\wedge\wedge\wedge}$ can be calculated.

$$\chi_{CB^{\wedge\wedge}} = \frac{K_a^{\wedge}K_a^{\wedge\wedge}[H^+]}{D} = a_1\frac{K_a^{\wedge}K_a^{\wedge\wedge}[H^+]}{D} + b_1\frac{K_a^{\wedge}K_a^{\wedge\wedge}[H^+]}{D} + c_1\frac{K_a^{\wedge}K_a^{\wedge\wedge}[H^+]}{D} \tag{B.2}$$

$a_1 + b_1 + c_1 = 1$

$$\chi_{CB^{\wedge\wedge\wedge}} = \frac{K_a^{\wedge}K_a^{\wedge\wedge}K_a^{\wedge\wedge\wedge}}{D} = a_2\frac{K_a^{\wedge}K_a^{\wedge\wedge}K_a^{\wedge\wedge\wedge}}{D} + b_2\frac{K_a^{\wedge}K_a^{\wedge\wedge}K_a^{\wedge\wedge\wedge}}{D} + c_2\frac{K_a^{\wedge}K_a^{\wedge\wedge}K_a^{\wedge\wedge\wedge}}{D} \tag{B.3}$$

$a_2 + b_2 + c_2 = 1$

Then the molar fractions of each species and their respective ionized forms can be presented as:

$$\chi_A + \chi_{A^-} + \chi_{A^{2-}} = \frac{a_0 K_a^{\wedge}[H^+]^2 + a_1 K_a^{\wedge} K_a^{\wedge\wedge}[H^+] + a_2 K_a^{\wedge} K_a^{\wedge\wedge} K_a^{\wedge\wedge\wedge}}{D} \tag{B.4}$$

$$\chi_B + \chi_{B^-} + \chi_{B^{2-}} = \frac{b_0 K_a^{\wedge}[H^+]^2 + b_1 K_a^{\wedge} K_a^{\wedge\wedge}[H^+] + b_2 K_a^{\wedge} K_a^{\wedge\wedge} K_a^{\wedge\wedge\wedge}}{D} \tag{B.5}$$

$$\chi_{Cc} + \chi_{Cc^-} + \chi_{Cc^{2-}} = \frac{c_0 K_a^{\wedge}[H^+]^2 + c_1 K_a^{\wedge} K_a^{\wedge\wedge}[H^+] + c_2 K_a^{\wedge} K_a^{\wedge\wedge} K_a^{\wedge\wedge\wedge}}{D} \tag{B.6}$$

Or expressed as in Appendix A:

$$\chi_A + \chi_{A^-} + \chi_{A^{2-}} = \frac{K_a[H^+]^2 + K_{A/A^-} K_a[H^+] + K_{A^-/A^{2-}} K_{A/A^-} K_a}{D} \tag{B.7}$$

$$\chi_B + \chi_{B^-} + \chi_{B^{2-}} = \frac{K_h[H^+]^2 + K_{B/B^-} K_h[H^+] + K_{B^-/B^{2-}} K_{B/B^-} K_h}{D} \tag{B.8}$$

$$\chi_{Cc} + \chi_{Cc^-} + \chi_{Cc^{2-}} = \frac{K_h K_t[H^+]^2 + K_{Cc/Cc^-} K_h K_t[H^+] + K_{Cc^-/Cc^{2-}} K_{Cc/Cc^-} K_h K_t}{D} \tag{B.9}$$

This is:

$$K_a = a_0 K_a^{\wedge} \qquad K_{A/A^-} K_a = a_1 K_a^{\wedge} K_a^{\wedge\wedge} \qquad K_{A^-/A^{2-}} K_{A/A^-} K_a = a_2 K_a^{\wedge} K_a^{\wedge\wedge} K_a^{\wedge\wedge\wedge}$$

$$K_h = b_0 K_a^{\wedge} \qquad K_{B/B^-} K_h = b_1 K_a^{\wedge} K_a^{\wedge\wedge} \qquad K_{B^-/B^{2-}} K_{B/B^-} K_h = a_2 K_a^{\wedge} K_a^{\wedge\wedge} K_a^{\wedge\wedge\wedge}$$

$$K_h K_t = c_0 K_a^{\wedge} \qquad K_{Cc/Cc^-} K_h K_t = c_1 K_a^{\wedge} K_a^{\wedge\wedge} \qquad K_{Cc^-/Cc^{2-}} K_{Cc/Cc^-} K_h K_t = a_2 K_a^{\wedge} K_a^{\wedge\wedge} K_a^{\wedge\wedge\wedge}$$

This permits to calculate all the equilibrium constants in the pseudo-equilibrium, since $K_a^{\wedge}$, $K_a^{\wedge\wedge}$ and $K_a^{\wedge\wedge\wedge}$ are obtained from the absorption spectra where three inflection points must be observed when the pH is plotted versus an specific wavelength. The constants in the equilibrium Ki, K_{Ct/Ct^-}, $K_{Ct^-/Ct^{2-}}$ also can be calculated if the next considerations are taken into consideration:

$$\chi_{CB'} = \frac{K_a'[H^+]^2}{D} = \frac{a_0 K_a'[H^+]^2 + b_0 K_a'[H^+]^2 + c_0 K_a'[H^+]^2 + d_0 K_a'[H^+]^2}{D} \tag{B.10}$$

$$\chi_{CB''} = \frac{K_a''[H^+]^2}{D} = \frac{a_0 K_a''[H^+]^2 + b_0 K_a''[H^+]^2 + c_0 K_a''[H^+]^2 + d_0 K_a''[H^+]^2}{D} \tag{B.11}$$

$$\chi_{CB'''} = \frac{K_a'''[H^+]^2}{D} = \frac{a_0 K_a'''[H^+]^2 + b_0 K_a'''[H^+]^2 + c_0 K_a'''[H^+]^2 + d_0 K_a'''[H^+]^2}{D} \tag{B.12}$$

$$a_0 + b_0 + c_0 + d_0 = 1 \qquad a_1 + b_1 + c_1 + d_1 = 1 \qquad a_2 + b_2 + c_2 + d_2 = 1$$

$$\chi_{Ct} + \chi_{Ct^-} + \chi_{Ct^{2-}} = \frac{d_0 K'_a [H^+]^2 + d_1 K'_a K''_a [H^+] + d_2 K'_a K''_a K'''}{D} \tag{B.13}$$

$$\chi_{Ct} + \chi_{Ct^-} + \chi_{Ct^{2-}} = \frac{K_h K_t K_i [H^+]^2 + K_{Ct/Ct^-} K_h K_t K_i [H^+] + K_{Ct^-/Ct^{2-}} K_{Ct/Ct^-} K_h K_t K_i}{D} \tag{B.14}$$

This is:

$$K_h K_t K_i = d_0 K'_a \qquad K_{Ct/Ct^-} K_h K_t K_i = d_1 K'_a K''_a \qquad K_{Ct^-/Ct^{2-}} K_{Ct/Ct^-} K_h K_t K_i = d_2 K'_a K''_a K'''$$

Once obtained the values of a, b, c and d, is easy to calculate all the equilibrium constants in the flavylium multi-state.

APPENDIX C

Mathematical deduction of the association constants in copigmentation process

Considering the pseudo-equilibrium between the flavylium cation ($\mathbf{AH^+}$) and the species after the fist acid-base reaction ($CB^\wedge$) and a 1:1 complexation with a co-pigment (CP) we have:

$$AH^+ + CP \overset{K_{AH^+CP}}{\rightleftharpoons} AH^+CP \tag{C.1}$$

$$A + CP \overset{K_{ACP}}{\rightleftharpoons} ACP \tag{C.2}$$

$$B + CP \overset{K_{BCP}}{\rightleftharpoons} BCP \tag{C.3}$$

$$Cc + CP \overset{K_{CcCP}}{\rightleftharpoons} CcCP \tag{C.4}$$

That can be reduced to Eq.C.1 and C.5:

$$CB^\wedge{}^+CP \overset{K_{CB^\wedge CP}}{\rightleftharpoons} CB^\wedge CP \tag{C.5}$$

$[CB^\wedge CP]$=$[ACP]$+$[BCP]$+$[CcCP]$

$$K_{CB^\wedge CP} = \frac{[CB^\wedge CP]}{[CB^\wedge][CP]} = \frac{[ACP]+[BCP]+[CcCP]}{[A][CP]+[B][CP]+[Cc][CP]} \tag{C.6}$$

Simplifying:

$$K_{CB^\wedge CP} = \frac{[CB^\wedge CP]}{[CB^\wedge][CP]} = \frac{K_{ACP}K_a + K_{BCP}K_h + K_{CcCP}K_hK_t}{K_a^\wedge} \tag{C.7}$$

Considering the mono-ionized species, which still have some importance in the anthocyanins copigmentation:

$$A^- + CP \rightleftharpoons A^-CP \tag{C.8}$$

$$B^- + CP \rightleftharpoons B^-CP \tag{C.9}$$

$$Cc^- + CP \rightleftharpoons Cc^-CP \tag{C.10}$$

That can be reduced to Eq.C.11:

$$CB^{\wedge -} + CP \rightleftharpoons CB^{\wedge -}CP \tag{C.11}$$

$$K_{(CB^{\wedge -}CP} = \frac{[CB^{\wedge -}CP]}{[CB^{\wedge -}][CP]} = \frac{[A^-CP]+[B^-CP]+[Cc^-CP]}{[A^-][CP]+[B^-][CP]+[Cc^-][CP]} \tag{C.12}$$

giving

$$K_{(CB^{\wedge -}CP} = \frac{K_{ACP/ACP^-}K_{A/A^-}K_a + K_{BCP/BCP^-}K_{B/B^-}K_h + K_{CcCP/CcCP^-}K_{Cc/Cc^-}K_hK_t}{K_{CB/CB^{\wedge -}}K_a^{\wedge}} \tag{C.13}$$

The complex set of equation can be extended even to another deprotonation, but for all practical purposes is now defined as a diprotic acid (after the third deprotonation, the anthocyanins are commonly unstable), summarized as $\mathbf{AH^+}$, $CB^{\wedge}$ and $CB^{\wedge -}$ in Eqs C.1, C.7 and C.13 respectably. In order to calculate the molar fractions in the pseudo-equilibrium, the mass balance results in:

$$\begin{aligned} C_0 = [AH^+]+[A]+[B]+[Cc]+[A^-]+[B^-]+[Cc^-]+[AH^+CP]+[ACP]+[BCP]+[CcCP] \\ +[A^-CP]+[B^-CP]+[Cc^-CP] \end{aligned} \tag{C.14}$$

In terms of $\mathbf{AH^+}$:

$$\begin{aligned} C_0 = [AH^+]\Bigg(1 + \frac{K_a}{[H^+]} + \frac{K_h}{[H^+]} + \frac{K_hK_t}{[H^+]} + \frac{K_{A/A^-}K_a}{[H^+]^2} + \frac{K_{B/B^-}K_h}{[H^+]^2} + \frac{K_{Cc/Cc^-}K_hK_t}{[H^+]^2} \\ + K_{AH^+CP}[CP] + K_{ACP}\frac{K_a}{[H^+]}[CP] + K_{BCP}\frac{K_h}{[H^+]}[CP] + K_{CcCP}\frac{K_hK_t}{[H^+]}[CP] \\ + \frac{K_{ACP/A^-CP}K_{ACP}K_a}{[H^+]^2}[CP] + \frac{K_{BCP/B^-CP}K_{BCP}K_h}{[H^+]^2}[CP] + \frac{K_{CcCP/Cc^-CP}K_{CcCP}K_hK_t}{[H^+]^2}[CP]\Bigg) \end{aligned} \tag{C.15}$$

$$C_0 = [AH^+](1 + K_{AH^+CP}[CP] + \frac{K_a + K_h + K_h K_t + K_{ACP} K_a [CP] + K_{BCP} K_h [CP] + K_{CcCP} K_h K_t [CP]}{[H^+]} + \frac{K_{A/A^-} K_a + K_{B/B^-} K_h + K_{Cc/Cc^-} K_h K_t}{[H^+]^2} + \frac{(K_{ACP/A^-CP} K_{ACP} K_a [CP] + K_{BCP/B^-CP} K_{BCP} K_h [CP] + K_{CcCP/Cc^-CP} K_{CcCP} K_h K_t)[CP]}{[H^+]^2}) \tag{C.16}$$

or simplifying

$$C_0 = [AH^+](1 + K_{AH^+CP}[CP] + \frac{K_a^\wedge + K_1[CP]}{[H^+]} + \frac{K_2 + K_3[CP]}{[H^+]^2}) \tag{C.17}$$

with

$$K_a^\wedge = K_a + K_h + K_h K_t$$
$$K_1 = K_{ACP} K_a + K_{BCP} K_h + K_{CcCP} K_h K_t$$
$$K_2 = K_{A/A^-} K_a + K_{B/B^-} K_h + K_{Cc/Cc^-} K_h K_t$$
$$K_3 = K_{ACP/A^-CP} K_{ACP} K_a + K_{BCP/B^-CP} K_{BCP} K_h + K_{CcCP/Cc^-CP} K_{CcCP} K_h K_t$$

The molar fraction can be written as:

$$\chi_{AH^+} = \frac{[AH^+]}{C_0} = \frac{1}{(1 + K_{AH^+CP}[CP]) + \frac{K_a^\wedge + K_1[CP]}{[H^+]} + \frac{K_2 + K_3[CP]}{[H^+]^2}} = \frac{\frac{1}{(1+K_{AH^+CP}[CP])}[H^+]^2}{[H^+]^2 + \frac{K_a^\wedge + K_1[CP]}{(1+K_{AH^+CP}[CP])}[H^+] + \frac{K_2 + K_3[CP]}{(1+K_{AH^+CP}[CP])}} \tag{C.18}$$

$$\chi_{AH^+CP} = \frac{[AH^+CP]}{C_0} = \frac{\frac{K_{AH^+CP}[CP]}{(1+K_{AH^+CP}[CP])}[H^+]^2}{[H^+]^2 + \frac{K_a^\wedge + K_1[CP]}{(1+K_{AH^+CP}[CP])}[H^+] + \frac{K_2 + K_3[CP]}{(1+K_{AH^+CP}[CP])}} \tag{C.19}$$

The sum of complexed and uncomplexed flavylium cations:

$$\chi_{AH^+} + \chi_{AH^+CP} = \frac{[H^+]^2}{[H^+]^2 + K_{a(CP)}^\wedge [H^+] + K_{a(CP)}^\wedge K_{a(CP)}^{\wedge\wedge}} \tag{C.20}$$

The values of $K_{a(CP)}^\wedge$ and $K_{a(CP)}^{\wedge\wedge}$ are obtained when the absorbance is plotted as function of pH. The constant K_{AH^+CP} is calculated representing the absorption of the flavylium cation at pH=1 as a function of increasing amounts of the co-pigment.
The mole fractions of **A** and **ACP** and their ionized forms is then obtained as:

$$\chi_A + \chi_{ACP} + \chi_{A^-} + \chi_{A^-CP} = \frac{\frac{K_a + K_{ACP} K_a [CP]}{(1+K_{AH^+CP}[CP])}[H^+] + \frac{K_{A/A^-} K_a + K_{ACP/A^-CP} K_{ACP} K_a [CP]}{(1+K_{AH^+CP}[CP])}}{[H^+]^2 + K_{a(CP)}^\wedge [H^+] + K_{a(CP)}^\wedge K_{a(CP)}^{\wedge\wedge}} \tag{C.21}$$

$$K_a^{\wedge} = K_a$$
$$K_1 = K_{ACP} K_a$$
$$K_2 = K_{A/A^-} K_a$$
$$K_3 = K_{ACP/A^-CP} K_{ACP} K_a$$

Identically for the hemiketal and the *cis*-chalcones:

$$\chi_B + \chi_{BCP} + \chi_{B^-} + \chi_{B^-CP} = \frac{\frac{(K_h + K_{BCP} K_h [CP])[H^+] + K_{B/B^-} K_h + K_{BCP/B^-CP} K_{BCP} K_h [CP]}{(1 + K_{AH^+CP}[CP])}}{[H^+]^2 + K^{\wedge}_{a(CP)}[H^+] + K^{\wedge}_{a(CP)} K^{\wedge\wedge}_{a(CP)}} \quad \text{(C.22)}$$

$$\chi_{Cc} + \chi_{CcCP} + \chi_{Cc^-} + \chi_{Cc^-CP} = \frac{\frac{(K_h K_t + K_{CcCP} K_h K_t [CP])[H^+] + K_{Cc/Cc^-} K_h K_t + K_{CcCP/Cc^-CP} K_{CcCP} K_h K_t [CP]}{(1 + K_{AH^+CP}[CP])}}{[H^+]^2 + K^{\wedge}_{a(CP)}[H^+] + K^{\wedge}_{a(CP)} K^{\wedge\wedge}_{a(CP)}} \quad \text{(C.23)}$$

Following the sequence in Appendix B for calculations of the a, b and c values.

$$\chi_{AH^+} + \chi_{AH^+CP} + \chi_A + \chi_{ACP} + \chi_{A^-} + \chi_{A^-CP} = \frac{[H^+]^2 + a_{0(CP)} K^{\wedge}_{a(CP)}[H^+] + a_{1(CP)} K^{\wedge}_{a(CP)} K^{\wedge\wedge}_{a(CP)}}{[H^+]^2 + K^{\wedge}_{a(CP)}[H^+] + K^{\wedge}_{a(CP)} K^{\wedge\wedge}_{a(CP)}} \quad \text{(C.24)}$$

where $a_{0(CP)}$ and $a_{1(CP)}$ are the mole fraction of **A** plus **ACP** and **A**$^-$ plus **A**$^-$**CP** respectably.

$$a_{0(CP)} K^{\wedge}_{a(CP)} = \frac{K_a + K_{ACP} K_a [CP]}{(1 + K_{AH^+CP}[CP])} \quad \text{(C.25)}$$

$$a_{1(CP)} K^{\wedge}_{a(CP)} K^{\wedge\wedge}_{a(CP)} = \frac{K_{ACP/A^-CP} + K_{ACP} K_a}{(1 + K_{AH^+CP}[CP])} \quad \text{(C.26)}$$

Proceeding identically for the other species:

$$\chi_B + \chi_{BCP} + \chi_{B^-} + \chi_{B^-CP} = \frac{b_{0(CP)} K^{\wedge}_{a(CP)}[H^+] + b_{1(CP)} K^{\wedge}_{a(CP)} K^{\wedge\wedge}_{a(CP)}}{[H^+]^2 + K^{\wedge}_{a(CP)}[H^+] + K^{\wedge}_{a(CP)} K^{\wedge\wedge}_{a(CP)}} \quad \text{(C.27)}$$

$$\chi_{Cc} + \chi_{CcCP} + \chi_{Cc^-} + \chi_{Cc^-CP} = \frac{c_{0(CP)} K^{\wedge}_{a(CP)}[H^+] + c_{1(CP)} K^{\wedge}_{a(CP)} K^{\wedge\wedge}_{a(CP)}}{[H^+]^2 + K^{\wedge}_{a(CP)}[H^+] + K^{\wedge}_{a(CP)} K^{\wedge\wedge}_{a(CP)}} \quad \text{(C.28)}$$

$$b_{0(CP)} K^{\wedge}_{a(CP)} = \frac{K_h + K_{BCP} K_h [CP]}{(1 + K_{AH^+CP}[CP])} \quad \text{(C.29)}$$

$$b_{1(CP)} K^{\wedge}_{a(CP)} K^{\wedge\wedge}_{a(CP)} = \frac{K_{BCP/B^-CP} + K_{BCP} K_h}{(1 + K_{AH^+CP}[CP])} \quad \text{(C.30)}$$

$$c_{0(CP)}K^{\wedge}_{a(CP)} = \frac{K_h K_h + K_{CcCP} K_h K_h [CP]}{(1 + K_{AH^+CP}[CP])} \tag{C.31}$$

$$c_{1(CP)}K^{\wedge}_{a(CP)}K^{\wedge\wedge}_{a(CP)} = \frac{K_{CcCP/Cc^-CP} + K_{CcCP} K_h K_t}{(1 + K_{AH^+CP}[CP])} \tag{C.32}$$

In summary, Equations C.25, C.29 and C.31 give the neutral constants K_{ACP}, K_{BCP} and K_{CcCP}, while the ionization constants complexes K_{ACP/ACP^-}, K_{BCP/BCP^-} and $K_{CcCP/CcCP^-}$ are given by Equations C.26, C.30 and C.32. Then is easy to prove that:

$$K_{ACP/ACP^-} = \frac{K_{ACP^-}}{K_{ACP}} K_{A/A^-} \tag{C.33}$$

$$K_{BCP/BCP^-} = \frac{K_{BCP^-}}{K_{BCP}} K_{B/B^-} \tag{C.34}$$

$$K_{CcCP/CcCP^-} = \frac{K_{CcCP^-}}{K_{CcCP}} K_{Cc/Cc^-} \tag{C.35}$$

If the equilibrium is considered, the contribution of the *trans*-chalcones should be added.

$$\begin{aligned} &\chi_{Ct} + \chi_{CtCP} + \chi_{Ct^-} + \chi_{Ct^-CP} \\ &= \frac{\frac{(K_h K_t K_i + K_{CtCP} K_h K_t K_i [CP])[H^+] + K_{Ct/Ct^-} K_h K_t K_i + K_{CtCP/Ct^-CP} K_{CtCP} K_h K_t K_i [CP]}{(1 + K_{AH^+CP}[CP])}}{[H^+]^2 + K'_{a(CP)}[H^+] + K'_{a(CP)}K''_{a(CP)}} \end{aligned} \tag{C.36}$$

$$\chi_{Ct} + \chi_{CtCP} + \chi_{Ct^-} + \chi_{Ct^-CP} = \frac{d_{0(CP)}K'_{a(CP)}[H^+] + d_{1(CP)}K'_{a(CP)}K''_{a(CP)}}{[H^+]^2 + K'_{a(CP)}[H^+] + K'_{a(CP)}K''_{a(CP)}} \tag{C.37}$$

$$d_{0(CP)}K'_{a(CP)} = \frac{K_h K_t K_i + K_{CtCP} K_h K_t K_i [CP]}{(1 + K_{AH^+CP}[CP])} \tag{C.38}$$

$$d_{1(CP)}K'_{a(CP)}K''_{a(CP)} = \frac{K_{CtCP/Ct^-CP} + K_{CtCP} K_h K_t K_i}{(1 + K_{AH^+CP}[CP])} \tag{C.39}$$

and

$$K_{CtCP/CtCP^-} = \frac{K_{CtCP^-}}{K_{CtCP}} K_{Ct/Ct^-} \tag{C.40}$$

Calculation of the Pigment/Co-pigment association constants

The association constants of some species from the flavylium multi-state with a co-pigment can be calculated directly from the spectra resulting from the titration. A variation of the Benesi-Hildebrand is applied the fitting to obtain K_{AH^+CP} (Eq.C.45). The Benesi-Hildebrand

equation can be described as:

$$A = A^{Y} + A^{YCP} + A^{CP} \tag{C.41}$$

where A is the observed absorbance at a specific wavelength, and A^{Y}, A^{YCP}, and A^{CP} are the contribution in absorbance of the pigment, the complex and the co-pigment respectively. Considering no absorption of the co-pigment, Eq.C.41 can be rewritten using the Beer's Law Equation $A = \epsilon bc$ as:

$$A = \epsilon_{Y} C_0 \chi_{Y} + \epsilon_{YCP} C_0 \chi_{YCP} \tag{C.42}$$

Considering **AH⁺** as the unique species at pH=1 for K_{AH^+CP} calculation, from Eq.C.1:

$$K_{AH^+CP} = \frac{[AH^+CP]}{[AH^+][CP]} \tag{C.43}$$

$$C_0 = [AH^+] + [AH^+CP] = [AH^+](1 + K_{AH^+CP}[CP]) \tag{C.44}$$

$$\chi_{AH^+} = \frac{[AH^+]}{C_0} = \frac{1}{1 + K_{AH^+CP}[CP]}$$

$$\chi_{AH^+CP} = \frac{[AH^+CP]}{C_0} = \frac{K_{AH^+CP}[CP]}{1 + K_{AH^+CP}[CP]}$$

Then, from Eq.C.42:

$$A = \frac{\epsilon_{AH^+} C_0 + \epsilon_{AH^+CP} C_0 K_{AH^+CP}[CP]}{1 + K_{AH^+CP}[CP]}$$

$$A = \frac{A_0 + A_f K_{AH^+CP}[CP]}{1 + K_{AH^+CP}[CP]} \tag{C.45}$$

where A_0 and A_f are the initial and final absorbance, respectively. When the association constant is very small the final absorbance could not be reached, limited by the solubility of the co-pigment.

Host-Guest association constants

The 1:1 Host-Guest complexation mathematical model can be described by the equilibrium:

$$\mathrm{G} + \mathrm{H} \overset{K_{11}}{\rightleftharpoons} \mathrm{HG} \tag{C.46}$$

Then, the following equations can be deduced:

$$[H]_0 = [H] + [HG] \tag{C.47}$$

$$[G]_0 = [G] + [HG] \tag{C.48}$$

$$K_{11} = \frac{[HG]}{[H][G]} \tag{C.49}$$

After some algebraic manipulations:

$$[H]^2K_1 + [H](K_{11}[G]_0 - K_{11}[H]_0 + 1) - [H]_0 = 0 \tag{C.50}$$

This is a quadratic equation that can be solved by the general expression: $[H] = -b \pm \sqrt[2]{(b^2 - 4ac)/(2a)}$. This method lead the direct calculation of the [H] in the equilibrium and the K_{11} can be calculated from Equation C.49.

The data A vs [H] obtained from the UV-Vis spectra is then fitted by Equation C.51, where A_0 is the absorption in the absence of the host and A_1 is the limiting spectroscopic signals of the complex 1:1. The Microsoft Excel Solver tool can be used to adjust the fitting.

$$A = \frac{A_0[G] + A_1[HG]}{[G]_0} \tag{C.51}$$

The 2:1 Host-Guest complexation mathematical model can be described by the equilibrium between two equilibrium reactions:

$$\mathrm{G} + \mathrm{H} \overset{K_{11}}{\rightleftharpoons} \mathrm{HG} \tag{C.52}$$

$$\mathrm{HG} + \mathrm{H} \overset{K_{21}}{\rightleftharpoons} \mathrm{H_2G} \tag{C.53}$$

Then, the following equations can be deduced:

$$[G]_0 = [G] + [HG] + [H_2G] \tag{C.54}$$

$$[H]_0 = [H] + [HG] + 2[H_2G] \tag{C.55}$$

$$K_{11} = \frac{[HG]}{[H][G]} \tag{C.56}$$

$$K_{21} = \frac{[H_2G]}{[H][HG]} \tag{C.57}$$

After some algebraic manipulations:

$$[G] + K_{11}[H][G] + K_{11}K_{21}[H]^2[G] - [G]_0 = 0 \tag{C.58}$$

$$[H] + K_{11}[H][G] + 2K_{11}K_{21}[H]^2[G] - [H]_0 = 0 \tag{C.59}$$

The Equation C.58 can be also written as:

$$[G] = \frac{[G]_0}{1 + K_{11}[H] + K_{11}K_{21}[H]^2} \tag{C.60}$$

combined with Equation C.59 the following cubic equation is obtained:

$$K_{11}K_{21}[H]^3 + (K_{11} + 2K_{11}K_{21}[G]_0 - K_{11}K_{21}[H]_0)[H]^2 + (K_{11}[G]_0 - K_{11}[H]_0 + 1)[H] - [H]_0 = 0 \tag{C.61}$$

The solution of the cubic Equation C.61 by the Newton-Ramphson algoritm, leads to [H] in the equilibrium. The equilibrium constants K_11 and K_21 can be calculated directly from Equations C.58, C.56 and C.57.

The data A vs [H] obtained from the UV-Vis spectra is fitted by Equation C.62, where A_0 is the absorption in the absence of the host, and A_1 and A_2 are the limiting spectroscopic signals of the complexes 1:1 and 2:1 respectively. The Microsoft Excel Solver tool can be used to adjust the fitting.

$$A = \frac{A_0[G] + A_1[HG] + A_2[H_2G]}{[G]_0} \tag{C.62}$$

ANNEX I

^{1}H NMR (400 MHz, DMSO) δ 7.08, 1.33.

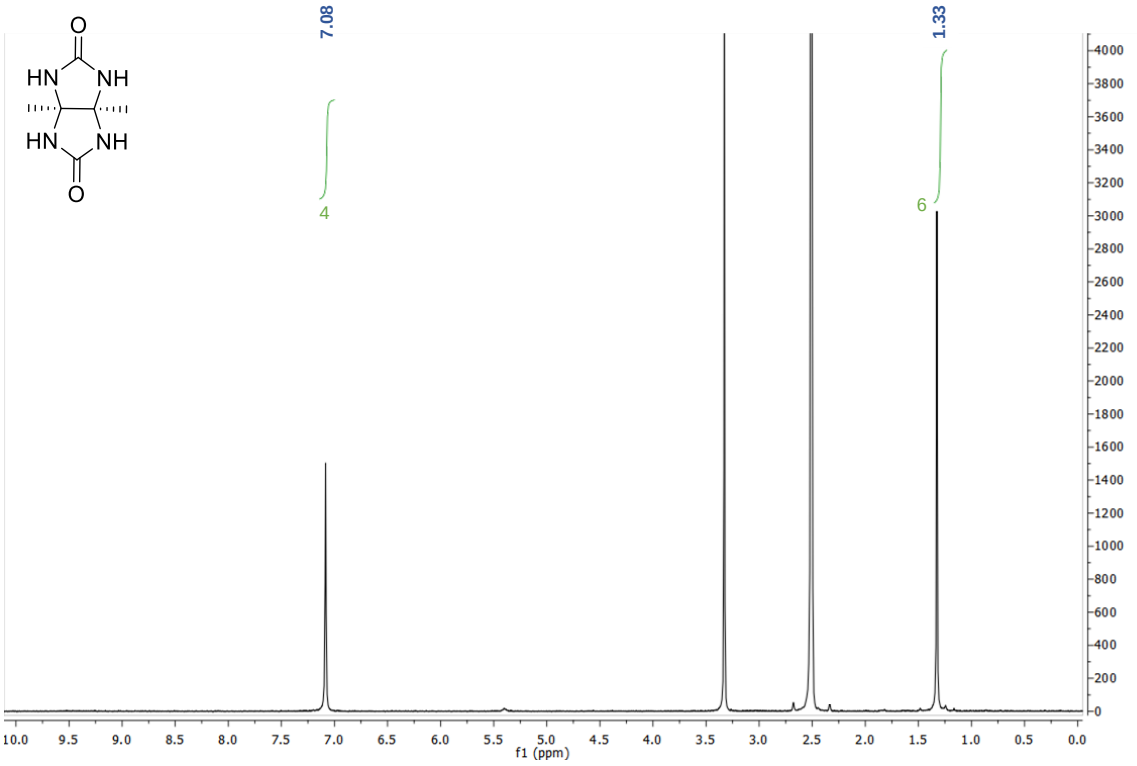

Figure A. ^{1}H NMR spectrum of compound 1 in DMSO.

^{1}H NMR (400 MHz, DMSO) δ 5.23, 4.99, 1.81.

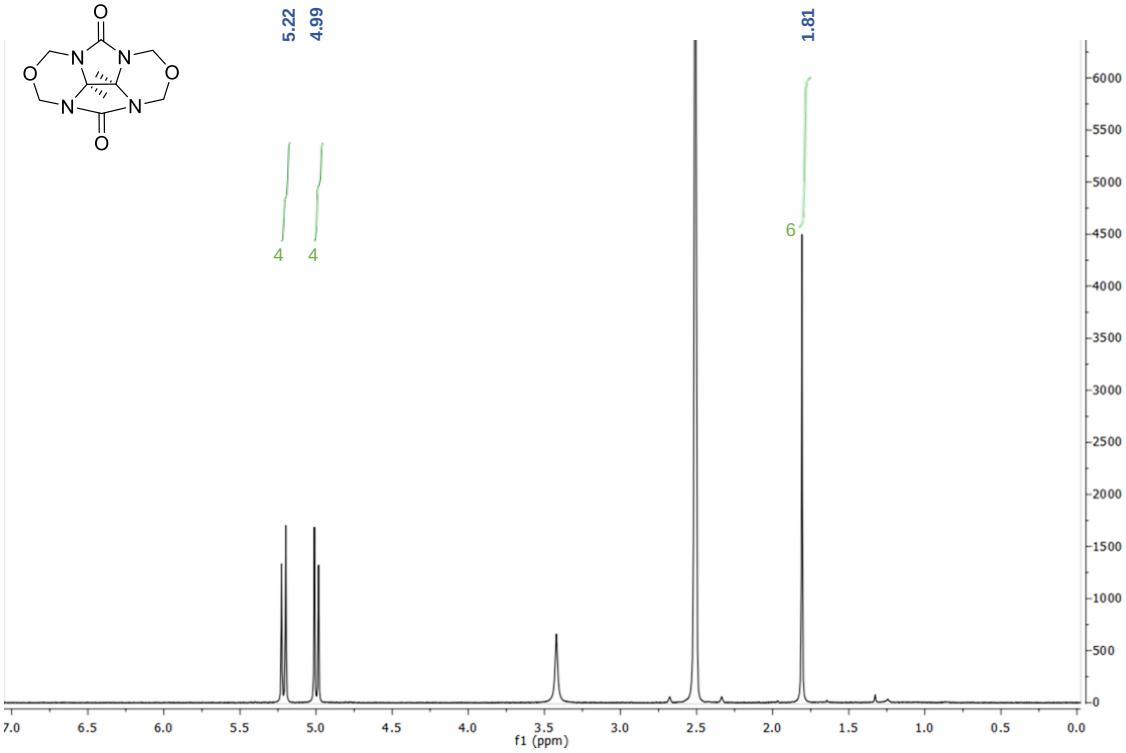

Figure B. ^{1}H NMR spectrum of compound 3 in DMSO.

^{1}H NMR (400 MHz, DMSO) δ 7.59, 5.50, 3.99, 1.55, 1.34.

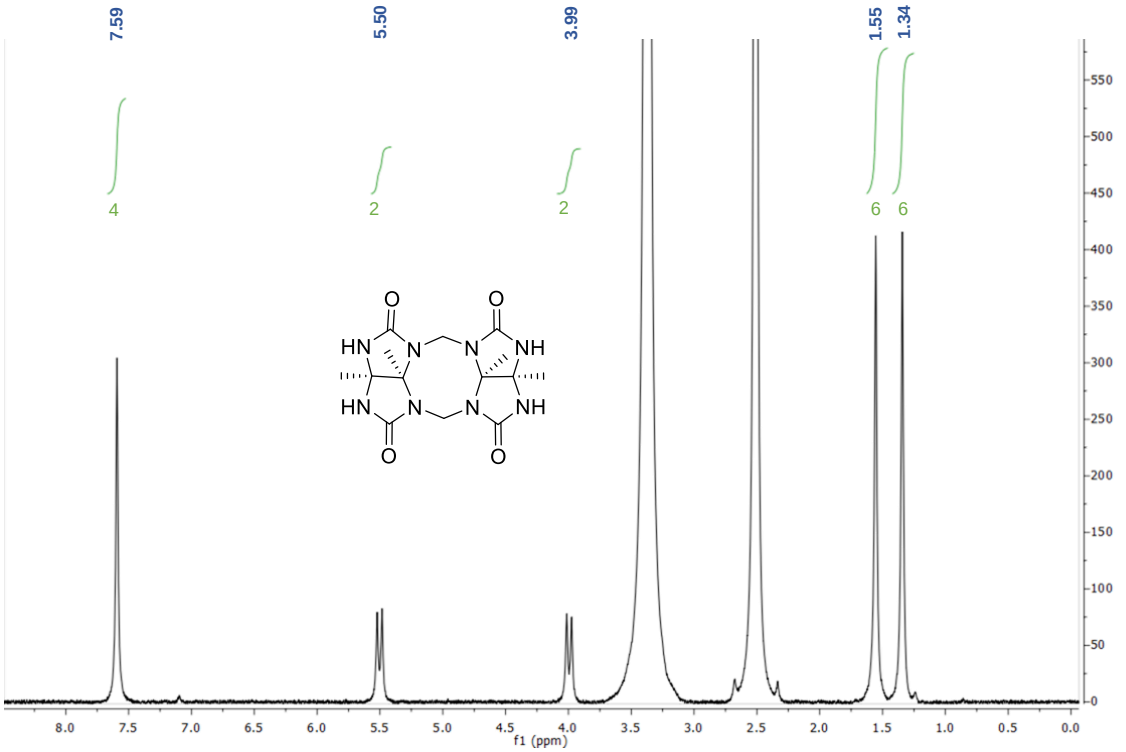

Figure C. ^{1}H NMR spectrum of compound 4 in DMSO.

^{1}H NMR (400 MHz, D_2O) δ 8.21, 7.56, 6.92, 4.24, 3.13, 2.27.

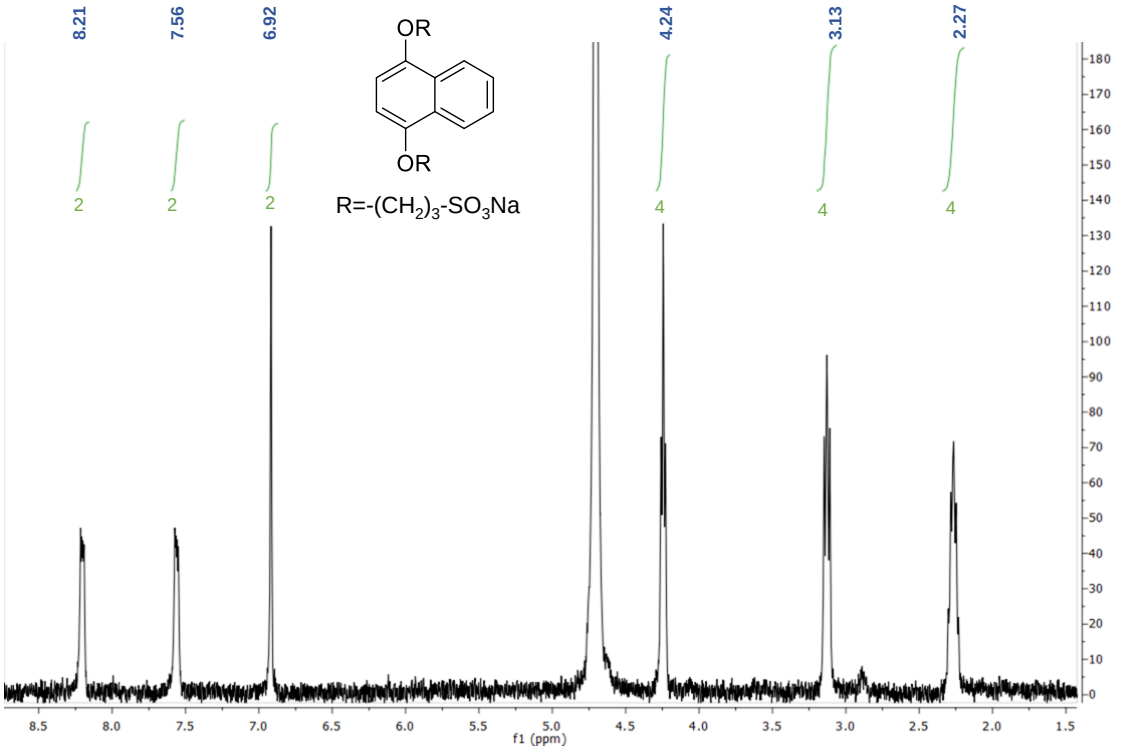

Figure D. ^{1}H NMR spectrum of compound 5 in D_2O.

^{1}H NMR (400 MHz, DMSO) δ 5.48, 5.16, 4.88, 4.33, 1.83, 1.65.

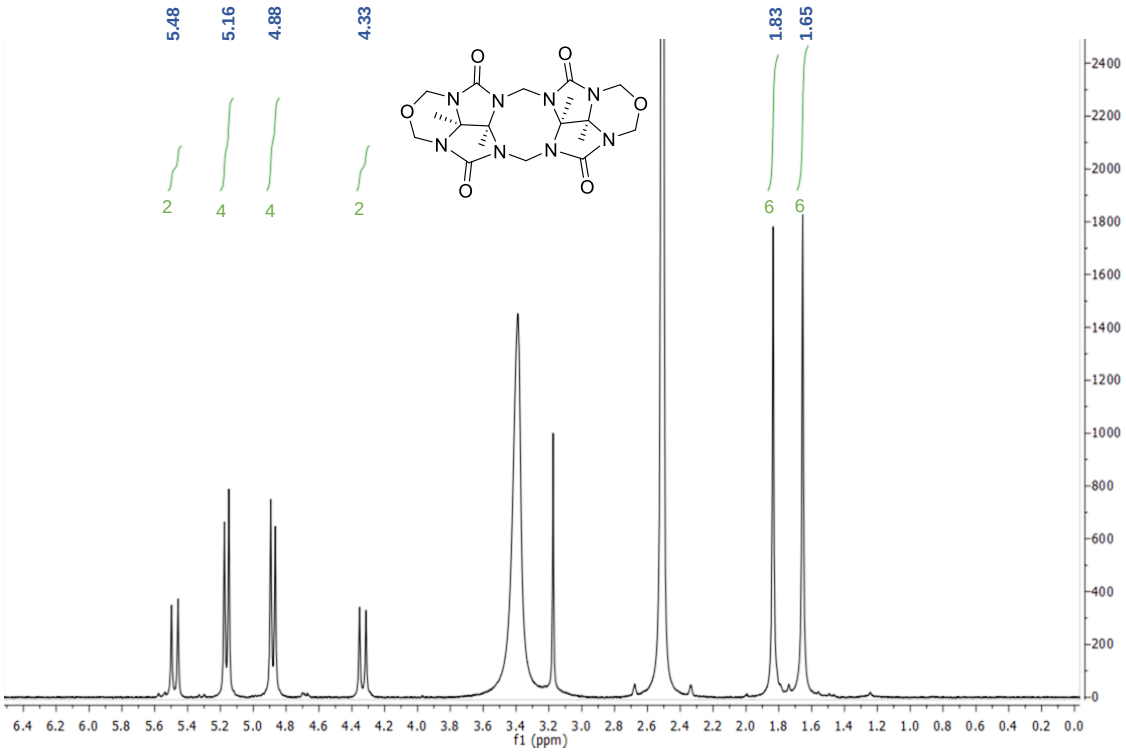

Figure E. ^{1}H NMR spectrum of compound 6 in DMSO.

^{1}H NMR (400 MHz, D_2O) δ 7.80, 7.41, 5.14, 4.32, 3.59, 2.79, 2.03, 1.75.

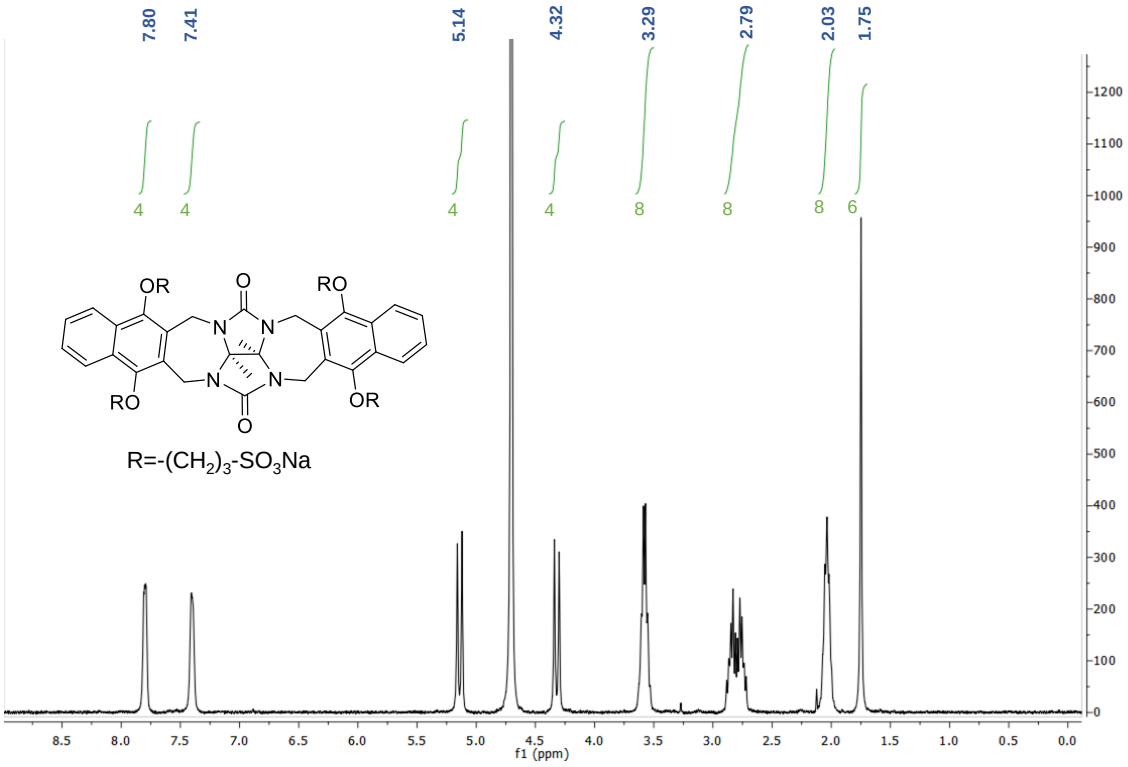

Figure F. ^{1}H NMR spectrum of CP1 in D_2O.

^{1}H NMR (400 MHz, D_2O) δ 7.75, 5.27, 5.11, 4.26, 4.17, 3.63, 3.18, 3.01, 2.85, 1.97, 1.74, 1.67, 1.62.

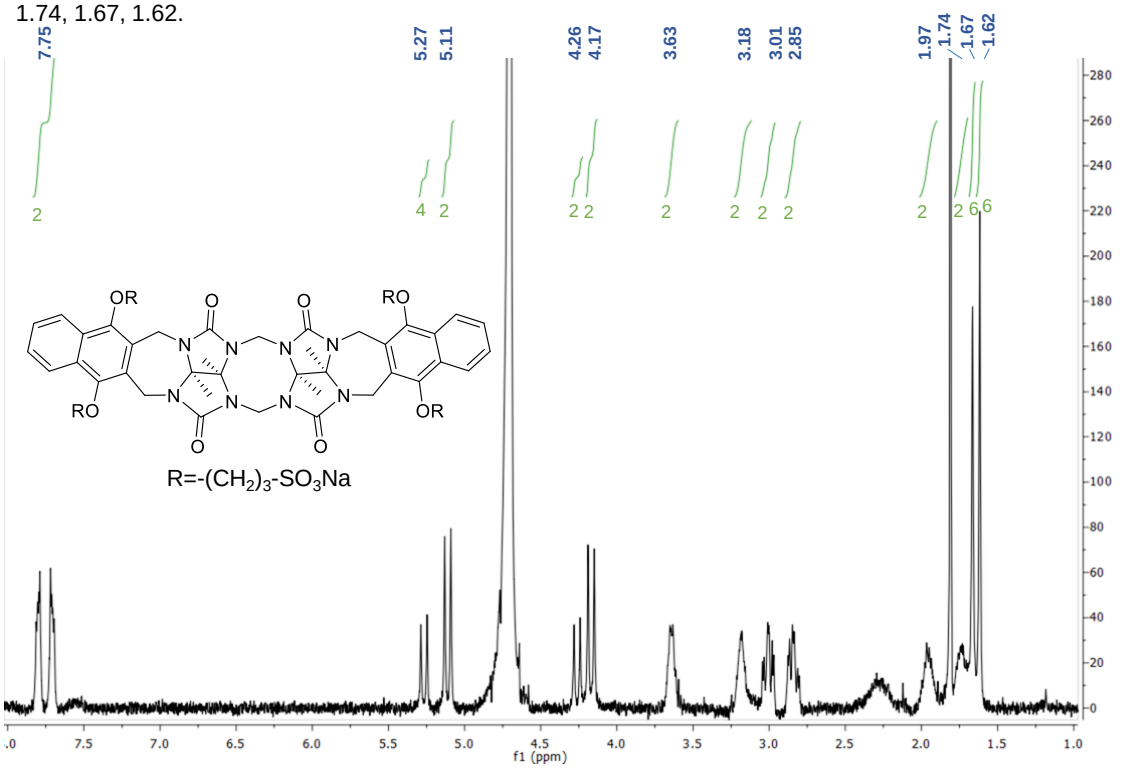

Figure G. ^{1}H NMR spectrum of CP2 in D_2O.

^{1}H NMR (400 MHz, D_2O) δ 7.47, 3.90.

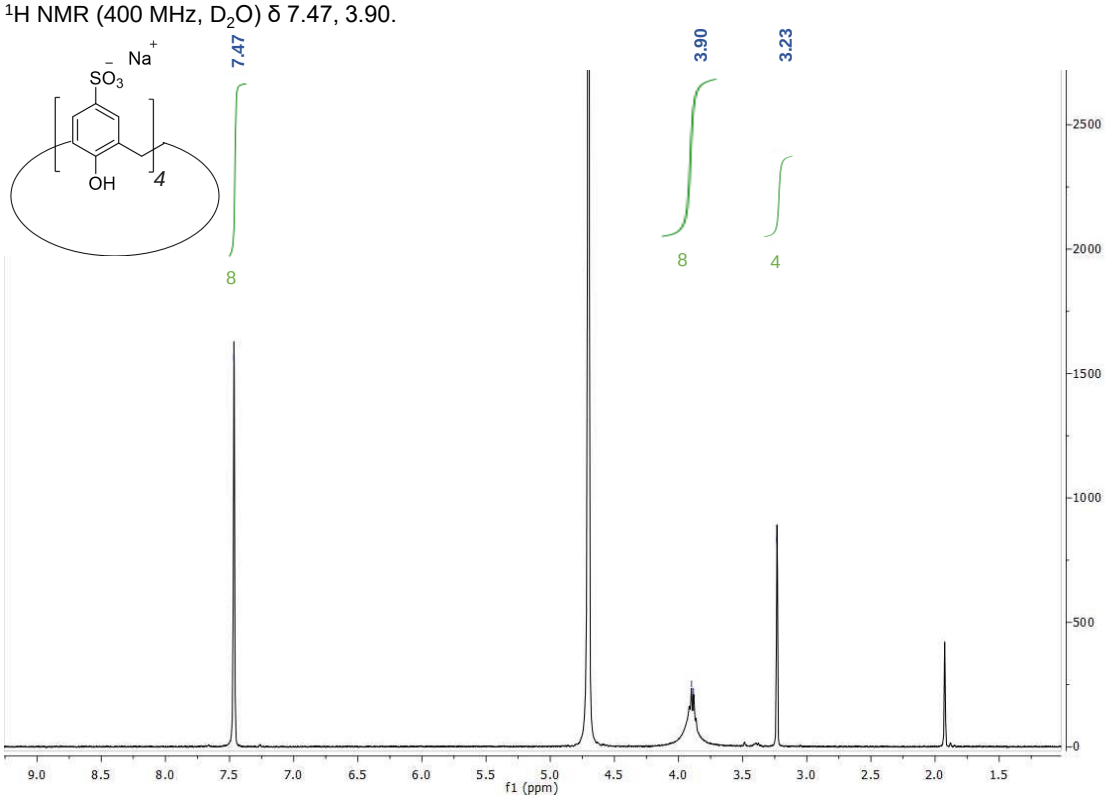

Figure H. ^{1}H NMR spectrum of *p*-sulfonated Calix[4]arene in D_2O.

^{1}H NMR (400 MHz, D_2O) δ 7.41, 3.88.

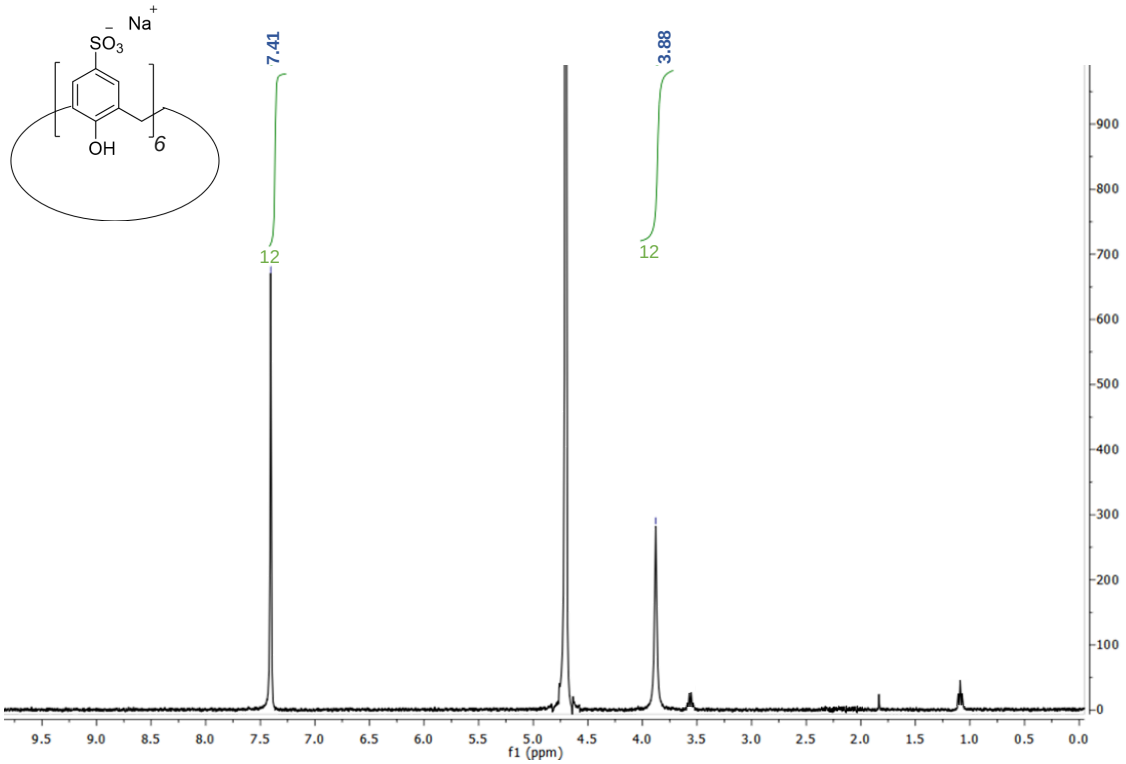

Figure H. ^{1}H NMR spectrum of *p*-sulfonated Calix[6]arene in D_2O.

^{1}H NMR (400 MHz, D_2O) δ 7.64, 4.11.

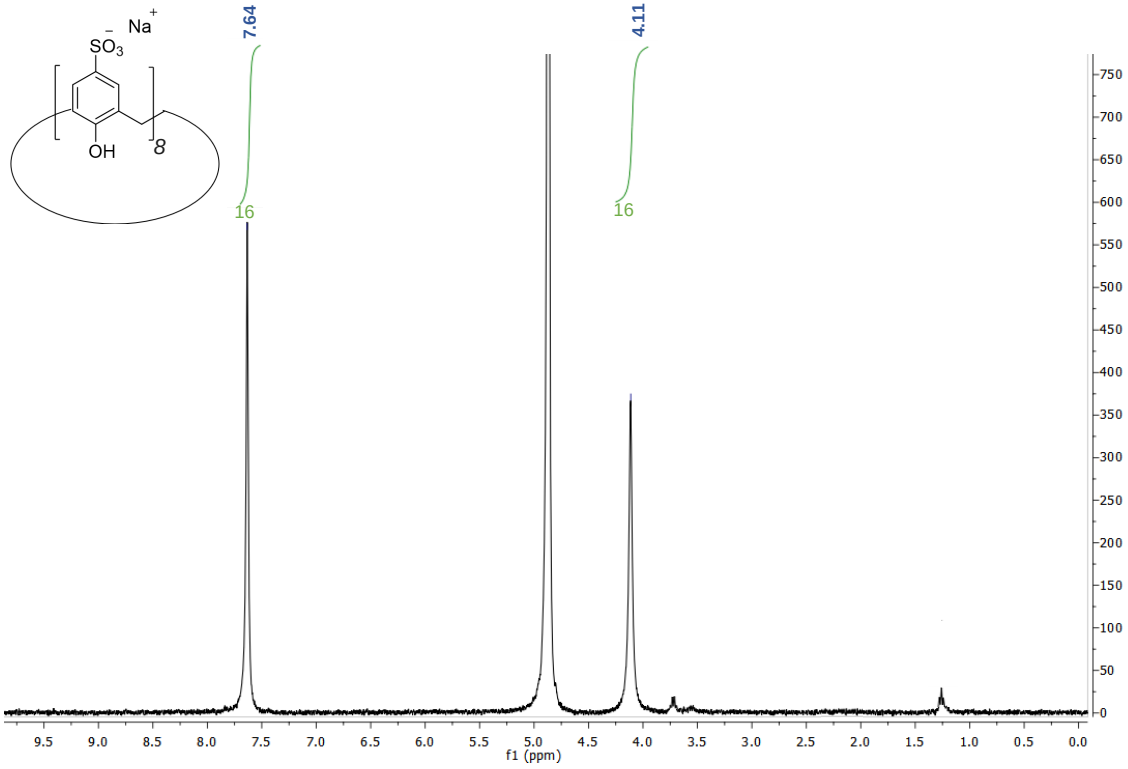

Figure I. ^{1}H NMR spectrum of *p*-sulfonated Calix[8]arene in D_2O.

^{1}H NMR (400 MHz, CD_3OD) δ 9.21, 8.65, 8.61, 7.70, 7.19.

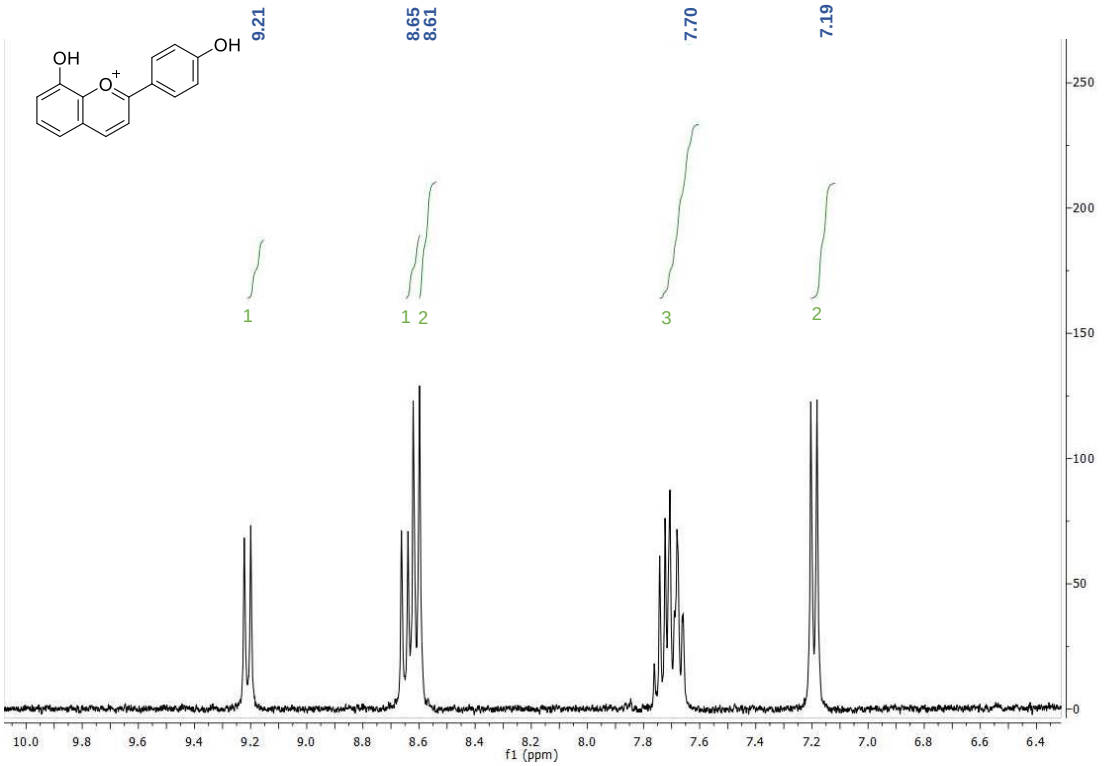

Figure I. ^{1}H NMR spectrum of the compound 84'OH in CD_3OD.

^{1}H NMR (400 MHz, CD_3OD) δ 9.01, 8.33, 7.54, 7.05, 4.16, 3.46, 3.06, 2.24.

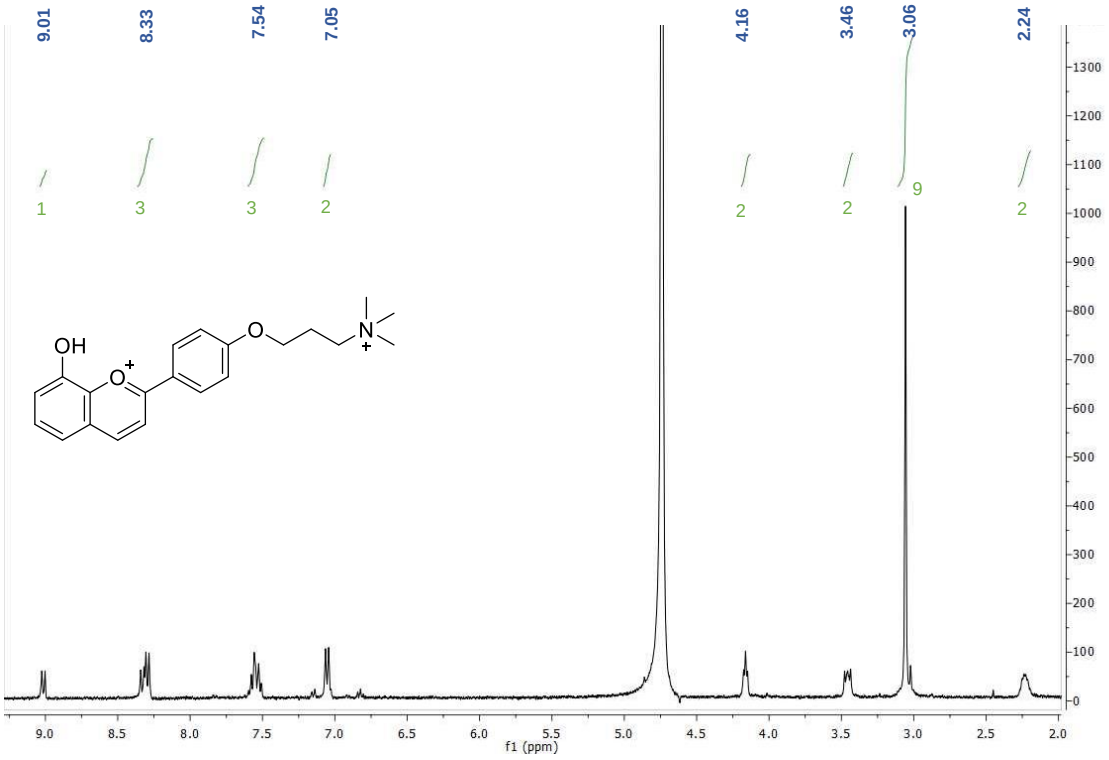

Figure I. ^{1}H NMR spectrum of the compound 8OH4'TMA in D_2O.